SISSA - International School for Advanced Studies

Deviations from General Relativity in Cosmology and Astrophysics

Thesis Submitted for the Degree of
"Doctor Philosophiæ"

Supervisors
Prof. Thomas P. Sotiriou
Prof. Ravi K. Sheth
Dr. Alessandra Silvestri

Candidate
Noemi Frusciante

October 2014

Contents

Abstract **v**

Collaborations **vii**

Notation **ix**

I Introduction **1**

1 General Relativity **3**
1.1 Einstein−Hilbert Action and Field Equations 4
1.2 On the Uniqueness of General Relativity Action 5

2 The Cosmological Standard Model **9**
2.1 The Cosmological Principle 11
2.1.1 The Friedmann-Lemaître-Robertson-Walker metric 11
2.2 The Stress Energy Tensor 13
2.3 Cosmological solutions to the ΛCDM model 14
2.4 Observational evidence for ΛCDM 17
2.5 Is the Cosmological Constant the Einstein's "greatest blunder"? . 19

3 Beyond the Cosmological Standard Model **21**
3.1 Fine-tuning problems in the early Universe: flatness, homogeneity and isotropy 21
3.1.1 The Inflation Paradigm 23
3.2 Cosmic Acceleration 26
3.2.1 The Cosmological Constant issue 26
3.2.2 Dark Energy 27
3.2.3 Quintessence model 28
3.3 The Dark Matter issue 29

II Dark Matter at Small and Large Scales 33

4 Dark Matter in Galaxies 35
4.1 Dark Matter halo density profiles . . . 36
4.2 MOND: Modifying the Newtonian Dynamics . . . 37
4.3 The Orion Dwarf Galaxy: a test for MOND . . . 38
4.3.1 Stellar Photometry . . . 39
4.3.2 HI surface density and kinematics . . . 39
4.3.3 The Circular Velocity . . . 40
4.3.4 Mass Modeling and Results . . . 44
4.3.5 Discussion . . . 48

5 The Bias factor and its implications in Cosmology 51
5.1 Lagrangian bias in the local bias model . . . 53
5.1.1 The Lognormal model and the usual expansion . . . 55
5.1.2 Normalizing density rather than overdensity: The general case . . . 58
5.1.3 Renormalized bias . . . 59
5.1.4 Relation to halo bias from the excursion set approach . . . 62
5.1.5 Discussion . . . 63

III Modifying General Relativity 67

6 Alternative theories of gravity with an extra scalar degree of freedom 69
6.1 Scalar-Tensor Theory . . . 72
6.1.1 f(R) Theory . . . 73
6.2 Generalized Galileon Theory . . . 75
6.3 Gradient expansion of superhorizon perturbations . . . 78
6.3.1 ADM formalism . . . 79
6.4 G-Inflation with shift symmetric Galileon . . . 80
6.4.1 Gradient expansion method: order analysis . . . 81
6.4.2 General solution . . . 83
6.4.3 Late time of inflation . . . 89
6.4.4 Discussion . . . 91

7 Effective Field Theory for Dark Energy and Modified Gravity 93
7.1 The effective field theory action and its formulation . . . 94
7.1.1 The background equations . . . 96
7.2 Quintessence and f(R) models mapping . . . 97
7.3 A Background Dynamical Analysis . . . 98

7.3.1 Dynamical System and Cosmological Viability 100
7.3.2 Stability Analysis 102
7.3.3 N^{th} order analysis: exploiting the recursive nature of the system 119
7.3.4 Discussion 123
7.4 Effective field theory for CAMB 125
7.4.1 Code implementation of the background cosmology 128
7.4.2 Scalar linear perturbations 130
7.4.3 Stability of perturbations in the dark sector 132
7.4.4 Observables 133
7.4.5 Numerical Results 135
7.4.6 $f(R)$ gravity: comparison and new results 136
7.4.7 Pure EFT parametrizations with phantom-divide crossing 144
7.4.8 EFTCosmoMC: sampling of the parameter space under stability conditions 146
7.4.9 Data sets and Results 147
7.4.10 Discussion 156

8 Conclusions **161**

A Dependence of equations of motion in general covariant scalar-tensor theory **165**

B Gradient expansion of the equations of motion in synchronous gauge **167**

C EFT background Dynamical analysis **169**
C.1 A complete second order analysis 169
C.2 N^{th} order analysis 171

D EFT: Contributions to the perturbative equations from second order operators **177**

Acknowledgments **181**

Bibliography **181**

Abstract

Two of the most prominent challenges of Modern Cosmology are the recent late-time accelerated expansion of the Universe and Dark Matter (DM).

DM is of fundamental importance in the process of structure formation at galactic, extragalactic and cosmic scales. It seems to dominate down to small galactocentric radii, as highlighted by the galaxies rotation curves and on cosmic scale, it is well known that the spatial distribution of galaxies is biased with respect to the underlying DM distribution. This relation is called "bias". Part of this thesis is devoted to the investigation of the DM issue. In particular, we study the DM density profile in the Orion dwarf galaxy. This galaxy is a good candidate to understand the physics of DM as in general, the kinematics of dwarf galaxies is dominated by this dark component. Moreover, due to the availability of high precision data, it becomes crucial to understand accurately the bias relation, so we elaborate on the Lagrangian bias, when the initial mass fluctuation field is considered Gaussian and the bias is local.

It is well known that the ΛCDM has been very successful in accounting for current cosmological data, although it suffers from some outstanding problems, such as the small value of Λ, DM problems on small scales, early Universe shortcomings and the lack of a correct scheme to quantize General Relativity. These lead people to propose and investigate alternative models, which are based on deviations from General Relativity at cosmic scales. The bulk of the present thesis is devoted to the study of gravity theories, which consider an extra scalar degree of freedom (DoF), in order to modify the gravitational interaction at large scales and account for the late time acceleration. In particular, we develop the gradient expansion formalism in order to explore the phenomenology associated with the non-linear derivative interactions of the most general scalar tensor theories that lead to second order field equations. This approach is very useful to probe on super horizon scale the Inflation scenario. Finally, in the quest of a model independent parametrization for gravity theories, the effective field theory formalism has been applied to the phenomenon of cosmic acceleration. It is developed using a perturbative approach in which an extra scalar DoF appears only at the level of perturbations. We investigate the viability of background functions by means of a thorough dynamical analysis. In conclusion, we present the implementation of this framework into CAMB/CosmoMC creating, what we dubbed, EFTCAMB/EFTCosmoMC. These codes will allow to test gravity theories with the most recent data releases.

Collaborations

This thesis is the result of the research done during my four years of Ph.D. and of collaborations with T. P. Sotiriou, R. K. Sheth, P. Salucci, A. Silvestri, J. M. Cannon, E. C. Elson, B. Hu, S.Y. Zhou, M. Raveri and D. Vernieri. The bulk of the present work is based on the following papers published in refereed Journals:

1. Marco Raveri, Bin Hu, Noemi Frusciante, Alessandra Silvestri,
   "Effective Field Theory of Cosmic Acceleration: constraining dark energy with CMB data",
   PRD **90** (2014) 043513 [arXiv:1405.1022 [astro-ph.CO]].
2. Bin Hu, Marco Raveri, Noemi Frusciante, Alessandra Silvestri,
   "Effective Field Theory of Cosmic Acceleration: an implementation in CAMB",
   PRD **89** (2014) 103530 [arXiv:1312.5742 [astro-ph.CO]].
3. Noemi Frusciante, Marco Raveri, Alessandra Silvestri,
   "Effective Field Theory of Dark Energy: a Dynamical Analysis",
   JCAP **1402**, 026 (2014) [arXiv:1310.6026 [astro-ph.CO]].
4. Noemi Frusciante, Shuang-Yong Zhou, Thomas P. Sotiriou,
   "Gradient expansion of superhorizon perturbations in G-inflation",
   JCAP **07**, 020, (2013) [arXiv:1303.6628 [astro-ph.CO]].
5. Noemi Frusciante & Ravi K. Sheth,
   "Lagrangian bias in the local bias model",
   JCAP 1211 (2012) 016, [arXiv:1208.0229v1 [astro-ph.CO]].
6. Noemi Frusciante, Paolo Salucci, Daniele Vernieri, Jhon. M. Cannon, Ed C. Elson,
   "The Distribution of Mass in the Orion Dwarf Galaxy",
   MNRAS **426**, 1, 751-757 (2012) [arXiv:1206.0314v1 [astro-ph.CO]].

Supplementary material includes:

- EFTCAMB/EFTCosmoMC package available at `http://www.lorentz.leidenuniv.nl/~hu/codes/`
- Bin Hu, Marco Raveri, Noemi Frusciante, Alessandra Silvestri
  "EFTCAMB/EFTCosmoMC: Numerical Notes v1.0",
  arXiv:1405.3590 [astro-ph.IM], (2014).

Notation

Here, we provide a brief guide to the notation and a list of acronyms.

$c = 1$	the speed of light is set to be equal to one;
G	Newtonian Gravitational Constant;
m_0	Planck mass;
$(-,+,+,+)$	metric signature;
$i, j, k...$	3D spatial indices in vectors and tensors;
$\mu, \nu, \gamma...$	4D indices in vectors and tensors;
$g_{\mu\nu}$	metric tensor;
g	determinant of the metric tensor $g_{\mu\nu}$
τ	conformal time;
t	cosmic time;
$\mathcal{H}$	Hubble parameter in conformal time;
H	Hubble parameter in cosmic time $H = \mathcal{H}/a$;
$R_{\mu\nu}$, R	Ricci tensor and its trace;
$T_{\mu\nu}$, T	Stress energy tensor and its trace;
$G_{\mu\nu}$	Einstein Tensor ($G_{\mu\nu} = R_{\mu\nu} - 1/2 g_{\mu\nu} R$);
ϕ	Scalar field;
χ_m	Matter fields;
S_m	Matter action of all matter fields, χ_m;
∇_μ	Covariant derivative;
$\bar{\nabla}$	Spatial covariant derivative;
Λ	Cosmological Constant;
δ	Perturbative density field ($\delta = \rho/\overline{\rho} - 1$).

Acronyms

ΛCDM	Λ Cold Dark Matter;
CC	Cosmological Constant Λ;
DM	Dark Matter;
GR	General Relativity;
FLRW	Friedmann-Lemaître-Robertson-Walker metric;
DE	Dark Energy;
MG	Modified Gravitational Theory;
LSS	Large Scale structure;
WMAP	Wilkinson Microwave Anisotropy Probe;
SDSS	Sloan Digital Sky Survey;
2dF	Two-degree-Field Galaxy Redshift Survey;
C.L.	Confidence Limits;
CMB	Cosmic Microwaves Background radiation;
BBN	Big Bang Nucleosynthesis;
EFT	Effective Field Theory for cosmic acceleration;
CAMB	Code for Anisotropies in the Microwave Background;
CosmoMC	Cosmological Monte Carlo code;
MGCAMB	Modification of Growth with CAMB;
WP	WMAP low-ℓ polarization spectra;
RC	Rotation Curve;
DoF	Degree of Freedom;
l.h.s	Left hand side;
r.h.s.	Right hand side;
w.r.t.	With respect to.

Part I

Introduction

Chapter 1

General Relativity

In 1915, Albert Einstein published the *Theory of General Relativity* (hereafter GR) in the *Annalen der Physik*, proposing to the academic world a new way to look at gravity: the gravitational field has to be thought of as geometrically related to the structure of space-time. The effect of the presence of a gravitational field directly translates into a curvature of the latter, which is dynamical described by a single geometrical quantity, the metric tensor $g_{\mu\nu}$. The mathematical language used to formulate the theory is that of differential geometry, a novelty in the field of physics. The resulting equations, known as Einstein's Equations are a set of partial differential equations, and are still the current description of gravity.

The first observational verification of the theory came only in 1919 by Eddington [1], who observed the bending of starlight by the Sun during a total solar eclipse. According to GR, the light of stars, passing near the Sun would be deflected by its gravitational field, and as a result the stars would occupy a position in the sky different than the actual one. This phenomenon can be verified only during a solar eclipse, as one can take pictures of the stars when the Sun is obscured. Eddington confirmed the GR expected value of 1.75 arcsec, which is twice the value predicted by the newtonian theory.

GR was soon proved to be the best mathematical description of physical phenomena involving the gravitational field. It has been tested on Solar System scales, where it describes the planetary orbits, including the anomaly in the orbit of Mercury. Further support to GR came from observations of distant binary millisecond pulsars [2]. First solutions to Einstein's Equations were found describing objects such as stars and black holes [3, 4, 5, 6] and, more generally, the collapse of spherical objects [7]. On cosmic scales, the theory allows to describe the Universe as a whole. This began what we know as Modern Cosmology, with several cosmological models proposed and tested.

This Chapter will provide a short introduction to the framework of GR. In Section 1.1, we briefly review the steps that led to the formulation of Einstein's Equations and the action from which they can be derived. Finally in Section 1.2, we shall comment on the uniqueness of the field equations and the action of GR.

1.1 Einstein−Hilbert Action and Field Equations

The equations of the gravitational field have been postulated by Einstein following some requirements in order to be considered viable. Locally a free-falling observer and an inertial observer are indistinguishable. This practically translates into the equivalence between the gravitational and the inertial mass (Equivalence Principle); a preferred system of reference does not exist, so the equations describing a physical phenomenon have the same form in all reference frames (Principle of Relativity); hence, the field equations should transform covariantly according to the Principle of General Covariance; they have to be of second order in the metric to avoid the Ostrogradski's instabilities [1] [8]; finally, in the weak field limit they have to recover the well known newtonian results. From an observational point of view the equations predictions must fit the observations. In the following we will illustrate how all these criteria come into play.

GR is constructed on a 4-dimensional manifold, called pseudo-Riemanian manifold, where the Levi-Civita connection $\Gamma^{\lambda}_{\mu\nu}$ is used to define the covariant derivative ∇_{μ}. The connection can be seen as describing the presence of gravitational forces or in absence of gravitational interactions, moving from an inertial frame to a non-inertial one, it provides the pseudo-forces. This shows the perfect equivalence between the inertial forces and the gravitational ones, accounting for the Equivalence Principle.
One important property of the Riemanian manifold is the contracted Bianchi identity, i.e.

$$\nabla^{\mu} G_{\mu\nu} = 0, \tag{1.1}$$

where $G_{\mu\nu}$ is the Einstein Tensor. It is defined as

$$G_{\mu\nu} = R_{\mu\nu} - \frac{1}{2} g_{\mu\nu} R, \tag{1.2}$$

where $g_{\mu\nu}$ is the metric tensor, $R_{\mu\nu}$ is the Ricci tensor and R is its trace. Then the relation (1.1) translates into four constraints on $R_{\mu\nu}$.

After some unsuccessful proposals, finally Einstein postulated that the equations of the gravitational field, known as Einstein's Equations, should be

$$G_{\mu\nu} = \frac{\kappa}{2} T_{\mu\nu}, \tag{1.3}$$

where $\kappa = 1/16\pi G$, G is Newtonian's constant and $T_{\mu\nu}$ is the stress-energy tensor, which accounts for the matter content. The contracted Bianchi identity implies a conservation equation for the stress-energy tensor, so one gets

$$\nabla^{\mu} T_{\mu\nu} = 0. \tag{1.4}$$

Einstein's Equations (1.3) are a set of 10 second order PDEs for the 10 components of the metric, which split into 4 constraints and 6 evolution equations.

[1] Let us consider a Lagrangian constructed with higher than one order derivatives, in such a way it is non degenerate, i.e. higher order derivatives can not be eliminated by subsequent integrations by part. Then, the corresponding field equations will be of higher order. Ostrogradski showed that such a Lagrangian leads to an Hamiltonian which is linear in the canonical momenta. Therefore, the system can not be stable.

They translate in mathematical form the relation between the geometrical description of space-time in the left hand side (l.h.s.) and the gravitational matter sector in the right hand side (r.h.s.).

Finally, it can be shown that they reproduce the weak field limit results. In fact, assuming a metric of the form

$$g_{\mu\nu} = \text{diag}(-1 + h_{00}, 1, 1, 1), \qquad h_{00} << 1 \tag{1.5}$$

where h_{00} is a small perturbation on a flat background, we find

$$\nabla^2 h_{00} = -\frac{\kappa}{2} T_{00}, \tag{1.6}$$

which is a generalization of the Poisson Equation, as h_{00} can be identified with the Newtonian potential ϕ_N.

Einstein's Equations can be rigorously derived from a variational principle. Hilbert and Einstein derived separately the equations for the gravitational field by varying the following action with respect to the metric

$$S = \frac{1}{\kappa} \int d^4x \sqrt{-g} R + S_m[g_{\mu\nu}, \chi_m], \tag{1.7}$$

where g is the determinant of the metric tensor $g_{\mu\nu}$. The first term in the r.h.s. is the Einstein-Hilbert action, while S_m is the action of all the matter fields, χ_m. The matter sector is minimally coupled to gravity to account for the Equivalence Principle. The variation of the action with respect to (w.r.t.) the metric leads to the field Eqs. (1.3), where the stress-energy tensor has been defined as

$$T_{\mu\nu} = -\frac{2}{\sqrt{-g}} \frac{\delta S_m}{\delta g^{\mu\nu}}. \tag{1.8}$$

By construction it can be inferred that $T_{\mu\nu}$ is a symmetric tensor. Moreover, because of the validity of the Equivalence Principle, the stress energy tensor is conserved, ensuring that test particles follow geodesics.

1.2 On the Uniqueness of General Relativity Action

In the previous Section, we have historically traced back the steps that led to the formulation of the gravitational field equations and the derivation of the equations from a variational principle. A simple question now arises: Are the Einstein field equations and the Einstein-Hilbert action unique and under which assumptions?

In order to construct the Einstein's Equations, which are of the form

$$B_{\mu\nu} = \frac{\kappa}{2} T_{\mu\nu}, \tag{1.9}$$

the following criteria on the tensor $B_{\mu\nu}$ need to be verified

1. constructed only with the metric tensor and its derivatives up to second order, i.e.

$$B_{\mu\nu}(g_{\mu\nu}, g_{\mu\nu,\rho}, g_{\mu\nu,\rho\lambda})\,; \tag{1.10}$$

2. divergence free: $\nabla^\nu B_{\mu\nu}$;

3. symmetric: $B_{\mu\nu} = B_{\nu\mu}$;

4. linear in $g_{\mu\nu,\rho\lambda}$.

Let us note that the 2nd and 3rd assumptions are requested because the l.h.s. of the field equations has to be consistent with the r.h.s., and we know the stress energy tensor satisfies these conditions.

In Refs. [9, 10, 11], it has been proved that the only tensor satisfying the above requirements in 4-dimensions is

$$B_{\mu\nu} = \eta G_{\mu\nu} - \lambda g_{\mu\nu}\,, \tag{1.11}$$

where η and λ are two constants. The above tensor gives rise to be the Einstein's Equations (1.3) with a zero matter tensor, plus eventually a constant term. Actually, this additional term plays is an important role in the cosmological framework to account for observational data.

Generalization of $B_{\mu\nu}$ came by Lovelock in 1971 [12, 13]. He relaxed the last assumption, including also non-linear terms in the second derivative of the metric. Moreover, he showed explicitly that the form of $B_{\mu\nu}$ could be generalized in n-dimensions. In particular, in Ref. [12], Lovelock proved that in 4-dimensions the general expression reduces to (1.11) and that the 3rd and 4th assumptions were redundant as implied by the first two. The corresponding general Lagrangian density $\mathcal{L}(g_{\mu\nu}; g_{\mu\nu,\alpha}; g_{\mu\nu,\alpha,\beta})$ constructed only with the metric tensor and its derivatives (up to second order) is of the form

$$\mathcal{L} = \sqrt{-g}\,(\eta R - 2\lambda) + \gamma \epsilon^{\mu\nu\alpha\beta} R^{\rho\sigma}{}_{\mu\nu} R_{\rho\sigma\alpha\beta} + \xi\sqrt{-g}(R^2 - 4R^\mu{}_\nu R^\nu{}_\mu + R^{\alpha\beta}{}_{\mu\nu} R^{\mu\nu}{}_{\alpha\beta}), \tag{1.12}$$

where γ, ξ are other two constants and $\epsilon^{\mu\nu\alpha\beta}$ is the Levi Civita tensor. Let us note that the 3rd and 4th terms in the above expression do not contribute to the field equations as they are boundary terms.

In Conclusion, according to the criteria (1)-(2), as they are the only necessary assumptions in 4-dimensions, the Einstein's Equations and the Einstein-Hilbert action are respectively the most general equations and action in 4-dimensions for the gravitational field.

The Lovelock's results are of fundamental importance when constructing theories of gravity which differ in the field equations from those of General Relativity (see Refs. [14, 15] for a general review). In order to include modifications in the gravity sector one has to consider one of the following options:

- include more fields beyond or rather than the metric tensor;
- allow for higher order field equations;
- allow for higher then 4-dimensions;
- break diffeomorphism invariance.

In this thesis, we will focus on modifications of GR which come from the first two points. In particular, we will consider theories which include one extra scalar field in the action and models described by dynamical 4th order field equations. The reason for not considering the other two points is the following. Higher dimensional theories have an effective description in 4-dimensions that is sufficient to describe low energy phenomena. Usually, diffeomorphism invariance can be restored via the Stückelberg technique [16], which actually introduces an extra field, bringing us back to the first point. In Part III, we will extensively comment on that points.

Chapter 2

The Cosmological Standard Model

Over the centuries, the description of the Universe was purely philosophical, related to religious and political ideas or pure speculations. The first attempt in constructing a "cosmological" model has to be traced back in ancient Greece. Ptolemy (II century) proposed the geocentric model for the Solar System, which assigns a central position to the Earth while assuming that planets and the Sun orbit around it. This model was purely based on observations of the apparent motion of stars in the sky and on the assumption that stars were at the same distance from the Earth. Ptolemy was also the first to make a star catalog that included 1022 stars, grouped into 48 constellations. The geocentric model was already present in many cultures, due to Aristotle's speculations, although no one before Ptolemy, had formalized the details of it.

It was in the early XVI, that the scientific approach began to make his way. In those years, the geocentric model has been questioned by Nicolaus Copernicus, who described in his *"De revolutionibus orbium coelestium"* an heliocentric model, in which the Sun occupies the central position. Subsequently, this idea was verified by Galileo Galilei, through astronomical observations. Finally in the XVII century, the present conception of the Solar System was pointed out by Johannes Kepler, who described in a mathematical language the physical properties of bodies (plantes) orbiting around a central star (the Sun). Kepler's work laid the foundations for Isaac Newton's intuition on the gravitation law that regulates the force between massive bodies.

It is in the early XX, that GR changed radically the way to approach the study of the Universe, the system *par excellence* dominated by gravitational interaction, and its substructures as clusters, galaxies, compact objects and stars. The whole Universe had started to be considered as a physical-mathematical system described through a set of equations, whose solutions provide us with important information about the geometry and the evolution of the Universe and its matter content. Thanks to the availability of more advanced surveys over the years, it has been possible to test the predictions of a theory using cosmological observations to ensure that "real world" behaves as predicted by a model. In this sense, the 1915 can be considered as the year of the birth of

the Modern Cosmology.

Since the publication of Einstein's theory, there were many solutions proposed to describe the evolution of the Universe. Let us recall the solution of a static Universe proposed by Einstein in 1917, the one describing an expanding empty Universe by de Sitter and that of an empty flat Universe by Minkowski. After the discovery of the recession of galaxies by Hubble (1929) [17], cosmologists have proposed models of an expanding Universe, whose matter content was not negligible. Over the years, the model that has been most successful is the result of the works by Friedmann, Lemaître, Robertson and Walker. They have proposed cosmological solutions based on the assumption that the Universe is homogeneous and isotropic on a large enough scale. This axiom, known as the Cosmological Principle, at that time was a real gamble, since there are no observational data to confirm these assumptions. In 1965, Penzias and Wilson discovered the Cosmic Microwaves Background radiation (CMB) giving an experimental confirmation of the Cosmological Principle.

A viable cosmological model has to account for the observational evidence. In particular, recent cosmological observations confirm that the Universe is undergoing a phase of accelerated expansion [18, 19]. The CMB together with the measurement of the abundance of the primordial elements produced during the Big Bang Nucleosynthesis (BBN), suggest the existence of a unknown component of non-baryonic matter, called Dark Matter (DM). Although DM particles are still far from being directly detected, they represent the 26.8% of the total energy content in the Universe, being only 4.9% the contribute of ordinary (baryonic) matter [20, 21]. Finally, every model has to make clear predictions to account for the distribution of large-scale structure which has been mapped by sky surveys, such as the Sloan Digital Sky Survey (SDSS) [22] and the Two-degree-Field Galaxy Redshift Survey (2dF) [23].

The Standard Cosmological Model or Λ Cold Dark Matter (ΛCDM) model, is the most widely used model to describe the dynamics and evolution of the Universe and that best fits the observational data. It is based on the Theory of General Relativity and the Cosmological Principle to describe on cosmic scales the gravitational field. It accounts for the cosmological observations related to the cosmic acceleration and DM. In fact, the ΛCDM model includes in the Einstein's Equations a cosmological constant term (CC called Λ) which behaves like a dark fluid with negative pressure that at late times gives rise to the observed accelerated expansion; it also includes a DM component with negligible pressure which moves slowly compared to the speed of light, hence the name cold. This particle is necessary to account for the required matter density component in the total energy-density budget of the Universe and for the observed large scale structure distribution.

This Chapter is organized as follows. In Section 2.1 we discuss the Cosmological Principle and in Section 2.1.1 we present the homogeneous and isotopic metric. In Section 2.2 we discuss the tensorial form of the stress energy tensor and in Section 2.3, we discuss the cosmological solutions to the Einstein's Equations, including also the CC term. In Section 2.4, we present in detail the observational evidence in support of the ΛCDM model and we provide the best fit parameter estimations for that model. Finally, in Section 2.5 we recap the historical introduction of the CC.

2.1 The Cosmological Principle

The Cosmological Principle extends on a cosmic scale the Copernican Principle, assuming that the Universe is homogeneous and isotropic on a large enough scale. The isotropy states that looking at the Universe from a position, such as the Earth, there are no preferred directions. The homogeneity ensures that on average over large distances, the Universe will look like the same for any observer at any point. These two conditions translate in saying that on cosmic scale the force governing the physical phenomena acts in a uniform manner. This clearly implies that inhomogeneity appears only on small distances.

The Cosmological Principle has been implicitly considered since 1915 in order to find cosmological solutions to the Einstein equations. It was in 1932 that Edward Milne [24] formulated the principle as we know it under the name "the extended principle of relativity", although in his work, he was very careful in defining it as an axiom, being a concept related more to a philosophical idea and to the perception (or extrapolation of local results) that the scientific community had about Universe rather than on observational evidence. In 1915, the idea of large-scale matter distribution was limited to the distribution of stars in the Milky Way and the assumption of isotropy was very risky and hasty at that time because of the missing data on galaxy redshifts in the Southern Hemisphere. However, the lack of real observational data, did not stop physicists from adopting the Cosmological Principle and attempting to find solutions that satisfy it.

Between the 20s and 30s, Friedmann, Lemaître, Robertson and Walker independently proposed an ansätz for the metric $g_{\mu\nu}$ in agreement with the Cosmological Principle to be used in the Einstein's Equations. This metric is still used today and remains the best way to parametrize the evolution of the Universe. Since then, many cosmological models have been proposed, based on that metric. In Section (2.3) we will present in detail cosmological solutions that are of interest for the standard cosmological model.

Nowadays, sky surveys provide maps of structures in the Universe, showing they are organized in galaxy groups, galaxy clusters, superclusters, walls and filament, separated by large voids, creating a sponge-like structure called the "Cosmic Web". These structures are clearly visible in the maps obtained with data by the SDSS [22] and the 2dF [23]. On large scales $\approx$ 100 Mpc, the maps show that the matter in the Universe can be considered homogeneously distributed. Inhomogeneities appear only when considering portions of Universe of size smaller then that. The CMB, which fills the entire Universe with a present day temperature of $2.725\,K$, offered the first real evidence for isotropy, which implies also the homogeneity. It has been observed that the CMB is isotropic to roughly one part in 100.000. In Conclusion, the large scale matter distribution and CMB data are strong observational evidence in support of the Cosmological Principle.

2.1.1 The Friedmann-Lemaître-Robertson-Walker metric

As stated in the first Chapter, the Universe can be described through a geometrical quantity, the metric $g_{\mu\nu}(t, x^i)$ as function of the time t and spatial

coordinates x^i. Making use of purely geometric considerations, it is possible to derive an appropriate form for the metric that describes an homogeneous and isotropic Universe, according to the Cosmological Principle.

Let us write the general form for the line element

$$ds^2 = g_{\mu\nu}dx^\mu dx^\nu = -\widetilde{g}_{00}dt^2 + 2g_{0i}dtdx^i + g_{ij}dx^i dx^j, \tag{2.1}$$

where $\widetilde{g}_{00}$ is the time-time component of the metric, g_{0i} is the off-diagonal time-space component, while g_{ij} is the space-space component and it is positively defined. In 4-dimensions i runs on the three spatial indices. Without loss of generality, we can choose a frame comoving with the observer. In this comoving frame, the time coordinate can be fixed such that $\widetilde{g}_{00} = 1$, as clocks are carried by the observer. Moreover, in order to avoid preferred directions in space, introduced by the time-space components of the metric, we require that $g_{0i} = 0$. Then, we are left with

$$ds^2 = -dt^2 + g_{ij}d^i dx^j = -dt^2 + dl^2, \tag{2.2}$$

where dl^2 is the 3-metric line element. Isotropy implies the spherical symmetry for g_{ij}, resulting in $dl^2 = a(t)^2(f(r)dr^2 + d\Omega^2)$, where $d\Omega^2 = r^2d\theta^2 + r^2sin^2(\theta)d\varphi^2$ is the solid angle and r is the comoving radial coordinate; while the homogeneity assumption fixes the function $f(r) = (1 - kr^2)^{-1/2}$, as the 3-space Ricci scalar for the above metric is a constant. Finally, we get the well known Friedmann-Lemaître-Robertson-Walker (FLRW) metric

$$ds^2 = -dt^2 + a(t)^2\left[\frac{dr^2}{1-kr^2} + r^2d\theta^2 + r^2sin^2(\theta)d\varphi^2\right], \tag{2.3}$$

where k is a constant representing the curvature of the space, it can assume the values $\{-1, 0, 1\}$ (after a suitable rescaling of the radial coordinate) corresponding to an Universe respectively hyperspherical, spatially flat and hyperbolic. The function $a(t)$ is called the scale factor.

Before concluding, a remarkable consequence of the Cosmological Principle and of the FLRW metric is the following. Considering two galaxies, their distances can be written as $l_{12} = a(t)x_{12}$, where x_{12} is constant in time, while it depends on the comoving distance between two galaxies. The same is true for another couple of galaxies, then $l_{34} = a(t)x_{34}$ and so forth. Assuming that the distance l_{12} changes by a small amount in a finite time interval, also the distance between the others galaxies will change by the same amount. Therefore, the geometry of the Universe is fully specified only through the unknown function $a(t)$. Moreover, if v is the recession velocity of two galaxies, we have

$$\dot{l} \equiv v = l\left(\frac{\dot{a}}{a}\right) = l\,H(t), \tag{2.4}$$

where overdot stands for derivatives w.r.t. the time coordinate and

$$H(t) \equiv \frac{\dot{a}(t)}{a(t)} \tag{2.5}$$

is the Hubble parameter. Evaluating the above relation at present time, we have

$$v = lH_0, \tag{2.6}$$

where H_0 is usually known as the Hubble constant and is the value of the Hubble parameter today. A recent estimate of this parameter was made by the *Planck* team, whose best fit value is $H_0 = 67.3 \pm 1.2$ km/s/Mpc at 68% confidence limits (hereafter C.L.). It is obtained combining the *Planck* temperature data with the *WMAP* [1] polarization at low multipoles [21]. The relation (2.6) is known as the Hubble law. It states that any given galaxy should recede from us at a speed proportional to its distance. This would mean that the recession velocity is increasing over time as the galaxy moves to greater and greater distances. Observational evidence of the recession of the galaxies has been obtained measuring the distance as function of the redshift of standard indicators, such as the Supernovae Ia and the Chepheids [26, 27]. The Hubble law gives rise also to implications in the past. According to it, the galaxies at a certain time t in the early Universe, would have been very close to one another, supporting the Big Bang theory.

2.2 The Stress Energy Tensor

In order to solve the Einstein's Equations, we need to define an appropriate form for the stress energy tensor $T_{\mu\nu}$. The stress energy tensor is a symmetric tensor ($T_{\mu\nu} = T_{\nu\mu}$) by definition as it is constructed by varying the matter action w.r.t. a symmetric tensor $g_{\mu\nu}$; it is a covariant tensor according to the Principle of General Covariance and from the validity of the Equivalence Principle follows

$$\nabla^{\mu} T_{\mu\nu} = 0. \tag{2.7}$$

Let us note that the conservation equation is also implied by the diffeomorphism invariance of S_m with the assumption that the matter fields satisfy their field equations. The relation (2.7) provides a sets of conserved equations which holds separately for all the matter species (if they are not coupled).

Usually, the stress-energy tensor is assumed to be described by a perfect fluid

$$T_{\mu\nu} = (\rho_i + p_i) u_{\mu} u_{\nu} + p_i g_{\mu\nu}, \tag{2.8}$$

where p_i and ρ_i are the pressure and density of the i-th matter fluid components and u_{μ} is the four-velocity.

According to the Cosmological Principle, the structures that make up the Universe can be considered statistically homogeneous distributed on large scale (~ 100 Mpc). Then as first approximation, the distribution of matter, can be considered homogeneous as well, meaning that the pressure and the density of the fluids are only time dependent. Observed inhomogeneities are treated as small deviations from an homogeneous background and can be studied with a perturbative approach (see Ref. [28] and references therein). Then, let us consider an inertial frame, comoving with the fluid, and the FLRW metric (Eq. (2.3)), we have

$$g_{\mu\nu} u^{\mu} u^{\nu} = -1, \tag{2.9}$$

with $u^k = 0$ for the spatial coordinates. Then the four velocity has components

$$u^{\mu} = (1, 0, 0, 0) \ . \tag{2.10}$$

[1] Wilkinson Microwave Anisotropy Probe (WMAP) [25].

It is straightforward to calculate the stress energy tensor components, which result in

$$T^{\mu}_{\nu} = \begin{pmatrix} -\rho_i(t) & 0 & 0 & 0 \\ 0 & p_i(t) & 0 & 0 \\ 0 & 0 & p_i(t) & 0 \\ 0 & 0 & 0 & p_i(t) \end{pmatrix},$$

and for the trace we get

$$T = 3p_i(t) - \rho_i(t). \tag{2.11}$$

We can now easily compute the conservation equation for the stress energy tensor (Eq. (2.7)), which holds separately for all the matter fluids (if they are not interacting) and it gives

$$\dot{\rho}_i(t) + 3H(t)\left[\rho_i(t) + p_i(t)\right] = 0. \tag{2.12}$$

2.3 Cosmological solutions to the ΛCDM model

The ΛCDM model is based on the theory of General Relativity and on the following field equations:

$$G_{\mu\nu} + \Lambda g_{\mu\nu} = \frac{\kappa}{2} T_{\mu\nu}, \tag{2.13}$$

where Λ is a constant, called Cosmological Constant (hereafter CC).
These equations differ from the ones of GR because of the additional CC term. Actually this term is expected in the general formulation of the gravitational field equations as shown by Lovelock (see Section 1.2).

Cosmological solutions can be obtained considering the FLRW metric (Eq. (2.3)) and for the stress energy tensor a perfect fluid form (Eq. (2.8)). Then, we get the well known Friedmann equations

$$\left(\frac{\dot{a}}{a}\right)^2 + \frac{k}{a^2} - \frac{\Lambda}{3} = \frac{8\pi G}{3}\rho, \tag{2.14}$$

$$\frac{\ddot{a}}{a} - \frac{\Lambda}{3} = -\frac{4\pi G}{3}(\rho + 3p), \tag{2.15}$$

where $\rho(t) = \sum \rho_i(t)$ and $p(t) = \sum p_i(t)$, the sum is over all the matter species. Note that we suppressed the time dependence for $a(t)$, $\rho(t)$ and $p(t)$ to simplify the notation. The system of Eqs. (2.12)-(2.14)-(2.15) is not enough to describe the evolution of the Universe since Eq. (2.14) and Eq. (2.15) are not independent equations. Then, we are left with two independent equations and three unknown functions $a(t)$, $p(t)$ and $\rho(t)$. In order to close the system we can specify an equation of state for the fluid components in order to relate the density and the pressure of the fluids. A further assumption is to consider a barotropic equation of state of the following form

$$p_i(t) = w_i(t)\rho_i(t), \tag{2.16}$$

where w_i is the adiabatic index ($=c_s^2/c^2$, where c_s is the sound speed of the fluid) and it depends on the matter species i. The Eq. (2.12) reads

$$\dot{\rho}_i = -3H(1 + w_i)\rho_i. \tag{2.17}$$

If w_i is a constant the above equation can be integrated and we get

$$\frac{\rho_i}{\rho_{i,0}} = \left(\frac{a}{a_0}\right)^{3(1+w_i)}, \tag{2.18}$$

where a_0 and $\rho_{i,0}$ are respectively the values of the scale factor and the density of the i-th fluid component at present time. The normalization is chosen such that $a_0 = 1$. Eq. (2.18) clearly shows that depending on the matter species, the density and hence the pressure will have a different scaling behavior with the scale factor, $a(t)$.

Before moving on, we want to show that moving the CC to the r.h.s. of Eqs. (2.14)-(2.15), it can be read as a "matter" component and then recast in a fluid form. The density for the CC is

$$\rho_\Lambda = \frac{\Lambda}{8\pi G}, \tag{2.19}$$

then its pressure obeys an equation of state defined by $w_\Lambda = -1$, resulting in $p_\Lambda(t) = -\rho_\Lambda(t)$. Hence, the CC has a non-dynamical equation of state, with a constant energy density, Eq. (2.19) and a negative pressure which acts as a repulsive force.

Now, let us define the density parameter of the i-th component, as follows

$$\Omega_i(t) \equiv \frac{\rho_i(t)}{\rho_c(t)} = \frac{8\pi G\rho_i(t)}{3H(t)^2}, \tag{2.20}$$

where $\rho_c(t)$ is the critical density defined via Eq. (2.14), neglecting Λ and the spatial curvature (k). The value of the critical density at present time is

$$\rho_{c,0} = \frac{3H_0^2}{8\pi G} = 1.88\, h^2\, 10^{-29}\, g\, cm^{-3}, \tag{2.21}$$

where $h = H_0/100\, km\, s^{-1} Mpc^{-1}$.
Following the same line, we can also define a quantity to parametrizes the deviations from spatial flatness, such as

$$\Omega_k \equiv -\frac{k}{\rho_c(t)}. \tag{2.22}$$

Then the Eq. (2.14) can be written as

$$\Omega_m(t) + \Omega_\Lambda(t) + \Omega_k(t) = 1, \tag{2.23}$$

where $\Omega_m(t)$, $\Omega_\Lambda(t)$ are respectively the density of the matter component (baryonic and DM, including massive neutrinos) and the CC. As they are time dependent functions, it is clear that their values change over the eras, so we do not expect their relative abundances to be fixed. Best fit values of the density parameters, evaluated at present time, were recently determined by the *Planck* Collaboration [21]

$$\Omega_{\Lambda,0} = 0.685^{+0.018}_{-0.016}\,(68\%\, C.L.),\ \Omega_{m,0} = 0.315^{+0.016}_{-0.018}\,(68\%\, C.L.), \tag{2.24}$$

$$\Omega_{k,0} = -0.037^{+0.043}_{-0.049}\,(95\%\,C.L.). \tag{2.25}$$

They are obtained combining the *Planck* temperature data with *WMAP* polarization at low multipoles. In what follows we will consider $\Omega_{k,0} = 0$. That is a good assumption as $\Omega_{k,0} \sim 0$ with an accuracy better than a percent [21].

Finally, we want to present the main solutions to the Friedman Eqs. (2.14)-(2.15) for the main transition eras, each of them characterized by a different behavior of the scale factor. In particular we will analyze three eras:

- Radiation dominated era (RDE): At early time the Universe has been dominated by relativistic particles whose barotropic coefficient is $w_r = 1/3$. The solution to the Friedmann equations is

$$\frac{a}{a_0} = \left(\frac{t}{t_0}\right)^{\frac{1}{2}}, \quad \rho_r = \rho_{r,0} a^{-4}, \quad H = \frac{1}{2t}, \tag{2.26}$$

  where $\rho_{r,0}$ is the present value of the radiation energy density. In the ΛCDM models there are two relativistic particles: neutrinos and photons.

- Matter dominated era (MDE): Matter components are pressureless fluids with a corresponding equation of state with $w_m = 0$. The solution to the Friedmann equations is

$$\frac{a}{a_0} = \left(\frac{t}{t_0}\right)^{\frac{2}{3}}, \quad \rho_m = \rho_{m,0} a^{-3}, \quad H = \frac{2}{3t}, \tag{2.27}$$

  where as before $\rho_{m,0}$ is the matter density today. In the ΛCDM scenario two matter components are considered: the baryons (b) and the cold dark matter particles (cdm), respectively with density parameters

$$\begin{aligned} \Omega_{b,0}h^2 &= 0.02205 \pm 0.00028\,(68\%\,C.L.), \\ \Omega_{cdm,0}h^2 &= 0.1199 \pm 0.0027\,(68\%\,C.L.). \end{aligned} \tag{2.28}$$

  They have been obtained considering both *Planck* temperature data and *WMAP* polarization at low multipoles [21].

  Due to the scaling solutions of the matter and radiation densities, we can infer that when the radiation component began to be negligible the matter component started to dominate the evolution of the Universe. It is possible to get an estimate of the time in which the two densities coincide, the so called Equivalence Era. It is useful to introduce at this point the *redshift* parameter, defined as

$$z = \frac{a_0}{a(t)} - 1, \tag{2.29}$$

  and in terms of z, the two densities read

$$\rho_m = \rho_{m,0}(1+z)^3, \quad \rho_r = \rho_{r,0}(1+z)^4. \tag{2.30}$$

  Equating the densities we get

$$1 + z_{eq} = \frac{\rho_{m,0}}{\rho_{r,0}} \approx 3000. \tag{2.31}$$

This redshift defines the era at which the RDE ended and the MDE started.

- Accelerating era: The Friedmann Eqs. (2.14)-(2.15) describe the accelerated expansion of the Universe through a dark fluid with a CC, which has a constant equation of state defined by $w_\Lambda = -1$. In this case the solution to the equations is

$$a(t) = a_0 e^{\sqrt{\frac{\Lambda}{3}}t}, \quad \rho_\Lambda = \frac{3H_0^2}{8\pi G}, \quad H = \sqrt{\frac{\Lambda}{3}}. \tag{2.32}$$

We can estimate the redshift at which the switch between matter domination and the recent acceleration took place. Equating the densities we get

$$(1 + z_{acc})^3 = \frac{\Omega_{\Lambda,0}}{\Omega_{m,0}}, \tag{2.33}$$

then $z_{acc} \sim 0.4$ confirming the very recent acceleration.

Ultimately, the overall evolution of the scale factor can be determined solving the following equation

$$\frac{H^2}{H_0^2} = \Omega_{r,0}a^{-4} + (\Omega_{b,0} + \Omega_{cdm,0})a^{-3} + \Omega_{\Lambda,0}, \tag{2.34}$$

which account for the evolution of all the three components.

2.4 Observational evidence for ΛCDM

Last decade is referred to as the era of Precision Cosmology, because of the large amount of high quality data. Sky surveys cover different scales and epochs, providing a detailed mapping of the galaxies distribution up to large scales as well as observations of active galactic nuclei, stars in our own Galaxy and planets. These data are of cosmological interest as from them we can infer important information about the early Universe, the origin of cosmic structure and the present day Universe. Moreover, they are used as test for theoretical predictions of a cosmological model.

The ΛCDM model is strongly supported by observational evidence, which make this model the best description of the observed Universe. We will discuss the evidence for the standard cosmological model and present the most recent best fit parameter estimations in support of it.

- Baryonic matter component: Today we have a precise estimation of the baryonic component in the Universe mainly due to the accuracy on measurements of light element abundance produced during the BBN. BBN is the process that leads to the production of the light elements in the very early stage of the Universe. It took place ~ 100 sec up to ~ 200 sec after the Big Bang, at temperature below 10^9 K. It lasted few minutes, after which the density and the temperature went down and no other processes occurred. The elements produced are hydrogen (about 75% in mass

abundance), helium-4 (25% by mass), deuterium (0.01% by mass), finally, litium-7 and beryllium-7 in trace. The origin of heavy elements can be traced back in the nucleosynthesis that happen in the cores of stars during their evolution.

Measurements of the light elements abundances can be obtained by looking at astronomical objects where the stellar nucleosynthesis is at early stages, such as high-z objects like quasars, or it is less efficient. Another independent observable is the CMB which also provide estimation of the light elements. The mass abundance for helium is expressed as $Y_P^{BBN} = 4n_{He}/n_b$ and the deuterium one as $Y_{DP}^{BBN} = 10^5 n_D/n_H$, where n_i is the number density. The best fit for the helium abundance is provided in Ref. [29] using spectroscopic observations of the chemical abundances in metal-poor HII regions and it is

$$Y_P^{BBN} = 0.2534 \pm 0.0083(68\%\, C.L.). \tag{2.35}$$

For the deuterium abundance, the value is

$$Y_P^{BBN} = 0.2534 \pm 0.0083(68\%\, C.L.), \tag{2.36}$$

which is obtained analyzing the metal-poor damped Lymanα system at $z = 3.04984$ in the QSO SDSSJ1419 +0829 [30].
According to the BBN abundances, it is possible to determine the baryon abundance in the Universe

$$\Omega_b h^2 = 0.0223 \pm 0.0009\,, \tag{2.37}$$

as estimated in Ref. [30].
An independent estimation of the helium mass fraction came from the CMB

$$Y_P = 0.266 \pm 0.021\ (Planck + WP + highL), \tag{2.38}$$

at 68% C.L. [21]. Due to the helium binding energy, Y_P differs from Y_P^{BBN} by 0.5%. The baryonic mass component is then estimated to be

$$\begin{aligned} &\Omega_b h^2 = 0.02207 \pm 0.00033\ (Planck), \\ &\Omega_b h^2 = 0.02217 \pm 0.00033\ (Planck + lensing), \\ &\Omega_b h^2 = 0.02205 \pm 0.00028\ (Planck + WP), \end{aligned} \tag{2.39}$$

at 68% C.L. [21]. They are obtained using the *Planck* temperature power spectrum data alone and in combination with *Planck* lensing and *WMAP* polarization at low multipoles in turns.
Current observations are in agreement with the theoretical predictions [31]

$$\Omega_{b,0} h^2 = 0.021,\ \ Y_P = 0.248. \tag{2.40}$$

- Cold Dark Matter: Closely related to the estimation of the baryonic component, it is the DM observational evidence. *Planck* Collaboration [21] found that the total matter density parameter is $\Omega_m = 0.315^{+0.016}_{-0.018}$ (68% C.L.) (which include also massive neutrinos), meaning that most of the

matter in the Universe is in form of a dark component. The best fit parameter estimation for the DM component at 68% C.L. [21] is

$$\begin{aligned}
&\Omega_{cdm,0}h^2 = 0.1196 \pm 0.0031 \ (Planck),\\
&\Omega_{cdm,0}h^2 = 0.1186 \pm 0.0031 \ (Planck + lensing),\\
&\Omega_{cdm,0}h^2 = 0.1199 \pm 0.0027 \ (Planck + WP).
\end{aligned} \tag{2.41}$$

Because of the above measurements on the baryonic component, we can infer that the DM nature is non-baryonic. Moreover, the demand of a DM component in the form of non-baryonic cold particle is necessary in order to make the predictions of structures formation, carried with N-body simulations, comparable to the observed structures in the Universe [32].

- Accelerating Universe: The recent accelerated expansion of the Universe is now strongly confirmed by different surveys (among others WMAP [25], SCP Union2.1 [33], SDSS [22], *Planck* [34]). A recent paper by the *Planck* Collaboration [21], shows the best fit values on $w = p/\rho$, which parametrizes the equation of state of a dark fluid. They are obtained combining the CMB data with lower redshift distance measurements, such as the Baryonic Acoustic Oscillations (BAO) [35, 36, 37, 38] and the Supernovae data: Union2.1 [26], in order to break the degeneracy in the parameter space and better constraint w. The results are

$$\begin{aligned}
&w = -1.13^{+0.24}_{-0.25} \ (95\%;\ Planck + WP + BAO),\\
&w = -1.09 \pm 0.17 \ (95\%;\ Planck + WP + Union2.1),
\end{aligned} \tag{2.42}$$

showing an overall agreement with the CC value $w_\Lambda = -1$, in particular the combination with the Union2.1 dataset is very consistent with a CC[2]. The CC density parameter for the ΛCDM model is estimated to be

$$\begin{aligned}
&\Omega_\Lambda = 0.686 \pm 0.020 \ (Planck),\\
&\Omega_\Lambda = 0.693 \pm 0.019 \ (Planck + lensing),\\
&\Omega_\Lambda = 0.685^{+0.018}_{-0.016} \ (Planck + WP),
\end{aligned} \tag{2.43}$$

at 68% C.L. [21].

2.5 Is the Cosmological Constant the Einstein's "greatest blunder"?

Before concluding this Chapter, we briefly discuss Einstein's primary idea on the Cosmological Constant.

In 1915, it was believed that the Universe did not change over time on large scales. Therefore, it was natural to look for static solutions to the Einstein's

[2] In the same work, combinations of the Planck data with cosmological data in Refs. [39, 40] show tension with $w_\Lambda = -1$ in some cases at more than 2σ. A dynamical parametrization for the dark fluid equation of state has been also analyzed. We will illustrate and comment on these results in the next Chapter. However, they conclude confirming that no significant evidences for deviations from a CC have been found.

Equations (1.3) with a nonzero matter content. When it was clear that such a solution was not admissible by the field equations, Einstein decided to add a new term to achieve the desired result. A non trivial but simple choice was to include a constant term to the action (1.7)

$$S = \frac{1}{\kappa}\int d^4x\sqrt{-g}\,[R - 2\Lambda] + S_m[\chi_m, g_{\mu\nu}], \tag{2.44}$$

which still provide second order equations (Eq. (2.13)). Einstein's idea was to balance the gravitational force with the CC, thus avoiding the collapse of the Universe due to the sole action of the gravity. The resulting field equations (2.13) indeed admit a static solution, although it is unstable to small perturbations. This model of Universe is known as the *Einstein Universe*.

Assuming a static spherical metric,

$$ds^2 = e^{\alpha(r)}dt^2 - e^{-\beta(t)}dr^2 - r^2d\theta^2 - r^2sin^2\theta d^2\varphi, \tag{2.45}$$

from the Eqs. (2.13), we can obtain a first rough estimate of the magnitude of the CC. The conservation equation (2.7) for a perfect fluid (Eq. (2.8)) reads

$$(\rho + p)\frac{d\alpha}{dr} = 0, \tag{2.46}$$

which allows for three conditions: 1) $\rho + p = 0$, 2) $\rho + p = 0 \cup \frac{d\alpha}{dr} = 0$ and 3) $\frac{d\alpha}{dr} = 0$. The first two describe, once included in the Einstein's Equations, respectively the *de Sitter Universe* and the *Minkowski Universe*, giving in both cases solutions in absence of a matter component. While the last condition is what we are looking for, because the equations describe an Universe filled with matter. Then the Eqs. (2.13) give the relation

$$\Lambda = 4\pi G(\rho + 3p) \approx \frac{4\pi G}{c^2}\rho_0 \approx 10^{-57}cm^{-2}\,, \tag{2.47}$$

where ρ_0 is the density of the Universe at present time. We have assumed an Universe filled only with dust for which $p = 0$.

In 1929, Edwin P. Hubble demonstrated that the Universe is expanding at an increasing rate [17], therefore a static model for the Universe was no longer considered. As a consequence, Einstein rejected the CC term, referring to it as his "greatest blunder". However as explained in the previous Sections, the CC was not entirely abandoned, indeed it is still the most viable alternative to account for the phenomenon of the recent acceleration of the Universe.

Chapter 3

Beyond the Cosmological Standard Model

Last Planck 2013 results support the ΛCDM model as the best description of the observed Universe. Nevertheless, the model fails in explaining observed phenomena such as homogeneity, isotropy and flatness of the Universe. Moreover, there are DM and Cosmological Constant problems. DM particle candidates have not yet been detected and some shortcomings arise when looking at small scales. The Cosmological Constant problems are due to the discrepancy between the predicted theoretical value of Λ and the observed one and to the coincidence problem at late time. Furthermore, an ultimate problem arises when one attempts to create a consistent quantum gravity description of General Relativity.

This Chapter will focus on the limitations of the standard cosmological model. In Section 3.1 we present the fine-tuning problems in the early Universe and in Section 3.1.1 we discuss a possible solution in the Inflationary framework. In Section 3.2 we explain the CC issues and we consider a different model for the dark fluid. Finally in Section 3.3 we discuss the DM problems.

Let us note that an alternative approach to the problems of ΛCDM relies in the modification of General Relativity at large scales. We will extensively discuss about this proposal in Part III.

3.1 Fine-tuning problems in the early Universe: flatness, homogeneity and isotropy

In this Section we are going to illustrate the cosmological fine-tuning problems affecting the ΛCDM model. These are the flatness, homogeneity and isotropy problems. The last two are usually know under the name of horizon problem. They concern the special initial conditions needed in order to have the observed late time Universe. Small departures from these conditions would lead to big changes in the present day Universe.

- Flatness problem: The present value of the total density of the Universe ($\rho_{tot,0}$) is measured to be very close to the critical density ρ_c and no

significant deviation from flatness has been found. Recent results by the *Planck* Collaboration [21] fix the value of the curvature density parameter at 95% C.L. to be very close to zero

$$\Omega_k = -0.037^{+0.043}_{-0.049}\,(Planck + WP), \tag{3.1}$$

$$\Omega_k = 0.0000^{+0.0066}_{-0.0067}\,(Planck + WP + BAO), \tag{3.2}$$

$$\Omega_k = -0.042^{+0.043}_{-0.048}\,(Planck + WP + highL), \tag{3.3}$$

$$\Omega_k = -0.0005^{+0.0065}_{-0.0066}\,(Planck + WP + highL + BAO), \tag{3.4}$$

which imply that $\Omega_{tot,0} = 1 - \Omega_k \approx 1$. Previous results, consistent with the above values, have been also found in Refs. [41, 42, 27].

The problem occurs because, the condition $\Omega_{tot} \sim 1$ is an unstable configuration, then a small deviation from it would lead to a different evolution. Using the Friedmann Equations it is possible to show that the present equality between the total density and the critical density implies in the early Universe that the total density parameter has been even closer to one. This point can be illustrated as follows. The Friedmann Equation (2.14) can be written as

$$\left(\Omega_{tot}^{-1} - 1\right) \rho a^2 = -\frac{3k}{8\pi G} = \text{const}\,. \tag{3.5}$$

We can evaluate the above relation at different epochs. Let us consider a redshift higher than $z_{eq} \sim 3000$, then from the above relation follows that

$$\left(\Omega_{tot}^{-1} - 1\right) = \left(\Omega_{tot,0}^{-1} - 1\right) \frac{1}{(1+z)^2}, \tag{3.6}$$

where we have used the radiation density profile (2.26) and the redshift definition Eq. (2.29). In particular, the predicted total density parameter at early time ($z = 10^{11}$, about 1 sec after the Big Bang) can be computed using the deduced limits $0.994 < \Omega_{tot,0} < 1.086$, from *Planck*. Then, we get

$$0.99999 < \Omega_{tot}(z = 10^{11}) < 1.00000, \tag{3.7}$$

which is actually very close to 1. This situation to be realized seems to indicate that $k = 0$. However, this condition requires fine-tuning in the initial conditions because $\Omega_{tot} = 1$ (k=0) is an unstable stationary point for the system and small deviations from $\Omega_{tot} \approx 1$ would lead to a collapsing (k=-1) or expanding (k=1) Universe. Moreover, in scenarios for which $\Omega_{tot} \neq 1$, structures would have no time to form.

- Horizon problem: why is Universe homogeneous and isotropic, if distant regions are not causally connected?
  Homogeneity and isotropy are the basic assumptions of the ΛCDM model and are observationally confirmed by large scale structure (LSS) sky surveys [22, 23] and CMB measurements [43, 25, 34]. Therefore, different regions (even the more distant) in the Universe are in equilibrium as they show the same physical properties, such as homogeneity, isotropy and temperature. In the ΛCDM model, it can be shown that if we observe two widely-separated regions in the Universe, their horizons will not overlap.

Hence, these regions can not reach the equilibrium as they are not causally connected. Therefore, homogeneity and isotropy are not theoretically explained in the ΛCDM scenario [44].

3.1.1 The Inflation Paradigm

Inflation is a short period after the Big Bang (10^{-36} to 10^{-33}) characterized by an accelerated expansion. A phase of acceleration ($\ddot{a} > 0$) can be obtained assuming the existence of a fluid with

$$\rho + 3p < 0. \tag{3.8}$$

As the density is positively defined, Inflation can occur only if the fluid's pressure results to be negative. Ordinary matter fluids (e.g. dust, radiation, perfect fluids) can not violate the Strong Energy Condition. [1] Therefore, also for the early accelerated expansion it seems we need an extra non-standard fluid component. Actually, the CC can be considered a possible candidate as its equation of state is $p_\Lambda = -\rho_\Lambda$, but it is has been shown that an initial phase dominated by this term would not end. In the context of GR another possibility is to consider matter fields, which satisfies Eq. (3.8). Usually, it is assumed that Inflation is driven by a scalar field ϕ, called *Inflaton*.

Several models have been proposed during the last years, spanning from canonical to non-canonical kinetic models, including also multi-fields Inflation. For a complete and comprehensive review see Refs. [45, 46]. Here, we will mention the minimally coupled slow-roll Inflation model described by a canonical kinetic term $\dot{\phi}^2/2$ and a potential $V(\phi)$, as it is the simplest model and it is consistent with the *Planck* data [47]. The field ϕ satisfies the Klein-Gordon and Friedmann Equations

$$\ddot{\phi} + 3H\dot{\phi} + V_\phi = 0, \tag{3.10}$$

$$H^2 = \frac{1}{3m_0^2}\left(\frac{1}{2}\dot{\phi}^2 + V(\phi)\right), \tag{3.11}$$

where $V_\phi \equiv \partial V(\phi)/\partial\phi$. The Friedmann Equation is obtained neglecting the matter and the spatial curvature. The first equation can be read as a conservation equation for the scalar field, for which we can define the pressure $p_\phi \equiv \dot{\phi}^2/2 - V(\phi)$ and the density $\rho_\phi \equiv \dot{\phi}^2/2 + V(\phi)$. Assuming $\dot{\phi}^2 < V(\phi)$ in order to have a negative pressure and requiring that the $\ddot{\phi}$ term be negligible, we get

$$3H\dot{\phi} \approx -V_\phi, \tag{3.12}$$

$$H^2 \approx \frac{1}{3m_0^2}V(\phi). \tag{3.13}$$

[1] The Strong Energy Condition states that for all future-pointing causal vectors V^μ holds:

$$\left(T_{\mu\nu} - \frac{1}{2}\,T\,g_{\mu\nu}\right) V^\mu\, V^\nu \geq 0. \tag{3.9}$$

For a perfect fluid the condition can be written as: $\rho + p \geq 0$ and $\rho + 3p \geq 0$.

The above conditions are known as the slow-roll conditions. They can be formally written in terms of two slow-roll parameters, defined as

$$\epsilon(\phi) = 4\pi G \left(\frac{V_\phi}{V}\right)^2, \tag{3.14}$$

$$\eta(\phi) = 8\pi G \frac{V_{\phi\phi}}{V}, \tag{3.15}$$

with $\epsilon << 1$ and $\eta << 1$. These conditions allow for the potential to dominate over the kinetic term, and together with the Eq. (3.12), they ensure that Inflation ends and reheating can occur [48, 49, 50, 51, 52]. Moreover, the slow roll conditions allow to restrict the form of the potential.

Inflation has been introduced in the early '80s, we refer the reader to the literature for further information on Inflationary models [53, 54, 55, 56, 57, 58, 59]. The need for an Inflationary phase, immediately after the Big Bang, was required to explain the problem of magnetic monopoles (see Refs. [60, 61, 62, 63, 64] for early works). In the early stages of the Universe, according to the Grand Unified Theory a large number of magnetic monopoles would have been created, which relic density should be observable today. At present no experimental evidence supports the existence of these magnetic monopoles. Before the Universe reaches the formation temperature of the magnetic monopoles, Inflation has the effect to decrease their production. Then their density today results to be reduced by many orders of magnitude, explaining why the magnetic monopoles have not been detected. Later, it became clear that this mechanism could also explain the fine-tuning cosmological problems (Flatness and Horizon Problems) [53] as well as the structure formation in the Universe. As postulated by Guth the scale factor should increase as

$$a(t) \sim e^{Ht}. \tag{3.16}$$

The exponential phase is known as de Sitter or inflationary phase. Under this condition the future light cone is strongly influenced, thus making possible that distant regions show the same conditions of temperature, homogeneity and isotropy. The rapid expansion would account for the right behavior for $|\Omega_{tot}^{-1} - 1|$, resulting in a spatially flat Universe.

The initial Inflationary phase explains the origin of the large scale structure of the Universe, as quantum fluctuations in the initial field constitute the seeds for the growth and subsequent formation of the structures. Many observational evidence coming from CMB and LSS data describe a flat FLRW Universe with *nearly* Gaussian scale invariant spectrum for the perturbations. In the previous Chapter we have already discussed about the observational evidence for a flat, homogeneous an isotropic Universe. Let us now focus on perturbations. The power spectrum is described by two parameters the amplitude A_s and its spectral scalar index n_s ($n_s = 1$ corresponds to a scale invariant Harrison Zeldovich (HZ) power spectrum [65, 66, 67]). Measuring n_s not only give us information about the shape of the primordial perturbations but allow us to select viable Inflationary models. *Planck* best fit estimations are

$$n_s = 0.9624 \pm 0.0075\,(Planck + WP), \tag{3.17}$$

$$n_s = 0.9653 \pm 0.0069\,(Planck + WP + lensing), \tag{3.18}$$

$$n_s = 0.9600 \pm 0.0071\,(Planck + WP + highL), \tag{3.19}$$
$$n_s = 0.9643 \pm 0.0059\,(Planck + WP + BAO), \tag{3.20}$$

which show tension with the HZ-power spectrum at 5σ [47]. These results rule out models such as the exponential potential [68] or the inverse power law potential [69], while they constraint the power low potential $\sim \phi^n$, such that n=2,4 are ruled out, while n=1 [70] is inside the 95% C.L. region.

Depending on the Inflationary models, non-Gaussianity (NG) can be generated and signatures of it can be used to rule out or significantly constraint inflationary models. For example, large value of NG are expected to be generated in multi fields models [71, 72, 73, 74] or in models with additional light fields (different from Inflaton) [75, 76, 77]. On the other hand, single field models generically predict a Gaussian spectrum of primordial perturbations, although if the slow-roll condition is temporarily violated, large non-Gaussianity can be generated even in a single field model [78]. Both n_s and NG measurements have to be considered a way to better understand the physical mechanisms behind the structures formation. If the primordial perturbations are NG, one can look at the Bispectrum (the 3-point correlation function), which generically can be written in Fourier space as

$$B(k_1, k_2, k_3) = f_{NL} F(k_1, k_2, k_3), \tag{3.21}$$

where f_{NL} is the non-linearity parameter, while $F(k_1, k_2, k_3)$ describes the configuration of the three wavevectors k_i.[2] A recent *Planck* analysis [83] on the angular Bispectrum of the CMB anisotropies constraints the value of the amplitude and shape of NG to

$$\begin{aligned} f_{NL}^{local} &= 2.7 \pm 5.8, \\ f_{NL}^{equil} &= -42 \pm 75, \\ f_{NL}^{ortho} &= -25 \pm 39, \end{aligned} \tag{3.22}$$

which let us to conclude that no evidence for NG have been found. These results favor the standard single-field, slow-roll inflationary models, while other models result to be strongly constrained.

Finally, on 17th March 2014 the BICEP2 Collaboration [84, 85] claimed the detection of inflationary gravitational waves in the B-mode of the CMB polarization. They fix for the tensor to scalar ratio parameter the value $r = 0.20^{+0.07}_{-0.05}$, which is in tension with $r = 0$ at 7.0σ. It has to be noted that this best fit value is obtained without accounting for the foreground's contribution, which should lower the estimated value. Further investigations are therefore required.

[2] The main configurations of triangles, which characterize the shape $F(k_1, k_2, k_3)$, are: Local for $k_1 << k_2 \cong k_3$ (squeezed triangles) in the case of multi-field models [71, 72, 73, 74], equilateral for $k_1 \approx k_2 \approx k_3$ in models as k-essence [79] or effective field theories [80], folded or flattened for $k_1 + k_2 \approx k_3$ in model with higher derivatives [81] and orthogonal for which a positive peak signal is generated for the equilateral configuration and a negative peak for the folded one, in general for single field models with non canonical kinetic term [82] or with higher derivatives [81].

3.2 Cosmic Acceleration

The late-time acceleration is perhaps the biggest challenge of Modern Cosmology. The observational data show that whatever causes the acceleration also accounts for 68% of the energy-density in the Universe.

In the previous Chapter, we have extensively discussed about the ΛCDM model, which theoretically is described by General Relativity with the addition of a CC term. The CC is characterized by a density that remains constant throughout the entire evolution of the Universe and an equation of state such that $w_\Lambda = -1$. As we will see in the next Section, the CC introduces some problems that go under the names *Cosmological Constant Problem* and the *Coincidence Problem*. Therefore, deviations from the ΛCDM model have been considered. The resulting models assume the existence of a dark fluid that permeates the Universe, the Dark Energy (DE), which is characterized by a dynamical or constant ($w_{DE} \neq -1$) equation of state.

Finally, a different approach is to consider the CC problems as an evidence of the lack of validity of General Relativity at large scales. This is why extensions to the theory of General Relativity have been taken into account as an alternative to the DE description. This alternative approach will be the central topic of Part III. Which is the best proposal in describing the acceleration, is not yet clear. Very often, it happens that the two descriptions are not distinguishable (e.g. Quintessence [86]), as in some cases modifications in the gravity sector give rise to an extra fluid component.

3.2.1 The Cosmological Constant issue

The CC is probably the easiest way to account for the recent acceleration. It naturally arises from the construction of a general action in 4-dimentions, as discussed in Section 1.2. The advantages of considering a CC have been exhaustively presented in the previous Chapter 2. In this Section, we will focus on two problems that put in tension the theoretical predictions and the observational evidences: the Cosmological Constant Problem and the Cosmic Coincidence Problem.

The value of the CC inferred from observation is

$$\Lambda_{obs} \sim \left(10^{-3}\, eV\right)^4, \tag{3.23}$$

which in terms of the Planck mass ($m_0 = 10^{18}\, GeV$) is $\Lambda_{obs} \sim 10^{-120}\, m_0^4$. From quantum field theory, we expect that particles in the Standard Model contribute to the value of the CC in a non negligible amount. The expected theoretical value is [3]

$$\Lambda_{th} \sim 10^{-60}\, m_0^4, \tag{3.24}$$

which is roughly 60 order of magnitude (in mass scale) larger than the observed value. The discrepancy between the theoretically predicted value and the one

[3] The stress energy tensor is of the form: $< T_{\mu\nu} >= - < \rho > g_{\mu\nu}$. In order to evaluate the energy density $< \rho >$, one can sum over the zero-point energies of a collection of independent harmonic oscillators (which are the representation of Standard Model fields) up to a cutoff Λ_{UV}, then $< \rho > \sim \Lambda_{UV}^4$. The cutoff is fixed to be $\Lambda_{UV} \sim 1$ Tev as Standard Model physics is well tested at ultraviolet (UV) scale. See Refs. [88, 15].

inferred by observations goes under the name *Old Cosmological Constant Problem* [87]. A *New Cosmological Constant Problem* also exists, which is why the observed CC has a remarkably low value. In Refs. [88, 89], S. Weinberg explains this small value with an anthropic argument: a larger value of the CC would not allow for structure formation to take place.

The second problem concerns the coincidence of living in the precise era of transition between the matter domination and the late time acceleration one, hence the name *Coincidence Problem*. More precisely, we are in the epoch in which the CC density has exceeded that of matter, being $z \sim 0.3$ the time at which $\rho_\Lambda = \rho_m$ (see Section 2.3). Observational data show that the present day cosmological density parameters of CC and matter component are of comparable magnitude, being $\Omega_\Lambda = 68\%$ and $\Omega_m = 31\%$ [21].

In conclusion, although the cosmological constant is well suited to account for the recent acceleration of the Universe, its introduction into the field equations implies shortcoming in the theoretical sector, which need to be solved in order to construct the right theory of gravity.

3.2.2 Dark Energy

Because of shortcoming in the ΛCDM model, Dark Energy (DE) models have been proposed. In general, one refers to DE as a fluid, which does not interact with the matter sector other than through gravity (as Λ), characterized by an equation of state with $w_{DE} = p_{DE}/\rho_{DE} < -1/3$, in order to give rise to the observed acceleration. The difference w.r.t. the CC resides in the equation of state, hence the CC can be considered as a special case of DE models. General DE models can allow for constant w_{DE}, but different from -1, corresponding to wCDM cosmologies, or dynamical w_{DE}. In the last case, one can assume a specific form as function of the scale factor, $w_{DE}(a)$ [90], such as the Chevallier-Polarski-Linder (CPL) [91, 92] parametrization

$$w_{DE}(a) = w_0 + w_a(1 - a), \tag{3.25}$$

where w_0 and w_a are constants, respectively the value of w_{DE} and its derivative evaluated at present time.

Deviations from the ΛCDM model have been investigated in the recent analysis by the *Planck* Collaboration [21], which shows some tensions with the ΛCDM model when Supernova data SNLS [93, 39] and H_0 measurements [40] are considered,

$$w_{DE} = -1.13^{+0.13}_{-0.14}\ (95\%;\ Planck + WP + SNLS), \tag{3.26}$$

$$w_{DE} = -1.24^{+0.18}_{-0.19}\ (95\%;\ Planck + WP + H_0). \tag{3.27}$$

In both cases the results are in favor of a phantom behavior, i.e. $w_{DE} < -1$, the first shows a 2σ tension with $w_\Lambda = -1$, while the second at more than 2σ. In the same paper a dynamical DE model has been considered, using the CPL parametrization and combining *Planck* data with both the SNLS and H_0 data sets. The results favor a dynamical DE at about 2σ.

A dynamical w_{DE} can be also the result of the parametrization of scalar fields, as in the case of Quintessence [94, 95, 96, 97, 98, 99, 100, 101, 102, 103],

k-essence [104, 105] and tachyons [106]. Usually, the field equation associated to the scalar field can be recast in the form of a conservation equation, in this sense the field is considered as a fluid component.

3.2.3 Quintessence model

A first hint, to solve problems related to the CC, was to extend the ΛCDM model introducing a scalar field ϕ. The simplest and probably the most common alternative model is the Quintessence. The name comes from latin "quinta essentia" (fifth element), as it was thought that a fifth element should contribute to the total energy budget of the Universe. We refer the reader to Ref. [86] for a complete and recent review or to the literature [94, 95, 96, 97, 98, 99, 100, 101, 102, 103].

Let us introduce the action of the Quintessence model

$$S = \int d^4x\sqrt{-g}\left[\frac{1}{2}m_0^2 R - \frac{1}{2}g^{\mu\nu}\partial_\mu\phi\partial_\nu\phi - V(\phi)\right] + S_m[g_{\mu\nu}, \chi_m]\,, \tag{3.28}$$

which is described by a canonical scalar field ϕ minimally coupled to gravity. Here, $V(\phi)$ is a potential while all the other quantities have been already defined in the previous Chapters. Varying the action with respect to the scalar field and assuming a spatially flat FLRW metric, one obtains

$$\ddot{\phi} + 3H\dot{\phi} - \frac{1}{a^2}\nabla^2\phi + \frac{dV(\phi)}{d\phi} = 0\,. \tag{3.29}$$

The field ϕ is usually written as the sum of an homogeneous part and a small perturbation, $\phi(t, x^i) = \phi(t) + \delta\phi(t, x^i)$. As it is expected that the scalar field mimics the CC on large scale, we can neglect the inhomogeneous part. Then, the Eq. (3.29) can be recast in the form of a conservation equation as

$$\dot{\rho}_\phi + 3H\left(\rho_\phi + p_\phi\right) = 0, \tag{3.30}$$

where

$$\rho_\phi = \dot{\phi}^2/2 + V(\phi), \tag{3.31}$$

$$p_\phi = \dot{\phi}^2/2 - V(\phi), \tag{3.32}$$

are respectively the density and pressure of the scalar field and the corresponding equation of state reads

$$w_\phi \equiv \frac{p_\phi}{\rho_\phi} = \frac{\dot{\phi}^2/2 - V(\phi)}{\dot{\phi}^2/2 + V(\phi)}. \tag{3.33}$$

The above relation makes manifest the dynamical nature of the Quintessence field, highlighting the difference with the CC. Quintessence models can be classified according to the dynamical evolution of w_ϕ. Caldwell and Linder [107] proposed two main classes: thawing models and freezing models.
In order to give rise to the late time acceleration the field has to satisfy the condition $p_\phi < -1/3\rho_\phi$. Moreover, as observations fix $w \approx -1$, the following slow-roll condition has to be considered

$$\dot{\phi}^2 << V(\phi), \tag{3.34}$$

according to which the potential is dominant w.r.t. the kinetic term ($\dot{\phi}^2$). This condition allows to restrict the very general form of the potential $V(\phi)$. Both early and late time accelerations can be described through a scalar field which violates the Strong Energy Condition. However, let us note that the scalar field responsible for the Inflation has a less restrictive condition, i.e. $\dot{\phi}^2 < V(\phi)$, but one has to assume that $\ddot{\phi}$ be negligible.

Quintessence model has been introduced in order to solve the CC issues. In that model as the role of the CC has been placed by the scalar field ϕ, we have to make sure that the field has a counterpart in the particle physics sector. In this regard, we can compute the mass of the field, which is defined as

$$m_\phi^2 \equiv \frac{\partial^2 V(\phi)}{\partial \phi^2}. \tag{3.35}$$

In the case of Quintessence, considering the slow-roll condition, one has from Eq. (3.29), that $H \sim \sqrt{\partial^2 V/\partial \phi^2}$, then the mass is proportional to the Hubble constant, setting the bound

$$|m_\phi| \lesssim H_0 \approx 10^{-33}\, eV\,. \tag{3.36}$$

A scalar field with such a low mass gives rise to a long range fifth force. On the other hand, having such a low mass for a scalar field does not seem to be technically natural from a quantum field theory point of view [108, 109]. Scalar field masses are quadratically divergent, as we already know from the Higgs field and the hierarchy problem. The fact that the mass of the Quintessence field is many orders of magnitudes smaller than that of the Higgs field make the problem much more pronounced.

Attempts to solve the Coincidence Problem have been made with specific models of Quintessence with a tracker behavior [101, 100, 103, 110]. In these models the field closely tracks the radiation or matter density for a time sufficiently long to eliminate the Coincidence Problem. However, tracker models depend strictly on the parameters of the potential, which in turn are difficult to constraint due to degeneracy in the parameter space [111].

3.3 The Dark Matter issue

The existence of a missing matter has been postulated since 1933 by Zwicky [112] to explain the high dispersion velocity of galaxies in the Coma Cluster, which required a bigger amount of non-luminous matter to justify the observations, hence the name Dark Matter (DM). The "proof" of its presence has been shown in many observations including rotation curves [112, 113, 114, 115, 116, 117], gravitational lensing [118], LSS [22], BBN [21, 29, 30], CMB [21]. Constraints on the nature of DM show that it is non-baryonic and it does not interact with other matter components other than via gravitational interactions. Finally, LSS simulations require a cold component to account for the observed matter distribution [32]. The best particle candidate is the Weakly Interacting Massive Particle (WIMP). Despite indirect observational evidence [119, 120], ground based experiments have not detected any signature for a DM particle [121].

In this Section we will focus on DM's shortcomings at a small scales. These are mainly related to discrepancies between N-body simulations and observa-

tional data. This leads us to wonder whether the standard cosmological model, on which simulations are based, can be reliable in its predictions. However, let us say, that at small scales, the approximations, that usually are used when studying the evolution of the Universe or perturbations, break down when one deals with fundamental structures, such as galaxies or clusters.

The first problem is the so called *Core-Cusp Problem*. It concerns the inner density profile of the DM halo in galaxies. Pure DM-simulations select a Navarro-Frenk-White (NFW) profile [122]. Such a cuspy profile in the interior of a galaxy is not favored by observations. One specific example is DDO 47, whose velocity field is clearly best fitted if the DM halo is cored; moreover, its (small) detected non-circular motions cannot account for the discrepancy between data and the NFW predictions [123]. An empirical profile has been proposed by Burkert [124], which at small radii reveals a core profile, which is more suitable to fit observations (e.g. [125, 126, 127, 128, 129, 130, 131]), while at large radii the profile is the same as for NFW. See also Section 4.1 for details about these density profiles. A problem between the simulations and observational data can be found in the assumptions used in running simulations. In fact, the baryonic component is usually ignored, instead it has been shown that it is crucial to solve the problem (e.g. Ref. [132]). In Ref. [133], it is shown that the inclusion of supernovae feedback in the simulation allow to form cored profiles.

A second problem related to N-body simulations is the *missing satellite problem* [134, 135]. A discrepancy between the predicted number of sub-halos in DM-only simulations and the observed number of satellites in the Milky Way has been found, casting doubt on the model used for the formation of structures. However, it is questionable whether this discrepancy is due to very faint satellites, that are difficult to detect or even to entire sub-halos which remain dark. The availability of data coming from wide field resolved star surveys has increased the discovery of faint satellites around the Milky Way (see for examples Refs. [136, 137]), although their number is not sufficient to explain such a difference. Moreover, as shown in Refs. [138, 139, 140] the inclusion of baryonic matter in the simulations allows to consider mechanisms for the suppression of the gas and star formation rate such as supernova feedback, stellar winds or photoevaporation, which actually make halos unobservable. These results are very encouraging as they reconcile the satellite population obtained in simulations to the observed one.

Finally, a third problem is the *Too Big Too Fail problem* [141]. In numerical simulations the most massive sub-halos are too dense to host the observed satellites. In fact, satellites in the Milky Way have circular velocities around 24 km/s, on the contrary simulated sub-halos reach velocities in the range 30-70 km/s. These results are obtained in DM-only simulations, in which the density profile for the halo is chosen to be the NFW. Inclusion of supernovae feedbacks in the simulations allow to flatten the central cusp, in that way the resulting circular velocity profiles do not exceed 20 km/s (at least in the inner 1 kpc) [133].

We may conclude that a deep knowledge of the physical process of galaxy formation at small scale is required as this seems to be the key to understand which processes need to be considered when running simulations. On the other hand, DM-only simulations are not enough to explain the physical processes of galaxy formation at small scale. Then, N-body simulations have to be improved in order to include the baryon's feedbacks such as supernovae explosions and

stellar wind.

Doubts about the validity of the standard cosmological model have given space to new scenarios, such as the inclusion in the simulations of Warm Dark Matter particles (WDM), which best candidates are sterile neutrinos and gravitinos. WDM particles might cure the shortcomings at small scales [142]. Modifications of the newtonian law have also been considered, such as Milgrom's proposal [143, 144], known as MOND (MOdified Newtonian Dynamics). In this approach instead of assuming the existence of a DM component, Milgrom postulates that newtonian force is modified at large radii, where the baryonic component seems to be ineffective to account for the galaxy kinematics. The details on the MOND paradigm will be discussed in the next Part II.

Part II

Dark Matter at Small and Large Scales

Chapter 4

Dark Matter in Galaxies

The most direct evidence of the existence on a missing component, the Dark Matter (DM), comes from observations of velocity profiles of galaxies [145]. Luminous matter in galaxies would show a velocity profile that is

$$V(r) \propto r^{-1/2}, \tag{4.1}$$

according to the newtonian law. Measurements of the velocity profile using doppler shift, show that the velocity instead of decreasing with the radius, actually remains constant. The resulting profile is known as flat Rotation Curve (RC). This behavior persists well outside the galaxy core, where no luminous matter is present. This would suggest an extra component which contributes to the matter profile giving rise to a distribution of the form

$$M(r) \propto r, \tag{4.2}$$

implying that the mass would increase with distance.

This aspect is most evident in Spiral galaxies, where observational data show that the mass in dark halos is about 10 times the stellar mass component. The RC in Spirals is obtained by measuring the gas emission lines in the disk, e.g. the neutral hydrogen (H I), or using satellite galaxy kinematics and weak lensing, providing a direct measurement of the radial distribution of the gravitational mass. In the central region of a galaxy, it is difficult to disentangle the dark and luminous component, as the mass model usually used to fit the inner region, accounts for both the components. In some cases, the dark component seems to dominates at all radii, as for the Low Surface Brightness galaxies (LSB) and Dwarf galaxies [146]. In particular the latter are an excellent laboratory to test models of mass, allowing to discriminate between different profiles, since about 90% of the total mass consists of a dark component.

DM in Elliptical galaxies contributes in the same amount as for Spirals (about 10% of the luminous mass). Unfortunately, in that case the DM can not be studied using RC as Ellipticals exhibit small or no rotational motions. However, excellent mass indicators are: the kinematics of globular clusters at 10-30 Kpc [147, 148], and at large radii (100-400 kpc) the one of Satellite galaxy [149], weak lensing and X-ray emission measurements, as some Elliptical galaxies are surrounded by X-ray emitting gas.

Today, the DM component is a real challenge in Astrophysics. It is the galaxy component less known, though perhaps the most studied. Many unknowns remain, such as determining exactly the shape, the size and mass of the dark halo. Furthermore, it is important to understand its composition from a particle point of view.

4.1 Dark Matter halo density profiles

A galaxy is usually modeled with an halo composed by DM, which surrounds the whole galaxy. In order to explain the flat RCs in galaxies, many density profiles for the dark halo have been proposed. In particular, numerical N-body simulations in the contest of ΛCDM were of fundamental importance in the study and determination of the main characteristics of the DM distribution. Their results show that the dark halo is well described by the NFW profile [122]

$$\rho_{NFW}(r) = \frac{\rho_s}{\frac{r}{r_s}\left(1+\frac{r}{r_s}\right)^2}, \tag{4.3}$$

where ρ_s and r_s are respectively the density and radius parameters, which vary depending on the halo. Usually r_s is parametrized through $r_s = R_{vir}/c$, where R_{vir} is the virial radius and c is the concentration parameter which in turn depends on the virial mass (M_{vir}) and redshift. The corresponding velocity profile of the RC is given by

$$V^2_{NFW}(r) = V^2_{vir}\frac{g(c)}{xg(cx)}, \tag{4.4}$$

where $x = r/R_{vir}$, $g(c) = [ln(1+c) - c/(1+c)]^{-1}$. At redshift $z = 0$ the concentration parameter can be approximated as [150]

$$c(M_{vir}) = 9.60\left(M_{vir}/10^{12}h^{-1}M_{\odot}\right)^{-0.075}. \tag{4.5}$$

More complicated forms for the concentration parameter which depend on z are also available [150]. This profile is in tension with the observational data, since it provides a cuspy core, while for the outer regions, RC profile has been proven successfully.

A phenomenological model has been proposed by Burkert [124], hence the name Burkert profile, to explain the RCs of dwarf galaxies and it is the following

$$\rho_r = \frac{\rho_0 r_0^3}{(r+r_0)(r^2+r_0^2)}, \tag{4.6}$$

where r_0 and ρ_0 are respectively the radius and the density of the core. This model is well suited to explain the density profile in the inner regions as well as at large radii, where the profile diverges as r, recovering the prediction of N-body simulation. The cored halo parametrization for the velocity profile results in the Halo Universal Rotation Curve (URCH) profile [151]:

$$\begin{aligned} V^2_{URCH}(r) = \quad & 6.4G\frac{\rho_0 r_0^3}{r}\left[\ln\left(1+\frac{r}{r_0}\right) - \arctan\left(\frac{r}{r_0}\right)\right. \\ & \left. + \frac{1}{2}\ln\left(1+\frac{r^2}{r_0^2}\right)\right], \end{aligned} \tag{4.7}$$

where the core radius r_0 and the central halo density ρ_0 are free parameters.

Another model is the one proposed by Einasto (1965) [152], which describes the variation of the density with the semi-major axis of the isodensity ellipsoid b

$$\rho(a) = \rho_0 \exp\left[\left(-\frac{b}{b_0}\right)^{\frac{1}{N}}\right]. \tag{4.8}$$

where b_0 is the effective radius and N characterizes the slope of the profile. Two particular cases are for $N = 4$, for which the profile reduces to the de Vaucouleurs density law for a spherical system, and for $N = 1$ it describes the exponential disk profile.

4.2 MOND: Modifying the Newtonian Dynamics

An alternative to Newtonian gravity was proposed by Milgrom [143, 144] in order to explain the phenomenon of mass discrepancy in galaxies. It was suggested that the true acceleration a of a test particle, at low accelerations, is different from the standard Newtonian acceleration, a_N:

$$a = \frac{a_N}{\mu(a/a_0)}, \tag{4.9}$$

where $\mu(a/a_0)$ is an interpolation function which runs smoothly from $\mu = a/a_0$ at $a << a_0$ to $\mu = 1$ at $a >> a_0$, with a_0 being the critical acceleration at which the transition, between the two regimes, occurs.

Different forms of the interpolation function are present in the literature. The standard interpolation function, known also as the old interpolation function is

$$\mu(a/a_0) = \frac{a/a_0}{\sqrt{1+(a/a_0)^2}}. \tag{4.10}$$

For this model, Begeman and collaborators (1991) [153] claim that the value of the critical acceleration is $a_0 = 1.21 \times 10^{-8}$ cm s^{-2}. In this framework, the circular velocity profile can be expressed as a function of a_0 and of the standard Newtonian contribution of the baryons to the RC, obtaining for it

$$V^2_{MOND,old}(r) = V^2_{bar}(r) + V^2_{bar}(r)\left[\sqrt{\frac{1+\left(2ra_0/V^2_{bar}\right)^2}{2}} - 1\right], \tag{4.11}$$

where V_{bar}=$(\mathrm{V}^2_D+\mathrm{V}^2_{\mathrm{gas}})^{1/2}$ includes the contribution of the disk (V_D) and gas (V_{gas}).

A new model was suggested by Famaey & Binney (2005) [154], known as the new interpolation function

$$\mu(a/a_0) = \frac{a/a_0}{1+a/a_0}. \tag{4.12}$$

In that case a_0 assumes the value 1.35×10^{-8}cm s^{-2} [155]. In contrast with the old interpolation function, the new form has the advantage of making

MOND compatible [156] with its relativistic version, Tensor-Vector-Scalar gravity (TeVeS) [157]. The corresponding velocity profile is [158]

$$V^2_{MOND} = V^2_{bar}(r) \left(\frac{\sqrt{1 + \frac{4a_0 r}{V^2_{bar}(r)}} + 1}{2} \right). \quad (4.13)$$

Both Eqs.(4.11)-(4.13) show that in the MOND framework the resulting RC is similar to the no-DM standard Newtonian one with an additional term that works to mimic and substitute the DM component [159].

4.3 The Orion Dwarf Galaxy: a test for MOND

The measurement of the RCs of disk galaxies is a powerful tool to investigate the nature of DM, including its content relative to the baryonic components and their distributions. In particular, dwarf galaxies are good candidates to reach this aim as their kinematics are generally dominated by the dark component, down to small galactocentric radii [160, 129, 127, 131, 161]. This leads to a reliable measurement of the dynamical contribution of the DM to the RC and hence of its density profile.

In Ref. [162] with P. Salucci, D. Vernieri, J. M. Cannon and E. C. Elson, we investigate the viability of some velocity profiles for the dark halo, using as test the RC of the Orion dwarf galaxy. As we will show below, the Orion dwarf is one of the few known galaxies whose kinematics *unambiguously* point towards a cored profile. This system is thus critically important for investigating the nature of the DM particle and of the evolution of DM halos. Moreover, this nearby system harbors an extended H I disk, and thus provides us with an important test of the MOND paradigm. Historically MOND has generally been successful in reproducing the RCs of spiral galaxies with only the (observed) luminous matter (e.g. Refs. [163, 164, 165]). However, cases of tension between data and the MOND formalism do exist [129].

It is important to stress that in order to derive the DM density profile or to test the MOND formalism, we must know the distribution of the ordinary baryonic components, as well as have reliable measurements of the gas kinematics. For the Orion dwarf, 21-cm H I surface brightness and kinematics have been published in Ref. [166]: their analysis provides a high quality, high resolution RC, that, in addition, can be easily corrected for asymmetric drift and tested for non-circular motions. This galaxy is a very useful laboratory in that a simple inspection of the RC ensures us that it shows a large mass discrepancy at all radii. Moreover, the baryonic components are efficiently modeled (i.e., no stellar bulge is evident and the stellar disk shows a well-behaved exponential profile, see Ref. [167]). The distance to the galaxy, which is critical for an unambiguous test of MOND [159], is estimated to be 5.4±1.0 Mpc [167]. It is important to stress that the distance of the Orion dwarf remains a significant source of uncertainty. In Ref. [167], the distance is estimated using the brightest stars method. The intrinsic uncertainty in this technique may allow a distance ambiguity much larger than the formal errors estimated by Ref. [167], because in their work this method yields a scatter as large as 50% in distance. Finally, the system's inclination (47°) is kinematically measured and is high enough to not affect the

estimate of the circular velocity. The properties described above make the Orion dwarf galaxy an attractive candidate to determine the underlying gravitational potential of the galaxy.

The present investigation is organized as follows. In Section 4.3.1 we present the stellar surface photometry. In Section 4.3.2, the H I surface density and kinematics data are presented and discussed; we also provide the analysis of possible non-circular motions of the neutral gas. In Section 4.3.4 we model the RC in the stellar disk using a cored/cusped halo framework and test the Orion kinematics against the NFW, URCH profiles and MOND formalism. A final discussion is in Section 4.3.5.

4.3.1 Stellar Photometry

Following the discussion in Ref. [166], the underlying stellar mass in the Orion dwarf is estimated using the near-infrared (IR) photometry (J and K_S bands) presented in Ref. [167]. Those authors find $(J - K_S) = +0.80$ and a total K_S magnitude of +10.90. We assume that the color difference between K and K_S is negligible; further, we assume $L_{K,\odot} = +3.33$ [168, 169]. Accounting for extinction, the total K-band luminosity of the Orion dwarf is $\sim 3.5 \times 10^8$ $L_\odot$. The mass of the stellar component was estimated by Ref. [166] to be $(3.7 \pm 1.5) \times 10^8$ $M_\odot$. The stellar surface brightness profile is well fitted by an exponential thin disk, with a scale length of $R_D = 25 \pm 1$ arcsec (equivalent to 1.33 ± 0.05 kpc at the adopted distance). Moreover, there are no departures from an exponential profile that would be indicative of a prominent central bulge.

4.3.2 HI surface density and kinematics

H I spectral line imaging was acquired with the *Very Large Array* and presented in Ref. [166]. We refer the reader to that work for a full discussion of the data handling, and we summarize salient details here. The final data cubes have a circular beam size of 20 arcsec, with a 3σ H I column density sensitivity of $N_{HI} = 1.5 \times 10^{19}$ cm^{-2}. The first three moment maps (i.e. the integrated H I intensity, the velocity field, and the velocity dispersion) are shown in Fig. 4.1.

The neutral gas disk of the Orion dwarf shows rich morphological and kinematic structure at this physical resolution. The outer disk contains tenuous H I gas, but column densities rise above the 5×10^{20} cm^{-2} level at intermediate radii. There is plentiful high-column density ($>10^{21}$ cm^{-2}) H I throughout the disk. The more or less parallel iso-velocity contours at inner radii are indicative of linear rotation (although almost certainly not solid body) and the curving of the outer contours suggests that the outer rotation curve has a fairly constant velocity. The outer disk contours show no evidence for a decrease in rotational velocity at large radii. In the central regions of the disk, however, some H I "holes" or "depressions" manifest a pronounced kink in these contours (consider the contours at 370 ± 20 km s^{-1}). The intensity weighted velocity dispersion averages to $\sim$7-8 km s^{-1} throughout the disk, although the innermost regions show dispersions above 10 km s^{-1}.

The total H I flux integral, proportional to the H I disk mass, was found to be

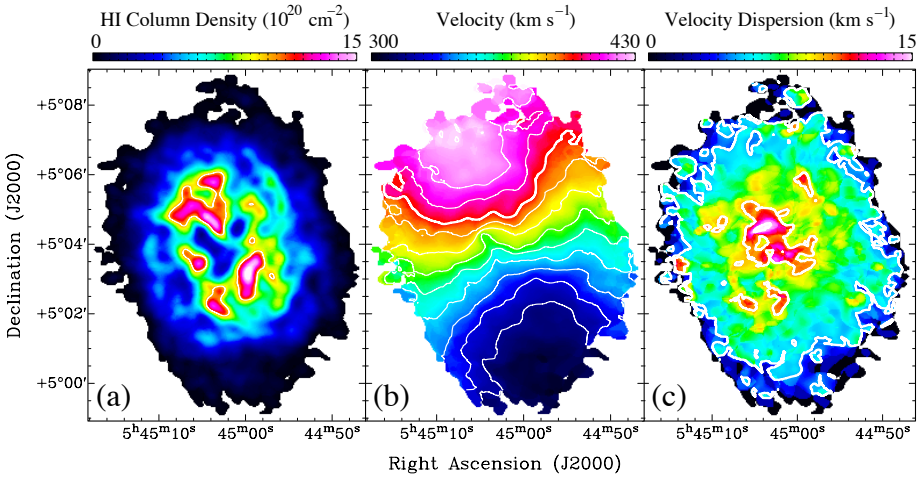

Figure 4.1: Comparison of the H I column density distribution (*a*), the intensity-weighted velocity field (*b*), and the intensity-weighted velocity dispersion (*c*); the beam size is 20 arcsec. The contour in (*a*) is at the 10^{21} cm^{-2} level; the contours in (*b*) show velocities between 320 and 420 km s^{-1}, separated by 10 km s^{-1}, and the thick white line corresponds to the 400 km s^{-1}contour; the contours in (*c*) are at the 5, 10, 15 km s^{-1} levels.

50.3 ± 5.1 Jy km s^{-1}, a value somewhat lower than the single-dish flux measure of 80.6±7.72 Jy km s^{-1} by Ref. [170]; the difference may arise from the lack of short interferometric spacings that provide sensitivity to diffuse structure. The total H I mass is found to be $M_{HI} = (3.5\pm0.5) \times 10^8 M_\odot$. After applying the usual 35% correction for Helium and molecular material, we adopt $M_{gas} = (4.7\pm0.7) \times 10^8 M_\odot$ as the total gas mass. In Fig. 4.2 we plot the 10 arcsec /20 arcsec resolution H I surface density, throughout the gas disk. A simple fit (valid out to the last measured point and for the scope of this work) yields:

$$\mu_{HI}(r) = \frac{-0.263r^3 + 1.195r^2 + 3.094r + 18.549}{0.154r^3 - 1.437r + 6.703} \; M_\odot/pc^2, \qquad (4.14)$$

where r is in kpc. The related fitting uncertainty on $\mu_{HI}(r)$ is about 20%.

Fig. 4.2 shows that the H I surface density rises from the center of the galaxy, reaches a maximum, and then declines exponentially. At the last measured point, i.e. out to $\sim$ 7 kpc, the profile has almost (though not completely) reached the edge of the H I disk and rapidly converges to zero. Note that, in Newtonian gravity, the outer gaseous disk contributes in a negligible way to the galaxy total gravitational potential.

4.3.3 The Circular Velocity

The channel maps of the Orion dwarf provide evidence of well-ordered rotation throughout the H I disk (see Ref. [166]). The intensity-weighted-mean velocity field (Fig. 4.1b) exhibits symmetric structure in the outer disk. Twisted iso-velocity contours at inner radii coincide with the H I holes near the center of the

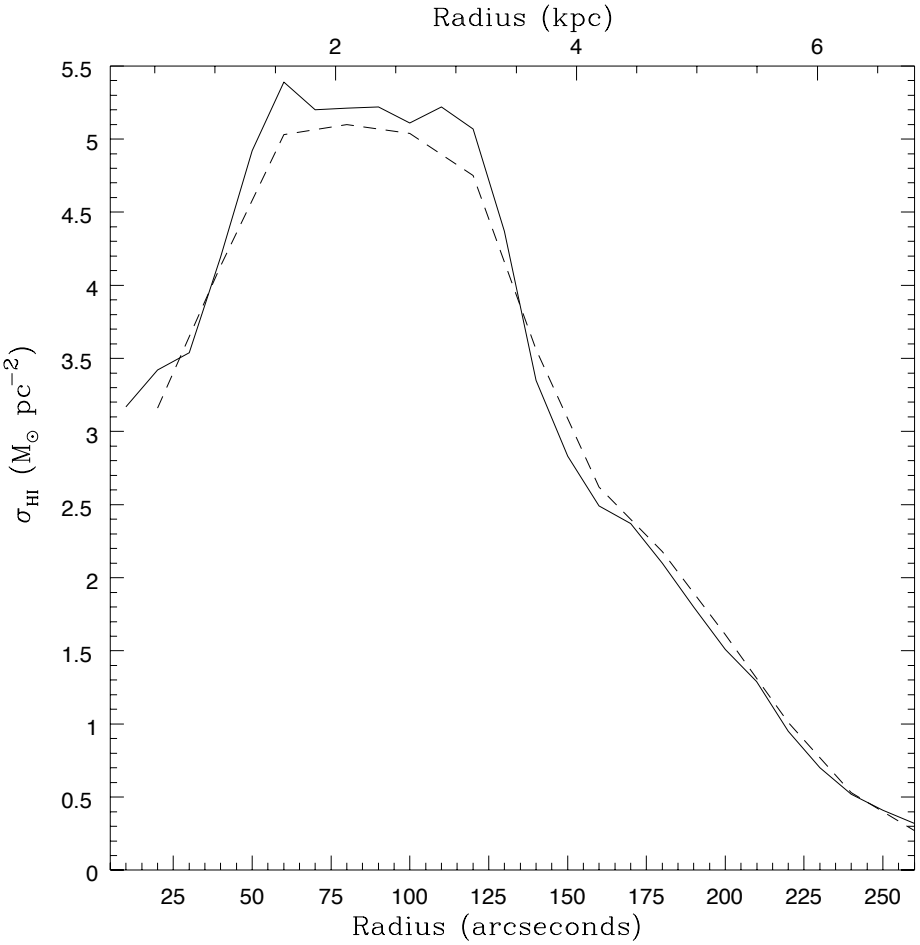

Figure 4.2: Radially averaged H I mass surface density profiles of the Orion dwarf, created by averaging H I emission in concentric rings emanating from the dynamical center found in our RC analysis. The solid/dotted lines were created from the 10 arcsec /20 arcsec resolution images.

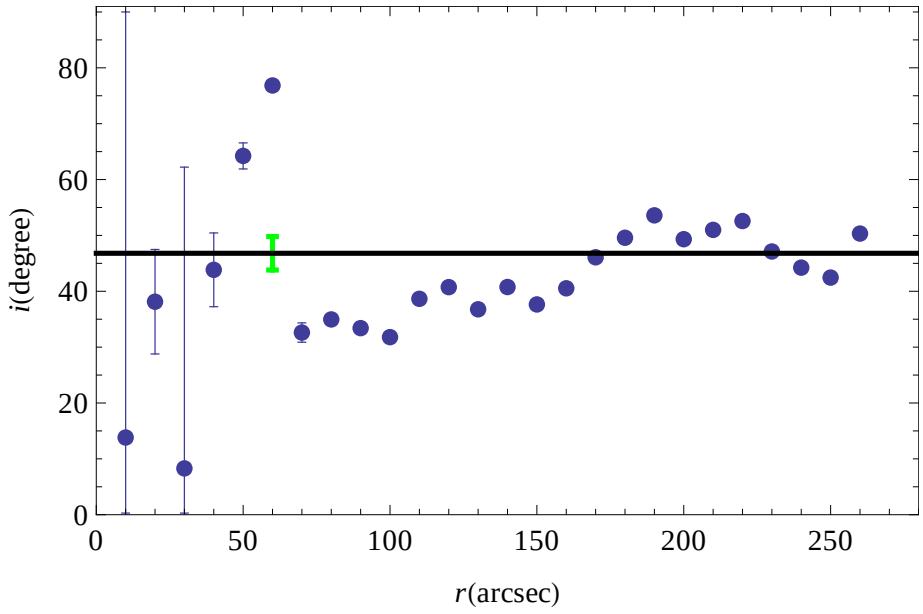

Figure 4.3: Inclination best fit (thick Black line) for high resolution (10″) data (filled Blue points). Errorbars are plotted and in most cases are smaller than the symbol size. The errors reported (by GIPSY/ROTCUR) include only errors on the fits, while the systematic error considered (3°) is shown as a Green errorbar.

disk. The disk is, therefore, dominated by circular motion. The RC of the galaxy was derived by fitting a tilted ring model to the intensity-weighted-mean velocity field using the GIPSY task ROTCUR. The routine carries out a least-squares fit to V_{los}, the line of sight-velocity. To derive the best-fitting model, an iterative approach was adopted in which the various combinations of the parameters were fitted. The final RC was extract by fixing all other parameters. The receding and approaching sides of the galaxy were fitted separately. The best fitting parameters are $i = (47 \pm 3)°$, $P.A. = (20 \pm 2)°$, $V_{\rm sys} = 368.5 \pm 1.0$ km/s, and $(\alpha_{2000},\delta_{2000})$ = (05:45:01.66, 05:03:55.2) for the dynamical center. We have realized that the inclination is not dependent on the radius, and the fit is shown in Fig. 4.3. Its weighted value is $(46.8 \pm 0.14)°$. Notice that because the errors reported by GIPSY/ROTCUR include only errors on the fits and systematics are not included, the 3° error estimate comes from attempting the ROTCUR fits in various orders (e.g., holding each variable fixed in turn). The resulting RC is shown in Fig. 4.4. Notice that in this object the disk inclination is determined kinematically and therefore it is quite accurate. No result of our work changes by adopting different values of i, inside the quoted errorbar.

The second-order moment map for the galaxy is shown in Fig. 4.1c. Throughout most of the disk, the velocity dispersion is roughly constant at $\sigma \simeq 7 \pm 2$ km/s, with a more complex behavior near the galaxy center and at the outermost radii. This velocity dispersion estimate allows us to derive the asymmetric drift correction to the RC yielded by the tilted ring model. The observed rotation

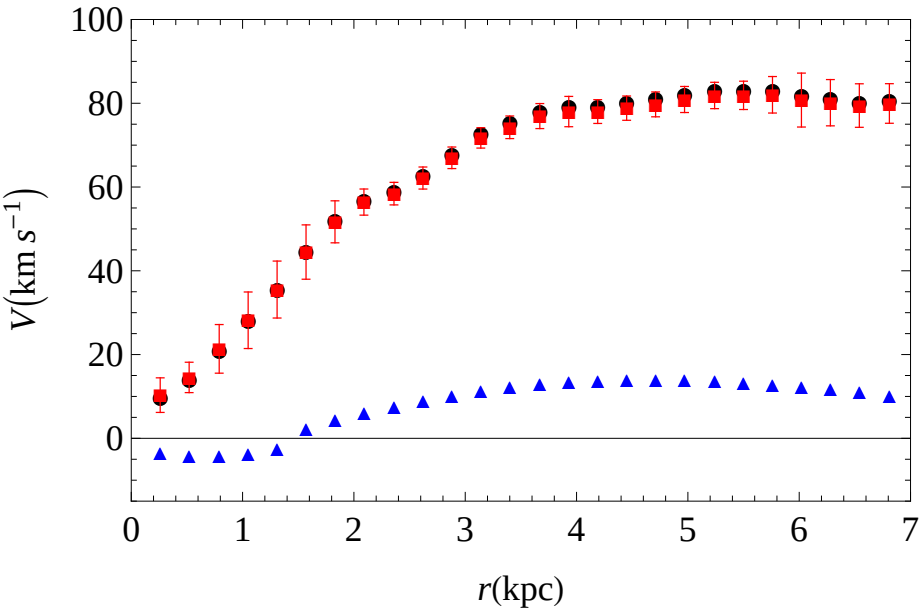

Figure 4.4: Rotation velocity corrected for asymmetric drift (filled black points), raw velocity data with error bars (filled red boxes) and the asymmetric drift correction (filled blue triangles).

velocity, V_{rot}, is related to the circular velocity V_c via

$$V_c^2(r) = V_{rot}^2(r) - \sigma^2(r) \left[\frac{dlog\ \mu_{\rm HI}(r)}{dlog\ r} + \frac{dlog\ \sigma^2(r)}{dlog\ r} \right]. \tag{4.15}$$

From an examination of Fig. 4.4 it is clear that the V_{rot} and V_c profiles differ by less than 1%. Throughout this work, we use the latter for the purposes of mass modeling. We notice that in very small dwarfs this correction is not negligible ($V_{rot} \sim \sigma$) and it introduces an uncertainty in the analysis, e.g. Ref. [171].

In summary, the Orion dwarf RC has a spatial resolution of 0.26 kpc (i.e. 0.2 R_D), and extends out to 5.1 R_D. The uncertainties on the RC are few km/s and the error on the RC slope $dlogV/dlogR < 0.1$.

Is the circular velocity given by Eq. (4.15) a proper estimate of the gravitational field? To further investigate the presence of non-circular motions within the H I disk that jeopardize the kinematics, we carried out a harmonic decomposition of the intensity-weighted velocity field to search for any significant non-circular components. This test is necessary in that the undetected presence of non-circular motions can lead to incorrect parametrization of the total mass distribution. Following Ref. [172], the line-of-sight velocities from the H I velocity field are decomposed into harmonic components up to order $N = 3$ according to

$$V_{los} = V_{sys} + \sum_{m=1}^{3} c_m \cos m\theta + s_m \sin m\theta, \tag{4.16}$$

where V_{sys} is the systemic velocity, c_m and s_m are the magnitudes of the harmonic components, m the harmonic number, and θ the azimuthal angle in the plane of the galaxy. The GIPSY task RESWRI was used to carry out the decomposition by fitting a purely circular model to the velocity field, subtracting it from the data, and then determining from the residual the magnitudes of the non-circular components. The tilted ring model fitted by RESWRI had its kinematic center fixed to that of the purely circular tilted ring model used to derive the RC above. The position angles and inclinations were fixed to constant values of 20° and 47°, respectively.

The parameters of the best-fitting model are shown in Fig. 4.5. Adjacent points are separated by a beam width in order to ensure that they are largely independent of one another. We argue that because the standard tilted ring model has fewer free parameters than the model incorporating the higher order Fourier components, it is not as essential to space the points on the rotation curve by a full beam width. Then in this model only 16 points are considered instead of the 26 points used in fitting the RC.

At inner radii the inferred non-circular motions are not negligible, but this is almost certainly due to the fact that the H I distribution over this portion of the disk is irregular, being dominated by the large central H I under-densities. The harmonic components of the outer disk are, instead, reliable and demonstrate the gas flow to be dominated by circular kinematics. The circular velocity so obtained well matches that found by means of the tilted ring model presented above. The amplitudes of c_2 and s_2 are too small to hide a cusp inside an apparently solid body RC (as suggested by Ref. [173]). These results provide further decisive support for the use of V_{rot} of the Orion dwarf as a tracer of its mass distribution.

4.3.4 Mass Modeling and Results

We model the Orion dwarf as consisting of two "luminous" components, namely the stellar and the gaseous disks, embedded in a dark halo. The stellar component is modeled as an exponential thin disk [174] with a scale length of 1.33 kpc. Any bulge component is assumed to be negligible in terms of mass. The dynamical contribution of the gas to the observed RC is derived from the H I total intensity map. A scaling factor of 1.33 is incorporated to account for the presence of Helium and other elements. For the dark halo we consider two different parametrizations of the mass distribution: a NFW profile Eq. (4.4) [175] and the cored profile of the URCH [151] Eq. (4.7).

The RC is modeled as the quadrature sum of the RCs of the individual mass components:

$$V_{mod}^2 = V_D^2 + V_{DM}^2 + V_{\rm gas}^2, \tag{4.17}$$

where V_D is the disk component, the V_{DM} is the DM halo, which in turn is parametrized by the NFW profile and the URCH one.

From Fig. 4.6 upper panel, it is evident that the URCH profile yields a total RC that fits the data extremely well, with best-fitting parameters of $r_0 = (3.14 \pm 0.32)$ kpc, $\mathrm{M}_D = (3.5 \pm 1.8) \times 10^8$ $\mathrm{M}_\odot$ and $\rho_0 = (4.1 \pm 0.5) \times 10^{-24} \mathrm{g/cm}^3$. More accurate statistics is not necessary; the mass model predicts all the $V(r)$ data points within their observational uncertainty.

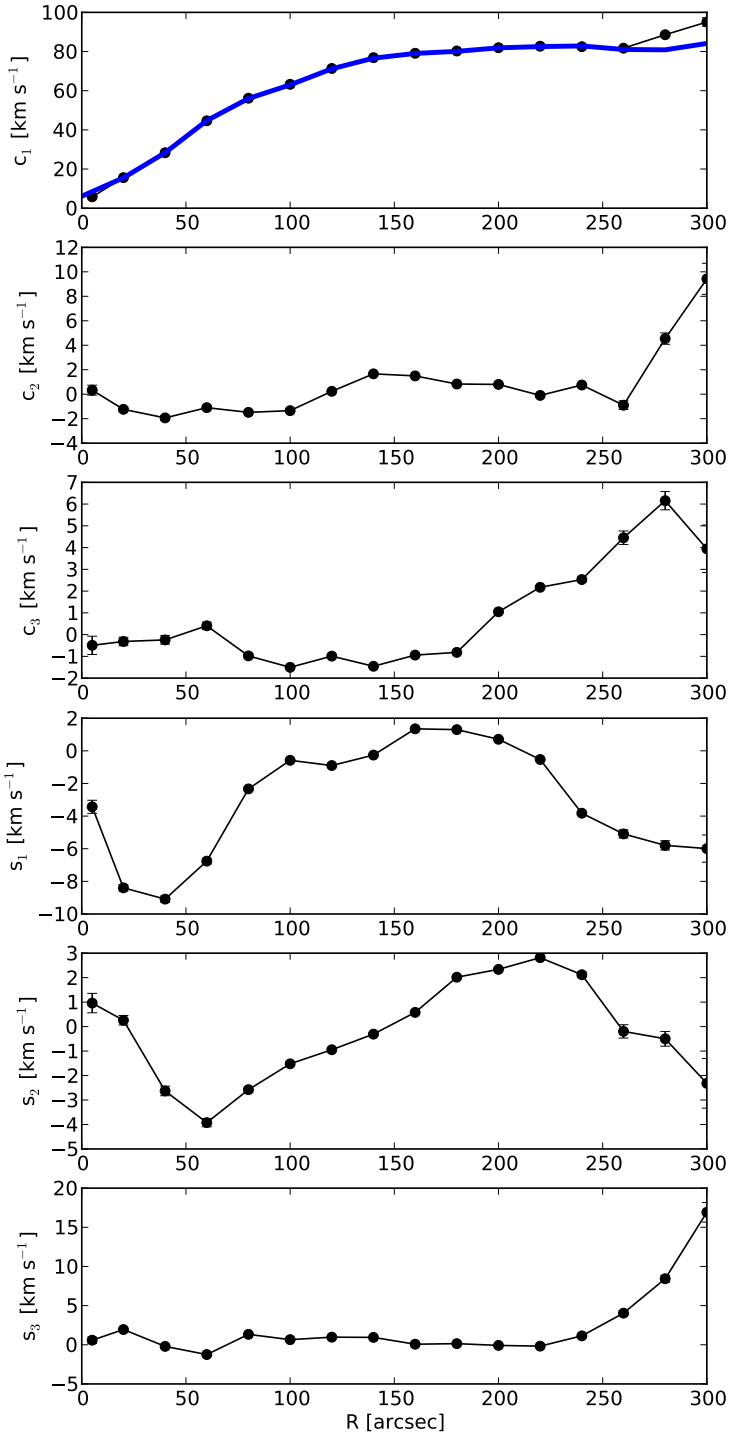

Figure 4.5: Non-circular velocity components as derived by carrying out a harmonic decomposition of the intensity-weighted-mean velocity field. The c_1 profile corresponds to the circular RC. The RC derived by fitting tilted ring model to the intensity-weighted-mean velocity field is shown as a solid blue curve.

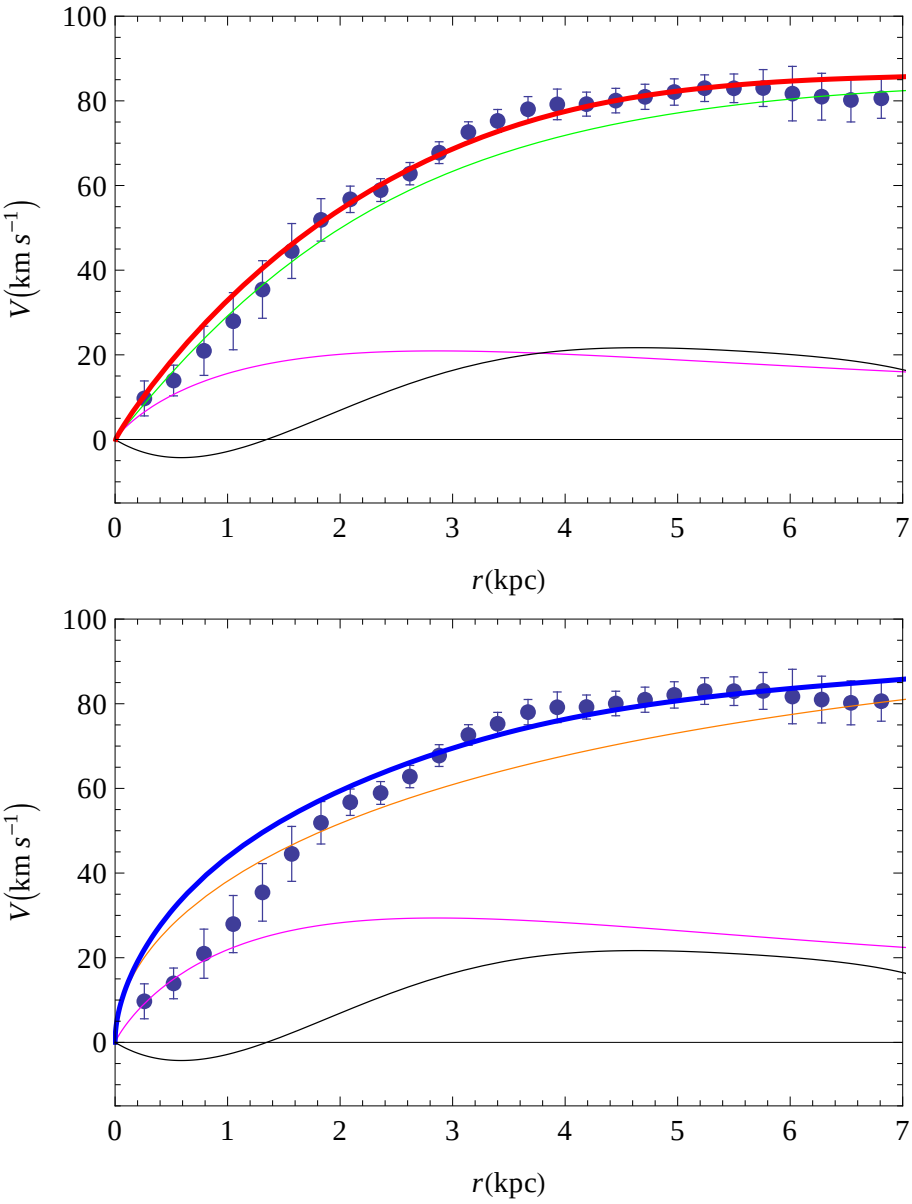

Figure 4.6: Upper panel: URC model of Orion dwarf. The circular velocity (filled circles with error bars) is modeled (thick Red line) by a Freeman disk (Magenta line), a URCH halo (Green line), and the H I circular velocity (Black line). Lower panel: NFW model of Orion dwarf. The circular velocity data (filled circles with error bars) is modeled (thick Blue line) including a Freeman disk profile (Magenta line), a NFW halo profile (Orange line) and the H I circular velocity (Black line). In both cases the values of the free parameters are reported in the text.

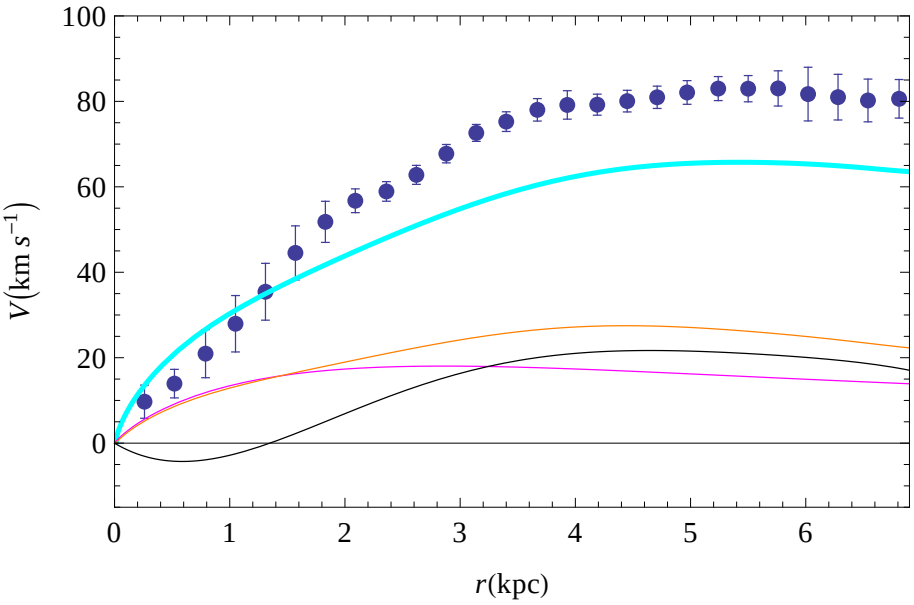

Figure 4.7: MOND model of Orion dwarf spiral. The circular velocity data (filled circles with error bars) is modeled with the MOND profile (thick Cyan line). Also shown are the (newtonian) Freeman disk contribution (Magenta line), the H I contribution (Black line) and the total baryonic contribution (Orange line).

Notice that the derived value of the disk mass agrees with the photometric estimate discussed above. The corresponding virial mass and radius of the DM halo are $M_{vir} = (5.2 \pm 0.5) \times 10^{10}$ $M_\odot$ (see Eq. (10) in Ref. [151]) and $R_{vir} = 95.5^{+5}_{-4}$ kpc [176], respectively. We note that the Orion dwarf has a mass 20 times smaller than that of the Milky Way, with the DM halo dominating the gravitational potential at all galactocentric radii. The baryonic fraction is $f_b = (M_D + M_{\rm gas})/M_{vir} = 0.016$, while the gas fraction is $M_{\rm gas}/M_{vir} = 9 \times 10^{-3}$.

The second model we will investigate is the NFW velocity profile, Eq. (4.4). We fitted the RC of the Orion dwarf by adjusting M_{vir} and M_D. The resulting best-fit values are $M_{vir} = (2.5 \pm 0.5) \times 10^{11}$ $M_\odot$ and $M_D = (6.9 \pm 1.7) \times 10^8$ $M_\odot$, but since $\chi^2_{\rm red} \simeq 3.3$, i.e. the fit is unsuccessful, the best-fit values of the free parameters and those of their fitting uncertainties do not have a clear physical meaning. We plot the results in the lower panel of Fig. 4.6. The NFW model, at galactocentric radii r<2 kpc, overestimates the observed circular velocity (see Fig. 4.6 lower panel).

Finally, we will consider an alternative to Newtonian gravity, MOND, which has been proposed in Refs. [143, 144] and presented in Section 4.2. In particular, for this analysis we adopt the new form for the interpolation function, Eq. (4.12). No results of this analysis would change by adopting the "standard" MOND interpolation function, Eq. (4.10).

The best-fitting MOND mass model is shown in Fig. 4.7. The model total RC (cyan line) completely fails to match the observations. We fix the stellar mass M_D at $M_D = 2.6 \times 10^8 M_\odot$. If we let the disk mass becomes higher, covering the

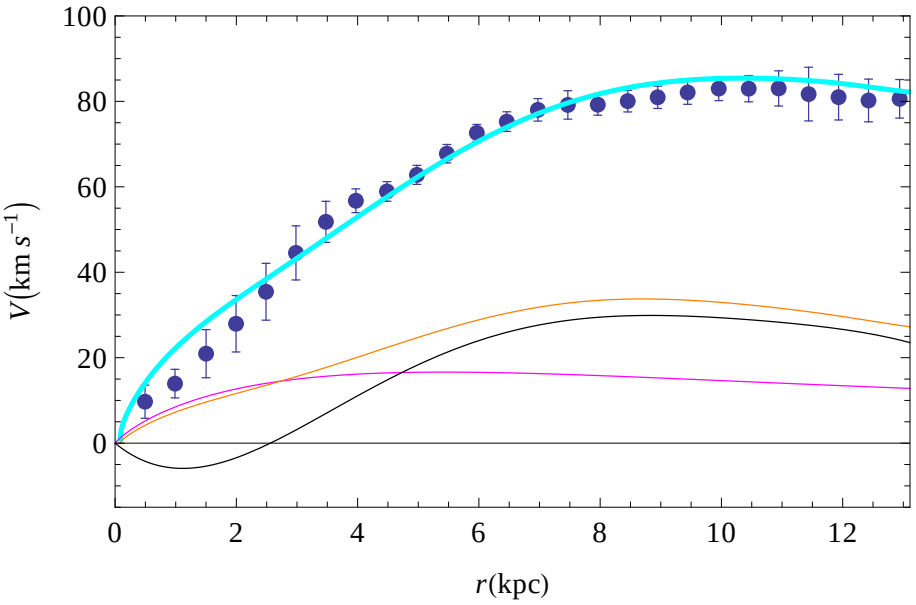

Figure 4.8: MOND model of Orion dwarf spiral for a distance from the galaxy of ∼10 Mpc, a factor 1.9 farther than the nominal distance. The legend to the lines is the same of Fig. 4.7. The resulting disk mass is $M_D = 4.2 \times 10^8$ $M_\odot$.

mass range estimated in Ref. [166], the fit is not even able to reproduce the RC at inner radii. Note that in the MOND formalism, the distance of the galaxy and the amount of gaseous mass are both crucial in deriving the model RC. To quantify the discrepancy of these observations with the MOND formalism, note that only if the Orion dwarf were 1.9 times more distant than the current estimate we would obtain a satisfactory fit to the RC (see Fig. 4.8).

4.3.5 Discussion

The Orion dwarf galaxy is representative of a population of dwarfs with a steep inner RC that gently flattens at the edge of the gas disk. The observed kinematics imply the presence of large amounts of DM also in the central regions. We have used new H I observations of the Orion dwarf to analyze its kinematics and derive the mass model. The derived RC is very steep and it is dominated by DM at nearly all galactocentric radii. Baryons are unable to account for the observed kinematics and are only a minor mass component at all galactic radii.

We have used various mass modeling approaches in this work. Using the NFW halo, we find that this model fails to match the observed kinematics (as occurs in other similar dwarfs). We show that non-circular motions cannot resolve this discrepancy. Then we modeled the galaxy by assuming the URCH parametrization of the DM halo. We found that this cored distribution fits very well the observed kinematics. Orion is a typical dwarf showing a cored profile of the DM density and the well-known inability of DM halo cuspy profiles to reproduce the observed kinematics. Finally, we find that the MOND model

is discrepant with the data if we adopt the literature galaxy distance and gas mass. The kinematic data can be reproduced in the MOND formalism if we allow for significant adjustments of the distance and/or value of the gas mass. Let us point out that the present interferometric observations may miss some of the objects's H I flux, although this may be limited in that the cubes do not have significant negative bowls. Obviously, for bigger values of the H I mass, the distance at which the baryon components would well fit the data will also somewhat decrease. It is worth stressing that there is a galaxy distance (albeit presently not-favored) for which MOND would strike an extraordinary success in reproducing the observed kinematics of the Orion dwarf.

The Orion dwarf has a favorable inclination, very regular gas kinematics, a small asymmetric drift correction, a well-understood baryonic matter distribution, and a large discrepancy between luminous and dynamical mass. All of these characteristics make this system a decisive benchmark for the MOND formalism and a promising target for further detailed studies. Of particular value would be a direct measurement of the distance (for example, infrared observations with the Hubble Space Telescope would allow a direct distance measurement via the magnitude of the tip of the red giant branch).

Chapter 5

The Bias factor and its implications in Cosmology

Observational data of the distribution of structures on large scales are one of the most important sources for understanding the properties and the statistics of the primordial density fluctuation field and the processes of structure formation. In particular, observational evidence show that the initial fluctuation field is nearly a Gaussian random field. Furthermore, these observations play a fundamental role in testing theoretical predictions of a cosmological model. Nevertheless, a main obstacle in comparing observations and theoretical predictions exists, Biasing.

DM is estimated to be about 84% of the total matter content in the Universe and luminous galaxies are considered biased tracers of the underlying distribution of this dark component [177, 178]. This relation is called bias. The real bias is very complicated as it depends on galaxy formation, galaxy types and it might be influenced by the redshift.

Let us define the (dark) matter density fluctuation field [1] and the number density fluctuation field of the biased tracer δ_b, as

$$\delta_m \equiv \frac{\rho_m - \overline{\rho}_m}{\overline{\rho}_m}, \qquad \delta_b \equiv \frac{n_b - \overline{n}_b}{\overline{n}_b}, \tag{5.1}$$

where ρ_m is the matter mass density, $\overline{\rho}_m$ is the mean background mass density, n_b is the tracer number density and $\overline{n}_b$ is the mean number of tracers. The relation between the spatial distribution of the biased tracer δ_b and the underlying matter density field δ_m can be defined through the bias factor

$$b \equiv \frac{\delta_b}{\delta_m}, \tag{5.2}$$

where with tracer we refer to galaxies, halos (in the case of halo model [179, 180, 181, 182]) or peaks (in the case of peaks model [177, 183, 178, 184, 185, 186]), depending on the model. As an example, in the current picture of structure formation, the halo model [182] provides a good description of bias factor. Galaxies

[1] In the following we will refer to the underlying Dark Matter distribution/mass density as matter distribution/mass density.

are considered to form in dark halos, which distribution follows the underlying matter one. A density profile for the DM in halos is obtained in N-body simulations and it is found to follow the NFW profile (Eq. (4.3)). In this context, it is clear that the physical properties of a galaxy are strongly determined by the halo's characteristics. Following this model, it is possible to define two types of bias: one between galaxies and halos distributions, called galaxy bias, and one between halos and the underlying matter distribution, the halo bias. The galaxy bias results to be fully specified through the halo bias once the halo occupation statistics is considered.

In general the bias factor can be deterministic or stochastic, linear or non-linear, constant or scale dependent, local or non-local. The real bias is expected to be a non-linear and stochastic function [187, 180, 188]. Nevertheless, on large scales the assumption that the bias is linear and deterministic is reasonable as for example, it arises in the peak model where the formation of non-linear structures is associated with peaks in the initial density fluctuation field. It has been shown that with this assumption the bias is scale independent on large scales, allowing to write the bias as a constant [189].

Models of bias have been proposed in the last years. They can be roughly divided in two groups, the Eulerian [190, 191, 192] and Lagrangian bias models. Lagrangian models are more physical motivated than the Eulerian ones, indeed the halo model [179, 180, 181, 182] and peaks model [177, 183, 178, 184, 185, 186] belong to the Lagrangian models. Let us explain the main difference between them. The Lagrangian model describes the bias of the initial number density field of the tracer w.r.t. the initial mass distribution of the dark component. On the other hand, the Eulerian bias describes the relation between these distributions after their evolution. At this point one might argue that the two bias factors can be related to each other, as the Eulerian fields are the result of the evolution of the initial Lagrangian ones. A full treatment of this point can be found in Refs. [193, 194, 195, 196]. Here, we will briefly recap the arguments therein. Initial fields evolve through non-linear processes. Then, the final mass density field is the result of the non-linear evolution of the initial mass density field as well as the final number density field arises from the non-linear process of evolution and formation of structures of the initial number density field. As the bias involves non-linear evolutions, which are non-local processes, this results is a non-local bias. In this regard, models of Lagrangian and Eulerian bias can be related to each other only when the bias is non-local. However, when considering sufficiently smoothed scales, local models have been considered for both Lagrangian and Eulerian bias. In that case, the number density field can be assumed to be locally determined by the matter density field, i.e. local bias. Let us note that local Lagrangian bias can be expressed by Eulerian bias only if that one is non-local.

Let us conclude the Section with a comment on the bias in theories which deviate from General Relativity. We will refer to them as Modified Gravity Theories (MG). A complete description of these theories is in Part III. Here, we want to point out that the bias factor for such theories is scale dependent even on large-linear scales, $b(t,k)$ [197, 198, 199]. In Ref. [197], the authors pointed out the following expression for a scale dependent bias in Fourier space

$$b(a,k) = 1 + (b_0 - 1)\frac{\delta_m(a_i,k)}{\delta_m(a,k)}, \tag{5.3}$$

where b_0 is the initial bias at some early time a_i, which is assumed to be scale independent. The reasons of a scale dependent bias and a modification in the clustering of galaxies are due to the scale dependence of the growth factor $D(t,k)$ and of a non-constant critical density δ_{sc} in the spherical collapse. In General Relativity, the growing solution for the density evolution equation can be straightforwardly obtained from the linearized Poisson and Euler equations. It is $\delta_m(t,k) = D(t)\delta_m(k)$, then the linear growth factor is a scale-independent function $D(t)$ on large-linear scales. Therefore, from Eq. (5.3) an initially scale independent bias, b_0, will remain scale independent. This result is no longer valid when considering deviations from GR. One of the effect of modifying GR is that in the newtonian limit the Poisson equation is defined through an effective newtonian function that is scale dependent, $G_{eff}(t,k)$, and the equation of evolution for the density perturbation in Fourier space results

$$\ddot{\delta}_m + 2H(t)\dot{\delta}_m = G_{eff}(k,t)\delta_m, \tag{5.4}$$

where dots stand for derivation w.r.t. time. This actually introduces a scale dependence in the growth factor, $\delta_m = D(t,k)\delta_m^i$ [198, 197, 200, 201, 202]. Furthermore, structures form at the peak of the density fluctuation field, when the initial overdensity is such that $\delta > \delta_{sc}$ and the collapse can occurs, δ_{sc} is the critical threshold for the spherical collapse. In GR, δ_{sc} does not depend on scale and it is the same for all masses, hence it is said to be a flat barrier. Successful MG should recover GR on small scales, where GR is well tested. Therefore, a screening mechanism is necessary in order to hide the modification (see Part III for details and examples). This practically introduces a scale beyond which GR is modified. The screening scale, R_S, depends on the particular theory considered. It is expected that if screening mechanisms are at play, they might change the scale at which the spherical collapse occurs. Usually, for MG the barrier depends on the mass of the density perturbation, which in turn depends on R_S [197, 202, 203, 204]. In Ref. [202], the authors investigated how the modification to standard gravity due to a Yukawa-like potential affects the spherical collapse. They found that patches which are smaller than R_S are unaffected by the modification, on the contrary those which are bigger than R_S do. In particular for that model, δ_{sc} is strongly mass dependent for masses larger than $\sim 10^{14}$ h^{-1} $\mathrm{M}_\odot$, where $\mathrm{M}_\odot$ is the solar mass. Let us note that the mass at $R_S = 5$ h^{-1} Mpc is $\sim 5\,10^{13}$ h^{-1} $\mathrm{M}_\odot$. Then, as expected δ_{sc} is a moving barrier only for patches with $r > R_S$, instead smaller halos are not affected by modification. In conclusion, modifications to the theory of General Relativity affect the clustering of structure in a such a way the bias factor is scale dependent even on linear scale.

5.1 Lagrangian bias in the local bias model

In the local bias model, the abundance of the biased tracers at a given position is assumed to be related to the mass at the same position. The simplest version of this model, in which the smoothed overdensity field of the biased tracers δ_b is treated as though it were a deterministic function of the (similarly smoothed) real-space mass overdensity field δ_m, has been the subject of much study [205, 190, 192]. Following Ref. [191], it has become common to write the local model

as

$$\delta_b = f(\delta_m) = \sum_{i>0} \frac{b_i}{i!} (\delta_m^i - \langle \delta_m^i \rangle), \tag{5.5}$$

where b_i is the bias coefficient of order i. Note that this model ensures $\langle \delta_b \rangle = 0$ by subtracting-off the $\langle \delta_m^i \rangle$ terms. One of the points we make in what follows is that one should, instead, normalize using a multiplicative factor which ensures that $\langle 1 + \delta_b \rangle = 1$. I.e., given an expansion of the form (5.5), one should always work with

$$\delta_B \equiv \frac{1 + \delta_b - \langle 1 + \delta_b \rangle}{\langle 1 + \delta_b \rangle}. \tag{5.6}$$

Although the model was invoked to describe the bias with respect to the late-time nonlinear Eulerian field δ_m^E, since it is only invoked on large scales, it is often assumed, and sometimes explicitly used, to describe the bias with respect to the initial Lagrangian field δ_m^L (on large scales, these are expected to be similar). However, the two best studied models of bias with respect to the Lagrangian field – those associated with peaks, and patches which form halos, in a Gaussian random field – behave rather differently from naive expectations based on the local bias model. In particular, in the local bias model calculation of the cross-correlation between the biased tracers and the initial field, $\langle \delta_b \delta_m \rangle$, one proceeds by writing the bias function as a Taylor series, and then expanding order by order in δ_m. This means that one expects higher-order terms to contribute. However, for peaks and in Gaussian initial conditions, the exact answer is $\langle \delta_b \delta_m \rangle = b_1 \langle \delta_m^2 \rangle$ [186]. Therefore, in the expansion referred to above, all the higher-order terms must cancel out. We show below that this is also true for another popular choice of the bias – a Lognormal mapping between the biased field and δ_m – and then that this is generically true in models where the bias is local and deterministic with respect to the initial Gaussian random field. I.e., the cross-correlation is always only linearly proportional to the auto-correlation signal of the DM, although, in general, the linear bias factor need not equal b_1 of the Taylor series. We then show that the auto-correlation function of the biased tracers can always be written as a Taylor series in the auto-correlation function of the original (unbiased) mass fluctuation field; derivatives and convolutions do not enter. Along the way, our analysis connects to recent work on renormalized bias [206], showing, e.g., that this renormalization is required if the Lognormal mapping is to make sensible predictions.

In the following, we present the results in Ref. [207]. The work is in collaboration with R. K. Sheth and it is organized as follows. In Section 5.1.1 we discuss the Lognormal mapping, since it turns out that all quantities of interest can be computed exactly (no truncation of the sums is required). These exact expressions exhibit some curious properties which are not obvious if one truncates the sums. Then we show that how one normalizes such purely formal expansions plays an important role, and why Eq. (5.6) is to be preferred over Eq. (5.5). Section 5.1.1 explores a more complex example in which some of this simplicity is lost, before showing the general result in Section 5.1.2. Section 5.1.3 shows how to proceed if the full expansion is not available, so one is constrained to work with a truncated series. Section 5.1.3 connects this analysis to some of the earliest work on this subject (Ref. [205]), discussing how the coefficients of the Taylor series expansion of δ_B in terms of δ_m are related to those obtained from expanding ξ_{BB} in terms of ξ_{mm}. Section 5.1.4 discusses halo bias in the

context of these results, and Section 5.1.4 revisits a technical point about halo bias, first made by Ref. [208] but often overlooked, which complicates the use of cross-correlations for testing the hypothesis that Lagrangian halo bias is indeed local, a subject of much recent interest [209, 194, 195, 210]. Finally, we discuss our results in Section 5.1.5.

5.1.1 The Lognormal model and the usual expansion

We begin with the usual model, Eq. (5.5), with $\delta_m = \delta_L$ to emphasize the fact that the mass field is for Lagrangian space, and recall that the $\langle \delta_L^k \rangle$ terms are inserted to guarantee that $\langle \delta_b \rangle = 0$. As an explicit example, we will consider the Lognormal transformation, which aims to map $1 + \delta_b \to \exp(b\delta_L)$. The parameter b is the one free parameter of this transformation: large values of b strongly enhance large values of δ_L.

Since the coefficients in the Taylor series are simply $b_k = b^k$, for a Gaussian distribution of δ_L, the additive correction terms can be summed explicitly:

$$\sum_{k>0} \frac{b_k}{k!} \langle \delta_L^k \rangle = \sum_{k>0} \frac{b^k}{k!} \langle \delta_L^k \rangle = \exp(b^2 \langle \delta_L^2 \rangle / 2) - 1. \tag{5.7}$$

This means that, in this expansion, the Lognormal model is really

$$\delta_b = \exp(b\delta_L) - 1 - [\exp(b^2 \langle \delta_L^2 \rangle / 2) - 1] = \exp(b\delta_L) - \exp(b^2 \langle \delta_L^2 \rangle / 2). \tag{5.8}$$

Notice that, as a result of this additive normalization term, $\delta_b \neq 0$ when $\delta_L = 0$.

The cross-correlation between the biased field and the original one can also be done analytically:

$$\langle \delta_b \delta_L \rangle = \sum_{k>0} \frac{b_k}{k!} \langle \delta_L^{k+1} \rangle = b \langle \delta_L^2 \rangle \exp\left(\frac{b^2 \langle \delta_L^2 \rangle}{2} \right) \tag{5.9}$$

where the final expression shows the result of evaluating the sum for the Lognormal coefficients. Finally, the auto-correlation, which can also be done analytically, yields:

$$\langle \delta_b^2 \rangle = \langle [\exp(b\delta) - \exp(b^2 \langle \delta_L^2 \rangle / 2)]^2 \rangle = \exp(b^2 \langle \delta_L^2 \rangle)[\exp(b^2 \langle \delta_L^2 \rangle) - 1]. \tag{5.10}$$

The treatment above ensures that $\langle \delta_b \rangle = 0$ by making an additive correction. However, because this additive correction term has, in effect, shifted the mean value of the transformation, one should really account for the fact that the definition of the mean density, with respect to which one would like to define the biased fluctuation field, has also been modified. This modification corresponds to accounting for the fact that, prior to adding these terms, $\langle 1 + \delta_b \rangle \neq 1$.

If one enforces $\langle 1 + \delta_b \rangle = 1$ by using a multiplicative factor rather than by an additive one, then one would write the Lognormal transformation as

$$1 + \delta_b = \exp(b\delta_L) \exp(-b^2 \langle \delta_L^2 \rangle / 2). \tag{5.11}$$

The first term on the right hand side is the same deterministic transformation of the variable as before, and the second, $\exp(-b^2 \langle \delta_L^2 \rangle / 2)$, is the multiplicative

factor that is required to ensure that $\langle 1+\delta_b\rangle = 1$. Note that this factor depends explicitly on the scale L on which the Lognormal transformation occurs, via $\langle\delta_L^2\rangle$. On large scales, $\langle\delta_L^2\rangle \ll 1$, making the overall normalization factor $\to 1$. In this limit, the Taylor series expansion of Eq. (5.11) has coefficients $b_k = b^k$, but otherwise, these coefficients generally pick up $\langle\delta_L^2\rangle$ dependent multiplicative correction factors.

Integrating over the underlying Gaussian distribution of δ_L shows that the cross-correlation between the biased field and the original one is

$$\langle(1+\delta_b)(1+\delta_L)\rangle = 1 + \langle\delta_b\delta_L\rangle = 1 + b\,\langle\delta_L^2\rangle, \tag{5.12}$$

whereas

$$\langle(1+\delta_b)^2\rangle = \exp[b^2\,\langle\delta_L^2\rangle]. \tag{5.13}$$

These expressions differ from Eqs. (5.9) and (5.10) for $\langle\delta_b\delta_L\rangle$ and $\langle\delta_b^2\rangle$ by one and two powers, respectively, of the multiplicative normalization factor associated with the Lognormal transformation (see discussion following Eq. (5.11)). Eq. (5.13) is the usual expression for the relation between the correlation function of the Lognormal field and that of the underlying Gaussian [211], suggesting that the present analysis is correct, and that of the previous Section is not. I.e., normalizing δ_b by subtracting a constant, rather than normalizing $1+\delta_b$ by a multiplicative constant is ill-advised. Moreover, notice that now the cross-correlation function is particularly simple: $\langle\delta_b\delta_L\rangle = b\,\langle\delta_L^2\rangle$, with *no* higher-order terms (Eq. (5.12)).

For what follows, it is useful to write out slightly more general expressions for the cross- and auto-correlations. The cross-correlation between the Lognormally biased field and the original Gaussian one smoothed on a different scale L' than that on which the bias was defined, and separated by a distance r, is

$$\langle\delta_b\delta_{L'}|r\rangle = b\,\langle\delta_L\delta_{L'}|r\rangle = b\,\xi_{LL'}(r), \tag{5.14}$$

where $\xi_{LL'}(r)$ denotes the correlation between the initial field when smoothed on scale L and when smoothed on scale L' and displaced by r. We note again that this expression is exact – it is remarkable that the cross-correlation function is just a linearly biased version of that of the underlying field, despite the fact that the transformation itself was highly nonlinear. Peaks in Gaussian fields exhibit this same simplicity [186]. Note in particular that the linear bias factor is the first term in the Taylor series of δ_b in the $\langle\delta_L^2\rangle \to 0$ limit. We show shortly that, although $\langle\delta_b\delta_{L'}|r\rangle \propto \langle\delta_L\delta_{L'}|r\rangle$ is generic, the constant of proportionality is not necessarily b_1, the first term in the Taylor series of the mapping between δ_b and δ_L.

The cross-correlation between two differently biased tracers b and b', defined using transformations on scales L and L', and separated by r, can also be computed exactly:

$$1 + \xi_{bb'}(r) \equiv \langle(1+\delta_b)(1+\delta_{b'})\rangle = \exp[bb'\,\xi_{LL'}(r)]. \tag{5.15}$$

This can be expanded as a series in $\langle\delta_L\delta_{L'}|r\rangle$ to yield:

$$\xi_{bb'}(r) \approx bb'\langle\delta_L\delta_{L'}|r\rangle + (bb')^2\frac{\langle\delta_L\delta_{L'}|r\rangle^2}{2} + \dots\ . \tag{5.16}$$

Therefore, if $b = b'$ and $L = L'$ then $\xi_{bb}(r) \approx b^2 \xi_{LL}(r)$, and

$$\frac{\langle \delta_b \delta_L | r \rangle^2}{\langle \delta_b \delta_b | r \rangle} \approx \xi_{LL}(r). \tag{5.17}$$

It turns out that this is a generic feature of local Lagrangian bias; it holds even when the constant of proportionality between $\langle \delta_b \delta_L | r \rangle$ and $\langle \delta_L^2 | r \rangle$ differs from b_1 of the Taylor series.

Before moving on, we note that the ratio $\rho^2 \equiv \langle \delta_b \delta_L \rangle^2 / \langle \delta_b^2 \rangle \langle \delta_L^2 \rangle$ is sometimes used to quantify the 'stochasticity' of the bias, where $\rho^2 < 1$ is taken to imply stochasticity. For the Lognormal mapping above, $\rho^2 = x/(\mathrm{e}^x - 1)$ with $x \equiv b^2 \langle \delta_L^2 \rangle$. This equals unity only when $\langle \delta_L^2 \rangle = 0$, despite the fact that the Lognormal mapping is explicitly deterministic. Clearly, ρ^2 is not a good indicator of stochasticity.

Approximate transformation for peaks

Suppose one smoothes a Gaussian random field with a filter of scale L_p. When the peak point process is smoothed with a filter of scale $L \gg L_p$, then Ref. [178] argue that it is useful to think of the smoothed field as defining a peak fluctuation field which is related to that of the initial Gaussian field by

$$1 + \delta_p = \exp(b\delta_L - c\delta_L^2/2) \sqrt{1 + c\langle \delta_L^2 \rangle} \, \exp\left(- \frac{b^2 \langle \delta_L^2 \rangle / 2}{1 + c \langle \delta_L^2 \rangle} \right). \tag{5.18}$$

(Note that we are normalizing using a multiplicative rather than additive factor.) The free parameters b and c are related to the properties of the peak (e.g., its height and curvature); they determine a rather complex normalization factor that, as before, depends on the smoothing scale via $\langle \delta_L^2 \rangle$ and tends to unity on large scales. In this limit, the first few bias coefficients associated with this transformation are $b_1 = b$, $b_2 = (b^2 - c)$, $b_3 = (b^3 - 3bc)$, and $b_4 = (b^4 - 6b^2c + 3c^2)$. (The structure of these terms means that b_k is very similar to the Hermite polynomial $H_k(b)$; in fact $b_k = H_k(b)$ when $c = 1$. This happens because the bias relation has the same form, $\exp(bt - t^2/2)$, as the generating function of the Hermites.) Note that the quantity $b_3 - b_1 b_2 = -2bc \neq 0$, in contrast to the Lognormal studied earlier. This will be matter of discussion in Section 5.1.3.

For this relation, the cross-correlation between such peaks and the field at a different position when smoothed on a different scale is

$$\langle \delta_p \delta_{L'} | r \rangle = \frac{b}{1 + c \langle \delta_L^2 \rangle} \, \xi_{LL'}(r). \tag{5.19}$$

As for the Lognormal transformation, this expression is exact for the peak approximated field we considered, and it is linearly proportional to $\xi_{LL'}(r)$; there are no higher order terms. However, in this case, the constant of proportionality equals the first term in the Taylor series of δ_p only in the $\langle \delta_L^2 \rangle \to 0$ limit; in general, they are different.

When the two smoothing scales are the same, then

$$1 + \langle \delta_p \delta_p | r \rangle = \left[1 - C^2 \, \xi_{LL}^2(r) \right]^{-1/2} \exp\left(\frac{B^2 \xi_{LL}(r)}{1 + C \, \xi_{LL}(r)} \right), \tag{5.20}$$

where

$$B \equiv \frac{b}{1+c\langle\delta_L^2\rangle} \quad \text{and} \quad C \equiv \frac{c}{1+c\langle\delta_L^2\rangle}. \tag{5.21}$$

To leading order in ξ_{LL}, this reduces to

$$\langle\delta_p\delta_p|r\rangle \approx B^2\xi_{LL}(r) + \frac{(B^2-C)^2}{2}\,\xi_{LL}^2(r) + \frac{(B^3-3BC)^2}{3!}\,\xi_{LL}^3(r) + \ldots \tag{5.22}$$

I.e., to leading order this transformation also satisfies Eq. (5.17) even though this bias factor is not the same as the leading order term in the Taylor expansion. On the other hand, if we view this final expression as the Taylor series expansion of the correlation function, then the coefficients of this expansion have the same structure as the $\sigma_L \to 0$ limit of δ_p. We will return to this shortly.

5.1.2 Normalizing density rather than overdensity: The general case

It was shown in the previous Sections that, for Lognormal-like, local, deterministic, Lagrangian bias functions, one should normalize the density of the biased field to unity (using a multiplicative factor), rather than the overdensity to zero (by subtracting a constant). We now study the general case.

If one starts with an arbitrary bias function of the form given by Eq. (5.5), then the correctly normalized bias field is simply defined by Eq. (5.6):

$$\delta_B \equiv \frac{1+\delta_b - \langle 1+\delta_b\rangle}{\langle 1+\delta_b\rangle} = \frac{\sum_{k=1}^{\infty}(b_k/k!)(\delta_L^k - \langle\delta_L^k\rangle)}{\sum_{k=0}^{\infty}(b_k/k!)\langle\delta_L^k\rangle}. \tag{5.23}$$

Note that this renders the coefficient b_0 redundant, so we can set it equal to unity (and redefine all other coefficients in units of b_0). This expression only differs from Eq. (5.5) because of the term in the denominator. In general, $\delta_B \neq 0$ when $\delta_L = 0$.

It is a simple matter to check that this works out correctly for a Lognormal. Moreover, it is straightforward to see that

$$\begin{aligned}\langle\delta_{L'}\delta_B|r\rangle &= \frac{\sum_{k=1}^{\infty}(b_k/k!)\langle\delta_{L'}\delta_L^k|r\rangle}{\sum_{k=0}^{\infty}(b_k/k!)\langle\delta_L^k\rangle} \\ &= \frac{\sum_{k=1}^{\infty}(b_k/k!)\langle\delta_L^{k+1}\rangle/\langle\delta_L^2\rangle}{\sum_{k=0}^{\infty}(b_k/k!)\langle\delta_L^k\rangle}\,\xi_{LL'}(r) \equiv B_L\,\xi_{LL'}(r),\end{aligned} \tag{5.24}$$

where the second equality used the fact that

$$\langle\delta_{L'}|\delta_L\rangle = \delta_L\,\frac{\langle\delta_{L'}\delta_L|r\rangle}{\langle\delta_L^2\rangle} = \delta_L\,\frac{\xi_{LL'}(r)}{\sigma_{LL}^2} \tag{5.25}$$

to write

$$\begin{aligned}\langle\delta_{L'}\delta_L^k|r\rangle &= \int d\delta_L \mathcal{P}(\delta_L)\,\delta_L^k \int d\delta_{L'}\mathcal{P}(\delta_{L'}|\delta_L)\,\delta_{L'} = \int d\delta_L\mathcal{P}(\delta_L)\,\delta_L^k\langle\delta_{L'}|\delta_L\rangle \\ &= \int d\delta_L\,\mathcal{P}(\delta_L)\delta_L^k\,\delta_L\,\frac{\xi_{LL'}(r)}{\langle\delta_L^2\rangle} = \frac{\langle\delta_L^2\rangle}{\langle\delta_L^{k+1}\rangle}\,\xi_{LL'}(r).\end{aligned} \tag{5.26}$$

Equation (5.24) shows that $\langle \delta_{L'} \delta_B | r \rangle$ is linearly proportional to $\xi_{LL'}(r)$, where the final equality defines the constant of proportionality B_L. Note that this is an exact statement, valid for any r, L or L', and for any local deterministic bias function. In particular, there is no requirement that r be large compared to either L or L', nor that L' be larger than the scale L on which the local transformation from the DM to the biased field is (assumed to be) monotonic and deterministic. Furthermore, notice that, although $B_L \neq b_1$ in general, they are indeed equal in the limit $\langle \delta_L^2 \rangle \to 0$. (Our Eq. (5.24) is consistent with Eq. (10) of Ref. [189], in the Lagrangian bias limit in which all their $C_{pq} = 0$; but our formulation highlights the fact that, in their expansion, all the higher order terms are proportional to powers of $\langle \delta_L^2 \rangle$, whereas none are proportional to powers of ξ.)

For similar reasons the auto-correlation function of the biased tracers will reduce to a series of the form

$$\langle \delta_{B'} \delta_B | r \rangle = B_L^2 \, \xi_{LL}(r) + \frac{C_L}{2} \, [\xi_{LL}(r)]^2 + \dots \tag{5.27}$$

This means that, to lowest order, Eq. (5.17) is satisfied even in the general case. Note that the auto-correlation function of the biased tracers can always be written as a series in ξ. E.g., terms involving derivatives or convolutions of ξ do not appear. This means that the power spectrum of a locally biased tracer will generically involve convolutions of the original $P(k)$. In this sense, local bias is simpler in real space than it is in Fourier space.

5.1.3 Renormalized bias

The analysis above highlighted the fact that it was important to include the multiplicative normalization factor when enforcing $\langle \delta_b \rangle = 0$. We illustrated this using the Lognormal, for which all the sums could be performed analytically. The question now arises as to what to do when this cannot be done.

The analysis above suggests that one should redefine the mean density, and hence all bias factors, order by order. This corresponds to truncating Eq. (5.6) rather than Eq. (5.5):

$$\delta_B^{(j)} = \frac{1 + \delta_b - \langle 1 + \delta_b \rangle_j}{\langle 1 + \delta_b \rangle_j} = \frac{\sum_{k=1}^{j} (b_k/k!)(\delta_L^k - \langle \delta_L^k \rangle)}{\sum_{k=0}^{j} (b_k/k!) \langle \delta_L^k \rangle}. \tag{5.28}$$

Hence, the cross-correlation between the mass and biased fields is

$$\langle \delta_{L'} \delta_B^{(j)} | r \rangle = \frac{\sum_{k=1}^{j} (b_k/k!) \langle \delta_L^k \delta_{L'} | r \rangle}{\sum_{k=0}^{j} (b_k/k!) \langle \delta_L^k \rangle}. \tag{5.29}$$

To 4th order in δ_L, this is

$$\begin{aligned} \langle \delta_{L'} \delta_B^{(4)} | r \rangle &= \frac{b_1 \, \langle \delta_{L'} \delta_L | r \rangle + (b_3/3!) \, \langle \delta_{L'} \delta_L^3 | r \rangle}{1 + (b_2/2) \langle \delta_L^2 \rangle + (b_4/4!) \langle \delta_L^4 \rangle} \\ &= \left[b_1 + \left(\frac{b_3}{2} - \frac{b_1 b_2}{2} \right) \langle \delta_L^2 \rangle \right] \xi_{LL'}(r) \equiv b_\times^{(4)} \xi_{LL'}(r), \end{aligned} \tag{5.30}$$

where the final equality defines $b_\times^{(4)}$. This differs from truncating Eq. (5.5) because of the term which is proportional to $b_1 b_2$. For the Lognormal transformation ($b_k = b_1^k$), $b_3 = b_1 b_2$ so the term that is higher order in σ is zeroed out in this expansion, whereas it would survive if we had started from Eq. (5.5). Thus, this approach correctly gets $\langle \delta_L \delta_B^{(4)} \rangle = b\,\xi(r)$. In fact, one can show that, for the Lognormal, $\langle \delta_L \delta_B^{(j)} \rangle = b \langle \delta_L^2 \rangle$ for any j. In this sense, this treatment is a significant improvement on the usual truncation of Eq. (5.5). However, since $b_3 \neq b_1 b_2$ in general, this approach would also lead one to conclude erroneously that the cross-correlation includes higher order terms when it does not. For example, for the approximate peaks-bias relation of Eq. (5.18), $b_3 - b_1 b_2 = -2bc \neq 0$. On the other hand, note that this expression returns $b_\times^{(4)} \equiv b - 2bc\langle\delta_L^2\rangle/2 = b(1 - c\langle\delta_L^2\rangle)$ which is indeed the exact answer, $b/(1 + c\langle\delta_L^2\rangle)$, expanded to first order in $\langle\delta_L^2\rangle$. That is to say, although the renormalization approach suggests more complexity than is present in the exact answer, it is at least self-consistent.

A similar calculation for the auto-correlation yields

$$\langle \delta_B^{(4)} \delta_B^{(4)} | r \rangle \equiv \xi_{bb}^{(4)}(r) = (b_\times^{(4)})^2\, \xi_{LL}(r) + \frac{b_2^2}{2}\, \xi_{LL}(r)^2. \tag{5.31}$$

Note that although truncating Eq. (5.5) has the same form, in this case, the coefficients are correct for a Lognormal, illustrating again that this is a better approach.

We are not the first to advocate normalizing by a multiplicative factor. Ref. [206] noted that this was advisable, especially in the context of truncated expansions. However, that analysis did not highlight the fact that this makes the Lagrangian bias so simple (our Eq. (5.24)). Rather, Ref. [206] went on to consider the implications in Fourier space, arguing that the $k = 0$ limit of the term which scales as $b_2^2/2$ should be removed from the definition of the bias, and instead absorbed into a shot-noise like term. This procedure has the virtue of making the bias defined by the auto-correlation equal the square of that defined by the cross-correlation by definition even in Fourier space, which is the scaling satisfied by the exact answer. In Ref. [212], it has bee argued that this may not be the best way to think on $b_2^2/2$ (or the higher order bias coefficients).

Relation to Szalay (1988)

In all essential respects, the analysis above is simply a restatement of results in Ref. [205]. For $y \equiv \delta_L / \langle \delta_L^2 \rangle^{1/2}$, Szalay assumed that the bias function $G(y)$ could have non-negative values only, and that

$$\langle G(y) \rangle = \int dy\, G(y)\, \frac{e^{-y^2/2}}{\sqrt{2\pi}} = 1. \tag{5.32}$$

Because $G \geq 0$, and $\langle G \rangle = 1$, his G is, in effect, our $1 + \delta_B$ of Eq. (5.23). He then expanded G in terms of Hermite polynomials:

$$G(y) = \sum_{k=0}^{\infty} \frac{B_k}{k!}\, H_k(y)\,, \tag{5.33}$$

where

$$B_k = \int dy\, \frac{e^{-y^2/2}}{\sqrt{2\pi}}\, G(y)\, H_k(y)\,, = \langle G(y)\, H_k(y) \rangle \tag{5.34}$$

and

$$H_k(y) = e^{y^2/2}\left(-\frac{d}{dy}\right)^k e^{-y^2/2}, \qquad \text{with} \qquad \langle H_m(y)\, H_n(y)\rangle = \delta_{nm}\, m!. \quad (5.35)$$

The orthogonality of the Hermite polynomials allowed him to show that

$$\begin{aligned}\langle G(y_1)G(y_2)\rangle &= \int dy_1\, \frac{e^{-y_1^2/2}}{\sqrt{2\pi}} \int dy_2\, \frac{e^{-v}}{\sqrt{2\pi(1-w_{12}^2)}} \sum_{k=0}^{\infty} \frac{B_k}{k!} H_k(y_1) \sum_{i=0}^{\infty} \frac{B_i}{i!}\, H_i(y_2) \\ &= \sum_{k=0}^{\infty} \frac{B_k^2}{k!}\, w_{12}^k\,, \end{aligned} \quad (5.36)$$

where $v = (y_2 - w_{12}y_1)^2/2(1-w_{12}^2)$ and $w_{12} \equiv \langle y_1 y_2|r\rangle \equiv \xi_{LL}(r)/\sigma_{\rm L}^2$. Comparison with Eq. (5.27) shows that his B_k are our B_L, C_L, etc., so they are complicated sums over the (renormalized) bias factors. This means they are, in general, $\sigma_{\rm L}$ dependent combinations of the coefficients b_k of the Taylor series expansion of δ_h on scale L.

Szalay did not compute the cross-correlation function, but it is straightforward to see that

$$\begin{aligned}\Big\langle y_2\, G(y_1)\Big\rangle &= \int dy_1\, \frac{e^{-y_1^2/2}}{\sqrt{2\pi}}\, w_{12}\, y_1 \sum_{k=0}^{\infty} \frac{B_k}{k!} H_k(y_1) \\ &= w_{12}\left\langle \sum_{k=0}^{\infty} \frac{B_k}{k!} H_k(y_1) H_1(y_1) \right\rangle \\ &= w_{12}\left\langle B_1\, H_1(y_1)^2 \right\rangle = B_1\, w_{12}, \end{aligned} \quad (5.37)$$

where we have used the fact that $H_1(y) = y$ and the orthogonality of the Hermite polynomials to simplify the expressions. Notice that the tracer-mass cross-correlation is indeed just linearly proportional to the auto-correlation of the mass, and the square of it is the leading order term of the auto-correlation function, consistent with Eq. (5.17).

We remarked earlier that the B_k values depend on the scale on which the transformation is applied. It is a simple matter to check that setting $B_k = (b\sigma_L)^k$ yields the correctly normalized Lognormal mapping considered earlier (Eq. (5.11)). Notice that in this case B_k is a separable function of a scale dependent piece σ_L^k, and a constant piece whose value is given by the large scale $\sigma_L \to 0$ limit of the Taylor series expansion of δ_h. That is to say, if one expands the (Lagrangian space) halo auto-correlation function in powers of the mass correlation ξ_{LL}, then the coefficient of the kth order term in the expansion is simply B_k^2, and this term is independent scale L, even though the bias coefficients in the Taylor expansion of the field $1 + \delta_h(\delta_L)$ itself do depend L. Therefore, the bias parameters estimated from a scatter plot of $1 + \delta_h$ versus δ_L 'run' with scale L, whereas those estimated from the correlation function do not.

We will return to this in the next Section, but note that it is not generic. E.g., for the peaks transformation of Eq. (5.18), $B_1 = B\,\sigma_L$, $B_2 = (B^2 - C)\,\sigma_L^2$, $B_3 = (B^3 - 3BC)\,\sigma_L^3$ etc., where B and C were defined in Eq. (5.21). I.e., the

B_k satisfy the same relations between the rescaled values B and C that the b_k do for b and c, but B and C differ from the peak-background split values (i.e. the large scale Taylor series coefficients of δ_h) b and c by a factor of $1 + c\sigma_L^2$.

5.1.4 Relation to halo bias from the excursion set approach

The analysis above made the point that the leading order bias factor for the cross-correlation is the leading order term in the Taylor series expansion of δ_h only in the (large-scale) $\sigma_{\rm L} \ll 1$ limit. So it is somewhat surprising that the differences between these two are sufficiently small as to have not attracted significant attention. In part, this is because the large scale halo bias factors, as determined from the excursion set approach, satisfy

$$b_k = \nu^{k-1}\, H_{k+1}(\nu)/\delta_c^k, \qquad \text{where} \qquad \nu \equiv \delta_c/\sigma_h \tag{5.38}$$

[213]. Here σ_h is related to the smoothing scale R_h which contains the halo mass M_h (i.e. $\bar\rho\,(4\pi/3)\,R_h^3 = M_h$), and δ_c is the overdensity associated with halo formation. Since these bias factors were determined from a physically motivated model, rather than an arbitrary formal expansion, they are already correctly normalized, in the sense that $\langle 1+\delta_h\rangle = 1$. This makes the renormalized δ_B of Eq. (5.23) equal to the original δ_h, so the renormalized large scale bias factors are simply those in Eq. (5.38).

What is remarkable about the excursion set approach is that, for any smoothing scale (larger than that on which the halos were defined) the associated B_k satisfy

$$B_k = \sigma_{\rm L}^k\, b_k \tag{5.39}$$

[186, 210]. I.e., just as for the Lognormal mapping (for which $b_k = b^k$), the B_k are separable functions of the scale independent piece b_k and the scale dependent piece $\sigma_{\rm L}$. Note that this separability is not general; e.g., it does not apply for the mapping in Eq. (5.18). When $k = 1$, this separability implies that $\langle \delta_h \delta_{\rm L} | r\rangle = \sigma_{\rm L}\, B_1\, w(r) = b_1 \sigma_{\rm L}^2 w(r) = b_1\, \xi(r)$. I.e., for excursion set halos, the cross-correlation measurement returns the large scale linear bias factor b_1 whatever the smoothing scale L, and whatever the separation r.

Inserting Eq. (5.39) in Eq. (5.36) indicates that if one expanded the halo auto-correlation function in powers of the mass correlation, then the coefficient of the kth order term in the expansion is simply b_k^2. Note again that this statement is not restricted to large scales. This simple prediction for halos in Lagrangian space has not been noticed before.

In addition, the higher order correlations of the halos are given by Szalay's Eq. (11). Like the two-point function, these can be written as sums of products of ξ. To order ξ^3, the three point function is given by

$$\begin{aligned}\zeta_{123} = \quad & b_1^2 b_2\,(\xi_{12}\xi_{23} + \xi_{23}\xi_{13} + \xi_{12}\xi_{13}) + b_2^3\,\xi_{12}\xi_{23}\xi_{13} \\ & + b_1 b_2 b_3 \left[\xi_{12}^2\,\frac{\xi_{23}+\xi_{13}}{2} + \xi_{23}^2\,\frac{\xi_{12}+\xi_{13}}{2} + \xi_{13}^2\,\frac{\xi_{12}+\xi_{23}}{2}\right], \end{aligned} \tag{5.40}$$

where ξ_{ij} denotes the two-point correlation function of the mass, smoothed on scale L at separation r_{ij}. For equilateral triangles, this simplifies to

$$\zeta_{\rm eq}(r) = 3\, b_1^2 b_2\, \xi_{LL}^2(r) + b_2^3\, \xi_{LL}^3(r) + 3\, b_1 b_2 b_3\, \xi_{LL}^3(r). \tag{5.41}$$

On the appropriate ensemble over which to average

The analysis above, like essentially all previous analyses in the literature to date, makes a technical assumption about how to compute the ensemble averages in Lagrangian space. Namely, it assumes that, for Gaussian initial conditions, this average is over a Gaussian probability distribution function. However, although averaging over the initial (Gaussian) pdf is technically correct for peaks, it is known to be incorrect for patches which are destined to form halos [208]. This is because, in the excursion set definition of halos, δ_L is required to be less than δ_c on all scales L larger than that on which the halo was defined: this constraint on all larger scales is, in effect, a nonlocal requirement. In practice, this means that the use of a Gaussian distribution for δ_L is, formally, inappropriate. As shown in Ref. [208] (see their Eq. (17)), a more careful treatment of this averaging, with the appropriate replacement of the Gaussian pdf yields

$$\delta_c \frac{\bar{\xi}_\times}{\sigma_L^2} = H_2(\nu) + (\nu_{10}^2 + 1)\,\mathrm{erfc}(\nu_{10}/\sqrt{2}) - \sqrt{2\nu_{10}^2/\pi}\, e^{-\nu_{10}^2/2}, \tag{5.42}$$

where $\nu_{10}^2 = \nu^2\,(\sigma_h^2/\sigma_L^2 - 1)$. When $\sigma_L \ll \sigma_h$, this expression asymptotes to $\bar{\xi}_\times \to b_1\,\sigma_L^2$ (recall that $b_1 = H_2(\nu)/\delta_c$), but in general the simple constant linear bias of the cross-correlation function between halos and mass is spoilt. E.g., as $\sigma_L \to \sigma_h$, the cross-correlation $\bar{\xi}_\times$ tends to δ_c.

It is a simple matter to extend this analysis to see how averages over the higher order Hermite polynomials associated with the higher order bias factors are modified, but this is beyond the scope of the present work. Measurements in simulations are needed to see if the range of scales over which the simple Gaussian averaged estimate is accurate – and hence all the power of the Hermite polynomials – is large enough to be interesting.

5.1.5 Discussion

In local bias models it is assumed that the biased field $1 + \delta_b$ can be written as a function of the underlying density field at the same position. We showed that, if the underlying field is Gaussian, then the cross-correlation between the biased field and the original one is linearly proportional to the auto-correlation function of the original field. This is an exact result, valid on all scales, and is not a consequence of truncating expansions, etc., as most previous treatments assume. While this is implicit in some previous work (e.g. Ref. [189]), it has not been highlighted before.

If one has been careful to ensure that $\langle 1 + \delta_b \rangle = 1$ (by using Eq. (5.6) rather than Eq. (5.5)), then the constant of proportionality is easily related to the first coefficient of the Taylor series expansion of the biased field, although they are not equal in general (Eq. (5.24)). In addition, we showed that, to leading order, the ratio of the square of the cross-correlation to the auto-correlation of the bias tracers equals the correlation function of the underlying field (Eqs. (5.27) and (5.17)).

We also explored the consequences of truncating these expansions, demonstrating that it is better to renormalize all truncated expansions (Eq. (5.28)) than to not. In this respect, our results agree with Ref. [206]. Indeed, although

our work has concentrated on Lagrangian bias, the multiplicative normalization (our Eq. (5.6)) also holds also for Eulerian mass field, although providing an explicit expression when the mass field is not gaussian is more complicated (see Ref. [206] for the implications in Fourier space).

Expanding the biased field using Hermite polynomials rather than powers of the overdensity, as was done by Ref. [205], provided a easy way to see a number of our results for local bias in the initial, Lagrangian, Gaussian field. Although the coefficients B_k of this expansion are functions of the scale on which the bias transformation is applied (Eq. (5.33)), for the Lognormal distribution, as well as for excursion set halos, the scale dependence of these coefficients is trivial: $B_k = b_k \sigma_{\rm L}^k$ (Eq. (5.39)), where b_k are the scale-independent peak-background split bias factors. (The Lognormal has $b_k = b^k$, whereas excursion set halos have b_k given by Eq. (5.38).) Therefore, if one expands the (Lagrangian space) halo auto-correlation function in powers of the mass correlation, then the coefficient of the kth order term in the expansion is simply b_k^2 (Eq. (5.36)). These coefficients for the expansion of $1+\xi_{hh}$ in powers of ξ_{LL} are independent of scale L, even though the bias coefficients in the Taylor expansion of the field $1+\delta_h(\delta_L)$ itself do 'run' with L. This property of halo bias in Lagrangian space has not been emphasized before.

The 'running' of the $1 + \delta_h(\delta_L)$ bias factors is most easily understood by noting that the Hermite polynomials arise naturally if one phrases the question of local bias in Fourier rather than real space [193], a connection made recently in Ref. [210, in particular, their Appendix B]. Moreover, Ref. [193] notes that it is better to work with 'renormalized' parameters c_n rather than the original bias parameters b_n (but see Ref. [210] for how this renormalization should actually be done). In effect, this corresponds to working with our Eq. (5.6) rather than Eq. (5.5); our analysis shows why this is necessary. This connection to Fourier space bias is rich, because we showed that the simple relation $B_k = b_k \sigma_{\rm L}^k$ is not generic. For the peaks transformation of Eq. (5.18), both b_k and B_k 'run' with L. Nevertheless, the B_k satisfy the same relations between the rescaled values that the original b_k (in the peak background split limit) do. Exploring whether this is generic is the subject of ongoing work.

Unfortunately, although the analysis based on Hermite polynomials is formally correct (and elegant), there are two reasons why, at least for describing halos, it cannot be valid for all smoothing scales L and separations r. First, halos do not overlap; this makes ξ_{hh} of the halo point process tend to -1 on scales smaller than $\sim R_h$ [179]. As a result, this halo exclusion limits the range in r over which the local model can be applied. The second is that, at least in the excursion set definition of halos, there is a nonlocal requirement on the density field: this was the subject of Section 5.1.4, which argued that this modifies the pdf over which one should compute ensemble averages. Accounting for this makes the ratio of the halo-mass cross-correlation bias scale dependent (our Eq. (5.42), which is Eq. (17) of Ref. [208]). The small scale limiting value of this modified expression yields δ_c, which is the correct 'one-halo' contribution to the Lagrangian space cross-correlation (the Lagrangian overdensity within a region which is destined to form a halo equals δ_c by definition), a fact which has not been emphasized before. This suggests that averaging over the more appropriate pdf not only leads to sensible results, but accounts for halo exclusion as well, so it may be worth exploring further. This may be particularly interesting

because, in the large separation limit, it leads to $\xi_{hh} - b_\times^2\,\xi_{mm} < 0$ (Eq. (27) of Ref. [208]).

There is a third reason why, at least for describing halos, the local bias model is unlikely to be valid for all smoothing scales L and separations r. This is related to the fact that the tidal field influences halo formation [214]. The correlation with the tidal field leads, generically, to nonlocal bias even in Lagrangian space. This is explored further in Ref. [215], where the nonlocal bias terms are shown to matter most for massive halos, though the nonlocal effects are subdominant on large scales.

If the gravitationally evolved nonlinear Eulerian mass field was a locally biased version of the initial field (it is not), then expanding in Hermite polynomials would also be the prefered way of describing halo bias (assuming the initial conditions were Gaussian). This is because local Lagrangian bias, with local nonlinear evolution, leads to local bias with respect to the Eulerian field. Conversely local bias with respect to the Eulerian field could be mapped back to local Lagrangian bias (with different bias factors, determined by the local linear-nonlinear mapping). Some of the scalings which are characteristic of local Lagrangian bias will survive in Eulerian bias as well. For example, the Lognormal transformation has one free parameter b. If we use b' to model the nonlinear mass field, and another b to model the biased tracers (incidentally, this means that one should think of the biased field $1+\delta_b$ as being the nonlinear field $1+\delta_{b'}$ raised to the b/b' power), then we may interpret our Eq. (5.15) as the Eulerian space cross-correlation between the biased field and the nonlinear mass field. Since $\langle\delta_b\delta_L|r\rangle$ and $\langle\delta_{b'}\delta_L|r\rangle$ equal $b\,\xi_{LL}(r)$ and $b'\,\xi_{LL}(r)$ for all r, one might naively have thought that $\langle\delta_b\delta_{b'}|r\rangle$ would also be linearly proportional to $\xi_{LL}(r)$. Not only is this not true, Eq. (5.15) shows that it is not proportional to $\xi_{b'b'}(r)$ either. In particular, Eq. (5.15) shows that in this model of local Eulerian bias, the cross-correlation is linearly proportional to the auto-correlation of the mass only when $\xi_{LL} \ll 1$ (i.e., for sufficiently large r). See Ref. [192] for more discussion of this limit of local Eulerian bias.

Recent work has emphasized the fact that because nonlinear evolution is nonlocal, local Lagrangian bias will lead to nonlocal Eulerian bias, and vice versa [193, 194, 195, 196]. The Hermite polynomials are the orthogonal polynomials associated with a Gaussian field. Therefore, the usefulness of Szalay's work for local Lagrangian bias suggests that, if bias is local with respect to the nonlinear, non-Gaussian field, then it would be natural to write Eulerian bias using the orthogonal polynomials of this non-Gaussian field. This is the subject of work in progress.

Finally, we note that our results depend only on the assumption that the Lagrangian matter field is Gaussian, so one might have thought that they also hold for modified gravity models. However, for such models, k-dependence of the linear growth factor is generic, with the consequence that the assumption that Lagrangian halo bias is local is no longer so attractive [204].

Part III

Modifying General Relativity

Chapter 6

Alternative theories of gravity with an extra scalar degree of freedom

An outstanding problem faced by Modern Cosmology is the recent phase of accelerated expansion of the Universe [18, 19]. In the context of General Relativity, it is possible to explain the cosmic acceleration adding an extra ingredient in the energy budget of the Universe. As discussed in Section 3.2, one can interpret the acceleration as the consequence of the negative pressure due to the inclusion of an extra fluid component, Dark Energy, which could be dynamical or constant (which includes Λ). In this case, Einstein's Equations are modified by adding an extra matter tensor accounting for the DE. The model which best describes the physical phenomena and accounts for cosmological observations is the ΛCDM (see Chapter 2). Despite its success, the need to go beyond the standard cosmological model stems from some outstanding problems (see Chapter 3). Moreover, GR description of space and time breaks down on scale around the Planck scale, where the theory can not be reconciled with quantum gravity.

One option is to consider these problems as a signal of the first real lack of our understanding of gravity and look for alternatives to General Relativity. In the following, we will refer to them as Modified Gravity Theories (MG). In this regard, several options can be taken into account. A good point to start is Lovelock's Theorem (Section 1.2) which gives us the following options,

1. include extra fields in the Lagrangian,
2. allow for higher order field equations,
3. break diffeomorphism invariance in the action,
4. assume higher than 4 dimensions for the space-time.

Considering one or more of these modifications, one can obtain field equations which differ from those of General Relativity. A plethora of models which allow for modifications in the gravity sector have been proposed and analyzed

in the past years. We refer the reader to the following reviews and references therein [216, 217, 14, 218, 15]. Let us briefly comment on the above points.

Extra fields in the Lagrangian can be scalars, vectors or tensors. Variation of the action w.r.t. the extra field(s) leads in general to an additional dynamical equation for the corresponding field(s). It is important to stress that usually modifications to GR involve only the gravitational action as matter fields are strongly constrained to be minimally coupled to metric only, due to the Equivalence Principle. Examples of MG theories with one extra scalar field are the Brans-Dicke theory [219] and Galileons [220, 221]. We will discuss them in detail respectively in Sections 6.1 and 6.2. Here, we want to note that although they have an additional field, their field equations remain of second order in the metric and the field. In particular the Galileon theory is the most general scalar field theory with field equations at second order. Moreover, the Galileon theory has been further generalized to include multi-scalar fields [222]. An example of theory which include a scalar and a vector field is TeVeS [157]. This theory is the relativistic generalization of the MOND paradigm, which modifies the Newton's law of gravity on small scales (see Part II). Furthermore, we mention also the Einstein-Æther theory [223] which includes in the action both a metric and a unit timelike vector field named æther. The introduction of a dynamical unit timelike vector breaks Lorentz symmetry. The resulting model allows to investigate the gravitational and cosmological effects of the æther. Finally, adding tensor fields in the action allows to construct massive spin 2 gravity theories, such as Massive Gravity [224].

The second option is to consider higher (than second) order field equations. This choice includes more degrees of freedom (DoFs) in the theory as more propagating modes appear. From a mathematical point of view higher order partial differential equations are more complicated to deal with and shortcomings can arise, e.g. Ostrogradski's instability [8]. An example of theory with higher order field equations is the f(R) theory [225]. It is a generalization of the Einstein-Hilbert action with a general function of the Ricci scalar which has 4-th order field equations in the metric tensor. However, let us note that $f(R)$ theory can be considered an exception as it can be recast in second order field equations being a special case of the Brans-Dicke theory [226] (see Section 6.1.1). This formulation makes explicit the extra dynamical DoF in the form of a scalar field and avoids the Ostrogradski's instability. Although very rarely, higher-order equations do not always lead to ghost instabilities.

The third option is to break diffeomorphism invariance. On the other hand, it is well known that diffeomorphism invariance can be restored by means of the Stückelberg technique [16]. It introduces a new field usually called Stückelberg field. This technique has been recently used in the formulation of the effective field theory of Inflation [80, 227] and cosmic acceleration [228, 229].

Finally, we comment about theories constructed in higher dimensions. Some examples are the Dvali-Gabadadze-Porrati (DGP) [230] and the Kaluza-Klein [231, 232, 233] theories, which generalize the GR action up to 5-dimentions. The Galileon theory has been also generalized to n-dimentions (and to multi-scalar fields) [222]. However, only 4-dimentions have been detected and in order to study low energy phenomena, the 4-dimentions effective description of such theories is sufficient.

Other modifications to General Relativity can be also considered. One can think to add non-local term in the action [234, 235, 236] or to add non dynamical field(s) in the action, as in the case of Auxiliary field(s) [237, 225, 238, 239, 240]. In this case an auxiliary field is algebraically determined by the field equations. However, in this thesis we will focus exclusively on theories with an extra (dynamical) scalar field in the actions or theories with higher order field equations.

Let us note that the division between models of DE and MG is not very stringent. When the modification in the gravitational action is induced by a scalar field, the equation obtained varying the action w.r.t. the field can be recast in a fluid form. The simplest example is the Quintessence model. Usually, this model is included in the DE class as it can be described with a dynamical equation of state. Actually, the pressure and the density of the fluid are due to the inclusion of a scalar field in the action which modifies the dynamics of the gravity (see Section 3.2.3). The same happens for Galileons where the modification of the extra field can be written in terms of an imperfect fluid [241].

As discussed above, modifications of gravity introduce additional DoFs. These extra DoFs need to be suppressed on Solar System scale where GR is well tested and where no extra DoFs have been found [242, 243]. Therefore, most viable MG models with extra scalar field(s) exhibit screening mechanisms able to hide the modification on Solar System scales in order to be consistent with local gravity experiments. There are different types of screening mechanisms [15], and they are classified depending on the nature of the physical interaction of the DoF, they are:

- Chameleon mechanism [244, 245, 246, 247]: This mechanism works in an environmental dependent way. The field's mass depends on the local energy density and in high energy density local environments, such as the Solar System, it is very large. As consequence, when the mass is high, the fifth force is suppressed. Therefore, the field is hidden in high energy density environments. On the contrary, in low energy density environments (as it is on cosmic scales) the field is very light and the fifth force is at play. Example of theories with such a mechanism are Scalar-Tensor theory [248, 249] and f(R) theory [250, 251].

- Vainshtein mechanism [252]: this mechanism is regulated by the non-linear self interaction of second derivatives of the field, which become important near a massive source. This results in hiding the modification to gravity in high energy density environments. Examples are the Galileon models [220] and Massive Gravity [224, 253, 254].

- k-mouflage mechanism [255]: It works as the Vainshtein mechanism with the difference that the screening is due to the first derivative interaction of the field.

- Symmetron mechanism [256, 257]: it depends on the vacuum expectation value, which in turn depends on the mass density. In local environments where the energy density is high this value is low and *vice versa*. As the scalar field couples to matter via the vacuum expectation value, it results to be decoupled from the matter in high energy density environment, hence it is hidden.

In theories that exhibit such mechanisms, modifications of the gravitational interaction become important only at large scales. It has become increasingly evident that the dynamics of perturbations can offer precious information to discern among candidate models, breaking, at least partially, the degeneracy that characterize them at the background level [258, 246, 259, 260, 261, 262, 263, 264, 265]. Ongoing and upcoming cosmological surveys will map matter and metric perturbations through different eras with exquisite precision. Combined with geometric probes, they will provide us with a set of independent measurements of cosmological distances and growth of structure. In the cosmological standard model, the rate of linear clustering can be determined from the expansion rate of the Universe; however this consistency relation is generically broken in models of MG and DE, even when they predict the same expansion history as ΛCDM. Therefore measurements of the growth of structure, such as weak lensing and galaxy clustering, add complementary constraining power to measurements of the expansion history via geometric probes. They can be used to perform consistency tests of ΛCDM *as well as* to constrain the parameter space of alternative approaches to the phenomenon of cosmic acceleration.

Over the past years there has been a lot of activity in the community to construct frameworks that would allow model-independent tests of gravity [266, 200, 267, 268, 269, 270, 271, 272, 273, 274, 275, 276, 277, 278, 279, 280, 281, 282, 283, 284, 285, 286, 287, 288, 289, 290, 291, 292, 293, 294, 295, 296, 297, 298, 299, 300, 301, 302, 303, 304, 305, 306, 307, 308, 309] with cosmological surveys like *Planck* [34], SDSS [22], DES [310], LSST [311], Euclid [312], WiggleZ Dark Energy Survey [313, 314] and CFHTLenS [315, 316, 317]. These are generally based on parametrizations of the dynamics of linear scalar perturbations, either at the level of the equations of motion, e.g. Ref. [298], of solutions of the equations, e.g. Refs. [270, 280, 295], or of the action, e.g. Refs. [318, 228, 229], with the general aim of striking a delicate balance among theoretical consistency, versatility and feasibility of the parametrization.

6.1 Scalar-Tensor Theory

A standard class of alternatives theories of gravity is represented by Scalar-Tensor Theory [248, 249], whose action is given by

$$\mathcal{S}_{ST} = \frac{1}{16\pi G}\int d^4x\sqrt{-g}\left(\phi R - \frac{\omega(\phi)}{\phi}\partial^\mu\phi\partial_\mu\phi - V(\phi)\right) + S_m[g_{\mu\nu},\chi_m] \quad (6.1)$$

where $\omega(\phi)$ is a function of the scalar field ϕ and $V(\phi)$ is a potential. For scalar tensor theories the modification of gravity is introduced by adding a scalar field in the action, which also includes a non minimally coupling between the field and the curvature. Variation of the action w.r.t. the metric led to the following equations

$$\begin{aligned} G_{\mu\nu} =& \frac{8\pi G}{\phi}T^m_{\mu\nu} + \frac{\omega(\phi)}{\phi^2}\left(\partial_\mu\phi\partial_\nu\phi - \frac{1}{2}g_{\mu\nu}\partial_\lambda\phi\partial^\lambda\phi\right) \\ &+ \frac{1}{\phi}\left(\nabla_\mu\nabla_\nu\phi - g_{\mu\nu}\Box\phi\right) - \frac{V(\phi)}{2\phi}g_{\mu\nu}. \end{aligned} \quad (6.2)$$

Combining the variation of the action w.r.t the scalar field with the trace of Eq. (6.2) leads to

$$\Box\phi = \frac{1}{3+2\omega}\left(8\pi G\, T^m + \phi\frac{dV}{d\phi} - 2V - \frac{d\omega}{d\phi}\partial^\sigma\phi\partial_\sigma\phi\right). \tag{6.3}$$

The scalar field equation relates the scalar field to the matter tensor which actually acts as a source for ϕ. Eqs. (6.2) describe the dynamics of the gravitational field. Action (6.1) and the Eqs. (6.2)-(6.3) are the generalization of the Brans and Dicke's theory (1961) [219], which can be obtained as the subclass of theories for which $\omega(\phi) = \omega_{BD}$ is a constant and $V(\phi) = 0$. Furthermore, it has been shown that $\omega(\phi) = 0$ corresponds to f(R) theory [226].

Constraints coming from Solar System can be imposed on the theory. Let us consider as a working example the case $\omega = \omega_0$ be a constant and a potential of the form $V(\phi) = m^2(\phi - \phi_0)^2$, where m and ϕ_0 are two constants. A generalization to a general potential can be found in Ref. [319]. Performing the newtonian approximation of this model, we can define the following post newtonian parameter (PPN) [320]

$$\gamma = \frac{2\omega_0 + 3 - e^{-m_{eff}r}}{2\omega_0 + 3 + e^{-m_{eff}r}}, \tag{6.4}$$

where the effective mass is

$$m_{eff} \equiv \frac{\partial^2 V}{\partial\phi^2} = \sqrt{\frac{2\phi_0}{2\omega_0+3}}m. \tag{6.5}$$

In GR the PPN parameter γ is equal to 1. From Eq. (6.4), γ approachs to 1 when $\omega_0 \to \infty$ or $m_{eff} \to \infty$. In these cases Einstein's Equations are satisfied. This parameter is strongly constrained by current observations in the Solar System [242, 243]

$$\gamma - 1 = (2.1 \pm 2.3) \times 10^{-5}. \tag{6.6}$$

$$\tag{6.7}$$

From this constraint, if we consider $m = 0$ it is possible to set a lower bound on ω_0

$$\omega_0 > 40000, \tag{6.8}$$

which makes the theory indistinguishable from GR at all scales and hence unappealing for cosmological purposes. This bound is still applicable in the most general case of $V(\phi) \neq 0$ or even when ω is a general function. However in that case the effective mass should be very light.

6.1.1 f(R) Theory

A simple modification to General Relativity is the inclusion of a general function of the Ricci scalar f(R) in the action [225, 238]. Let us briefly review the most important aspect of the f(R) theory.

We consider the following Lagrangian in Jordan frame

$$S = \int d^4x\sqrt{-g}\,[R + f(R)] + S_m[g_{\mu\nu}, \chi_m]\,, \tag{6.9}$$

where $f(R)$ is a generic function of the Ricci scalar and the matter sector is minimally coupled to gravity. Variation of the action w.r.t. the metric gives the following equations

$$(1+f_R)R_{\mu\nu} - \frac{1}{2}[R+f(R)]g_{\mu\nu} - [\nabla_\mu\nabla_\nu - g_{\mu\nu}\Box]\, f_R = \frac{\kappa}{2}T^{(m)}_{\mu\nu}\,, \tag{6.10}$$

with trace equation given by

$$3\,\Box f_R + f_R R - 2f(R) - R = \frac{\kappa}{2}T^{(m)}\,, \tag{6.11}$$

where $f_R \equiv df(R)/dR$. Let us note that we have used the metric formalism in deriving the field equations. A different approach is the one of Palatini [321], in which the metric tensor $g_{\mu\nu}$ and the $\Gamma^\alpha_{\mu\nu}$ are considered independent from each other. Then, the above equations differ from the ones obtained in the Platini formalism. In what follows, we will focus on the metric approach.

The trace equation can be written as a second order equation with an effective potential U_{eff}

$$\Box f_R = \frac{1}{3}\left\{\frac{\kappa}{2}T^{(m)} - f_R R + 2\,[R+f(R)]\right\} \equiv \frac{\partial U_{eff}}{\partial f_R}, \tag{6.12}$$

where one can define the effective mass as

$$\tilde{m}^2_{eff} = \frac{\partial^2 U_{eff}}{\partial f_R^2} = \frac{1}{3}\left[\frac{1+f_R}{f_{RR}}R\right]. \tag{6.13}$$

The range of the fifth force, due to the modification of the action, is described by the Compton wavelength

$$\lambda_C = \frac{2\pi}{\tilde{m}_{eff}}, \tag{6.14}$$

then when the mass is large the fifth force is suppressed as it acts at very small distances, hiding the modifications. On the contrary, when the mass is light, for examples at cosmic scales, λ_C is very large and the modification is at play. This is how the Chameleon mechanism works.

The fifth force is the manifestation of the presence of an extra dynamical DoF. A clear approach to figure out which is the dynamical DoF, is to consider the following action

$$S = \int d^4x\sqrt{-g}\,[\psi + f(\psi) + \phi(R-\psi)] + S_m[g_{\mu\nu},\chi_m]\,. \tag{6.15}$$

Varying the action w.r.t. ϕ, we get $R=\psi$, then this action is dynamical equivalent to action (6.9). The variation w.r.t. ψ yields $\phi = 1 + f'(\psi)$ where prime is the derivative w.r.t. ψ. Then, the action can be written as

$$S = \int d^4x\sqrt{-g}\,[\phi R - V(\phi)] + S_m[g_{\mu\nu},\chi_m]\,. \tag{6.16}$$

where $V(\phi) = f'(\psi) - f(\psi)$. From this action we can infer that: 1) the extra DoF is $\phi = 1 + f_R$, 2) it is equivalent to action (6.1) for $\omega = 0$, 3) the field equations now are of the second order then the theory avoids Ostrogradski's instability, as previous stated.

In the last decades, f(R) theory has been extensively studied in cosmology in order to explain the late time acceleration and as an alternative to the quintessence model in the early inflationaly epoch. Starobinsky in 1980 [322] proposed a model with $f(R) = \alpha R^2$ to describe the early expansion, for which once the condition $\alpha R^2 << R$ is satisfied, inflation can end. Moreover, it has been shown that the Starobinsky model is consistent with the observed CMB temperature anisotropies, confirming it as a viable alternative [47]. In the case of the late time cosmic expansion, several models for the form of the f(R) function have been proposed, some of them have been ruled out by both Solar System and cosmological tests, such as $f(R) = \alpha/R^n$ with $\alpha > 0$ and $n > 0$ [238]. Finally, it has been pointed out that the conditions for a viable f(R) models are [264] 1) $1 + f_R > 0$ as $G_{eff} = G/(1 + f_R)$, 2) $f_{RR} > 0$ for $f_{RR} << R$ to avoid tachyonic instabilities, 3) $f_R < 0$ from BBN and CMB constraints and finally 4) $|f_R|$ today should be less than 10^6.

6.2 Generalized Galileon Theory

Galileon models were originally introduced as an effective, infrared gravitational modification which can lead to self-accellerating solutions [220]. The first formulation has been obtained as the decoupling limit of the DGP model [230], for which the 3+1-dimentions Minkowski space is embedded in a 4+1-dimentions Minkowski space. The modification to General Relativity is obtained introducing the "Galileon", a scalar field with a galilean(-like) symmetry $\phi \to \phi + b_\mu x^\mu + c$ (b_μ, c being constant), hence the name of this new class of theories.

The Galileon Lagrangian contains more than two derivatives but nevertheless leads to second order equations of motion, thus avoiding Ostrogradski ghosts [8]. The generic structure of the Galileon Lagrangian is

$$\mathcal{L}_n \sim \partial\phi \cdot \partial\phi \left(\partial^2\phi\right)^{n-2}, \tag{6.17}$$

up to $n = 5$, as higher order Lagrangians are total derivatives.

Coupling the Galileon covariantly to gravity and insisting on the requirement that the scalar and the metric satisfy second order equations, forces one to abandon galilean symmetry [221], ordinary shift symmetry $\phi \to \phi + c$ can be retained [323] or abandoned as well. In the Covariant Galileon formulation, extra terms non minimally coupled to the metric appear in the action. Finally, a more general covariant action have been constructed in Ref. [324, 325], which allows also to explore modifications to gravity coming from extra dimentions. It is known as Generalized Galileon action. The 4-dimensional version of the action given in Ref. [325] has been shown [326] to be equivalent to the most general action for a scalar coupled to gravity that leads to second order equations of motion, given by Horndeski in the 1970s [327]. The Galileon model has also been generalized in various other directions, see e.g. Refs. [328, 329, 330, 331, 332, 333, 334, 335] and references therein.

The 4-dimentions action for Generalized Galileon is

$$S = \int d^4x\sqrt{-g}\sum_{i=2}^{5}\left(\mathcal{L}_i\right), \tag{6.18}$$

with

$$\mathcal{L}_2 = K(\phi, X), \tag{6.19}$$

$$\mathcal{L}_3 = -G_3(\phi, X)\Box\phi, \tag{6.20}$$

$$\mathcal{L}_4 = G_4(\phi, X)R + G_{4X}\left[(\Box\phi)^2 - (\nabla_\mu\nabla_\nu\phi)^2\right], \tag{6.21}$$

$$\mathcal{L}_5 = G_5(\phi, X)G_{\mu\nu}\nabla^\mu\nabla^\nu\phi - \frac{G_{5X}}{6}\left[(\Box\phi)^3 - 3\,(\Box\phi)\,(\nabla_\mu\nabla_\nu\phi)^2 + 2\,(\nabla_\mu\nabla_\nu\phi)^3\right], \tag{6.22}$$

where $K(\phi, X)$ and $G_i(\phi, X)$ are general functions of ϕ and $X = -\partial_\mu\phi\partial^\mu\phi/2$. We will refer to them as galileon functions and a subscript ϕ or X denotes partial differentiation respectively w.r.t. ϕ or X [1]. Varying the action w.r.t. the metric and the scalar field, one obtains the equations of motion for the metric, to which we will refer to as Einstein's Equations and the scalar field equation. For sake of brevity, here we do not rewrite these equations, while we refer the reader to Ref. [326].

The Generalized Galileon formulation allows a model independent analysis of a large class of single field modified gravity models. In fact, particular choices of the galilean functions correspond to well known models, such as

- For $K \neq 0$ and $G_i = 0$, we recover k-inflation [79]
- Generalized Brans-Dicke theories [336]

  $$K = B(\phi)X,\;\; G_3 = \xi(\phi)\partial^\mu\phi\partial_\mu\phi,\;\; G_4 = F(\phi),\;\; G_5 = 0, \tag{6.23}$$

  where $B(\phi)$, $\xi(\phi)$ and $F(\phi)$ are functions of the scalar field.
- Covariant Galileon [221]

  $$K = c_2X,\;\; G_3 = c_3X,\;\; G_{4,X} = c_4X,\;\; G_{5,X} = c_5X, \tag{6.24}$$

  with $c_i = const.$ For $c_4 = c_5 = 0$ one has the Cubic Covariant Galileon [221].

The interest in these theories arises in the possibility to describe the early time Inflation epoch [337, 323, 338, 339, 326, 340, 341, 342, 343, 344, 345] as well as to account for the late time acceleration [346, 347, 348, 349, 350, 351]. There are some known novel features in such scenarios: to name a few, the null energy condition can be drastically violated without developing instabilities [337]; a large tensor-to-scalar power spectrum ratio is allowed [323]; there are new shapes of the three-point function and potentially large four-point function [339]. Moreover, Galileon theories exhibit a screening mechanism on small scale, the so called Vainshtein mechanism [252, 352]. The field ϕ decouples from matter due to its non-linear derivative self-interactions which become important in local high energy density environment. This mechanism allows these theories to recover GR on length scale smaller than the Vainshtein radius. Let us

[1] Let us explicitly define:

$$(\nabla_\mu\nabla_\nu\phi)^2 = \nabla_\mu\nabla_\nu\phi\nabla^\mu\nabla^\nu\phi\,,$$
$$(\nabla_\mu\nabla_\nu\phi)^3 = \nabla_\mu\nabla_\nu\phi\nabla^\nu\nabla^\lambda\phi\nabla_\lambda\nabla^\mu\phi\,.$$

explain it with an example [15, 353, 354]. We consider the Lagrangian of the Cubic Galileon

$$\mathcal{L}_\phi = -3(\partial\phi)^2 - \frac{1}{\hat{\Lambda}^3}(\partial\phi)^2\Box\phi + \frac{\beta}{m_0}\phi T^{(m)} \tag{6.25}$$

where β parametrizes the gravitational coupling and $\hat{\Lambda}$ is the strong-coupling scale of the theory. We expect that the term $(\partial\phi)^2\Box\phi/\hat{\Lambda}^3$ becomes important near a massive source in order to screen the Galileon field. The spherically-symmetric profile for the scalar field, i.e. $\phi = \phi(r)$ can be obtained analytically from the field equations around a static point source of mass M with $T^{(m)} = -M\delta\bar{x}$ by solving

$$6\phi' + \frac{4}{\hat{\Lambda}^3}\frac{(\phi')^2}{r} = \frac{\beta M}{4\pi r^2 m_0}, \tag{6.26}$$

where prime is the derivative w.r.t. the radial coordinate. By computing the solution far from and close to the source we can define the Vainshtein radius as the radius at which the transition between this two regime occurs,

$$r_V \equiv \frac{1}{\hat{\Lambda}}\left(\frac{\beta M}{m_0^2}\right)^{1/3}. \tag{6.27}$$

Let us also define a *classical* parameter which will allow to understand in which regime non-linearities become important

$$\alpha_{cl} \equiv \frac{\partial^2\phi}{\hat{\Lambda}^3}. \tag{6.28}$$

Far from the source we have

$$\phi'(r >> r_V) \cong \frac{\beta}{3}\frac{M}{8\pi m_0 r^2}, \tag{6.29}$$

and the force due to the Galileon field w.r.t that of newtonian gravity is

$$\frac{F_\phi}{F_N} \sim \frac{\beta^2}{3} \tag{6.30}$$

where the force mediated by the scalar field has been defined as $\vec{F}_\phi = \frac{\beta}{m_0}\vec{\nabla}\phi$. The classical parameter is

$$\alpha_{cl} \sim \left(\frac{r_V}{r}\right)^3 << 1, \tag{6.31}$$

then non-linearities are unimportant. Near the source, we have

$$\phi'(r << r_V) \sim \frac{1}{\sqrt{r}}, \tag{6.32}$$

and the ratio between the Galileon force and the newtonian one is

$$\frac{F_\phi}{F_N} \sim \left(\frac{r}{r_V}\right)^{3/2} << 1, \tag{6.33}$$

Than, the Galileon force is strongly suppressed on scales smaller than the Vainshtein radius, and

$$\alpha_{cl} \sim \left(\frac{r_V}{r}\right)^{3/2} >> 1. \tag{6.34}$$

Then $\partial^2\phi >> \hat{\Lambda}^3$ as it should be, near a massive source.

6.3 Gradient expansion of superhorizon perturbations

Inflation is a powerful paradigm that addresses various fine-tuning problems in the early Universe and accounts for the nearly scale invariant primordial perturbations that are needed for structure formation. As we extensively discussed in Section 3.1.1, substantial non-Gaussianity can be generated in inflation models with multiple scalar fields or with non-canonical kinetic terms. Furthermore, if the slow-roll condition is temporarily violated, large non-Gaussianity can be generated even in a single field model [78]. In this respect, non-Gaussianity can be used to rule out or constraint different inflationary models. All Inflationary models have to deal with the recently released results by *Planck* Collaboration [83] that are consistent with a Gaussian spectrum of primordial perturbations.

To tackle non-Gaussianity from inflation models, traditional linear perturbation theory is inadequate. A natural approach is to go beyond the linear order and work with second order cosmological perturbation theory [355, 356, 357, 358, 359, 360, 361]. While this approach usually applies to primordial perturbations up to the horizon exit, an alternative approach naturally tackles the superhorizon perturbations — gradient expansion [362, 363, 364, 365, 366, 367, 368, 369, 370, 371, 372, 373, 374]. In gradient expansion, physical quantities are expanded in terms of their inverse wavelengths, as compared to a pivotal length scale ($\epsilon \sim L_p/L_{phys}$), so every spatial derivative adds one perturbative order, $\partial_i \sim \epsilon$, hence the name. This is different from usual cosmological perturbation theory where the expansion is in terms of perturbative field amplitudes. In the context of cosmology, particularly in the inflationary epoch when physical modes are stretched well outside the quasi-constant Hubble horizon, the Hubble length can be naturally chosen as the pivotal length scale. Therefore, this approach can be used to evaluate and evolve non-Gaussiantites at superhorizon scales, complementary to usual non-linear perturbation theory. The leading order gradient expansion is often called the separate universe approach [375] or δN formalism [376, 377], which is sufficient for many purposes. However, the next-to-leading order gradient corrections can be as important, for example, in some multi-field models or when the slow-roll condition is violated [378, 374]. A beyond-δN formalism scheme has recently been proposed [374].

In Ref. [379], with S. -Y. Zhou and T. P. Sotiriou, we developed the superhorizon gradient expansion formalism for G-inflation [323], up to second order in gradient expansion. We focus on the subclass of actions for which the scalar enjoys shift symmetry ($\phi \to \phi + c$), as they are closer to the original idea of the Galileon and significantly simpler. Additionally, this will allow to explore the phenomenology associated with the non-linear derivative interactions of the scalar. Abandoning shift symmetry leads, amongst other terms, to allowing a potential for the scalar, which can lead to similar phenomenology and, therefore, obscures the role of the Galileon-type terms.

During the preparation of our paper [379], Ref. [373] appeared, which also develops the superhorizon gradient expansion formalism for G-inflation without assuming shift symmetry. However, there are major differences: On the technical side, we work in the synchronous gauge, while Ref. [373] prefers the uniform expansion gauge; On the more substantial side in Ref. [373] it is assumed that

$\partial_t h_{ij}(t,x)$ (see Eq. 6.64) is $\mathcal{O}(\epsilon^2)$, while we do not impose such condition. In this respect our results are more general.

The work is organized as follows. In Section 6.3.1 we perform $3+1$ decomposition of the equations of motion. In Section 6.4 we present the model we use to perform the analysis. In Section 6.4.1, we establish the gradient expansion orders of relevant quantities. The equations of motion are solved up to $\mathcal{O}(\epsilon^2)$ and the general solution is summarized in Section 6.4.2,. In Section 6.4.3, we simplify the general solution in the de Sitter limit. Note that in Section 6.4.2, Section 6.4.3 and Appendix B, we mostly suppress the background quantities' order indication $^{(0)}$ to simplify the equations. We conclude and discuss some future perspectives in Section 6.4.4.

6.3.1 ADM formalism

In order to perform the gradient expansion formalism, it is useful to decompose the equations of motion according to the Arnowitt-Deser-Misner (ADM) prescription [380, 381, 382, 383, 384]. The formalism supposes a 3+1 decomposition of the space-time, then the metric can be written as

$$\mathrm{d}s^2 = -N^2\mathrm{d}t^2 + \gamma_{ij}(\mathrm{d}x^i + N^i\mathrm{d}t)(\mathrm{d}x^j + N^j\mathrm{d}t), \tag{6.35}$$

where N and N_i are respectively the lapse and shift functions, and γ_{ij} is the three dimensional metric. To reduce redundant gauge degrees of freedom and simplify equations, we make use of a gauge condition:

$$N = 1, \qquad N^i = 0, \tag{6.36}$$

which implies

$$g_{tt} = -1, \quad g_{ti} = 0, \quad g_{ij} = \gamma_{ij}, \tag{6.37}$$
$$g^{tt} = -1, \quad g^{ti} = 0, \quad g^{ij} = \gamma^{ij}. \tag{6.38}$$

Here latin indices (except for t) run from 1 to 3 and they are raised and lowered with γ^{ij} and γ_{ij} respectively. This is called synchronous gauge, where the proper time distance between two neighboring hypersurfaces along the normal vector coincides with the coordinate time distance ($N = 1$, proper time slicing) and the spatial coordinates are such that clocks are synchronized between different hypersurfaces ($N^i = 0$). In synchronous gauge, equations can be very much simplified. Note, however, that there is residual gauge freedom, which will be discussed in Section 6.4.2.

Now, the spatial γ_{ij} can be considered as a fundamental dynamical variable. Another fundamental variable after the $3+1$ decomposition is the extrinsic curvature, which in synchronous gauge is simply

$$\mathcal{K}_{ij} = -\Gamma^t_{ij} = -\frac{1}{2}\dot{\gamma}_{ij}, \tag{6.39}$$

and its trace is defined as $\mathcal{K} = \gamma^{ij}\mathcal{K}_{ij}$. It is useful to decompose the spatial metric and the extrinsic curvature as

$$\gamma_{ij} = a^2(t)e^{2\zeta(t,\mathbf{x})}h_{ij}(t,\mathbf{x}), \tag{6.40}$$
$$\mathcal{K}^i_j = \frac{1}{3}\mathcal{K}(t,\mathbf{x})\delta^i_j + A^i_j(t,\mathbf{x}), \tag{6.41}$$

where $a(t)$ is the scale factor of the fiducial FLRW background, $\zeta(t,\mathbf{x})$ is related to the curvature perturbation, $h_{ij}(t,\mathbf{x})$ is defined to have a unit determinant $\det[h_{ij}]=1$, and A^i_j is the traceless part of $\mathcal{K}^i_j$. These definitions lead to the following relations

$$\mathcal{K} = -3\left[\frac{\dot{a}}{a}+\dot{\zeta}\right], \tag{6.42}$$

$$\dot{h}_{ij} = -2h_{ik}A^k_j. \tag{6.43}$$

To decompose the equations of motion, we make use of some well-known results which do not make reference to any specific gauge. Using the ADM variables, the unit normal 1-form and vector can be written respectively as $n_\mu=(-N,0,0,0)$ and $n^\mu=(1/N,-N^1/N,-N^2/N,-N^3/N)$. Making use of the Gauss-Codazzi relations (see e.g. Ref. [385]), we can write the Ricci tensor and Ricci scalar respectively as

$$\begin{aligned} R_{\mu\nu} = {} & n_\mu n_\nu\left(\frac{1}{N}\mathcal{L}_{\mathbf{m}}\mathcal{K}+\frac{1}{N}\nabla^\lambda\nabla_\lambda N-\mathcal{K}^\rho_\sigma\mathcal{K}^\sigma_\rho\right)-2n_{(\mu}\nabla_{\nu)}\mathcal{K}+2n_{(\mu|}\nabla_\sigma\mathcal{K}^\sigma_{|\nu)} \\ & -\frac{1}{N}\mathcal{L}_{\mathbf{m}}\mathcal{K}_{\mu\nu}-\frac{1}{N}\nabla_\mu\nabla_\nu N+{}^{[3]}R_{\mu\nu}+\mathcal{K}\mathcal{K}_{\mu\nu}-2\mathcal{K}^\sigma_\mu\mathcal{K}_{\nu\sigma}, \end{aligned} \tag{6.44}$$

$$R = {}^{[3]}R+\mathcal{K}^2+\mathcal{K}^\rho_\sigma\mathcal{K}^\sigma_\rho-\frac{2}{N}\mathcal{L}_{\mathbf{m}}\mathcal{K}-\frac{2}{N}\nabla^\sigma\nabla_\sigma N, \tag{6.45}$$

where $m^\mu=Nn^\mu$, $\mathcal{L}_{\mathbf{m}}$ is the Lie derivative along m^μ, ${}^{[3]}R$ the Ricci scalar, and ${}^{[3]}R_{\mu\nu}$ the Ricci tensor of the spacelike hypersurfaces. In the next Section we also make use of the Laplacian, which is decomposed as

$$\Box\phi = -n^\rho\partial_\rho(n^\sigma\partial_\sigma\phi)+\mathcal{K}n^\sigma\partial_\sigma\phi+\nabla^\sigma\ln N\partial_\sigma\phi+\nabla^\sigma\nabla_\sigma\phi, \tag{6.46}$$

where ϕ is a scalar field.

6.4 G-Inflation with shift symmetric Galileon

Among the most general action for shift-symmetric generalized Galileon models, we consider the simplest one which includes the characteristic "Galileon interactions", i.e. terms that contain second order derivatives of ϕ

$$S=\int \mathrm{d}^4x\sqrt{-g}\left(\frac{m_0^2}{2}R+K(X)-G_3(X)\Box\phi\right), \tag{6.47}$$

without assuming any specific forms for the unspecified functions $K(X)$ and $G_3(X)$. Even though it is not the most general action, it is closer to the original idea of Galileon and it allows to explore the phenomenology associated with the non-linear derivative interactions of the scalar field, avoiding the presence of a potential for the scalar that may mask or imitate the real field interaction. This action was firstly considered in Ref. [350].

The equations of motion, to which we will refer to as the Einstein equations, reduce to

$$m_0^2G_{\mu\nu}=T^\phi_{\mu\nu}, \tag{6.48}$$

with

$$T^{\phi}_{\mu\nu} = (K_X - G_{3X}\Box\phi)\partial_\mu\phi\partial_\nu\phi - 2\partial_{(\mu}G_3\partial_{\nu)}\phi + g_{\mu\nu}(K + \partial_\sigma G_3\partial^\sigma\phi). \quad (6.49)$$

Note that the energy momentum tensor takes the form of an imperfect fluid [241], thus this model does not fall under the existing formalism for a perfect fluid.

Thanks to the shift symmetry, the equation of motion for ϕ can be given in terms of the current

$$J^\mu = (K_X - G_{3X}\Box\phi)\partial^\mu\phi - G_{3X}\partial^\mu X, \quad (6.50)$$

as

$$\nabla_\mu J^\mu = 0. \quad (6.51)$$

It is worth mentioning that the scalar equation of motion is implied by the Einstein equations, i.e., once the Einstein equations are satisfied, the scalar equation of motion is automatically satisfied. In fact, this applies to any covariant scalar-tensor system, as we show in Appendix A.

In the synchronous gauge ($N = 1, N^i = 0$), the Einstein equations are greatly simplified:

$$m_0^2 G_{tt} = T^{\phi}_{tt}, \quad (6.52)$$
$$m_0^2 G_{ti} = T^{\phi}_{ti}, \quad (6.53)$$
$$m_0^2 G^i_j = T^{\phi}\big|^i_j, \quad (6.54)$$

with

$$G_{tt} = \frac{1}{2}\left({}^{[3]}R + \mathcal{K}^2 - \mathcal{K}^i_j\mathcal{K}^j_i\right), \quad (6.55)$$
$$G_{ti} = -\bar\nabla_k\mathcal{K}^k_i + \bar\nabla_i\mathcal{K}, \quad (6.56)$$
$$G^i_j = {}^{[3]}G^i_j - \dot{\mathcal{K}}^i_j + \mathcal{K}\mathcal{K}^i_j - \frac{1}{2}\delta^i_j\left(-2\dot{\mathcal{K}} + \mathcal{K}^2 + \mathcal{K}^k_l\mathcal{K}^l_k\right), \quad (6.57)$$
$$T^{\phi}_{tt} = K_X\dot\phi^2 - K - G_{3X}\Box\phi\dot\phi^2 - G_{3X}\dot\phi\dot X - G_{3X}\partial_k X\partial^k\phi, \quad (6.58)$$
$$T^{\phi}_{ti} = K_X\dot\phi\partial_i\phi - G_{3X}\Box\phi\dot\phi\partial_i\phi - G_{3X}\dot X\partial_i\phi - G_{3X}\partial_i X\dot\phi, \quad (6.59)$$
$$\begin{aligned} T^{\phi}\big|^i_j = {} & K_X\partial^i\phi\partial_j\phi - G_{3X}\Box\phi\partial^i\phi\partial_j\phi - G_{3X}\partial^i X\partial_j\phi - G_{3X}\partial^i\phi\partial_j X \\ & + \left(G_{3X}\partial^k\phi\partial_k X + K - G_{3X}\dot X\dot\phi\right)\delta^i_j, \end{aligned} \quad (6.60)$$

where $\Box\phi = -\ddot\phi + \mathcal{K}\dot\phi + \nabla^\sigma\nabla_\sigma\phi$. The scalar equation of motion is given by

$$\partial_\mu J^\mu + \frac{1}{2}\partial_\mu\ln\gamma J^\mu = \dot J^t + (3H + 3\dot\zeta)J^t + 3\partial_i\zeta J^i + \partial_i J^i = 0, \quad (6.61)$$

where $\gamma = \det[\gamma_{ij}]$ and $H = \dot a/a$ is the usual Hubble parameter.

6.4.1 Gradient expansion method: order analysis

In standard cosmological perturbation theory one expands perturbatively in the field amplitudes. To tackle non-Gaussianities in inflation models, second order perturbation theory is often used within the Hubble horizon. However,

for physics processes at superhorizon scales one usually resorts to the gradient expansion technique. Note that the separate universe approach or the δN formalism is simply the leading order gradient expansion [386]. Assuming the characteristic spatial length is L_{phys}, the dimensionless perturbative expansion parameter is

$$\epsilon \sim \frac{H^{-1}}{L_{phys}} \ll 1. \tag{6.62}$$

This means in particular that every spatial partial derivative carries an order of ϵ

$$\partial_i \sim \mathcal{O}(\epsilon), \tag{6.63}$$

while the time derivative is considered $\mathcal{O}(\epsilon^0)$. The superhorizon gradient expansion is complimentary to the usual non-linear cosmological perturbation analysis and may capture fully nonlinear (in terms of the field amplitudes) physics at superhorizon scales, while the equations are still tractable due to the perturbative approach.

To perform the superhorizon perturbation analysis, we first need to deduce the starting orders for various quantities of interest. First, note that the equations of motion at $\mathcal{O}(\epsilon^0)$ should simply determine the evolution of the scale factor $a(t)$ and the scalar, as the space-time is supposed to be described by an FLRW line element. Given the definition (6.40), one can infer that h_{ij} should start with $h^{(0)}_{ij}(\mathbf{x})$; otherwise the $\mathcal{O}(\epsilon^0)$ equation would pick up terms involving $\partial_t h^{(0)}_{ij}(t, \mathbf{x})$, which is non-FLRW. From the scalar's equation of motion Eq. (6.61), we can infer that at $\mathcal{O}(\epsilon^0)$ the scalar field should be spatially homogeneous, meaning that ϕ starts with $\phi^{(0)}(t)$. Unlike previous work on this subject (see e.g. Ref. [373]), we do not impose any conditions on the higher orders of these quantities. Therefore, we have

$$\text{starting order of } \dot{h}_{ij} = \mathcal{O}(\epsilon), \tag{6.64}$$

$$\text{starting order of } \partial_i \phi = \mathcal{O}(\epsilon^2). \tag{6.65}$$

Expanding Eq. (6.43) perturbatively (for $n \geq 1$)

$$\dot{h}^{(n)}_{ij} = -2 \sum_{p=0}^{n-1} h^{(p)}_{ik} \left(A^{(n-p)} \right)^k_j \tag{6.66}$$

and making use of Eq. (6.64), we can infer that

$$\text{starting order of } A^k_j = \mathcal{O}(\epsilon). \tag{6.67}$$

Expanding Eq. (6.53), we infer that

$$\partial_i \mathcal{K}^{(0)} = 0. \tag{6.68}$$

Therefore, $\mathcal{K}^{(0)}$ is a function of t. From the definition (6.42), and given that one can always redefine the scalar factor $a(t)$ to absorb $\zeta^{(0)}(t)$, it follows that

$$\text{starting order of } \dot{\zeta} = \mathcal{O}(\epsilon), \tag{6.69}$$

$$\mathcal{K}^{(0)} = -3\frac{\dot{a}}{a} = -3H(t), \tag{6.70}$$

$$\mathcal{K}^{(n)} = -3\dot{\zeta}^{(n)}, \qquad n \geq 1, \tag{6.71}$$

where $H(t)$ is the usual Hubble parameter.

Using Eq. (6.65), we may expand X as

$$X = X^{(0)}(t,\mathbf{x}) + X^{(1)}(t,\mathbf{x})\epsilon + X^{(2)}(t,\mathbf{x})\epsilon^2 + \mathcal{O}(\epsilon^3), \tag{6.72}$$

where

$$X^{(n)} = \frac{1}{2}\sum_{p=0}^{n} \dot{\phi}^{(p)}\dot{\phi}^{(n-p)} + \mathcal{O}(\epsilon^4). \tag{6.73}$$

We also need to perturbatively expand functions of X, such as $K(X)$. To this end, we should consider $X = X(\epsilon)$ according to Eq. (6.72) and Taylor-expand, for example, $K(X(\epsilon))$ around $\epsilon = 0$ as

$$\begin{aligned} K(X) &= K(X^{(0)}) + K_X(X^{(0)})X^{(1)}\epsilon + \frac{1}{2}\Big[K_{XX}(X^{(0)})X^{(1)2} \\ &+ 2K_X(X^{(0)})X^{(2)}\Big]\epsilon^2 + \mathcal{O}(\epsilon^3). \end{aligned} \tag{6.74}$$

In summary, the various quantities of interest, to be determined in the next section, are expanded as follows:

$$\zeta = \zeta^{(0)}(\mathbf{x}) + \zeta^{(1)}(t,\mathbf{x})\epsilon + \zeta^{(2)}(t,\mathbf{x})\epsilon^2 + \mathcal{O}(\epsilon^3), \tag{6.75}$$

$$\phi = \phi^{(0)}(t) + \phi^{(1)}(t,\mathbf{x})\epsilon + \phi^{(2)}(t,\mathbf{x})\epsilon^2 + \mathcal{O}(\epsilon^3)\,, \tag{6.76}$$

$$A^i_j = A^{(1)i}_{\ \ j}(t,\mathbf{x})\epsilon + A^{(2)i}_{\ \ j}(t,\mathbf{x})\epsilon^2 + \mathcal{O}(\epsilon^3), \tag{6.77}$$

$$h_{ij} = h^{(0)}_{ij}(\mathbf{x}) + h^{(1)}_{ij}(t,\mathbf{x})\epsilon + h^{(2)}_{ij}(t,\mathbf{x})\epsilon^2 + \mathcal{O}(\epsilon^3)\,, \tag{6.78}$$

$$\mathcal{K}^i_j = -H(t)\delta^i_j + \mathcal{K}^{(1)i}_{\ \ j}(t,\mathbf{x})\epsilon + \mathcal{K}^{(2)i}_{\ \ j}(t,\mathbf{x})\epsilon^2 + \mathcal{O}(\epsilon^3), \tag{6.79}$$

$$\mathcal{K} = -3H(t) + \dot{\zeta}^{(1)}(t,\mathbf{x})\epsilon + \dot{\zeta}^{(2)}(t,\mathbf{x})\epsilon^2 + \mathcal{O}(\epsilon^3). \tag{6.80}$$

6.4.2 General solution

Now, we solve the equations of motion perturbatively, up to the $\mathcal{O}(\epsilon^2)$ order, to obtain the general solutions. These solutions will be parametrized by a few unspecified spatial functions, which describe the physical degrees of freedom (modulo residual gauge freedom) that may evolve as the Universe expands. The gradient expansions of Einstein's equations up to order $\mathcal{O}(\epsilon^2)$ are listed in Appendix B.

In the following, to simplify the equations, we will mostly suppress the background quantities' order indication $^{(0)}$. For example, $\dot{\phi}^{(0)}$ is written as $\dot{\phi}$ if there is no confusion.

- The $\mathcal{O}(\epsilon^0)$ order

  For the $\mathcal{O}(\epsilon^0)$ order, all spatial derivatives are absent. As desired, the equations of motion reduced to the conventional background FLRW case:

$$3m_0^2H^2 = -K + 2K_X X + 6H\dot{\phi}G_{3X}X, \tag{6.81}$$

$$-m_0^2\left(2\dot{H} + 3H^2\right) = K - 2G_{3X}X\ddot{\phi}, \tag{6.82}$$

$$\dot{J}^{t\,(0)} + 3HJ^{t\,(0)} = 0, \tag{6.83}$$

where $J^{t(0)} = K_X\dot{\phi}+6HG_{3X}X$. Note that only two of the three equations are independent.

- The $\mathcal{O}(\epsilon)$ order

  The tt component of Einstein's equation is given by

$$\left(\frac{1}{2}\ \dot{\phi}K_X + \dot{\phi}K_{XX}X + 9HG_{3X}X + 6HG_{3XX}X^2\right)\dot{\phi}^{(1)} = \\ = \left(3m_0^2H - 3\dot{\phi}G_{3X}X\right)\dot{\zeta}^{(1)}, \tag{6.84}$$

  which can be re-written as

$$\dot{\phi}^{(1)} = \mathcal{A}^0\dot{\zeta}^{(1)}, \tag{6.85}$$

  where

$$\mathcal{A}^0(t) = \frac{6m_0^2H - 6\dot{\phi}G_{3X}X}{\dot{\phi}K_X + 2\dot{\phi}K_{XX}X + 18HG_3 3XX + 12HG_{3XX}X^2}. \tag{6.86}$$

  The ij component of Einstein's equation naturally splits into a trace part and a traceless part. The trace part gives rise to another relation between $\phi^{(1)}$ and $\zeta^{(1)}$:

$$-2G_3 3XX\ddot{\phi}^{(1)} + \left(\dot{\phi}K_X - 2\dot{X}(G_{3X} + G_{3XX}X)\right)\dot{\phi}^{(1)} \\ +2m_0^2\left(\ddot{\zeta}^{(1)} + 3H\dot{\zeta}^{(1)}\right) = 0. \tag{6.87}$$

  Combining Eq. (6.85) and Eq. (6.87), we get, after integration,

$$\zeta^{(1)}(t,\mathbf{x}) = C_\zeta^{(1)}(\mathbf{x})\int^t \frac{\mathrm{d}t'}{\bar{a}(t')^3}, \tag{6.88}$$

  where

$$\bar{a}(t) = \exp(\int^t \mathrm{d}t'\mathcal{H}^0(t')), \tag{6.89}$$

$$\mathcal{H}^0(t) = \frac{\left(\dot{\phi}K_X - 2\dot{X}(G_{3X} + G_{3XX}X)\right)\mathcal{A}^0 - 2G_{3X}X\dot{\mathcal{A}}^0 + 6m_0^2H}{6M_{pl}^2 - 6G_{3X}X\mathcal{A}^0}, \tag{6.90}$$

  and $\mathcal{C}_\zeta^{(1)}(\mathbf{x})$ is an unspecified spatial function from the first integration. There would be another unspecified spatial function from the second integration ($C_\zeta'^{(1)}(\mathbf{x})$), which has been absorbed into $\zeta^{(0)}(\mathbf{x})$. We will see in the next section that $\mathcal{H}^0$ approaches the Hubble constant H for near de Sitter expansion, in which case $\dot{\zeta}^{(1)}$ scales as $1/a^3(t)$. Now, $\phi^{(1)}$ is given by

$$\phi^{(1)}(t,\mathbf{x}) = C_\zeta^{(1)}(\mathbf{x})\int^t \frac{\mathrm{d}t'\mathcal{A}^0(t')}{\bar{a}(t')^3} + C_\phi^{(1)}(\mathbf{x}), \tag{6.91}$$

  where $C_\phi^{(1)}(\mathbf{x})$ is an integration spatial function. The traceless part of Einstein's equation's ij component is simply

$$\dot{A}^{(1)i}_{\ \ j} + 3HA^{(1)i}_{\ \ j} = 0, \tag{6.92}$$

whose solution is

$$A^{(1)i}{}_j(t,\mathbf{x}) = \frac{C_A^{(1)i}{}_j(\mathbf{x})}{a^3}, \tag{6.93}$$

where the unspecified spatial function $C_A^{(1)i}{}_j(\mathbf{x})$ is symmetric and traceless. From Eq. (6.43), we have

$$h_{ij}^{(1)}(t,\mathbf{x}) = -2h_{ik}^{(0)}(\mathbf{x})C_A^{(1)k}{}_j(\mathbf{x})\int^t \frac{\mathrm{d}t'}{a(t')^3}, \tag{6.94}$$

where the would-be integration spatial function $C_h^{(1)}{}_{ij}(\mathbf{x})$ has been absorbed into $h_{ik}^{(0)}(\mathbf{x})$. As expected, the scalar equation of motion is solved by the solution obtained above.

Before moving on to solve higher order equations, we note that defining a curvature perturbation that is conserved in time is trivial in our formalism. By virtue of the tt component of Einstein's equation (6.85), one can define a conserved curvature perturbation at $\mathcal{O}(\epsilon)$

$$\mathcal{R}^{(1)} = \zeta^{(1)} - \int^t \frac{\mathrm{d}t'}{\mathcal{A}^0(t')}\dot{\phi}^{(1)}(t'). \tag{6.95}$$

As we will see in Section 6.4.3, because of the shift symmetry, de Sitter expansion is an attractor of the system. For quasi-de Sitter expansion, i.e., for the late time of inflation, $\mathcal{A}^0 \simeq$ constant and we can write $\mathcal{R}^{(1)}$ as

$$\mathcal{R}^{(1)} \simeq \zeta^{(1)} - \frac{1}{\mathcal{A}^0}\phi^{(1)}. \tag{6.96}$$

- The $\mathcal{O}(\epsilon^2)$ order

  The tt component of the Einstein equation gives

$$\mathcal{A}^0\dot{\zeta}^{(2)} - \dot{\phi}^{(2)} = \mathcal{C}^0\left(\dot{\zeta}^{(1)}\right)^2 - \frac{\mathcal{C}_3^0}{2}{}^{[3]}R^{(2)} + \frac{\mathcal{C}_3^0}{2}A^{(1)k}{}_jA^{(1)j}{}_k, \tag{6.97}$$

  where ${}^{[3]}R^{(2)}$ is the 3D Ricci scalar for the $\mathcal{O}(\epsilon^0)$ order metric $\gamma_{ij} = a(t)^2e^{2\zeta^{(0)}(\mathbf{x})}h_{ij}^{(0)}(\mathbf{x})$ and $\mathcal{C}^0$, $\mathcal{C}_1^0$, $\mathcal{C}_2^0$ and $\mathcal{C}_3^0$ are again background quantities, defined respectively as

$$\mathcal{C}^0(t) = \mathcal{C}_1^0(\mathcal{A}^0)^2 + \mathcal{C}_2^0\mathcal{A}^0 - 3\mathcal{C}_3^0, \tag{6.98}$$

$$\begin{aligned}\mathcal{C}_1^0(t) = {}& \frac{\frac{1}{2}K_X + 4K_{XX}X + 2K_{XXX}X^2 + 9H\dot{\phi}G_{3X}}{\dot{\phi}K_X + 2\dot{\phi}K_{XX}X + 18HG_{3X}X + 12HG_{3XX}X^2} \\ & + \frac{21H\dot{\phi}G_{3XX}X + 6H\dot{\phi}G_{3XXX}X^2}{\dot{\phi}K_X + 2\dot{\phi}K_{XX}X + 18HG_{3X}X + 12HG_{3XX}X^2},\end{aligned} \tag{6.99}$$

$$\mathcal{C}_2^0(t) = \frac{18G_{3X}X + 12G_{3XX}X^2}{\dot{\phi}K_X + 2\dot{\phi}K_{XX}X + 18HG_{3X}X + 12HG_{3XX}X^2}, \tag{6.100}$$

$$\mathcal{C}_3^0(t) = \frac{m_0^2}{\dot{\phi}K_X + 2\dot{\phi}K_{XX}X + 18HG_{3X}X + 12HG_{3XX}X^2}. \tag{6.101}$$

Integrating this equation, we get the solution of $\phi^{(2)}$ in terms of $\zeta^{(2)}$:

$$\phi^{(2)}(t,\mathbf{x}) = \int^t \mathrm{d}t' \mathcal{A}^0(t')\dot{\zeta}^{(2)}(t',\mathbf{x}) - \left(\mathcal{C}_\zeta^{(1)}(\mathbf{x})\right)^2 \int^t \frac{\mathrm{d}t'\mathcal{C}^0(t')}{\bar{a}(t')^6} + \frac{{}^{[3]}R^{(2)}(\mathbf{x})}{2}\int^t \frac{\mathrm{d}t'\mathcal{C}_3^0(t')}{a(t')^2} - \frac{C_A^{(1)}{}^k_j(\mathbf{x})C_A^{(1)}{}^j_k(\mathbf{x})}{2}\int^t \frac{\mathrm{d}t'\mathcal{C}_3^0(t')}{a(t')^6}, \tag{6.102}$$

where an integration spatial function has been absorbed into $C_\phi^{(1)}(\mathbf{x})$, and ${}^{[3]}R^{(2)}(\mathbf{x})$ (the Ricci scalar of the metric $e^{2\zeta^{(0)}(\mathbf{x})}h_{ij}^{(0)}(\mathbf{x})$) is related to ${}^{[3]}R^{(2)}$ (the Ricci scalar of the metric $a(t)^2e^{2\zeta^{(0)}(\mathbf{x})}h_{ij}^{(0)}(\mathbf{x})$) by

$${}^{[3]}R^{(2)}(\mathbf{x}) = a(t)^2\,{}^{[3]}R^{(2)}. \tag{6.103}$$

The trace part of Einstein's equation's ij component is given by

$$\begin{aligned} &-m_0^2\left(2\ddot{\zeta}^{(2)} + 6H\dot{\zeta}^{(2)} + 3\left(\dot{\zeta}^{(1)}\right)^2 + \frac{1}{2}A^{(1)}{}^k_l A^{(1)}{}^l_k + \frac{1}{6}\,{}^{[3]}R^{(2)}\right) \\ &= -2G_{3X}X\ddot{\phi}^{(2)} + \left(\dot{\phi}K_X - 2\dot{X}(G_{3X}+G_{3XX}X)\right)\dot{\phi}^{(2)} + \mathcal{D}^0\left(\dot{\phi}^{(1)}\right)^2, \end{aligned} \tag{6.104}$$

where

$$\begin{aligned} \mathcal{D}^0(t) = \Big(&\frac{1}{2}K_X + K_{XX}X - \ddot{\phi}G_{3X} - 5\ddot{\phi}G_{3XX}X - 2\ddot{\phi}G_{3XXX}X^2 \\ &+ 2\left(3\mathcal{H}^0 - \partial_t \ln \mathcal{A}^0\right)\dot{\phi}(G_{3X}+G_{3XX}X)\Big). \end{aligned} \tag{6.105}$$

Combining with Eq. (6.97), we get

$$\begin{aligned} \zeta^{(2)}(t,\mathbf{x}) = &\left(C_\zeta^{(1)}(\mathbf{x})\right)^2 \int^t \frac{\mathrm{d}t''}{\bar{a}(t'')^3}\int^{t''}\frac{\mathrm{d}t'\mathcal{E}_1^0(t')}{\bar{a}(t')^3} \\ &+ {}^{[3]}R^{(2)}(\mathbf{x})\int^t \frac{\mathrm{d}t''}{\bar{a}(t'')^3}\int^{t''}\frac{\mathrm{d}t'\mathcal{E}_3^0(t')\bar{a}(t')^3}{a(t')^2} \\ &+ C_A^{(1)}{}^k_l(\mathbf{x})C_A^{(1)}{}^l_k(\mathbf{x})\int^t \frac{\mathrm{d}t''}{\bar{a}(t'')^3}\int^{t''}\frac{\mathrm{d}t'\mathcal{E}_2^0(t')\bar{a}(t')^3}{a(t')^6}, \end{aligned} \tag{6.106}$$

where two integration spatial functions have been absorbed into $C_\zeta^{(1)}(\mathbf{x})$ and $\zeta^{(0)}(\mathbf{x})$ respectively, and $\mathcal{E}_1^0$, $\mathcal{E}_2^0$ and $\mathcal{E}_3^0$ are background quantities, defined respectively as

$$\begin{aligned} \mathcal{E}_1^0(t) = &\frac{\left(\dot{\phi}K_X - 2\dot{X}(G_{3X}+G_{3XX}X)\right)\mathcal{C}^0 + 2G_{3X}X(6\mathcal{H}^0\mathcal{C}^0 - \dot{\mathcal{C}}^0)}{2m_0^2 - 2G_{3X}X\mathcal{A}^0} \\ &- \frac{+\mathcal{D}^0\left(\mathcal{A}^0\right)^2 + 3m_0^2}{2m_0^2 - 2G_{3X}X\mathcal{A}^0}, \end{aligned} \tag{6.107}$$

$$\mathcal{E}_2^0(t) = \frac{\left(\dot{\phi}K_X - 2\dot{X}(G_{3X}+G_{3XX}X)\right)\mathcal{C}_3^0 + 2G_{3X}X(6H\mathcal{C}_3^0 - \dot{\mathcal{C}}_3^0) - m_0^2}{4m_0^2 - 4G_{3X}X\mathcal{A}^0}, \tag{6.108}$$

$$\mathcal{E}_3^0(t) = -\frac{\left(\dot{\phi}K_X - 2\dot{X}(G_{3X} + G_{3XX}X)\right)\mathcal{C}_3^0 + 2G_{3X}X(2H\mathcal{C}_3^0 - \dot{\mathcal{C}}_3^0) + \frac{1}{3}m_o^2}{4m_0^2 - 4G_{3X}X\mathcal{A}^0}. \tag{6.109}$$

The traceless part of Einstein's equation's ij component is given by

$$\dot{A}^{(2)i}{}_j + 3HA^{(2)i}{}_j + 3\dot{\zeta}^{(1)}A^{(1)i}{}_j - \left({}^{[3]}R^{(2)i}{}_j - \frac{1}{3}\delta^i_j\,{}^{[3]}R^{(2)}\right) = 0, \tag{6.110}$$

which gives rise to the solution

$$\begin{aligned} A^{(2)i}{}_j(t,\mathbf{x}) = \quad & -\frac{3C_\zeta^{(1)}(\mathbf{x})C_A^{(1)i}{}_j(\mathbf{x})}{a^3}\int^t \frac{\mathrm{d}t'}{\bar{a}(t')^3} \\ & + \frac{{}^{[3]}R^{(2)i}{}_j(\mathbf{x}) - \frac{1}{3}\delta^i_j\,{}^{[3]}R^{(2)}(\mathbf{x})}{a^3}\int^t \mathrm{d}t' a(t'), \end{aligned} \tag{6.111}$$

where again an integration spatial function has been absorbed into $C_A^{(1)k}{}_j(\mathbf{x})$ and ${}^{[3]}R^{(2)i}{}_j(\mathbf{x})$ (the Ricci tensor of the metric $e^{2\zeta^{(0)}(\mathbf{x})}h^{(0)}_{ij}(\mathbf{x})$) is related to ${}^{[3]}R^{(2)i}{}_j$ (the Ricci tensor of the metric $a(t)^2e^{2\zeta^{(0)}(\mathbf{x})}h^{(0)}_{ij}(\mathbf{x})$) by

$${}^{[3]}R^{(2)i}{}_j(\mathbf{x}) = a(t)^2\,{}^{[3]}R^{(2)i}{}_j. \tag{6.112}$$

From Eq. (6.43), we can derive

$$\begin{aligned} h^{(2)}_{ij}(t,\mathbf{x}) = {} & 6h^{(0)}_{ik}(\mathbf{x})C_\zeta^{(1)}(\mathbf{x})C_A^{(1)k}{}_j(\mathbf{x})\int^t\frac{\mathrm{d}t''}{a(t'')^3}\int^{t''}\frac{\mathrm{d}t'}{\bar{a}(t')^3} \\ & + 4h^{(0)}_{il}(\mathbf{x})C_A^{(1)l}{}_k(\mathbf{x})C_A^{(1)k}{}_j(\mathbf{x})\int^t\frac{\mathrm{d}t''}{a(t'')^3}\int^{t''}\frac{\mathrm{d}t'}{a(t')^3} \\ & - 2h^{(0)}_{ik}(\mathbf{x})\left({}^{[3]}R^{(2)k}{}_j(\mathbf{x}) - \frac{1}{3}\delta^k_j\,{}^{[3]}R^{(2)}(\mathbf{x})\right)\int^t\frac{\mathrm{d}t''}{a(t'')^3}\int^{t''}\mathrm{d}t' a(t'), \end{aligned} \tag{6.113}$$

where an integration spatial function has been absorbed into $h^{(0)}{}_{ij}(\mathbf{x})$. The ti component of Einstein's equation at the $\mathcal{O}(\epsilon^2)$ order become constraints for the $\mathcal{O}(\epsilon)$ order quantities

$$-2m_0^2\partial_i\dot{\zeta}^{(1)} - m_0^2\bar{\nabla}_k^{(1)}A^{(1)k}_i = (K_X\dot{\phi} + 6HG_{3X}X)\partial_i\phi^{(1)} - 2G_{3X}X\partial_i\dot{\phi}^{(1)}, \tag{6.114}$$

where $\bar{\nabla}_k^{(1)}$, of order $\mathcal{O}(\epsilon)$ itself, is the covariant derivative associated with the $\mathcal{O}(\epsilon^0)$ order metric $e^{2\zeta^{(0)}(\mathbf{x})}h^{(0)}_{ij}(\mathbf{x})$. This gives rise to 3 constraints on the unspecified integration functions $C_A^{(1)i}{}_j(\mathbf{x})$.

Summary

Here we summarize the solution obtained up to the $\mathcal{O}(\epsilon^2)$ order:

$$\zeta(t,\mathbf{x}) = \zeta^{(0)}(\mathbf{x}) + C_\zeta^{(1)}(\mathbf{x})\int^t\frac{\mathrm{d}t'}{\bar{a}(t')^3} + \left(C_\zeta^{(1)}(\mathbf{x})\right)^2\int^t\frac{\mathrm{d}t''}{\bar{a}(t'')^3}\int^{t''}\frac{\mathrm{d}t'\mathcal{E}_1^0(t')}{\bar{a}(t')^3}$$

$$+ C_A^{(1)}{}^k_l(\mathbf{x}) C_A^{(1)}{}^l_k(\mathbf{x}) \int^t \frac{\mathrm{d}t''}{\bar{a}(t'')^3} \int^{t''} \frac{\mathrm{d}t' \mathcal{E}_2^0(t') \bar{a}(t')^3}{a(t')^6}$$

$$+ {}^{[3]}R^{(2)}(\mathbf{x}) \int^t \frac{\mathrm{d}t''}{\bar{a}(t'')^3} \int^{t''} \frac{\mathrm{d}t' \mathcal{E}_3^0(t') \bar{a}(t')^3}{a(t')^2} + \mathcal{O}(\epsilon^3), \tag{6.115}$$

$$\phi(t,\mathbf{x}) = \phi^{(0)}(t) + C_\phi^{(1)}(\mathbf{x}) + C_\zeta^{(1)}(\mathbf{x}) \int^t \frac{\mathrm{d}t' \mathcal{A}^0(t')}{\bar{a}(t')^3} + \int^t \mathrm{d}t' \mathcal{A}^0(t') \dot{\zeta}^{(2)}(t',\mathbf{x})$$

$$- \left(C_\zeta^{(1)}(\mathbf{x}) \right)^2 \int^t \frac{\mathrm{d}t' \mathcal{C}^0(t')}{\bar{a}(t')^6} + \frac{{}^{[3]}R^{(2)}(\mathbf{x})}{2} \int^t \frac{\mathrm{d}t' \mathcal{C}_3^0(t')}{a(t')^2}$$

$$- \frac{C_A^{(1)}{}^k_j(\mathbf{x}) C_A^{(1)}{}^j_k(\mathbf{x})}{2} \int^t \frac{\mathrm{d}t' \mathcal{C}_3^0(t')}{a(t')^6} + \mathcal{O}(\epsilon^3), \tag{6.116}$$

$$A^i_j(t,\mathbf{x}) = \frac{C_A^{(1)}{}^i_j(\mathbf{x})}{a^3} - \frac{3 C_\zeta^{(1)}(\mathbf{x}) C_A^{(1)}{}^i_j(\mathbf{x})}{a^3} \int^t \frac{\mathrm{d}t'}{\bar{a}(t')^3}$$

$$+ \frac{{}^{[3]}R^{(2)}{}^i_j(\mathbf{x}) - \frac{1}{3}\delta^i_j {}^{[3]}R^{(2)}(\mathbf{x})}{a^3} \int^t \mathrm{d}t' a(t') + \mathcal{O}(\epsilon^3), \tag{6.117}$$

$$h_{ij}(t,\mathbf{x}) = h_{ij}^{(0)}(\mathbf{x}) - 2 h_{ik}^{(0)}(\mathbf{x}) C_A^{(1)}{}^k_j(\mathbf{x}) \int^t \frac{\mathrm{d}t'}{a(t')^3}$$

$$+ 6 h_{ik}^{(0)}(\mathbf{x}) C_\zeta^{(1)}(\mathbf{x}) C_A^{(1)}{}^k_j(\mathbf{x}) \int^t \frac{\mathrm{d}t''}{a(t'')^3} \int^{t''} \frac{\mathrm{d}t'}{\bar{a}(t')^3}$$

$$+ 4 h_{il}^{(0)}(\mathbf{x}) C_A^{(1)}{}^l_k(\mathbf{x}) C_A^{(1)}{}^k_j(\mathbf{x}) \int^t \frac{\mathrm{d}t''}{a(t'')^3} \int^{t''} \frac{\mathrm{d}t'}{a(t')^3}$$

$$- 2 h_{ik}^{(0)}(\mathbf{x}) \left({}^{[3]}R^{(2)}{}^k_j(\mathbf{x}) - \frac{1}{3}\delta^k_j {}^{[3]}R^{(2)}(\mathbf{x}) \right) \int^t \frac{\mathrm{d}t''}{a(t'')^3} \int^{t''} \mathrm{d}t' a(t') + \mathcal{O}(\epsilon^3), \tag{6.118}$$

where $\mathcal{A}^0$ is defined by Eq. (6.86), $\bar{a}(t)$ is defined by Eq. (6.89), $\mathcal{C}^0$, $\mathcal{C}_1^0$, $\mathcal{C}_2^0$ and $\mathcal{C}_3^0$ are defined by Eqs. (6.98-6.101) respectively, $\mathcal{E}_1^0$, $\mathcal{E}_2^0$ and $\mathcal{E}_3^0$ are defined by eqs. (6.107-6.109) respectively, ${}^{[3]}R^{(2)}{}^i_j(\mathbf{x})$ and ${}^{[3]}R^{(2)}(\mathbf{x})$ are 3D curvature tensors of the metric $e^{2\zeta^{(0)}(\mathbf{x})} h_{ij}^{(0)}(\mathbf{x})$.

There are several unspecified spatial functions in the general solution: $\zeta^{(0)}(\mathbf{x})$, $h_{ij}^{(0)}(\mathbf{x})$, $C_\zeta^{(1)}(\mathbf{x})$, $C_\phi^{(1)}(\mathbf{x})$ and $C_A^{(1)}{}^i_j(\mathbf{x})$ (all other unspecified spatial functions have been absorbed into this set of functions). These functions play the role of initial data for the dynamical degrees of freedom, so counting the pieces of initial data and taking into account any constraints between them can be used in order to determine the number of degrees of freedom. However, properly counting the physical degrees of freedom requires determining whether there are any degrees of freedom that can be removed using residual gauge freedom.

$h_{ij}^{(0)}(\mathbf{x})$ is symmetric and has a unit determinant and $C_A^{(1)}{}^i_j(\mathbf{x})$ is symmetric and traceless, so they each have 5 degrees of freedom. 3 components of $C_A^{(1)}{}^i_j(\mathbf{x})$ are related to other unspecified spatial functions respectively by the constraint equations (6.114). In order to determine how many of these degrees of freedom are pure gauge we need to consider the residual gauge freedom. Performing the infinitesimal coordinate transformation

$$x^\mu \to \bar{x}^\mu = x^\mu + \eta^\mu \tag{6.119}$$

and requiring that the synchronous gauge condition on the lapse N and shift N^i are respected, one straighforwadly obtains that η^μ should be of the form

$$\eta^0 = \eta^0(\mathbf{x}), \tag{6.120}$$

$$\eta^i = \int^t \mathrm{d}t' \gamma^{ij}(t', \mathbf{x}) \partial_j \eta^0(\mathbf{x}) + \tilde{\eta}^i(\mathbf{x}), \tag{6.121}$$

(η^μ may be chosen as $\mathcal{O}(\epsilon)$). From this we infer that the residual gauge freedom amounts to 4 functions of space. 3 of those can be chosen so as to eliminate 3 spatial functions in $h^{(0)}_{ij}(\mathbf{x})$ and 1 chosen so as to eliminate $C^{(1)}_\phi(\mathbf{x})$. Therefore, we may count the degrees of freedoms as follows:

$$\zeta^{(0)}(\mathbf{x}) \qquad \text{1 scalar growing mode } = \text{ 1 component,} \tag{6.122}$$

$$h^{(0)}_{ij}(\mathbf{x}) \qquad \text{2 tensor growing modes } = \text{ 5 components } - \text{ 3 gauge DoFs,} \tag{6.123}$$

$$C^{(1)}_\zeta(\mathbf{x}) \qquad \text{1 scalar decaying mode } = \text{ 1 component,} \tag{6.124}$$

$$C^{(1)i}_{A\ \ j}(\mathbf{x}) \qquad \text{2 tensor decaying modes } = \text{ 5 components } - \text{ 3 constraints.} \tag{6.125}$$

In this scalar-tensor system, one expects three physical degrees of freedom, one for the scalar mode and two for the tensor modes. As it is a second order system, each physical degree of freedom contains two phase-space degrees of freedom, so one should expect six free spatial functions. This is indeed what the counting reveals.

6.4.3 Late time of inflation

At the end of the last section, we claimed that $C^{(1)}_\zeta(\mathbf{x})$ represents a decaying mode. However, this is actually not obvious from the general solution given above. After all, $\bar{a}(t)$ is not the scale factor $a(t)$ but is given by a rather complicated expression in terms of background quantities. Additionally, $\mathcal{C}^0_n$ and $\mathcal{E}^0_n$ also have time dependence. In this section, we would like to briefly re-derive the solution for an important special case, the late time of inflation. This will not only allows us to show explicitly that $C^{(1)}_\zeta(\mathbf{x})$ represents a decaying mode, but it will demonstrate how one can eliminate the gauge mode $C^{(1)}_\phi(\mathbf{x})$ on inflationary backgrounds. Moreover, the assumption of quasi-de Sitter expansion drastically simplifies the solution and allows an intuitive understanding of its behavior. Physically, perturbations coming from the late time of inflation are observationally most important, as it is these perturbations that seed the large scale structure of the observable Universe. Note that, similar to the previous section, we mostly suppress the background quantities' order indication $^{(0)}$ to simplify the equations.

Eq. (6.83) can be integrated to get

$$K_X \dot{\phi} + 6HG_{3X}X \propto a(t)^{-3}, \tag{6.126}$$

which is an attractor of the dynamical system. So for the later time of inflation J^t essentially vanishes. In this limit, the background equations of motion can

be simplified to

$$K = -3m_0^2 H^2, \tag{6.127}$$

$$K_X = -3G_{3X} H\dot{\phi}, \tag{6.128}$$

and $\dot{\phi}$ and H become constant and $a \propto e^{Ht}$ [326]. Furthermore, we have

$$\mathcal{H}^0 \to H, \qquad \bar{a}(t) \to a(t). \tag{6.129}$$

The background quantities defined in the last section now all become constant and can also be simplified:

$$\mathcal{A}^0 = \frac{3M_{pl}^2 H - 3\dot{\phi}G_{3X}X}{\dot{\phi}K_{XX}X + 6HG_{3X}X + 6HG_{3XX}X^2}, \tag{6.130}$$

$$\mathcal{C}^0 = \mathcal{C}_1^0(\mathcal{A}^0)^2 + \mathcal{C}_2^0\mathcal{A}^0 - 3\mathcal{C}_3^0, \tag{6.131}$$

$$\mathcal{C}_1^0 = \frac{-\frac{5}{2}K_X + 4K_{XX}X + 2K_{XXX}X^2 + 21H\dot{\phi}G_{3XX}X + 6H\dot{\phi}G_{3XXX}X^2}{2\dot{\phi}K_{XX}X + 12HG_{3X}X + 12HG_{3XX}X^2}, \tag{6.132}$$

$$\mathcal{C}_2^0 = \frac{9G_{3X}X + 6G_{3XX}X^2}{\dot{\phi}K_{XX}X + 6HG_{3X}X + 6HG_{3XX}X^2}, \tag{6.133}$$

$$\mathcal{C}_3^0 = \frac{M_{pl}^2}{2\dot{\phi}K_{XX}X + 12HG_{3X}X + 12HG_{3XX}X^2}, \tag{6.134}$$

$$\mathcal{D}^0 = -\frac{3}{2}K_X + K_{XX}X + 6H\dot{\phi}G_{3XX}X, \tag{6.135}$$

$$\mathcal{E}_1^0 = -\frac{\dot{\phi}K_X\mathcal{C}^0 + \mathcal{D}^0\left(\mathcal{A}^0\right)^2 + 3M_{pl}^2}{2M_{pl}^2 - 2G_{3X}X\mathcal{A}^0}, \tag{6.136}$$

$$\mathcal{E}_2^0 = -\frac{\dot{\phi}K_X\mathcal{C}_3^0 + M_{pl}^2}{4M_{pl}^2 - 4G_{3X}X\mathcal{A}^0}, \tag{6.137}$$

$$\mathcal{E}_3^0 = \frac{1}{3}\mathcal{E}_2^0. \tag{6.138}$$

Note that we have assumed $\dot{\phi}K_{XX}X + 6HG_{3X}X + 6HG_{3XX}X^2 \neq 0$ and $\mathcal{A}^0 + 6M_{pl}^2 H/\dot{\phi}K_X \neq 0$, which, by using the background EoMs, is equivalent to $G_{3X}(K_X - K_{XX}X) + K_X G_{3XX}X \neq 0$ and $K(G_{3X}K_X - 2G_{3X}K_{XX}X + 2K_X G_{3XX}X) + K_X^2 G_{3X}X \neq 0$. So the Covariant Cubic Galileon case is included in our solution. We will not discuss the special cases where any of the aforementioned quantities actually vanish, but it is easy to follow our formalism in the last section to get the relevant results. The constraint Eq. (6.114) now becomes

$$2(G_{3X}X\mathcal{A}^0 - m_0^2)\partial_i C_\zeta^{(1)}(\mathbf{x}) = m_0^2\bar{\nabla}_k^{(1)}C_A^{(1)}{}_i^k(\mathbf{x}). \tag{6.139}$$

Finally, the solution for the late time of inflation is given by

$$\zeta(t,\mathbf{x}) = \zeta^{(0)}(\mathbf{x}) - \frac{C_\zeta^{(1)}(\mathbf{x})}{3Ha^3} + \frac{\mathcal{E}_1^0\left(C_\zeta^{(1)}(\mathbf{x})\right)^2}{18H^2a^6} + \frac{\mathcal{E}_2^0 C_A^{(1)}{}_l^k(\mathbf{x})C_A^{(1)}{}_k^l(\mathbf{x})}{18H^2a^6} - \frac{\mathcal{E}_3^{0[3]}R^{(2)}(\mathbf{x})}{2H^2a^2} + \mathcal{O}(\epsilon^3), \tag{6.140}$$

$$\phi(t,\mathbf{x}) = \phi^{(0)}(t) + C_\phi^{(1)}(\mathbf{x}) - \frac{\mathcal{A}^0 C_\zeta^{(1)}(\mathbf{x})}{3Ha^3} + \mathcal{A}^0\zeta^{(2)}(t,\mathbf{x}) + \frac{\mathcal{C}^0\left(C_\zeta^{(1)}(\mathbf{x})\right)^2}{6Ha^6} - \frac{\mathcal{C}_3^0\,{}^{[3]}R^{(2)}(\mathbf{x})}{4Ha^2} + \frac{\mathcal{C}_3^0 C_A^{(1)\,k}{}_j(\mathbf{x}) C_A^{(1)\,j}{}_k(\mathbf{x})}{12Ha^6} + \mathcal{O}(\epsilon^3), \tag{6.141}$$

$$A_j^i(t,\mathbf{x}) = \frac{C_A^{(1)\,i}{}_j(\mathbf{x})}{a^3} + \frac{C_\zeta^{(1)}(\mathbf{x}) C_A^{(1)\,i}{}_j(\mathbf{x})}{Ha^6} + \frac{{}^{[3]}R^{(2)\,i}{}_j(\mathbf{x}) - \frac{1}{3}\delta^i_j\,{}^{[3]}R^{(2)}(\mathbf{x})}{Ha^2} + \mathcal{O}(\epsilon^3), \tag{6.142}$$

$$h_{ij}(t,\mathbf{x}) = h_{ij}^{(0)}(\mathbf{x}) + \frac{2h_{ik}^{(0)}(\mathbf{x}) C_A^{(1)\,k}{}_j(\mathbf{x})}{3Ha^3} + \frac{2h_{ik}^{(0)}(\mathbf{x})\left({}^{[3]}R^{(2)\,k}{}_j(\mathbf{x}) - \frac{1}{3}\delta^k_j\,{}^{[3]}R^{(2)}(\mathbf{x})\right)}{3H^2a^2} + \frac{3h_{ik}^{(0)}(\mathbf{x}) C_\zeta^{(1)}(\mathbf{x}) C_A^{(1)\,k}{}_j(\mathbf{x}) + 2h_{il}^{(0)}(\mathbf{x}) C_A^{(1)\,l}{}_k(\mathbf{x}) C_A^{(1)\,k}{}_j(\mathbf{x})}{9H^2a^6} + \mathcal{O}(\epsilon^3). \tag{6.143}$$

Now, we want to explicitly do away with the gauge mode $C_\phi^{(1)}(\mathbf{x})$ in the case of near de Sitter inflation by re-slicing. To this end, we choose

$$\bar{t} = t + \eta^0(\mathbf{x}), \tag{6.144}$$

$$\bar{x}^i = x^i + \eta^i, \tag{6.145}$$

with

$$\eta^0(\mathbf{x}) = \frac{C_\phi^{(1)}(\mathbf{x})}{\dot{\phi}^{(0)}}, \tag{6.146}$$

$$\eta^i = \int^t \mathrm{d}t' \gamma^{ij}(t',\mathbf{x})\partial_j\eta^0(\mathbf{x}) = -\frac{h_{(0)}^{ij}(\mathbf{x})\partial_j C_\phi^{(1)}(\mathbf{x})}{2H\dot{\phi}^{(0)}e^{2\zeta^{(0)}(\mathbf{x})}a(\bar{t})^2} + \mathcal{O}(\epsilon^3). \tag{6.147}$$

Let us consider the effects of the temporal transformation on $\phi^{(0)}(t)$: Taylor expansion yields $\phi^{(0)}(t) = \phi^{(0)}(\bar{t}) - C_\phi^{(1)}(\mathbf{x}) + \mathcal{O}(\epsilon^3)$, which straightforwardly removes the constant mode in Eq. (6.141). Though far less obvious, any other effect of the temporal or the spatial part of he transformation leads to corrections that are either $\mathcal{O}(\epsilon^3)$ or can be absorbed in redefinitions of $C_\zeta^{(1)}(\mathbf{x})$ and $C_A^{(1)\,i}{}_j(\mathbf{x})$. The end result is that by re-slicing one can eliminate $C_\phi^{(1)}(\mathbf{x})$ with all the other terms in the solution unchanged.

6.4.4 Discussion

In Ref. [379], we have developed the superhorizon gradient expansion formalism for G-Inflation, a novel inflation model characterized by its higher order derivative interactions. We have solved the equations of motion of Galileon inflation up to second order in gradient expansion in the synchronous gauge, and obtained the general solution without imposing extra conditions on the first order quantities. We have identified the physical degrees of freedom in the solution, taking particular care in keeping track of the residual gauge freedom left after imposing the synchronous gauge condition. We have also defined a

curvature perturbation $\mathcal{R}^{(1)}$ conserved up to first order. Finally, we have considered the special case of quasi-de Sitter expansion and we have showed that the general solution is substantially simplified in this case.

Non-Gaussianity in primordial perturbations can be a powerful probe of different inflation models and the associated fundamental theory on which they are based. The gradient expansion technique (valid outside the horizon) is complementary to usual second-order perturbative theory (applied inside the horizon), rather than a complete alternative. In rough terms, one uses usual nonlinear perturbative theory to calculate the generation of non-Gaussianties inside the horizon and uses the gradient expansion to evolve the non-Gaussianities outside the horizon. Evolution of non-Gaussianities outside the horizon is often tackled with the separate Universe approximation, which is just the leading order gradient expansion. However, this approximation may be inadequate in some multi-field models or when the slow-roll condition is temporally violated [378, 374], in which case a gradient expansion to second order is needed.

With the formalism developed here, the natural next step is to calculate non-Gaussianities in G-inflation at superhorizon scales. In combination with the conventional non-linear perturbation analysis inside the horizon, one can then use the existing data to constrain the model parameters (see Ref. [387] for an attempt in this direction for k-inflation). Unfortunately, this is not something that can be done straightforwardly in our case. First of all, there is an important difficulty one has to overcome: after expanding to second order in the gradient expansion, the usual curvature perturbation is not conserved in time and one has to find a new non-linear curvature perturbation. A new curvature perturbation has actually been found in Ref. [373] (in uniform Hubble gauge), but under the assumption that the starting order of $\dot{\gamma}_{ij}$ is the second order in the gradient expansion, which largely simplifies the whole calculation. But it is unclear how restrictive this condition is and our results seem to indicate that it is not generically justified. Without this assumption, identifying the conserved curvature perturbation is a pending, quite non-trivial task. The development of the gradient expansion formalism is only one of the necessary tools for calculating the bispectrum. Some of the other tools already exist (e.g., the second order perturbation analysis inside the horizon).

Another potential application of the formalism developed here can be to gain general insight on the non-linear behavior of Galileon fields. A key feature of Galileon gravity is that it is supposed to give rise to $\mathcal{O}(1)$ corrections to general relativity at large distances and yet satisfies stringent constraints at short distances, such as in the solar system where any modification is typically constrained below $\mathcal{O}(10^{-5})$. This is achieved due to the high degree of non-linearity of the Galileon derivative interactions and the phenomenon is called the Vainshtein mechanism, originally discovered in massive gravity [252, 335]. This mechanism is not easy to see in perturbation theory due to its non-linear nature, and the full non-linear problem is difficult to solve. It would be interesting to use the gradient expansion in order to get a deeper understanding of the behaviour of these non-linear interactions, at least in the regime where it is applicable.

Finally, an interesting extension of this work would be to develop a superhorizon gradient expansion for multi-Galileon inflationary scenarios. Having multiple fields is a typical way to generate non-Gaussianity. Non-Gaussianity in the multi-Galileon model has been discussed in Refs. [340, 341].

Chapter 7

Effective Field Theory for Dark Energy and Modified Gravity

A plethora of models addressing the phenomenon of cosmic acceleration have been proposed and analyzed in the past fifteen years [216, 217, 14, 218], and it has become increasingly evident that the dynamics of perturbations will offer fundamental information to discriminate among proposed models [258, 246, 259, 260, 261, 262, 263, 264, 265].

Anticipating a wealth of high precision large scale structure data from ongoing and upcoming surveys, such as *Planck* [34], SDSS [22], DES [310], LSST [311] and Euclid [312], it is important to identify a model-independent way of testing the theory of gravity against the evolution of linear cosmological perturbations. To this extend, several proposals have been put forward [266, 200, 267, 268, 269, 271, 272, 273, 274, 275, 276, 278, 279, 280, 281, 282, 283, 284, 286, 287, 388, 288, 290, 291, 292, 293, 294, 296, 297, 298, 299].

In the quest for the optimal framework to perform cosmological tests of gravity, some authors have recently proposed an 'effective' approach to unify single field DE and MG modeling [228, 229, 389], inspired by effective field theories of inflation [80, 390] and large scale structure [391, 392, 393]. We will refer to it as the *effective field theory of cosmic acceleration* (hereafter EFT). The aim of this approach is that of creating a model independent framework that encompasses single-field DE/MG models with a well defined Jordan frame, where all matter minimally couples to gravity, describing the evolution of the background cosmology and of perturbations with a finite number of functions of time introduced at the level of the action. The action is written in unitary gauge, in terms of an expansion in the operators that are compatible with the residual symmetries of unbroken spatial diffeomorphisms, organized in powers of the number of perturbations and derivatives. There is a finite number of such operators that enter the action multiplied by time-dependent coefficients to which we will refer as EFT functions; in particular, the background dynamics is determined solely by three EFT functions, that are the coefficients of the three background operators; while the general dynamics of linear scalar perturbations

is affected by a total of six operators, and can therefore be analyzed in terms of six time-dependent functions.

Despite this model-independent construction, there is a precise mapping that can be worked out between the EFT action and the action of a given single field DE/MG model that introduces a single scalar field and has a well defined Jordan frame [394, 395]. Therefore, the EFT formalism can be used in two ways: as a general model-independent framework to test the theory of gravity on large scales, studying the effects of the different operators and the constraints that can be put by data on their coefficients; as a unifying language to analyze specific single scalar field DE/MG models, once the chosen model is mapped into the EFT framework. We refer the reader to Refs. [228, 394, 395] for a detailed illustration of the mapping and a complete inventory of the models that can be cast in the EFT language.

The advantage in using such a kind of approach is clear, but as for all theories or parametrizations of a class of models, also the EFT formalism suffers from some limitations as discussed in Refs. [228, 229]. As already mentioned, one of the assumptions on which the EFT is built, is the validity of the weak equivalence principle, which limits its range of applicability to models for which a Jordan frame can be defined. Moreover, neither vector or tensor fields can be included in this description. Modifications to gravity which include higher-dimensional theories are not allowed. Finally, the EFT formalism describes only low energy cosmological phenomena. Despite the inherent limitations, the EFT framework includes most of the viable approaches to the phenomenon of cosmic acceleration that will undergo scrutiny with upcoming cosmological surveys. We shall mention, among others, the Horndeski class which includes quintessence, k-essence, $f(R)$, covariant Galileon, the effective 4-dimentions limit of DGP [220] and more.

In this Chapter we will present three works: one in collaboration with M. Raveri and A. Silvestri [396] and two in collaboration with B. Hu, M. Raveri and A. Silvestri [397, 398]. In particular in Section 7.1, we briefly review the EFT formulation. In Section 7.3 the viability of three background functions is investigated by means of a thorough dynamical analysis. While in Section 7.4 we introduce EFTCAMB and EFTCosmoMC, which implement the EFT formalism into the public Einstein-Boltzmann solver *Code for Anisotropies in the Microwave Background* (CAMB) [399, 400] and *Markov-Chain Monte-Carlo* code (CosmoMC) [401].

7.1 The effective field theory action and its formulation

The action of the effective field theory for cosmic acceleration [228, 229] is constructed in unitary gauge and Jordan frame, in conformal time it reads

$$S = \int d^4x\sqrt{-g}\left\{\frac{m_0^2}{2}\left[1+\Omega(\tau)\right]R + \Lambda(\tau) - a^2c(\tau)\delta g^{00}\right.$$
$$\left. + \frac{M_2^4(\tau)}{2}(a^2\delta g^{00})^2 - \frac{\bar{M}_1^3(\tau)}{2}a^2\delta g^{00}\delta\mathcal{K}^\mu{}_\mu - \frac{\bar{M}_2^2(\tau)}{2}(\delta\mathcal{K}^\mu{}_\mu)^2\right.$$

$$- \frac{\bar{M}_3^2(\tau)}{2}\delta\mathcal{K}^{\mu}{}_{\nu}\delta\mathcal{K}^{\nu}{}_{\mu} + \frac{a^2\hat{M}^2(\tau)}{2}\delta g^{00}\delta R^{(3)} + m_2^2(\tau)(g^{\mu\nu}+n^{\mu}n^{\nu})\partial_{\mu}(a^2g^{00})\partial_{\nu}(a^2g^{00}) + \dots \Big\} + S_m[\chi_m, g_{\mu\nu}], \tag{7.1}$$

where m_0 is the bare Planck mass, R is the Ricci scalar, $\delta g^{00} = g^{00} + 1$, $\delta R^{(3)}$, $\delta\mathcal{K}^{\nu}{}_{\mu}$ and $\delta\mathcal{K}^{\mu}{}_{\mu}$ are the perturbations respectively to the upper time-time component of the metric, the three dimensional spatial Ricci scalar, the extrinsic curvature and its trace. The vector n^{μ} is the normal to surfaces of constant time. In this thesis, our notation follows more closely that one of Ref. [229], however we work in conformal time and we multiply the Ricci scalar by $1+\Omega$ instead of simply Ω for reasons of accuracy in the numerical calculations. The functions Ω, Λ and c are free functions of the time coordinate τ and are the only ones which affect the background dynamics, hence the name background functions. In particular, the function $1+\Omega$, in the Jordan frame parametrizes the coupling to gravity, while in the Einstein frame the same function would describe the coupling of the scalar DoF to matter. $\{M_2, \bar{M}_1, \bar{M}_2, \bar{M}_3, \hat{M}_2, m_2\}$ are functions of time with dimensions of mass. The operators multiplied by these functions contribute only to the equations for perturbations, along with the background ones. The ellipses in the action stand for higher order terms, e.g. $(\delta g^{00})^3$. S_m is the action for all matter fields, χ_m.

The EFT approach has one extra dynamical scalar DoF as one would expect in both DE/MG models. In action (7.1) it is hidden inside the metric. While the unitary gauge is particularly suited for the construction of the general action (7.1), in order to study dynamical perturbations it is more convenient to make manifest the scalar DoF via the Stückelberg technique [16]. Pratically, one has to restore the time diffeomorphism invariance by mean of an infinitesimal time coordinate transformation while spatial coordinates remain unchanged, i.e.

$$\tau \to \tau + \pi(x^{\mu}). \tag{7.2}$$

The transformation introduces a new scalar field π, known as the Stückelberg field, that realizes the symmetry nonlinearly. In the context of the effective field theory of Inflation [80], the Stückelberg field is associated to the Goldstone boson, while in our case the time translation invariance is no longer realized by the Goldstone scalar mode.

Making manifest the extra scalar DoF will modify all the EFT functions which are typically Taylor expanded in π according to

$$f(\tau) \to f(\tau + \pi(x^{\mu})) = f(\tau) + \dot{f}(\tau)\pi + \frac{\ddot{f}(\tau)}{2}\pi^2 + \dots, \tag{7.3}$$

where dots stand for derivatives w.r.t. conformal time. Operators that are not fully diffeomorphism invariant transform according to the tensor transformation law, generating dynamical terms for π. For a complete description see Refs. [80, 228, 229].

Then the action with the Stückelberg field is

$$
\begin{aligned}
S = \int d^4x\sqrt{-g}\Bigg\{ & \frac{m_0^2}{2}\left[1+\Omega(\tau+\pi)\right]R + \Lambda(\tau+\pi) - c(\tau+\pi)a^2\Bigg[\delta g^{00} - 2\frac{\dot\pi}{a^2} \\
& +2\mathcal{H}\pi\left(\delta g^{00} - \frac{1}{a^2} - 2\frac{\dot\pi}{a^2}\right) + 2\dot\pi\delta g^{00} \\
& +2g^{0i}\partial_i\pi - \frac{\dot\pi^2}{a^2} + g^{ij}\partial_i\pi\partial_j\pi - \left(2\mathcal{H}^2+\dot{\mathcal{H}}\right)\frac{\pi^2}{a^2} + ...\Bigg] \\
& + \frac{M_2^4(\tau+\pi)}{2}a^4\left(\delta g^{00} - 2\frac{\dot\pi}{a^2} - 2\frac{\mathcal{H}\pi}{a^2} + ...\right)^2 \\
& - \frac{\bar M_1^3(\tau+\pi)}{2}a^2\left(\delta g^{00} - 2\frac{\dot\pi}{a^2} - 2\frac{\mathcal{H}\pi}{a^2} + ...\right)\left(\delta\mathcal{K}^\mu{}_\mu + 3\frac{\dot{\mathcal{H}}}{a}\pi + \frac{\bar\nabla^2\pi}{a^2} + ...\right) \\
& - \frac{\bar M_2^2(\tau+\pi)}{2}\left(\delta\mathcal{K}^\mu{}_\mu + 3\frac{\dot{\mathcal{H}}}{a}\pi + \frac{\bar\nabla^2\pi}{a^2} + ...\right)^2 \\
& - \frac{\bar M_3^2(\tau+\pi)}{2}\left(\delta\mathcal{K}^i{}_j + \frac{\dot{\mathcal{H}}}{a}\pi\delta^i{}_j + \frac{1}{a^2}\bar\nabla^i\bar\nabla_j\pi + ...\right)\left(\delta\mathcal{K}^j{}_i + \frac{\dot{\mathcal{H}}}{a}\pi\delta^j{}_i\right. \\
& \left. + \frac{1}{a^2}\bar\nabla^j\bar\nabla_i\pi + ...\right) \\
& + \frac{\hat M^2(\tau+\pi)}{2}a^2\left(\delta g^{00} - 2\frac{\dot\pi}{a^2} - 2\frac{\mathcal{H}}{a^2}\pi + ...\right)\left(\delta R^{(3)} + 4\frac{\mathcal{H}}{a}\bar\nabla^2\pi + ...\right) \\
& + m_2^2(\tau+\pi)\left(g^{\mu\nu}+n^\mu n^\nu\right)\partial_\mu\left(a^2g^{00} - 2\dot\pi - 2\mathcal{H}\pi + ...\right)\partial_\nu\left(a^2g^{00} - 2\dot\pi\right. \\
& \left. - 2\mathcal{H}\pi + ...\right) + ...\Big\} + S_m[\chi_m, g_{\mu\nu}],
\end{aligned}
\tag{7.4}
$$

where $\bar\nabla$ indicates three dimensional spatial derivatives. Note that the conformal scale factor has been already Taylor expanded in π according to Eq. (7.3) and that our Stückelberg field is defined w.r.t. to conformal time, therefore there is a factor of a of difference w.r.t. the Stückelberg field of Refs. [228, 229].

7.1.1 The background equations

Varying the background part of the action (7.4), with respect to the metric and assuming a flat FLRW metric, one obtains the modified Friedmann equations:

$$
\mathcal{H}^2 = \frac{a^2}{3m_0^2(1+\Omega)}(\rho_m + 2c - \Lambda) - \mathcal{H}\frac{\dot\Omega}{1+\Omega}, \tag{7.5}
$$

$$
\dot{\mathcal{H}} = -\frac{a^2}{6m_0^2(1+\Omega)}\left(\rho_m + 3P_m\right) - \frac{a^2(c+\Lambda)}{3m_0^2(1+\Omega)} - \frac{\ddot\Omega}{2(1+\Omega)}, \tag{7.6}
$$

where $\mathcal{H} = \dot a/a$ and ρ_m and P_m are, respectively, the energy density and pressure of the matter components, for which we assume a perfect fluid form with the standard continuity equation:

$$
\dot\rho_m = -3\mathcal{H}(\rho_m + P_m). \tag{7.7}
$$

Eqs. (7.5)-(7.6) can be recast in the following, more conventional, form

$$\mathcal{H}^2 = \frac{a^2}{3m_0^2(1+\Omega)}\left(\rho_m + \rho_Q\right), \tag{7.8}$$

$$\dot{\mathcal{H}} = -\frac{a^2}{6m_0^2(1+\Omega)}\left(\rho_m + 3P_m + \rho_Q + 3P_Q\right), \tag{7.9}$$

if one defines

$$\rho_Q \equiv 2c - \Lambda - \frac{3m_0^2\mathcal{H}\dot{\Omega}}{a^2},$$
$$P_Q \equiv \Lambda + \frac{m_0^2}{a^2}\left(\ddot{\Omega} + \mathcal{H}\dot{\Omega}\right). \tag{7.10}$$

The latter can be interpreted as, respectively, the energy density and pressure of the effective dark fluid. Combining Eqs. (7.7), (7.8) and Eq. (7.9) one obtains the following continuity equation for this dark component:

$$\dot{\rho}_Q = -3\mathcal{H}\left(\rho_Q + P_Q\right) + \frac{3m_0^2}{a^2}\mathcal{H}^2\dot{\Omega}, \tag{7.11}$$

which tells us that the energy density ρ_Q is conserved only in the case of $\Omega =$ const., i.e. a minimally coupled theory.

The covariant, background-independent approach that we adopt [228, 229], aims at offering a general framework to study the evolution of cosmological perturbations in a model independent way. In the latter context, it is common to fix the background history to the one of ΛCDM, or something close to that, and to focus on the dynamics of perturbations. This is justified by the fact that the cosmological concordance model is in very good agreement with current observables constraining the expansion history and that most alternative models are highly degenerate with it at the level of background dynamics, while predicting modifications at the level of perturbations. In the EFT framework this practice would translate into assuming that the background is given *a priori*, i.e. typically it is chosen to be close to the ΛCDM one, and one focuses on the coefficients of the second order operators. If we were to fix the expansion history, we could use Eqs. (7.5)-(7.6) to eliminate two of the three EFT functions, typically $\Lambda(t)$ and $c(t)$, as

$$c = -\frac{m_0^2\ddot{\Omega}}{2a^2} + \frac{m_0^2\mathcal{H}\dot{\Omega}}{a^2} + \frac{m_0^2(1+\Omega)}{a^2}(\mathcal{H}^2 - \dot{\mathcal{H}}) - \frac{1}{2}(\rho_m + P_m), \tag{7.12}$$

$$\Lambda = -\frac{m_0^2\ddot{\Omega}}{a^2} - \frac{m_0^2\mathcal{H}\dot{\Omega}}{a^2} - \frac{m_0^2(1+\Omega)}{a^2}(\mathcal{H}^2 + 2\dot{\mathcal{H}}) - P_m. \tag{7.13}$$

This however would still leave us with one completely undetermined function of time, $\Omega(\tau)$ for which we should make some arbitrary choice. In Ref. [396] with M. Raveri and A. Silvestri, we perform instead an investigation of viable analytical forms of the three EFT background functions by means of a dynamical analysis of the background cosmology. The analysis is shown in Section 7.3.

7.2 Quintessence and f(R) models mapping

The EFT framework allows to study a specic single field DE/MG model once the mapping into the EFT language is known. We refer the reader to Refs. [228, 394,

395] for a complete list of the theories that can be cast in the EFT framework and for an exhaustive theoretical treatment of models already mapped into this language. Here we will show two simple examples:

- As illustrated in Refs. [228, 229], the minimally coupled Quintessence mapping into EFT functions is very straightforward. The typical action for such a model consists

$$S_\phi = \int d^4x\sqrt{-g}\left[\frac{m_0^2}{2}R - \frac{1}{2}\partial^\nu\phi\partial_\nu\phi - V(\phi)\right]. \tag{7.14}$$

  The second term can be written as

$$-\frac{1}{2}g^{\mu\nu}\partial_\mu\phi\partial_\nu\phi \;\rightarrow\; \frac{\dot{\phi}^2}{2}g^{00}, \tag{7.15}$$

  substituting back into the action, we get

$$S_\phi \rightarrow \int d^4x\sqrt{-g}\left[\frac{m_0^2}{2}R + \frac{\dot{\phi}^2}{2}\delta g^{00} + \frac{\dot{\phi}^2}{2} - V(\phi)\right]. \tag{7.16}$$

  The EFT functions can be written as

$$\Omega(t) = 0,\;\; c(t) = \frac{\dot{\phi}^2}{2},\;\; \Lambda(t) = \frac{\dot{\phi}^2}{2} - V(\phi). \tag{7.17}$$

- The second example is the f(R) theory [228]. Let us start with the action

$$S_f = \int d^4x\frac{m_0^2}{2}[R + f(R)], \tag{7.18}$$

  and Taylor expand around a background value of the Ricci scalar, $R^{(0)}$ up to second order

$$S_f \rightarrow \int d^4x\frac{m_0^2}{2}\left\{\left[1 + f_R(R^{(0)})\right]R + f(R^{(0)}) - R^{(0)}f_R(R^{(0)})\right\}. \tag{7.19}$$

  It is easy to deduce that the corresponding EFT functions are

$$\Omega(t) = f_R(R^{(0)}), \qquad \Lambda(t) = \frac{m_0^2}{2}f(R^{(0)}) - R^{(0)}f_R(R^{(0)}), \qquad c(t) = 0, \tag{7.20}$$

  where $f_R \equiv \frac{df}{dR}$.

7.3 A Background Dynamical Analysis

The effective field theory approach to cosmic acceleration has been conjectured as a unified description of DE/MG to apply to tests involving data on linear cosmological perturbations, therefore it is generally assumed that a background evolution will be specified *a priori*; in other words, the background functions will be chosen to closely mimic the evolution of the standard cosmological model (ΛCDM), and one focuses on effects at the level of perturbations. However,

fixing the expansion history does not determine all the EFT functions, and there remain one completely free function of time out of the original three. Given this high degree of freedom, and given that the remaining function affects also the evolution of perturbations, it is important to explore what general viability/compatibility rules can be placed on the background EFT functions by requiring that the corresponding model gives a viable expansion history, rather than fixing the latter *a priori*.

In Ref. [396], with M. Raveri and A. Silvestri, we investigated the cosmological viability of the three EFT background functions by means of a thorough dynamical analysis of the background evolution. The machinery that we set up serves different purposes. It offers a general scheme for performing dynamical analysis of DE/MG models within the model independent framework of EFT; the general results, obtained with this technique, can be projected into specific models. It also can be used to determine appropriate ansätze for the three EFT background functions when studying the dynamics of cosmological perturbations in the context of large scale structure tests of gravity.

In the last Section, we presented the background equations in conformal time, while in Ref. [396] we work in cosmic time, i.e. $dt = ad\tau$. Before moving to the central part of this work, let us briefly revisit the action using the cosmic time

$$S = \int d^4x\sqrt{-g}\left[\frac{m_0^2}{2}\Omega(t)R + \Lambda(t) - c(t)\delta g^{00}\right] + S_{\rm DE}^{(2)} + S_m[g_{\mu\nu}], \qquad (7.21)$$

where all the quantities of interest have been already defined. We have not written explicitly all the quadratic (and higher) order operators that describe the dynamics of perturbations, as they are not of relevance for our analysis of the background, rather collecting them into $S_{\rm DE}^{(2)}$. In cosmic time the modified Friedmann equations read

$$3m_0^2\Omega H^2 + 3m_0^2 H\dot{\Omega} = \sum_i \rho_i - \Lambda + 2c, \qquad (7.22)$$

$$3m_0^2 H^2\Omega + 2m_0^2\dot{H}\Omega + m_0^2\ddot{\Omega} + 2m_0^2 H\dot{\Omega} = -\sum_i p_i - \Lambda, \qquad (7.23)$$

where in this case the dot indicates derivation w.r.t. cosmic time and ρ_i and p_i are, respectively, the background energy density and pressure of the i-th matter component, for which we assume a perfect fluid form. We will consider two distinct components, i.e. dust with zero pressure (that we will indicate with a subscript 'm') and radiation with $p_r = 1/3\,\rho_r$. Their continuity equations in cosmic time read:

$$\dot{\rho}_m = -3H\rho_m, \qquad (7.24)$$

$$\dot{\rho}_r = -4H\rho_r. \qquad (7.25)$$

Finally we rewrite the continuity equation for the effective DE component

$$2\dot{c} - \dot{\Lambda} = 3m_0^2\dot{H}\dot{\Omega} - 6Hc + 6m_0^2H^2\dot{\Omega}\,. \qquad (7.26)$$

Equations (7.22)-(7.26) are all the equations we have at our disposal to study the dynamics of the background.

The presentation is organized as follows. In Section (7.3.1) we set up the dynamical system, describe the strategy to make it autonomous and then proceed with the dynamical analysis at different, increasing, orders in Section (7.3.2), investigating the cosmology of selected trajectories. In Section (7.3.3) we exploit the recursive nature of our system of equations, as well as the results from the previous analyses, to perform the dynamical analysis at a generic order N. Finally we discuss our results and conclude in Section (7.3.4).

7.3.1 Dynamical System and Cosmological Viability

In this Section we will set up the necessary ingredients to perform a dynamical analysis of the effective field theory of cosmic acceleration. We need to rewrite the equations for the background into an autonomous system of first ODEs, for which we can then study the stability around equilibrium points. To this purpose, we introduce the following dimensionless variables:

$$x = \frac{c}{3m_0^2H^2\Omega}, \quad y = \frac{c-\Lambda}{3m_0^2H^2\Omega}, \quad u = \frac{\rho_r}{3m_0^2H^2\Omega},$$

$$\alpha_0 = -\frac{\dot{\Omega}}{H\,\Omega}, \ldots, \alpha_n = -\frac{\Omega^{(n+1)}}{H\Omega^{(n)}}, \lambda_0 = -\frac{\dot{c}-\dot{\Lambda}}{H(c-\Lambda)}, \ldots, \lambda_m = -\frac{(c-\Lambda)^{(m+1)}}{H\,(c-\Lambda)^{(m)}}, \ldots \tag{7.27}$$

where the indices n, m are unbounded from above. Using Eqs. (7.22)-(7.26), we can write the following set of first order ODEs:

$$\frac{dx}{d\ln a} = \lambda_0 y - 6x - 2\alpha_0 + x\alpha_0 - (\alpha_0 + 2x)\frac{\dot{H}}{H^2}, \tag{7.28a}$$

$$\frac{dy}{d\ln a} = \left(\alpha_0 - \lambda_0 - 2\frac{\dot{H}}{H^2}\right) y, \tag{7.28b}$$

$$\frac{du}{d\ln a} = \left(\alpha_0 - 4 - 2\frac{\dot{H}}{H^2}\right) u, \tag{7.28c}$$

$$\frac{d\alpha_{n-1}}{d\ln a} = \left(-\alpha_n + \alpha_{n-1} - \frac{\dot{H}}{H^2}\right)\alpha_{n-1}, \quad (n \geq 1) \tag{7.28d}$$

$$\frac{d\lambda_{m-1}}{d\ln a} = \left(-\lambda_m + \lambda_{m-1} - \frac{\dot{H}}{H^2}\right)\lambda_{m-1}, \quad (m \geq 1) \tag{7.28e}$$

where

$$\frac{\dot{H}}{H^2} = -\frac{3}{2} - \frac{3}{2}x + \frac{3}{2}y + \alpha_0 - \frac{1}{2}\alpha_1\alpha_0 - \frac{1}{2}u. \tag{7.29}$$

This is a nonlinear, non-autonomous system that, however, displays a hierarchical structure in the equations for the $\alpha's$ and $\lambda's$. We will shortly describe our strategy to approach it.

Eq. (7.22) can be read as a constraint equation

$$\Omega_m = \frac{\rho_m}{3{m_0}^2\Omega H^2} = 1 - x - y - u - \alpha_0, \tag{7.30}$$

with $\Omega_m \geq 0$. When describing the cosmology of the different points, we will consider also the following parameters:

$$\Omega_{\rm DE} = x+y+\alpha_0, \qquad \Omega_{\rm r} = u, \qquad w_{\rm eff} \equiv -1-\frac{2}{3}\frac{\dot{H}}{H^2} = x-\frac{2}{3}\alpha_0+\frac{1}{3}\alpha_1\alpha_0-y+\frac{1}{3}u, \tag{7.31}$$

respectively the DE and radiation fractional energy density and the effective equation of state. Note that what we define the fractional density parameters, are the standard ones rescaled by the function $\Omega(t)$, as it is common to do in presence of a conformal coupling [402].

In order to solve system (7.28) we first need to make it autonomous. The simplest option corresponds to setting α_0, λ_0 to constant and evolve only the three core equations (7.28a)-(7.28c); we refer to this case as the zero-th order one and analyze it sampling the space (α_0, λ_0) to find viable cosmologies. As we discuss in detail in Section 7.3.2, this case corresponds to assuming that Ω and $c-\Lambda$ are power laws in the scale factor. To go beyond this zero-th order analysis, we can start exploring the hierarchy of equations (7.28d) and (7.28e), by setting α_N and λ_M constant for given $N, M \geq 1$. We are then left with a $(3+N+M)$-dimensional system formed by the three core equations for $\{x, y, u\}$, plus N equations for $\alpha_0, \ldots, \alpha_{N-1}$ and M equations for $\lambda_0, \ldots, \lambda_{N-1}$. We perform the dynamical analysis of this system sampling the space (α_N, λ_M) and determining the regions for which one can obtain viable expansion histories. What is the corresponding form of the EFT functions that we explore at this order? Let us develop the following argument in terms of Ω; it is then trivial to reproduce it for $c-\Lambda$. From the definition of the $\alpha's$, we see that fixing $\alpha_N = {\rm const}$ gives

$$\Omega^{(N)}(t) = \Omega^{(N)}(t_0) a^{-\alpha_N}, \tag{7.32}$$

where t_0 is the present time. Now that we have an expression for the N^{th} derivative of Ω, we can use it to write

$$\Omega(t) = \sum_{i=0}^{N-1} \frac{\Omega^{(i)}(t_0)}{i!}(t-t_0)^i + \Omega^{(N)}(t_0)\int_{t_0}^{t} \frac{(t-\tau)^{N-1}}{(N-1)!} a^{-\alpha_N}(\tau)\, d\tau, \tag{7.33}$$

that shows that the constant α_N ($N \geq 1$) parametrizes the remainder in a Taylor expansion of order $N-1$ around the present time for the function $\Omega(t)$. Notice that in order for the above argument to hold one does not necessarily need t_0 to be the present time (with $a_0 = 1$); the latter can be the desired choice in view of constraining the form of the EFT functions at recent times [228], where they are expected to have a non-trivial dynamics and where they are more likely to be probed. However, one can in principle choose any other t_0 that is suited to one's purpose, as long as a is rescaled by a_0 in Eqs. (7.32) and (7.33). In the following Sections, we separately analyze the stability of the system (7.28) at different orders. In particular, after analyzing the zero-th order case in Section 7.3.2, we maintain λ_0 constant and focus on the α channel of the system, solving $3+N$ equations for the variables $\{x, y, u, \alpha_0, \ldots, \alpha_N\}$. In other words, we focus on the class of models for which $c-\Lambda$ is a power law in the scale factor, while the conformal factor Ω can be increasingly general as we go up with the order. Alternatively one could fix Ω to a constant and open the λ channel, which would correspond to exploring all minimally coupled models

of DE. Finally, one could work with both channels and, for instance, explore, within this parametrized framework the full class of Horndeski theories [327]. While we leave the former, as well as the most general case, for future work, we want to stress that the machinery set up in our work is quite general and easily applicable to the other cases mentioned above.

Finally, let us point out that the structure of the system is such that the planes $y = 0$, $u = 0$, $\alpha_i = 0$, $\lambda_j = 0$ are all invariant manifolds, which implies that trajectories starting on one of these planes remain on it. This ensures that viable trajectories identified at a given order, will exist at all higher orders. We exploit this feature at the end of this Section, when we reconstruct the dynamics at a generic order $N \geq 3$.

7.3.2 Stability Analysis

The dynamics of system (7.28) can be studied analyzing the evolution around fixed/critical points, i.e. points p_i satisfying the equilibrium condition

$$\frac{dp_i}{d\ln a} = 0. \tag{7.34}$$

In the following we briefly summarize the general procedure; for an exhaustive description of the technique, and for some applications to cosmological models we refer the reader to [403, 404, 405, 406, 216, 407, 408]. After determining its fixed points, one proceeds to calculate the eigenvalues μ_i of the Jacobian matrix $\mathcal{M}$ of the system in order to linearize it around each critical point. This determines the stability nature of the point, in other words it controls how the system behaves when approaching the point. We are interested in hyperbolic critical points, since around these the linearized dynamical system is a good approximation of the full nonlinear system. By definition a critical point is said to be hyperbolic if all eigenvalues of $\mathcal{M}$ have $Re(\mu_i) \neq 0$. Hyperbolic critical points are robust, in the sense that small perturbations do not change qualitatively the phase portrait near the equilibrium. For an n-dimensional system one has n eigenvalues for each point and the stability depends on the nature of these eigenvalues, according to the following classification:

- All μ_i are real and have the same sign:
  - Negative eigenvalues → Stable node/ Attractor;
  - Positive eigenvalues → Unstable node;
- All μ_i are real and at least one positive and one negative → Saddle points;
- At least one eigenvalue is real and there are pairs of complex eigenvalues:
  - All eigenvalues have negative real parts → Stable Focus-Node;
  - All eigenvalues have positive real parts → Unstable Focus-Node;
  - At least one positive real part and one negative → Saddle Focus.

A working cosmological model needs to first undergo a radiation dominated era, followed by a matter era, and then enter a phase of accelerated expansion

(DE) as indicated by observations [18, 19]. In terms of critical points we need two saddle points for the radiation and the matter dominated eras, followed by a late time accelerated attractor, i.e. a stable node with $w_{\rm eff} < -\frac{1}{3}$. In addition we impose the constraints that $\Omega_m \geq 0$ and $\Omega_r \geq 0$, given that matter and radiation energy densities should be positively defined, and $\Omega(t) > 0$ to guarantee a stable gravity [409, 410]. On the other hand, we allow the effective dark energy density to be negative since this quantity may not correspond to the energy density of an actual fluid, and may indeed be negative in some models of modified gravity [402]. Finally, in reconstructing viable trajectories, we require that the matter era is long enough to allow for structure formation.

Zero$^{\rm th}$ order analysis

The simplest option to make the system (7.28) autonomous is setting α_0 and λ_0 to constant and evolve only the core equations (7.28a)-(7.28c). The corresponding behavior of the EFT functions is

$$\Omega(t) = \Omega_0\, a^{-\alpha_0}, \qquad c(t) - \Lambda(t) = (c-\Lambda)_0 a^{-\lambda_0}, \tag{7.35}$$

where the constants will depend on the initial conditions and their value does not affect the stability analysis.

Unless $\alpha_0 = 0$, the system (7.28a)-(7.28c) is not closed due to the dependence on α_1 through $\dot{H}/H^2$. We can use (7.28d) for $n = 1$ to get

$$\frac{\dot{H}}{H^2} = \frac{1}{2-\alpha_0}\left(2\alpha_0 - \alpha_0^2 - 3 + 3y - 3x - u\right) . \tag{7.36}$$

The resulting critical points of the system and the analysis of their stability are shown in Tab. 7.1. We find that the same results are still valid if $\alpha_0 = 0$. In what follows we present their eigenvalues and discuss the cosmological viability.

- P_1: *matter point*
  The eigenvalues and the relative eigenvectors of the linearized system around the first critical point are:

$$\begin{aligned} &\mu_1 = -1, && \mu_2 = \alpha_0 - 3, && \mu_3 = 3 - \lambda_0. \\ &\vec{u}_1 = \left(\frac{\alpha_0}{6-3\alpha_0}\,,\,0\,,\,1\right), && \vec{u}_2 = (1\,,\,0\,,\,0)\,, && \vec{u}_3 = \left(\frac{\alpha_0-\lambda_0}{\alpha_0+\lambda_0-6}\,,\,1\,,\,0\right). \end{aligned} \tag{7.37}$$

  This point displays a scaling solution for which matter and DE coexists with a constant ratio between their energy densities. We are primarily interested in the matter configuration, since this is the only critical point of the zeroth order system that can provide a matter dominated critical point. If we require $\Omega_m \approx 1$, then we have $\alpha_0 \approx 0$, which combined with the requirements of having a saddle, gives $\alpha_0 = 0 \wedge \lambda_0 < 3$.

- P_2: *stiff matter point*

$$\begin{aligned} &\mu_1 = 2 - \alpha_0, && \mu_2 = 3 - \alpha_0, && \mu_3 = -\alpha_0 - \lambda_0 + 6. \\ &\vec{u}_1 = (-1\,,\,0\,,\,1), && \vec{u}_2 = (1\,,\,0\,,\,0), && \vec{u}_3 = (-1\,,\,1\,,\,0). \end{aligned} \tag{7.38}$$

This point is a DE dominated critical point; it is a stable node with accelerated expansion only if $\alpha_0 > 3 \wedge \alpha_0 + \lambda_0 > 6$. For $\alpha_0 = 0$, it has $w_{\rm eff} = 1$, which corresponds to a stiff matter behavior that could be of interest for modeling early stages of the Universe [101].

- P_3: *DE point*

$$\begin{aligned}
&\mu_1 = \lambda - 4, \quad \mu_2 = \lambda_0 - 3, \\
&\mu_3 = \alpha_0 + \lambda_0 - 6. \\
&\vec{u}_1 = \left(\frac{\lambda_0 - 2\alpha_0}{3(\alpha_0 - 2)} \, , -\frac{\alpha_0 + \lambda_0 - 6}{3(\alpha_0 - 2)} \, , 1 \right), \quad \vec{u}_2 = \left(\frac{\alpha_0 - \lambda_0}{\alpha_0 + \lambda_0 - 6} \, , 1 \, , 0 \right), \\
&\vec{u}_3 = (-1 \, , 1 \, , 0) \, .
\end{aligned} \tag{7.39}$$

This is the second DE dominated critical point of the zero-th order system; it exhibits a correct cosmological behavior, i.e. $w_{\rm eff} < -\frac{1}{3}$, if $(\alpha_0 \geq 3 \wedge \alpha_0 + \lambda_0 < 6) \vee (\alpha_0 < 1 \wedge \lambda_0 < \alpha_0 + 2) \vee (1 \leq \alpha_0 < 3 \wedge \lambda_0 < 3)$.

- P_4: *radiation point*

$$\begin{aligned}
&\mu_1 = 1, \quad \mu_2 = \alpha_0 - 2, \quad \mu_3 = 4 - \lambda_0. \\
&\vec{u}_1 = \left(\frac{\alpha_0}{6 - 3\alpha_0} \, , 0 \, , 1 \right), \quad \vec{u}_2 = (-1 \, , 0 \, , 1) \, , \\
&\vec{u}_3 = \left(\frac{\lambda_0 - 2\alpha_0}{3(\alpha_0 - 2)} \, , -\frac{\alpha_0 + \lambda_0 - 6}{3(\alpha_0 - 2)} \, , 1 \right).
\end{aligned} \tag{7.40}$$

This point is characterized by $\Omega_m = 0$ and a coexistence of radiation and DE with a constant energy density ratio; in other words it is a scaling radiation point. We will focus on its radiation dominated version, since it is the only point that can supply a radiation era for the zero-th order trajectories. It can be be easily seen that it corresponds to a saddle with $w_{\rm eff} = \frac{1}{3}$ if $\alpha_0 = 0 \wedge \lambda_0 \neq 4$.

Combining all the information above, we conclude that viable cosmological models for the zero-th order case, can be recovered setting $\alpha_0 = 0$ and $\lambda_0 < 3$, and they are characterized by the transitions $P_4 \to P_1 \to P_3$ (radiation$\to$ matter $\to$ DE attractor). One can actually further constrain the space (α_0, λ_0). Indeed, a peculiar feature of the zero-th order system is the disposition of the critical points. A careful analysis of the eigenvectors (7.37)-(7.40), shows that for any pair of critical points the heteroclinic orbits, i.e. the lines connecting the two points, are straight lines. This is valid for any choice of (α_0, λ_0) and it allows us to put a stricter bound on λ_0 by requiring a long enough matter era for the trajectories of interest. Let us elucidate this point. The ΛCDM model corresponds to $\alpha_0 = \lambda_0 = 0$ and its trajectory is such that it starts very close to the radiation saddle point P_4, then it passes close to the matter saddle P_1 and finally it reaches the DE attractor P_3, always moving very close to the heteroclinic orbits that connect these three critical points. The time spent by this trajectory in the last transition gives a handle on the proper duration of the matter era for trajectories that aim to be cosmologically viable. Since after we set $\alpha_0 = 0$ the coordinates of P_1 and P_4 are fixed (i.e. independent on λ_0), we can use the constraint on the position of P_3 to put a stringent bound on λ_0;

Point	$[x_c, y_c, u_c]$	Stability	$\Omega_{\rm DE}$	$w_{\rm eff}$
P_1	$\left[-\frac{1}{6}\alpha_0(1+\alpha_0), 0, 0\right]$	**Stable node:** $\lambda_0 > 3 \wedge \alpha_0 \leq 2$ **Saddle point:** $(\lambda_0 < 3 \wedge \alpha_0 \leq 2) \vee (\alpha_0 > 3 \wedge \lambda \neq 3)$	$-\frac{1}{6}(\alpha_0 - 5)\alpha_0$	$-\frac{\alpha_0}{3}$
P_2	$[1-\alpha_0, 0, 0]$	**Stable node:** $\alpha_0 > 3 \wedge$ $\alpha_0 + \lambda_0 > 6$. **Unstable node:** $\alpha_0 < 2 \wedge$ $\alpha_0 + \lambda_0 < 6$ **Saddle point:** otherwise	1	$1 - \frac{2\alpha_0}{3}$
P_3	$\left[\frac{1}{12}(-\alpha_0^2 - \alpha_0(\lambda_0+4) + 2\lambda_0), \frac{1}{12}(\alpha_0-2)(\alpha_0+\lambda_0-6), 0\right]$	**Stable node:** $(\alpha_0 \geq 3 \wedge$ $\alpha_0 + \lambda_0 < 6) \vee$ $(\alpha_0 < 3 \wedge \lambda_0 < 3)$. **Unstable node:** $(\lambda_0 > 4 \wedge \alpha_0 \geq 2) \vee$ $(\alpha_0 + \lambda_0 > 6$ $\wedge \alpha < 2)$. **Saddle point:** otherwise	1	$\frac{1}{3}(-\alpha_0 + \lambda_0 - 3)$
P_4	$\left[-\frac{\alpha_0^2}{4}, 0, \frac{1}{4}(\alpha_0-2)^2\right]$	**Unstable node:** $\alpha_0 > 2 \wedge \lambda_0 < 4$ **Saddle point:** $(\alpha_0 > 2 \wedge \lambda_0 > 4) \vee$ $(\alpha_0 < 2 \wedge \lambda_0 \neq 4)$	$-\frac{1}{4}(\alpha_0 - 4)\alpha_0$	$\frac{1-\alpha_0}{3}$

Table 7.1: Hyperbolic critical points and stability analysis for the *zero-th order* system. The additional constraints $\Omega_m \geq 0$ and $\Omega_r \geq 0$ have been imposed. We have $\mathcal{D} \equiv \{\alpha_0, \lambda_0 \in \mathbb{R}\}$.

indeed if we change the latter, and hence move P_3, the duration of the matter era will change significantly. In other words, we need P_3 to be always close to its ΛCDM position, and this forces $\lambda_0 \sim 0$.

In summary, *viable cosmological models for the zero-th order case, can be recovered setting* $\alpha_0 = 0$ and $\lambda_0 \approx 0$, *and they are characterized by the transitions* $P_4 \to P_1 \to P_3$. Notice that $\alpha_0 = 0$ implies that the conformal factor $\Omega(t)$ is a constant, which just rescales the Planck mass.

Reconstructing quintessence models

We shall now show how the results of this general dynamical analysis can be used to constrain specific models of DE. As an example, we choose to interpret the results of the zero-th order analysis within the context of quintessence by using the matching in [228, 229]. Given that c and Λ for quintessence models assume the following forms:

$$c = \frac{\dot{\phi}^2}{2}\,, \qquad c - \Lambda = V(\phi) = (c-\Lambda)_0 a^{-\lambda_0}, \tag{7.41}$$

one immediately notices that the bound $\alpha_0 = 0$ for the zero-th order analysis, translates into the constraint that any quintessence model with a potential which

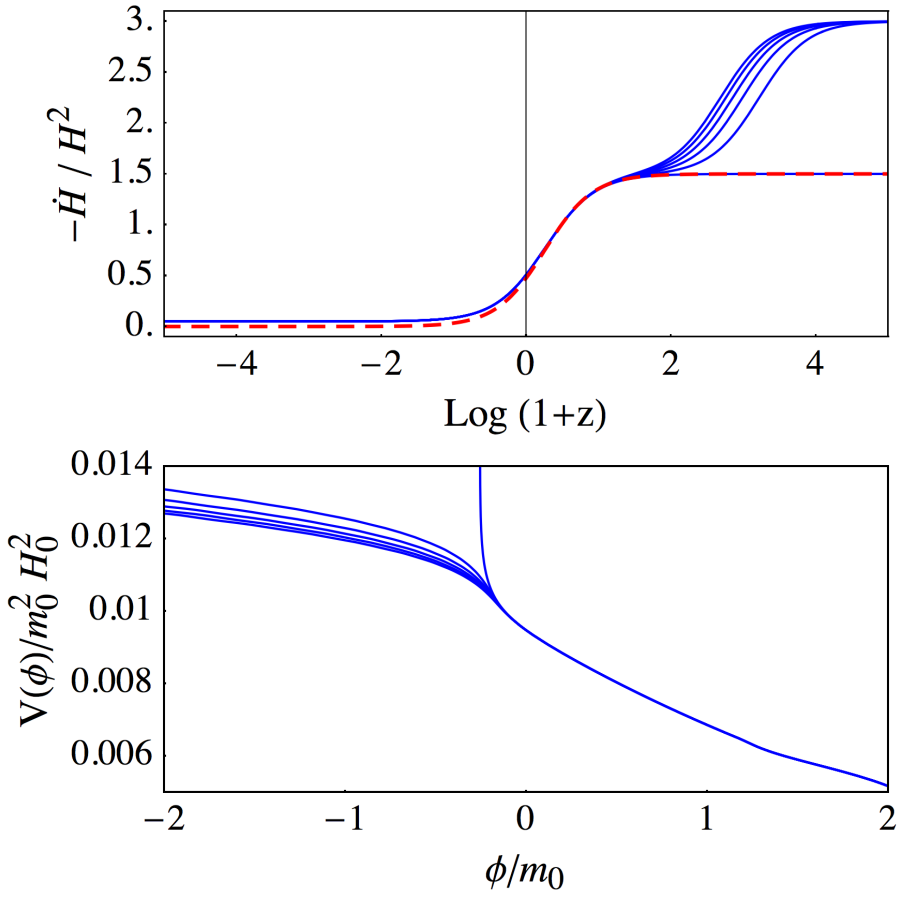

Figure 7.1: The slow roll parameter and the quintessence potential reconstructed for several trajectories of the $\alpha_0 = 0$, $\lambda_0 = 0.1$ model (blue lines). The red dashed line represents the behavior of the Planck [21] best fit ΛCDM model.

is a power law in the scale factor, cannot have a power law behavior for the conformal factor Ω, and therefore at this order is forced to be minimally coupled.

Among the models selected in this way, we will choose for our example those corresponding to the value $\lambda_0 = 0.1$. For simplicity we do not include radiation in this numerical study since it will not alter much the reconstruction. We choose initial conditions so that the present day matter density matches the Planck ΛCDM best fit value [21] and we sample the trajectories that undergo a $P_1 \to P_3$ transition. Then using Eq. (7.41) we reconstruct the time evolution of the quantities of interest, i.e. the slow-roll parameter and the the potential. We show the outcome in Fig. 7.1, where one can notice that the late time DE attractor corresponds to slow roll behavior which makes the field behave approximately like a cosmological constant. On the other hand at early times the field is rolling down the potential very fast as the DE component behaves like stiff matter, as expected since the unstable stiff-matter point, P_2, serves as the starting point for the numerically reconstructed trajectories. The corresponding

potential is monotonically decreasing and positively defined.

First order analysis

We now start exploring the hierarchy of equations for the $\alpha' s$. The immediate generalization of the previous model is the one obtained by letting α_0 vary, while fixing (α_1, λ_0) to constant. As discussed at the beginning of this Section, this corresponds to setting

$$\dot{\Omega}(t) = \dot{\Omega}_0 a^{-\alpha_1}, \qquad c(t) - \Lambda(t) = (c-\Lambda)_0 a^{-\lambda_0}, \tag{7.42}$$

where again the constants will depend on the initial conditions and do not affect the stability analysis. Our system of equations is now formed by Eqs. (7.28a)-(7.28c) along with Eq. (7.28e) with $n = 1$ and the constraint (7.30). The system has nonlinear quadratic terms and, for different values of the parameters (α_1, λ_0), it can display a wide range of behaviors.

The critical points of the system and the stability properties according to their eigenvalues are summarized in Tab. 7.2. In what follows we give a more detailed overview of each point, reporting the corresponding eigenvalues.

- P_1: *matter point*
  The linearized system around the first critical point has the following eigenvalues:
  $$\mu_1 = -3, \quad \mu_2 = \frac{3}{2} - \alpha_1, \quad \mu_3 = -1, \quad \mu_4 = 3 - \lambda_0. \tag{7.43}$$
  It corresponds to a matter dominated solution ($w_{\rm eff} = 0$) which is a saddle point for $\lambda_0 \neq 3 \wedge \alpha_1 < \frac{3}{2} \vee \lambda_0 < 3 \wedge \alpha_1 > \frac{3}{2}$.

- P_2: *stiff matter point*
  $$\mu_1 = 3, \quad \mu_2 = 3 - \alpha_1, \quad \mu_3 = 6 - \lambda_0, \quad \mu_4 = 2. \tag{7.44}$$
  This point corresponds to unstable solutions with a stiff matter equation of state, which could be relevant in the early stages of the Universe [101].

- P_3: *DE point*
  $$\mu_1 = -6 + \lambda_0, \quad \mu_2 = -3 + \lambda_0, \quad \mu_3 = -\alpha_1 + \frac{\lambda_0}{2}, \quad \mu_4 = -4 + \lambda_0. \tag{7.45}$$
  It gives a DE dominated solution which is accelerated for $\lambda_0 < 2$. For $\lambda_0 < 0$ the point has a phantom equation of state. In particular we have a late time accelerated attractor (i.e. a stable node), with $a \propto t^{2/\lambda_0}$, for $(\alpha_1 > 1 \wedge \lambda_0 < 2) \vee (\lambda_0 < 2\alpha_1 \wedge \alpha_1 \leq 1)$.

- P_4: *phantom DE point*
  $$\mu_1 = -5+2\alpha_1, \quad \mu_2 = -3+\alpha_1, \quad \mu_3 = -2+2\alpha_1-\lambda_0, \quad \mu_4 = 2(\alpha_1-3). \tag{7.46}$$
  It has a DE dominated solution with an accelerated expansion for $\alpha_1 < 3$, (with a phantom equation of state for $\alpha_1 < 2$). Furthermore, the point is a saddle for $\alpha_1 < \frac{5}{2} \wedge \lambda_0 > -2 + 2\alpha_0$ with $a \propto t^{\frac{1}{\alpha_1 - 2}}$.

Point	$[x_c, y_c, u_c, \alpha_{0,c}]$	Stability	$\Omega_{\rm DE}$	$w_{\rm eff}$
P_1	$[0,0,0,0]$	**Stable node:** $\lambda_0 > 3 \wedge \alpha_1 > \frac{3}{2}$ **Saddle point:** otherwise	0	0
P_2	$[1,0,0,0]$	**Unstable node:** $\alpha_1 < 3 \wedge \lambda_0 < 6$ **Saddle point:** otherwise	1	1
P_3	$\left[\frac{\lambda_0}{6}, 1-\frac{\lambda_0}{6}, 0, 0\right]$	**See Fig. 7.2.**	1	$\frac{1}{3}(\lambda-3)$
P_4	$[-1,0,0,2]$	**Stable node:** $\alpha_1 < \frac{5}{2} \wedge 2-2\alpha_1+\lambda_0 > 0$, **Unstable node:** $\alpha_1 > 3 \wedge 2-2\alpha_1+\lambda_0 < 0$, **Saddle point:** otherwise	1	$\frac{1}{3}(-7+2\alpha_1)$
P_5	$[\frac{1}{3}(-3+5\alpha_1-2\alpha_1^2), , 0, 0, -3+2\alpha_1]$	**Stable node:** $\alpha_1 < \frac{3}{2} \wedge \lambda_0 > 3$ **Saddle point:** $\alpha_1 < \frac{3}{2} \wedge \lambda_0 < 3 \vee \alpha_1 > 3 \wedge \lambda_0 > 3 \vee \alpha_1 > 3 \wedge \lambda_0 < 3 \vee \lambda_0 \neq 3 \wedge \frac{3}{2} < \alpha_1 < \frac{5}{2}$	$-4+\frac{11\alpha_1}{3}-\frac{2\alpha_1^2}{3}$	$1-\frac{2\alpha_1}{3}$
P_6	$[\frac{1}{6}[-2\alpha_1^2+\alpha_1(\lambda_0-4)+3\lambda_0], \frac{1}{6}(-3+\alpha_1)(-2+2\alpha_1-\lambda_0), 0, 2\alpha_1-\lambda_0]$	**See Fig. 7.2.**	1	$\frac{1}{3}(-3-2\alpha_1+2\lambda_0)$
P_7	$[0,0,1,0]$	**Saddle point:** $\lambda_0 \neq 4 \wedge \alpha_1 \neq 2$	0	$\frac{1}{3}$
P_8	$[-(-2+\alpha_1)^2, 0, , (-3+\alpha_1)^2, 2(-2+\alpha_1)]$	**Saddle point:** $\alpha_1 \neq 3 \wedge \alpha_1 \neq 2 \wedge \lambda_0 \neq 4$	$-8+6\alpha_1-\alpha_1^2$	$\frac{1}{3}(5-2\alpha_1)$

Table 7.2: Hyperbolic critical points of the *first order* analysis (α_1, λ_0 = constant), for which we have imposed the additional constraints $\Omega_m \geq 0$ and $\Omega_r \geq 0$. We have $\mathcal{D} \equiv \{\alpha_1, \lambda_0 \in \mathbb{R}\}$.

- P_5: *matter scaling point*

$$\begin{aligned}\mu_1 &= \frac{1}{4}\left(-21+13\alpha_1-2\alpha_1^2-\sqrt{81-42\alpha_1+29\alpha_1^2-20\alpha_1^3+4\alpha_1^4}\right),\\ \mu_2 &= \frac{1}{4}\left(-21+13\alpha_1-2\alpha_1^2+\sqrt{81-42\alpha_1+29\alpha_1^2-20\alpha_1^3+4\alpha_1^4}\right),\\ \mu_3 &= 3-\lambda_0, \quad \mu_4=-1. \end{aligned} \tag{7.47}$$

For this critical point we have a matter scaling solution with $\Omega_m = 5-\frac{11}{3}\alpha_1+\frac{2}{3}\alpha_1^2$ and $\Omega_{\rm DE} = -4+\frac{11\alpha_1}{3}-\frac{2\alpha_1^2}{3}$. The constraint on the positiveness of the matter density gives $\alpha_1 \geq 3 \vee \alpha_1 \leq \frac{5}{2}$. In our work we do not perform a full analysis of scaling solutions, but we rather focus on the two extrema for which either of the two components has fractional energy density equal to unity. We leave the full analysis of the scaling regime for future work. For this specific point it means that we consider only the case for which $\Omega_m = 1$ and the case for which $\Omega_{\rm DE} = 1$. Both points do not display the proper cosmology and therefore we do not consider P_5 any further.

- P_6: *DE point*

$$\begin{aligned}\mu_1 &= \lambda_0-3, \quad \mu_2 = \lambda_0-4,\\ \mu_3 &= \frac{1}{4}\left(-12-2\alpha_1^2-3\lambda_0+\alpha_1(10+\lambda_0)\right.\\ &\quad \left.-\sqrt{-3+\alpha_1}\,W\right),\\ \mu_4 &= \frac{1}{4}\left(-12-2\alpha_1^2-3\lambda_0+\alpha_1(10+\lambda_0)\right.\\ &\quad \left.+\sqrt{-3+\alpha_1}\,W\right), \end{aligned} \tag{7.48}$$

where $W = \sqrt{-48+4\alpha_1^3-4\alpha_1^2(\lambda_0-1)-8\lambda_0+5\lambda_0^2+\alpha_1(32-12\lambda_0+\lambda_0^2)}$. The point P_6 gives a DE dominated solution, with $a(t) \propto t^{\frac{1}{\lambda_0-\alpha_1}}$, which gives an accelerated expansion for $\lambda_0-\alpha_1<1$ (phantom if $\alpha_1>\lambda_0$). The results of the stability analysis around this critical point are summarized in Fig. 7.2; one can identify regions in the space (α_1,λ_0) for which the point is a late time attractor, as well as regions for which it is a stable focus-node. The latter one is an asymptotically stable point and corresponds to the case in which the system undergoes oscillations prior to reaching the equilibrium.

- P_7: *radiation point*

$$\mu_1=-2, \quad \mu_2=1, \quad \mu_3=-\alpha_1+2, \quad \mu_4=4-\lambda_0. \tag{7.49}$$

It corresponds to a standard radiation point with $w_{\rm eff}=\frac{1}{3}$ and can be a saddle for $\alpha_1 \neq 2$ and $\lambda_0 \neq 4$.

- P_8: *radiation scaling point*

$$\mu_1=1, \quad \mu_2=2(\alpha_1-3), \quad \mu_3=-6+5\alpha_1-\alpha_1^2, \quad \mu_4=4-\lambda_0. \tag{7.50}$$

This point exhibits a radiation scaling behavior since $\Omega_m=0$ while Ω_r and $\Omega_{\rm DE}$ can be both non-vanishing. However one cannot in general find values of (α_1,λ_0) that give either a proper DE or radiation dominated cosmology.

As we already discussed, a working cosmological model needs to first undergo a radiation dominated era, followed by a matter dominated era (that needs to be long enough to allow for proper structure formation) and finally it has to approach an accelerated phase. The only critical point which corresponds to a proper radiation domination in the first order system is P_7, which is a saddle for $\alpha_1 \neq 2$ and $\lambda_0 \neq 4$; a good critical point for a matter era is P_1, which can be a saddle with $a \propto t^{2/3}$. From this point the system can move to an accelerated expansion phase by going toward the late time attractors P_3, P_4 or P_6 (as well as the stable-focus version of P_6), depending on the values of α_1, λ_0. Therefore we have three types of cosmologically viable trajectories, that can be identified by the last transition that they undergo: $P_1 \to P_3$, $P_1 \to P_4$ and $P_1 \to P_6$ (with and without oscillations). In the next subsection we investigate numerically each of these cases. Finally, we give a graphical representation of the regions in (α_1, λ_0) for which the different transitions can take place in Fig. 7.2.

Numerical investigation of different transitions

We shall now investigate numerically the structure of the phase space for some models that display the different types of possible transitions discussed above. In order to facilitate the visualization of the phase space, we neglect radiation.

Let us briefly describe the procedure that we follow for this numerical investigation.

We set initial conditions in order to reproduce the ΛCDM matter density [21] at some given initial redshift and we systematically sample trajectories that cross the plane so defined. After the integration of the equations of motion we notice that, even if nothing a priori suggests it, the trajectories that depart from constant matter density planes remain quite close to them. It is then possible to visualize the behavior of the three dimensional system by projecting the trajectories on these planes, and compactifying the latter via

$$x_P = \frac{x}{\sqrt{1+x^2+y^2}}\,, \qquad y_P = \frac{y}{\sqrt{1+x^2+y^2}}. \tag{7.51}$$

After this operation we obtain the phase space plots that are shown in Figs. 7.3-7.4. In what follows we discuss the different types of transitions recovered with the technique just described; in particular we choose four different combinations of values for (α_1, λ_0), according to the previous analysis (e.g. Fig. 7.2), to focus each time on a different type of trajectory among the cosmologically viable ones.

$P_1 \to P_3$ transition. We start with the model corresponding to $\alpha_1 = 0.1$ and $\lambda_0 = 0$. This choice of values allows us to recover trajectories that mimic very closely the ΛCDM trajectory, shown as a red line in Fig. 7.3a. Notice that for this choice of α_1, λ_0, there is an alternative stable attractor, P_4, which gives a phantom DE. We set initial conditions to reproduce $\Omega_m^0 = 0.31$ and evolve the system to obtain the phase space plot shown in Fig. 7.3a. One can notice that the phase space is dominated in the past by trajectories moving away from the unstable point P_2. These trajectories can be divided in several groups. The first one is made by trajectories that leave P_2 and reach infinity. Obviously these correspond to unphysical solutions since the matter density and/or $w_{\rm eff}$ would go to infinity as well. The second group is made of trajectories that leave P_2 to

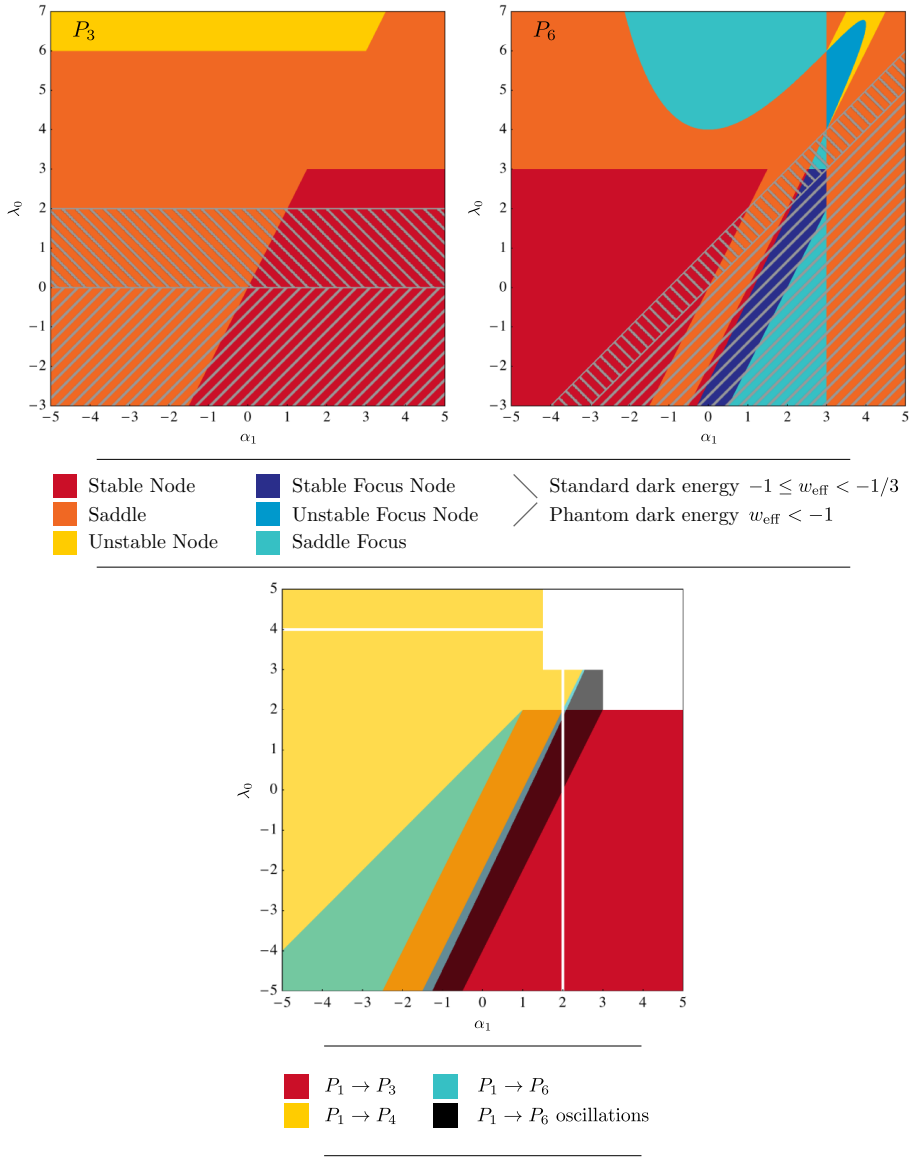

Figure 7.2: The top right panel shows the results of the stability analysis of the *first order* system around P_3. The panel at the to left illustrates the stability around P_6. The bottom panel shows the combined results of the *first order* analysis: regions in the (α_1, λ_0) plane which allow the different transitions discussed in Section 7.3.2 are shown in different colors.

go to P_3 and exhibit a cosmological behavior that is very similar to the ΛCDM one. The third family of trajectories leave P_2 to go to P_4 that is the phantom DE attractor, while the fourth family of trajectories is made up by solutions that leave infinity and go to P_4 and P_3. It is worth noticing that we find again the $P_2 \to P_1 \to P_3$ transition that we had found for the zero-th order system. In

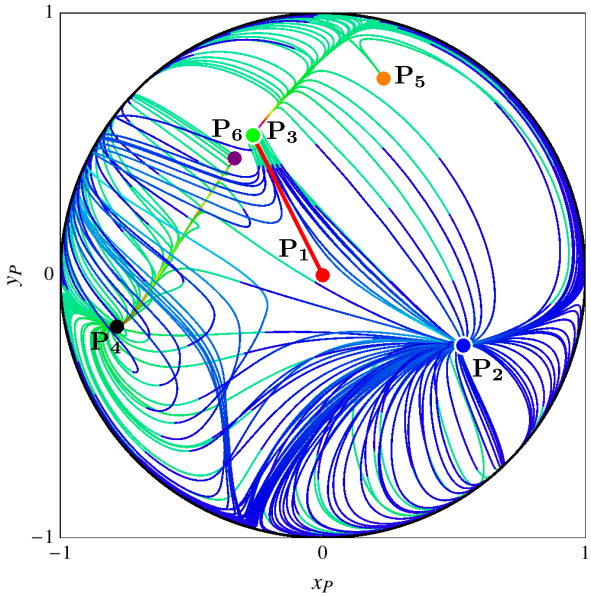

P_1: matter dominated saddle
P_2: stiff matter unstable node
P_3: dark energy stable node
P_4: dark energy attractor $w_{\rm eff} = -7/3$
P_5: stiff matter saddle
P_6: dark energy saddle

(a) The $\alpha_1 = 0.1$, $\lambda_0 = 0$ model.

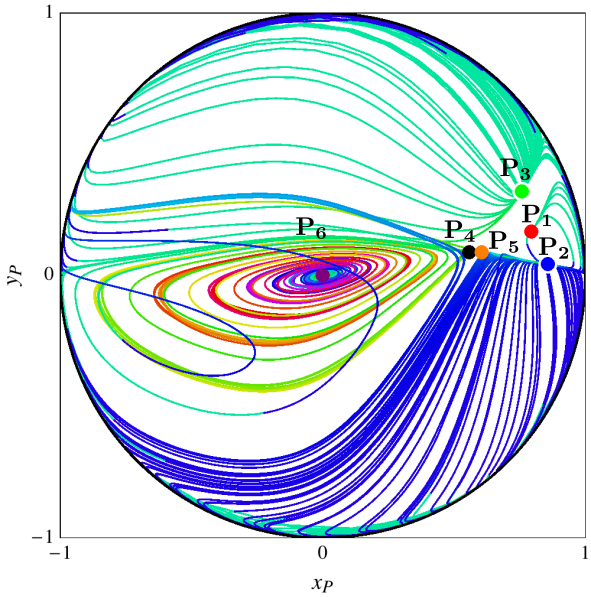

P_1: matter dominated saddle
P_2: stiff matter unstable node
P_3: dark energy attractor
P_4: dark energy saddle, $w_{\rm eff} = -0.7$
P_5: matter scaling saddle, $\Omega_m = 0.04, w_{\rm eff} = -1.7$
P_6: dark energy stable focus, $w_{\rm eff} = -1.7$

(b) The $\alpha_1 = 2.4$, $\lambda_0 = 1.3$ model.

Figure 7.3: The phase space numerical investigation of different DE models for the *first order* system. Initial conditions are evolved both in the past (blue lines) and in the future (green line). The red line in (a) corresponds to the ΛCDM trajectory.

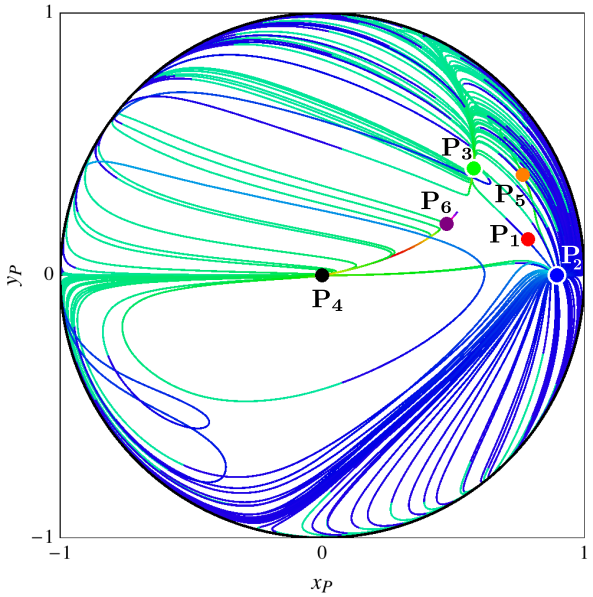

P_1: matter dominated saddle
P_2: stiff matter unstable node
P_3: dark energy attractor
P_4: dark energy attractor, $w_{\rm eff} = -2$
P_5: matter scaling saddle, $\Omega_m = 3.3, w_{\rm eff} = 0.67$
P_6: dark energy saddle, $w_{\rm eff} = -1.3$

(a) The $\alpha_1 = 0$, $\lambda_0 = -1/2$ model.

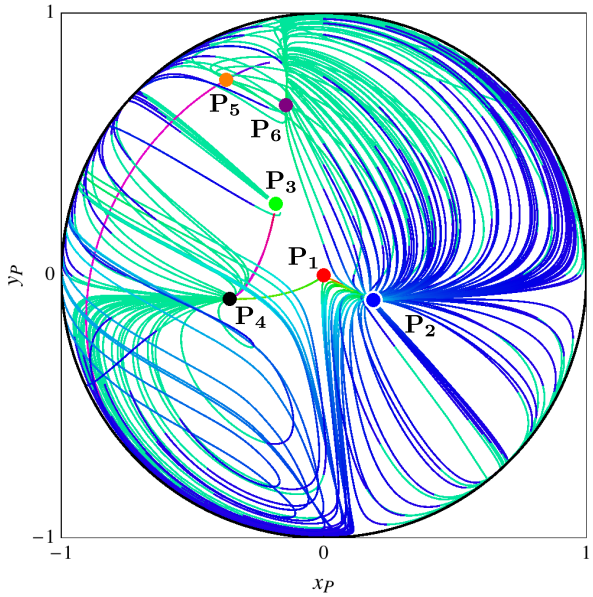

P_1: matter dominated saddle
P_2: stiff matter unstable node
P_3: dark energy saddle $w_{\rm eff} = -1.7$
P_4: dark energy attractor, $w_{\rm eff} = -3.7$
P_5: matter scaling saddle, $\Omega_m = 15, w_{\rm eff} = 2.3$
P_6: dark energy attractor, $w_{\rm eff} = -1$

(b) The $\alpha_1 = -2$, $\lambda_0 = -2$ model.

Figure 7.4: The phase space numerical investigation of different DE models for the *first order* system. Initial conditions are evolved both in the past (blue lines) and in the future (green line).

fact, the eigenvector that corresponds to the positive eigenvalue of P_1 is aligned with the eigenvector that corresponds to the negative eigenvalue of P_3 and the same holds for P_1 and P_2. As we already discussed, this gives rise to a family of cosmologically viable trajectories (noticeable in Fig. 7.3a) that move very close to the heteroclinic orbits connecting these points.

$P_1 \to P_6$ transition with oscillations. We now investigate numerically a model which displays a $P_1 \to P_6$ transition with oscillations (Fig. 7.3b). We obtain this behavior by setting $\alpha_1 = 2.4$ and $\lambda_0 = 1.3$. This time we impose initial conditions such that $\Omega_m = 1$ at high redshift (i.e. $z = 1000$), to evolve the system more into the future than in the past. Doing so, we avoid the dominance of the unstable point P_2 and are able to show a richer set of trajectories in the phase space plot. The most interesting family of trajectories corresponds to trajectories that either start at P_2 or infinity at early times, then pass close to P_1 crossing the $\Omega_m = 1$ plane and then move close to P_4, and start circling toward P_6. The background cosmology of one of such trajectories is shown in Fig. 7.5.

$P_1 \to P_4$ transition. In order to numerically recover a model which displays a $P_1 \to P_4$ transition, we choose $\alpha_1 = -1/2$ and $\lambda_0 = 0$. The points P_1 and P_2 exhibit basically the same behavior as in the previous models, however for the chosen values of α_1, λ_0 both P_3 and P_4 play the role of a DE attractor, with different w_{eff}. This time we impose initial conditions to match the matter density today. In Fig. 7.4a we can see as a result that we obtain two different types of trajectories that go from P_1 to P_4. The first set departs from P_2 and, after passing close to the matter saddle point P_1, go to the DE attractor P_4. The second one starts at infinity, then passes close to P_1 and eventually moves towards P_4. We plot the cosmological behavior of a trajectory that undergoes this transition in Fig. 7.5.

$P_1 \to P_6$ transition. The last transition we want to discuss is the $P_1 \to P_6$. In order to obtain trajectories with this behavior we set $\alpha_1 = -2$ and $\lambda_0 = -2$ and impose appropriate initial conditions in order to have equivalence between DM and DE density at the same redshift as the Planck best fit ΛCDM model [21]. As we can see from the resulting phase space plot in Fig. 7.4b, the system displays a clear transition from P_1 to P_6 for the trajectories that start close to P_2. In Fig. 7.5 we show the cosmological behavior of one of these trajectories.
The selected values for α_1, λ_0, allow also different types of trajectories, as can be read off Fig. 7.2. In particular we can recognize two sets of trajectories that show a P_1 to P_4 transition. The first set of trajectories starts in P_2 and move toward P_1, but are then deviated towards P_4 instead of P_6. The second set of trajectories starts at infinity, approaches P_1 and then moves towards P_4. Noticeably in the phase space plot in consideration (Fig. 7.4b), one ca observe non-trivial heteroclinic orbits joining P_1 and P_4, P_4 to P_3 and P_6 to P_5.

In summary, from the numerical investigation of the different transitions, we have learned that in general trajectories that undergo a $P_1 \to P_3$ transition are those that closely resemble the ΛCDM cosmology. Models involving other transitions, such as $P_1 \to P_4$ or $P_1 \to P_6$, display trajectories that are quite different from the ΛCDM one, but still can give viable cosmologies as can be noticed in Fig. 7.5.

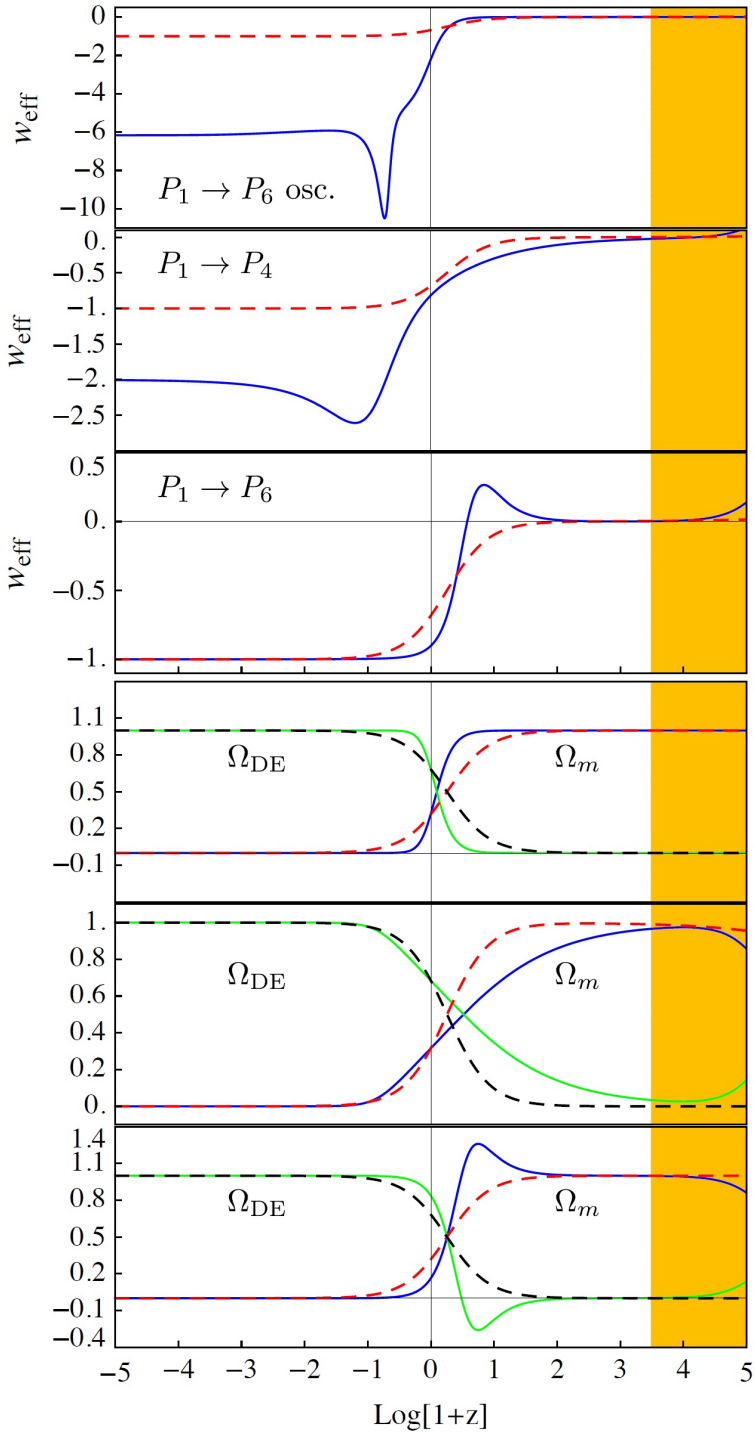

Figure 7.5: The top 3 panels shows the behavior of the effective equation of state for ΛCDM (red dashed line) and three different DE models (blue continuous line) corresponding to different types of trajectories identified in the *first order* system and described in Section 7.3.2. The bottom 3 panels shows the evolution of matter and DE densities for the ΛCDM model (respectively the red and black dashed lines) and the different DE models (respectively the blue and green solid lines), for the same transitions in the top 3 panels. The yellow area represents the region in which we expect a non-negligible contribution from radiation which was not considered when constructing these numerical DE models.

Second order analysis

We now proceed to the second order by allowing both α_0 and α_1 to vary, while fixing α_2 and λ_0 to constant. The models under consideration will then be characterized by

$$\ddot{\Omega}(t) = \ddot{\Omega}_0 a^{-\alpha_2}\,, \qquad c(t) - \Lambda(t) = (c-\Lambda)_0 a^{-\lambda_0}. \tag{7.52}$$

As it can be seen from (7.28), α_2 is the first of the $\alpha' s$ that does not enter the core equations (7.28a)-(7.28c); it is therefore from this order on, that we start to observe some of the effects of the recursive nature of Eqs. (7.28d). As we will shortly show, the majority of the critical points for the second order system are just trivial extensions of the critical points of the first order case; they replicate the values for the coordinates $\{x_c, y_c, u_c, \alpha_{0,c}\}$ and come in two copies distinguished by the value of α_1, being it equal or different from zero. The latter difference reflects into a different dynamics for $\Omega(t)$, which can be richer for the points with $\alpha_1 \neq 0$. To highlight this splitting of the points, we shall label with the subscript a the duplicates of the first order critical points that have $\alpha_1 = 0$, and with b the duplicates that have $(\alpha_1 \neq 0)$. This splitting trend will become regular from the next order on and it will help us in Section 7.3.3 for the classification of the points at a generic order N.
The details of all the critical points and their stability are shown in Tabs. C.1-C.2 in Appendix C.1. In what follows we briefly comment on the characteristics of the cosmologically interesting points.

- *Matter points*
  There are two critical points that are matter dominated with $w_{\text{eff}} = 0$ and both of them represents the extension to one higher dimension of the P_1 critical point found in the first order analysis. Their coordinates and the eigenvalues of the linearized system are:

$$P_{1a} \equiv (0,0,0,0,0) \qquad \mu_1 = -3,\ \mu_2 = -1,\ \mu_3 = \frac{3}{2},\ \mu_4 = \frac{3}{2} - \alpha_2,$$
$$\mu_5 = 3 - \lambda_0. \tag{7.53a}$$
$$P_{1b} \equiv \left(0,0,0,0,\alpha_2 - \frac{3}{2}\right) \quad \mu_1 = -3,\ \mu_2 = -1,\ \mu_3 = 3 - \alpha_2,\ \mu_4 = -\frac{3}{2} + \alpha_2,$$
$$\mu_5 = 3 - \lambda_0. \tag{7.53b}$$

  The first one, P_{1a}, is a viable saddle point for $\lambda_0 \neq 3 \wedge \alpha_2 \neq \frac{3}{2}$ while the second one, P_{1b}, is a saddle for $\lambda_0 \neq 0 \wedge \alpha_2 \neq \frac{3}{2} \wedge \alpha_2 \neq 3$. As we can notice the stability requirements are quite mild if compared to the constraints that we found at the previous orders. As a result the vast majority of second order models will have two cosmologically viable matter configurations distinguished by the behavior of $\Omega(t)$. When passing close to P_{1a} models will be characterized by $\ddot{\Omega} \ll \dot{\Omega} \ll \Omega$ which means that the coupling to matter will be frozen at a certain value until the model moves toward DE domination. On the other hand the second configuration corresponds to a matter era in which $\Omega(t)$ has a non-trivial dynamics.

- *Stiff-matter points*
  There are two P_2-like critical points with a stiff matter equation of state,

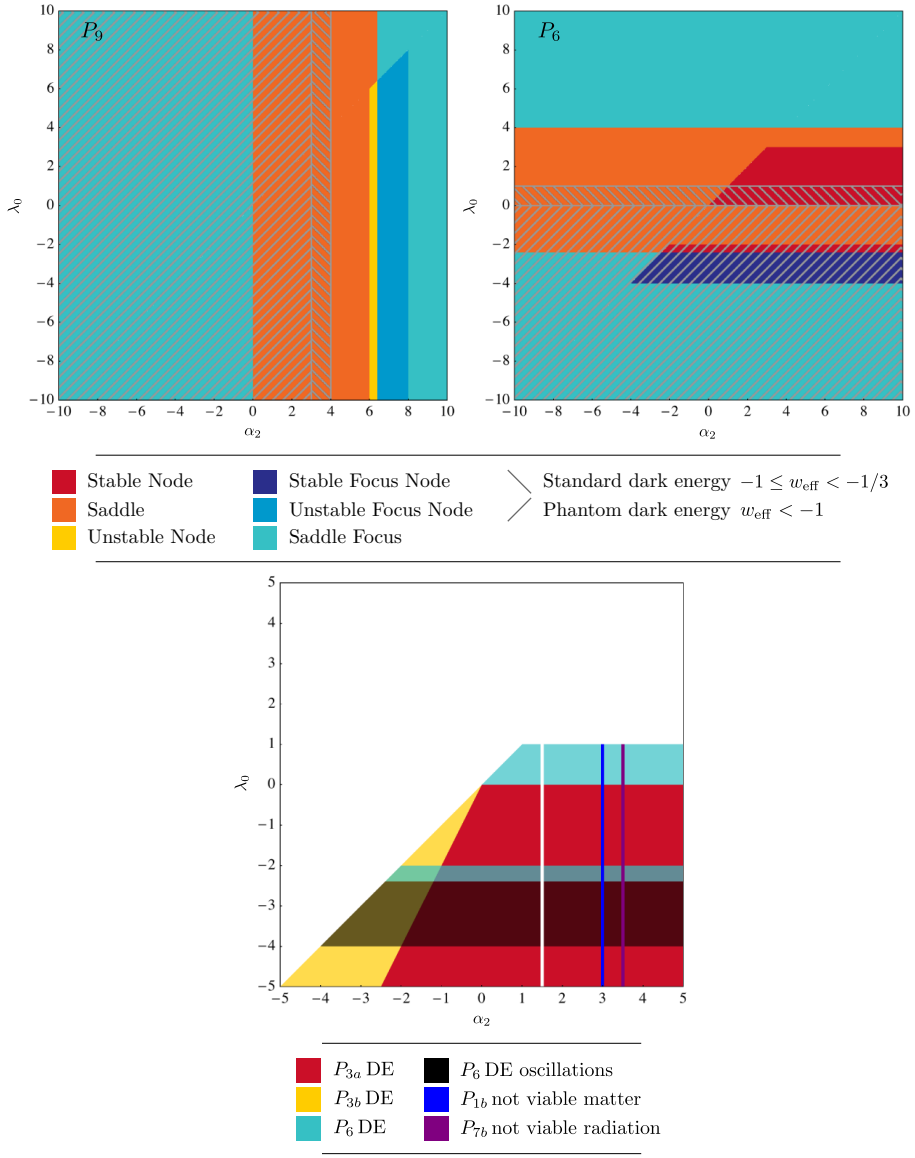

Figure 7.6: The top left panel shows the results of the stability analysis of the *second order* system around P_9 (see Appendix C.1). The top right panel at the center illustrates the stability of the system around P_6. The bottom panel shows the combined results of the *second order* analysis. Regions in the (α_2, λ_0) plane which allow the different transitions discussed in Section 7.3.2 are shown in different colors.

$w_{\rm eff} = 1$:

$$P_{2a} \equiv (1,0,0,0,0) \qquad \mu_1 = 2,\ \mu_2 = 3,\ \mu_3 = 3,\ \mu_4 = 3-\alpha_2,$$
$$\mu_5 = 6-\lambda_0. \tag{7.54a}$$
$$P_{2b} \equiv (1,0,0,0,-3+\alpha_2) \qquad \mu_1 = 2,\ \mu_2 = 3,\ \mu_3 = 6-\alpha_2,\ \mu_4 = \alpha_2-3,$$
$$\mu_5 = 6-\lambda_0. \tag{7.54b}$$

Their unstable configuration, which might be relevant for the early stages of the Universe, can be obtained for $\alpha_2 < 3 \wedge \lambda_0 < 6$ in the case of P_{2a}, and for P_{2b} is $3 < \alpha_2 < 6 \wedge \lambda_0 < 6$ in the case of P_1. Again the two realizations of this point correspond to different behaviors of the conformal coupling $\Omega(t)$.

- *Dark energy points*
  We have also two DE dominated points from the splitting of the first order P_3 point:

$$P_{3a} \equiv \left(\frac{\lambda_0}{6}, 1-\frac{\lambda_0}{6}, 0, 0, 0\right) \qquad \mu_1 = \lambda_0 - 6,\ \mu_2 = \lambda_0 - 4,\ \mu_3 = \lambda_0 - 3,$$
$$\mu_4 = \frac{\lambda_0}{2},\ \mu_5 = \frac{1}{2}(\lambda_0 - 2\alpha_2). \tag{7.55a}$$
$$P_{3b} \equiv \left(\frac{\lambda_0}{6}, 1-\frac{\lambda_0}{6}, 0, 0, \alpha_2 - \frac{\lambda_0}{2}\right) \quad \mu_1 = \alpha_2 - \frac{\lambda_0}{2},\ \mu_2 = \lambda_0 - 6,\ \mu_3 = \lambda_0 - 3,$$
$$\mu_4 = \lambda_0 - 4,\ \mu_5 = \lambda_0 - \alpha_2. \tag{7.55b}$$

  They both have $w_{\rm eff} = -1 + \lambda_0/3$ and are cosmologically viable late time DE attractors respectively for $(\alpha_2 \geq 0 \wedge \lambda_0 < 0) \vee (\alpha_2 < 0 \wedge \lambda_0 < 2\alpha_2)$ and for $\alpha_2 < 0 \wedge \lambda_0 > 2\alpha_2 \wedge \lambda_0 < \alpha_2$.
  The other viable DE attractor is the second order equivalent of the DE dominated P_6 (7.48):

$$P_6 \equiv \left(\frac{\lambda_0}{2}, 1+\frac{\lambda_0}{2}, 0, -\lambda_0, 0\right) \quad \mu_1 = \lambda_0 - 4,\ \ \mu_2 = \lambda_0 - \alpha_2,$$
$$\mu_3 = -3 - \frac{3}{4}\lambda_0 + \frac{1}{4}\sqrt{3}\sqrt{48 + 8\lambda_0 - 5\lambda_0^2},$$
$$\mu_4 = \lambda_0 - 3,\ \mu_5 = -3 - \frac{3}{4}\lambda_0 - \frac{1}{4}\sqrt{3}\sqrt{48 + 8\lambda_0 - 5\lambda_0^2}, \tag{7.56}$$

  which is an accelerated attractor with a viable equation of state for $(\alpha_2 > 1 \wedge 0 < \lambda_0 < 1) \vee (0 < \alpha_2 \leq 1 \wedge 0 < \lambda_0 < \alpha_2)$. From the full stability graphical analysis, reported in Fig. 7.6, we can notice that this point can be an accelerated attractor for a wider range of (α_2, λ_0), however for some intervals it would have $w_{\rm eff} < -2$, which is a value already excluded by experiments, e.g. Refs. [21, 411], and hence we have considered a more conservative region.

- *Radiation points*
  Two radiation dominated critical points are provided by the splitting of the

first order point P_7:

$$P_{7a} \equiv (0,0,1,0,0) \;\; \mu_1 = -2,\; \mu_2 = 1,\; \mu_3 = 2,\; \mu_4 = \frac{3}{2} - \alpha_2,\; \mu_5 = 4 - \lambda_0. \tag{7.57a}$$

$$P_{7b} \equiv \left(0,0,1,0,-\frac{3}{2}+\alpha_2\right) \;\; \mu_1 = -2,\; \mu_2 = 1,\; \mu_3 = \frac{7}{2} - \alpha_2,\; \mu_4 = \alpha_2 - \frac{3}{2},$$
$$\mu_5 = 4 - \lambda_0. \tag{7.57b}$$

They are a saddle respectively for $\lambda_0 \neq 4 \wedge \alpha_2 \neq \frac{3}{2}$ and $\lambda_0 \neq 4 \wedge \alpha_2 \neq \frac{7}{2} \wedge \alpha_2 \neq \frac{3}{2}$. A viable radiation era can also be provided by P_{10} (see Tab. C.2) which is a radiation-DE scaling critical point. The stability analysis of this critical point is too complicated to be shown because of the complexity of its eigenvalues; nevertheless we can deduce the stability conditions for the configurations of cosmological interest. For instance for $\alpha_2 = \frac{7}{2}$ this point supplies a good radiation dominated point which is a saddle if $\lambda_0 \neq 4$. We cannot instead identify a region of (α_2, λ_0) where this point would provide a viable DE candidate.

Combining the above results, we can see that for the second order system there is a wide variety of possible transitions between viable critical points that will give rise to a working cosmological model. This is somewhat expected given that we are moving up the α channel and allowing more and more general behaviors of the function $\Omega(t)$. The combined results of the second order dynamical analysis are shown in Fig. 7.6. In general the stability requirements for a viable radiation and matter era are much less stringent than those for the first order system. Indeed, except for a discrete set of values of α_2, λ_0, generally there are two points that can give a radiation era, i.e. P_{7a} or P_{7b}, as well as two points that can provide a matter era, i.e. P_{1a} or P_{1b}. The values of α_2 that do not allow either a viable matter or radiation critical point are shown in Fig. 7.6 as, respectively, straight blue and purple lines. A stronger selection of viable regions in the (α_2, λ_0) plane is imposed by requiring that the possible DE points, P_{3a}, P_{3b}, P_6, have a proper cosmology and stability.

7.3.3 N^{th} order analysis: exploiting the recursive nature of the system

In the previous Sections we performed a dynamical analysis of the system (7.28) cutting the hierarchy of equations (7.28d) at increasingly higher orders, up to the second, while keeping λ_0 constant. At each order we determined the critical points, their stability and cosmological features. The reason for treating separately the zero, first and second order is twofold. First, it allows us to study gradually more and more general models, recognizing at each order some characteristic features and cosmological viability conditions. Second, since α_2 is the first of the $\alpha' s$ not to enter the core equations (7.28a)-(7.28c), we expect that from the third order up the system will display a regular pattern in the critical points that reflects the recursive structure of the equations (7.28d). We saw glimpses of this pattern already in the second order system in Section 7.3.2, but it is not until we have $N \geq 3$ that it displays fully. We will

now exploit this feature to reconstruct the dynamical properties of the system at any given order $N \geq 3$, building on the findings of the lower order analyses. We neglect radiation for simplicity (our results can be easily extended to include it), so we are left with an $N+2$ dimensional system for the variables $\{x, y, \alpha_0, \alpha_1, \ldots, \alpha_{N-1}\}$. When writing the coordinates of the critical points we use the general structure $(x_c, y_c, \alpha_{0,c}, \alpha_{1,c}, \alpha_{n,c})$, with $n = 2, .., N-1$, which allows us to treat separately α_0, α_1 from α_n with $n \geq 2$, given that the former enter the core equations (7.28a)-(7.28c) and do not obey the general rules that we are about to derive.

By looking at system (7.28), one notices that the set of variables $\{x, y, \alpha_0\}$ depends on the α_n, $n \geq 2$, only through α_1. We can therefore use α_1 as a pivot variable and split the original system into two blocks: the block of equations (7.28a), (7.28b), (7.28d) with $n = 1$ and the block of equations (7.28d) with $n \geq 2$. We start by solving the equations of the first block, and determine solutions for $(x_c, y_c, \alpha_{0,c})$ as functions of α_1. We then turn to the second block and notice that one can generally distinguish two cases: those characterized by $\alpha_{1,c} = 0$ and those with $\alpha_{1,c} \neq 0$. In the former case, the two blocks are independent, while in the latter all the coordinates of the critical points will be affected by the equations of the second block. The general structure of the points for which $\alpha_1 = 0$ can then be recovered as follows. One starts solving the first block of equations, which can be done quite straightforwardly, to determine $\{x_c, y_c, \alpha_{0,c}\}$. Then one turns the attention to the second block, with $n \geq 3$ since $\alpha_{1,c} = 0$, and finds that there are three types of general solutions for this block: one in which all $\alpha_{n,c} = 0$, the second where all $\alpha_{n,c} \neq 0$ and the last case in which there will be different combinations of $\alpha' s$ equal or not to zero (hence the name *combinations* in what follows). A combination is specified by the location of all the zero terms; once these are given, the values of the $\alpha' s \neq 0$ are uniquely determined and can be reconstructed, after some lengthy algebra, solving the corresponding equations. Let us illustrate the general rules for the specific expressions of the non-zero $\alpha' s$, by using the following representative *combination*:

$$\alpha_{n,c} \equiv (\,\emptyset\,,\, \underbrace{\alpha_{q,c}, \ldots \alpha_{j,c} \ldots, \alpha_{s,c}}_{\text{block} \neq 0,\ j=q,\ldots s}\,,\, \emptyset\,,\, \underbrace{\ldots \alpha_{j,c} \ldots}_{\text{block} \neq 0}\,,\, \emptyset\,,\, \underbrace{\alpha_{k,c}, \ldots \alpha_{l,c} \ldots, \alpha_{N-1,c}}_{\text{block} \neq 0,\ l=k,\ldots,N-1}\,), \tag{7.58}$$

where $\emptyset \equiv (0, \ldots, 0)$.
The elements in the non-zero blocks which are followed by a zero block have:

$$\alpha_{j,c} = (s+1-j)\frac{\dot{H}}{H^2}, \tag{7.59}$$

where $q \leq j \leq s$, with α_q being the first non-zero term in the block and α_s the last one. The particular *combination* shown in (7.58) ends with a non-zero block; the elements of such a block obeys the following specific rule:

$$\alpha_{l,c} = \alpha_N + (N-l)\frac{\dot{H}}{H^2}, \tag{7.60}$$

where $k \leq l \leq N-1$, with α_k being the first non-zero term in the block. Every time we substitute into (7.59) and (7.60) the specific value of $\dot{H}/H^2(x_c, y_c, \alpha_{0,c}, \alpha_{1,c})$ that corresponds to the point in consideration.

The solutions for which the variable α_1 assumes a non-zero value are a little trickier to treat as the components $(x_c, y_c, \alpha_{0,c})$ of the critical points will be affected by the equations of the second block, we find that also in this case the critical points can generally be separated in the three above cases based on the structure of the α_n, $n \geq 2$, block for which the general rules (7.59)-(7.60) still apply.

Using the above technique we are able to reconstruct all the critical points of system (7.28) at a given order N. In particular, we find that they can be organized in families characterized by the same cosmological behavior. These families, in most of the cases, can be directly connected to the critical points that we have analyzed in the previous Sections, as expected because of the structure of our system and its invariant manifolds (as mentioned at the end of the introductory part of Section 7.3.1). Therefore one can identify the main critical points of cosmological interest, or in other words get a good sense of the cosmologies encoded in the EFT formalism, already at the lower orders. Going to higher orders allows to analyze more and more general models.

In what follows we describe only the families of critical points that allow for a viable cosmology, leaving the discussion of the remaining critical points for Appendix C.2. We generally indicate with s the position of the last term in a non-zero block within the combination, and with k the position of the first non-zero term in the last non-zero block that, for some cases, closes the combination.

- *Matter points:*
  This family includes 2^{N-1}, P_1-like, critical points characterized by a well defined cosmology ($\Omega_m = 1$):

$$P_{1a} \equiv (0, 0, 0, 0, \alpha_{n,c} = 0), \tag{7.61a}$$

$$P_{1b} \equiv \left(0, 0, 0, \alpha_N - \frac{3}{2}(N-1), \alpha_{n,c} = \alpha_N - \frac{3}{2}(N-n)\right), \tag{7.61b}$$

$$P_{1c} \equiv (0, 0, 0, \text{combinations}). \tag{7.61c}$$

  The latter point includes all $(2^{N-1} - 2)$ possible combinations constructed via Eqs. (7.59) and (7.60) with $\dot{H}/H^2 = -1$. All critical points correspond to matter domination, therefore, instead of performing the full stability analysis, we simply determine the intervals for which they are saddle points. The eigenvalues of the linearized system around P_{1a} and P_{1b} are:

$$P_{1a} : \mu_1 = -3,\ \mu_2 = \frac{3}{2} - \alpha_N,\ \mu_3 = 3 - \lambda_0,\ \mu_4 = \cdots = \mu_{N-1} = \frac{3}{2}, \tag{7.62a}$$

$$P_{1b} : \mu_1 = -3,\ \mu_2 = \frac{3}{2}N - \alpha_N,\ \mu_3 = 3 - \lambda_0,$$
$$\mu_4 = \cdots = \mu_{N-1} = \alpha_N - \frac{3}{2}(N-h), \tag{7.62b}$$

  where $h = 1, .., N-1$. As we can see these points have only one possible stability configuration having two eigenvalues of opposite sign, therefore as long as they are hyperbolic they are saddles. The first one is hyperbolic if $\lambda_0 \neq 3$ and $\alpha_N \neq 3/2$ while for the second one we should have $\alpha_N \neq \frac{3}{2}(N-h)$, $\alpha_N \neq \frac{3}{2}N$ and $\lambda_0 \neq 3$. As for the last sub-family of critical points,

P_{1c}, the analysis of the eigenvalues reveals that this is a set of saddle points regardless of the particular combination as for each combination at least two eigenvalues have opposite sign. Despite the complexity of the structure of the combinations, we are able to determine that all of them are hyperbolic if: $\lambda_0 \neq 3$ and $\alpha_N \neq \frac{3}{2}(N-h)$ with $h = 1, \ldots, N-1$.

- *Stiff-matter points:*

$$P_{2a} \equiv (1,0,0,0,\alpha_{n,c}=0), \tag{7.63a}$$
$$P_{2b} \equiv (1,0,0,\alpha_N - 3(N-1), \alpha_{n,c} = \alpha_N - 3(N-n)), \tag{7.63b}$$
$$P_{2c} \equiv (1,0,0,\text{combinations}),\ \alpha_{j,c} = -3(s+1-j)\ , \quad \alpha_{l,c} = \alpha_N - 3(N-l). \tag{7.63c}$$

The points in this family have $\Omega_{\rm DE} = 1$ and $w_{\rm eff} = 1$, therefore representing a set of 2^{N-1} stiff-matter critical points. The structure and the cosmology of these critical points suggest a similarity with the P_2 critical point we analyzed in the previous Sections. These critical points could be of interest in the early stages of the Universe as unstable critical points [101], which is the only configuration we analyze in what follows. The first two critical points have eigenvalues:

$$P_{2a} : \mu_1 = 3 - \alpha_N,\ \mu_2 = 6 - \lambda_0,\ \mu_3 = \mu_4 = \cdots = \mu_{N-1} = 3, \tag{7.64a}$$
$$P_{2b} : \mu_1 = 3,\ \mu_2 = 3N - \alpha_N,\ \mu_3 = 6 - \lambda_0, \quad \mu_4 = \cdots = \mu_{N-1} = \alpha_N - \frac{3}{2}(N-1-h), \tag{7.64b}$$

where $h = 1, .., N-1$. The first critical point is unstable for $\alpha_N < 3 \wedge \lambda_0 < 6$ while the unstable configuration of the second one is obtained if $3/2\,(N-2) < \alpha_N < 3N \wedge \lambda_0 < 6$. For the last sub-family, P_{2c}, there is only one combination which shows an unstable configuration and it is the one with $\alpha_1 = 0$ and $\alpha_{n,c} \neq 0$ for $n = 2, \ldots, N-1$ which is unstable if $\lambda_0 < 6 \wedge 3 < \alpha_N < 3(N-1)$. Most of the other combinations are saddle points.

- *Dark Energy points:*

$$P_{3a} \equiv \left(\frac{\lambda_0}{6}, 1 - \frac{\lambda_0}{6}, 0, \alpha_{n,c} = 0\right), \tag{7.65a}$$
$$P_{3b} \equiv \left(\frac{\lambda_0}{6}, 1 - \frac{\lambda_0}{6}, 0, \alpha_N - \frac{\lambda_0}{2}(N-1), \alpha_{n,c} = \alpha_N - \frac{\lambda_0}{2}(N-n)\right), \tag{7.65b}$$
$$P_{3c} \equiv \left(\frac{\lambda_0}{6}, 1 - \frac{\lambda_0}{6}, 0, \text{combinations}\right),\ \alpha_{j,c} = -(s+1-j)\frac{\lambda_0}{2}\ , \quad \alpha_{l,c} = \alpha_N - \frac{\lambda_0}{2}(N-l). \tag{7.65c}$$

This family corresponds to a set of 2^{N-1} DE dominated critical points with $\Omega_{\rm DE} = 1$ and $w_{\rm eff} = \frac{\lambda_0}{3} - 1$. From the structure of these points we can immediately recognize a similarity with the P_3 critical point analyzed in the previous Sections. We are interested in the stable configuration for this family.

The eigenvalues of the system around the first two points are:

$$P_{3a} : \mu_1 = \lambda_0 - 6,\ \mu_2 = \lambda_0 - 3,\ \mu_3 = \frac{\lambda_0}{2} - \alpha_N,\ \mu_4 = \cdots = \mu_{N-1} = \frac{\lambda_0}{2}, \tag{7.66a}$$

$$P_{3b} : \mu_1 = \lambda_0 - 6,\ \mu_2 = \lambda_0 - 3,\ \mu_3 = \frac{\lambda_0}{2},$$
$$\mu_4 = \cdots = \mu_{N-1} = \frac{\lambda_0}{2} + \alpha_N - \frac{3}{2}(N - h + 1), \tag{7.66b}$$

where $h = 1, \ldots, N-1$. The stability analysis reveals that P_{3a} is a stable accelerated attractor if $(\alpha_N > 0 \wedge \lambda_0 < 0) \vee (\lambda_0 < 2\alpha_N \wedge \alpha_N \leq 0)$ while P_{3b} displays this cosmological behavior if $(\lambda_0 < 0 \wedge \alpha_N \leq 3) \vee (\alpha_N > 3 \wedge \lambda_0 < 6 - 2\alpha_N)$. The last sub-family P_{3c} does not contain any stable solution, and as a consequence will be not further considered.

The points discussed above represent all the hyperbolic, cosmologically viable, critical points of the system (7.28) at a given order $N \geq 3$ (with $\lambda_0 =$ constant). Since we neglected radiation, the families of critical points which are of cosmological interest and that can be used to construct transitions from a matter era to a DE one are, respectively, the P_1-like and P_3-like family. Each family contains several critical points, therefore there are many possible specific transitions; in particular at a given order N, there are 2^{N-1} matter points and 2 DE points. Analogously to what happens in the second order case, the intervals of cosmological viability for (α_N, λ_0) are strongly influenced by the stability requirements of the DE points, while the requirements for a good matter era are significantly easier to satisfy, and only exclude some values. Once one selects the values of (α_N, λ_0) according to the intervals reported above, the trajectories of the dynamical system will generally start at early times in the neighborhood of a P_2-like unstable node then approach a P_1-like matter point, finally moving away from it heading towards a P_3-like de-Sitter attractor. Different trajectories will correspond to different behaviors of the EFT functions $\Omega(t)$ and $c(t)$. Let us conclude pointing out that viable transitions have $\lambda_0 < 0$, which implies that $c(t) - \Lambda(t)$ will be a growing function of time for all viable trajectories at the N^{th} order.

7.3.4 Discussion

In Ref. [396], we performed a thorough dynamical analysis of the background cosmology within the effective field theory for cosmic acceleration [228, 229]. In particular we investigated general conditions of cosmological compatibility for the three functions of time that describe the background dynamics in this formalism (EFT functions). While the system of equations is undetermined, we identified a set of variables that allows one to transform it into an infinite-dimensional system characterized by an important recursive structure. We then studied several autonomous cases of increasingly higher dimension corresponding to more and more general models of dark energy and modified gravity within the EFT framework. Furthermore, exploiting the recursive nature of the full system of equations, as well as our findings at the lower orders, we drew some general conclusions on its dynamics and cosmological behavior.

Our set of dynamical variables contains two infinite series of variables α_n and λ_m, defined as ratios of subsequent derivatives of, respectively, the EFT functions Ω and $c-\Lambda$, (7.27). These variables are such that their corresponding equations assume a hierarchical structure. One can truncate these series at any desired order, and study the corresponding autonomous system. We focused on the α channel, keeping always λ_0 constant. In other words, we focused on the class of models for which $c-\Lambda$ is a power law in the scale factor, while the conformal factor Ω can be increasingly general as we go up with the order. Alternatively one could fix Ω to a constant and open the λ channel, which would correspond to exploring all minimally coupled models of DE. Finally, one could work with both channels and, for instance, explore, within this parametrized framework the full class of Horndeski theories [327]. While we leave the former for future work, we want to stress that the machinery set up here is general and easily applicable to the other cases mentioned above.

As we showed in Eq. (7.33), our set up allows us to find a general expression for Ω consisting, at a given order N, of a Taylor expansion of order $N-1$ in time and the corresponding remainder that is parametrized in terms of α_N. Since we include the remainder, increasing the order of the analysis is not a matter of increasing the precision of the Taylor expansion but rather it allows the investigation of a wider class of models of DE/MG with the most diverse coupling. An analogous argument could be repeated for $c-\Lambda$.

Focusing on the α variables, while keeping λ_0 constant, we analyzed the system at increasingly higher order. At each order we found the critical points and analyzed their stability and cosmological nature, determining regions in the plane (α_N, λ_0) which allow for viable cosmological trajectories. The simplest case we analyzed was the zero-th order one, obtained setting α_0 to constant. It corresponds to a power law behavior for the EFT functions. After finding the critical points, we performed a stability analysis and determined the cosmology of each point as function of α_0, λ_0. The general result of the zero-th order analysis is that viable cosmological models can be recovered setting $\alpha_0 = 0$ and $\lambda_0 \approx 0$ and there is really only one viable transition between cosmologically interesting critical points. Given that $\alpha_0 = 0$, the corresponding models will be characterized by a constant conformal factor Ω, which is just a rescaling of the Planck mass. In Section 7.3.2 we showed how these findings, projected onto models of quintessence, imply that a quintessence model with a potential which is a power law in the scale factor, cannot have a power law behavior for Ω and therefore, at this order is forced to be minimally coupled. We then proceeded with the analysis of the first and second order systems, finding, as expected, a richer set of cosmologies. We identified respectively the (α_1, λ_0) and (α_2, λ_0) regions which result in cosmologically compatible EFT functions.

At the second order we started to notice some reflections of the recursive nature of the equations for the $\alpha's$. In particular, we found that the majority of the critical points for the second order system are just trivial extensions of the critical points of the first order case, that come in two copies with similar cosmology but a different dynamics of the conformal factor $\Omega(t)$. The recursive nature of the dynamical system fully displays when $N \geq 3$, which is part of the reason why we treated separately the zero, first and second order cases. In Section 7.3.3 we showed how to exploit this recursive feature to reconstruct the critical points, their stability and their corresponding cosmological dynamics

at any given order $N \geq 3$. We identified regions in $(\alpha_N,\ \lambda_0,\ N)$ space that allow compatible forms of the EFT functions; in particular, all viable models correspond to a function $c - \Lambda$ that grows in time.

Our methodology offers a general tool to perform the dynamical analysis of DE/MG models within the EFT language. We have used it to explore models with an increasingly more general conformal coupling; we leave the analysis of other realizations for future work. Finally, let us point out that here we have chosen not to perform a full analysis of the scaling configurations, but rather focused on the two extreme cases for which either of the two components in the configuration has fractional energy density equal to unity. While we leave a thorough investigation of the scaling regime for future work, we expect that the scaling points that we found, especially at the order $N \geq 3$, will display a rich phenomenology of late-time scaling cosmologies that could provide a dynamical solution to the coincidence problem.

Our results can be applied to the numerical investigations of the dynamics of linear perturbations within the model-independent framework of EFT. Given the generality of the formalism, there is a high degree of freedom so that even after fixing the expansion history one is left with a completely undetermined function of time out of the three original EFT functions. As such, a designer approach that fixes the background cosmology (typically to ΛCDM) and uses the Friedmann equations to reconstruct the corresponding behavior of the EFT functions, may not be the optimal way to proceed. With our technique we are able to explore the cosmological dynamics of several forms of the EFT functions and determine general conditions of cosmological compatibilty at different order. This will help us in choosing appropriate ansätze for the EFT background functions to input in our Einstein-Boltzmann code, EFTCAMB [397], to study the evolution of linear perturbations.

7.4 Effective field theory for CAMB

In this Section we focus on the implementation of the EFT approach to cosmic acceleration in CAMB/CosmoMC [399, 400, 401], creating what we will refer to as EFTCAMB/EFTCosmoMC [397, 398]. These works are in collaboration with B. Hu, M. Raveri and A. Silvestri.

EFTCAMB, is a powerful and versatile tool that can be used for several objectives [397]. It can be employed to evolve the full dynamics of linear scalar perturbations of a broad range of single field DE/MG models, once the model of interest is mapped into the EFT formalism. It offers a numerical implementation of EFT as a model-independent framework to test gravity on cosmological scales. To interface EFTCAMB with cosmological data sets, we equipped it with a modified version of CosmoMC, namely EFTCosmoMC [398], creating a bridge between the EFT parametrization of the dynamics of perturbations and observations. EFTCAMB/EFTCosmoMC will be of great use for upcoming cosmological surveys, such as Euclid [312, 412], that aim at testing the underlying theory of gravity on large scales.

One of the virtue of the code is that it does not rely on any quasi-static (QS) approximation. When fitting to data or performing forecasts for upcoming surveys, one generally focuses on sub-horizon scales and neglects the time

derivatives of the gravitational potentials and scalar fields w.r.t. their spatial gradients, i.e. one assumes the QS regime. In Fourier space, this brings the Einstein and scalar field equations to an algebraic form and simplifies significantly both the theoretical and the numerical setup. A widely used parametrization of modified gravity that relies on the QS approximation is the one introduced in Refs. [270] and commonly referred to as the BZ parametrization. While the QS description of the growth of structure generally gives a good representation of the evolution on sub-horizon scales (see e.g. Ref. [413] for an analysis in $f(R)$ gravity), and significantly reduces the computing time, it might loose out on some dynamics at redshifts and scales that would leave an imprint within the reach of some ongoing and upcoming surveys [414, 415]. At the level of model-independent tests of gravity, implementations that do not employ the QS approximation are the Parametrized Post-Friedmann (PPF) modules of Refs. [269, 416] as well as MGCAMB [417, 418]. The former uses a full set of equations for all linear scales, obtained by the interpolation between the super-horizon and the QS regime and it relies on three free functions and one parameter; however, in order to study specific models, one needs to work out interpolations and fits to the these functions and parameters for each case. The latter relies on a generic parametrization of the Poisson and anisotropy equation to form a complete and general set of equations for all linear scales, allowing for model-independent analysis of modified growth such as those of Refs. [287, 276, 297]; however, one has to restrict to the QS regime in order to study a specific model. We shall mention also ISiTGR [285, 289], which is an integrated set of modified modules for use in testing whether observational data are consistent with general relativity on cosmological scales. EFTCAMB is a full Einstein-Boltzmann code which does not rely on any QS approximation and is very general in terms of models and parametrizations that it can handle. We will illustrate the importance of allowing for full dynamics in view of upcoming data in Section 7.4.6, by showing how, for some models, the time dependence of the scalar DoF can have a non-negligible effect on the lensing of the Cosmic Microwave Background (CMB) detected by *Planck* [419].

Our code solves the full Klein-Gordon equation for the Stückelberg field, which in the EFT formalism encodes the departures from the standard cosmological model, as opposed to macroscopic hydrodynamic/fluid treatments [291, 420, 421]. This allows us to maintain an approach which is closer to the true nature of the theory as well as to have a direct control and easier interpretation of the possible instabilities related to this DoF as we discuss in Section 7.4.3. Furthermore, with our method we can easily evolve perturbations in models that cross the phantom-divide, as we will illustrate in Section 7.4.7.

We focus on cosmological observables of interest for ongoing and upcoming surveys, in particular showing outputs of our code for the CMB temperature-temperature auto-correlation, the CMB lensing potential auto-correlation, the cross-correlation between temperature and lensing potential for the CMB and the matter power spectrum. We consider several models. To start with, we focus on $f(R)$ models that reproduce a ΛCDM expansion history and we compare our outputs to those of the common implementation of these theories in MGCAMB [417, 418, 413]. This allows us to perform a consistency check of our code as well as to identify some peculiar features in the power spectra contributed by the sub-horizon dynamics of the scalaron, which is neglected by the

QS implementation of $f(R)$ in MGCAMB. We then extend to designer $f(R)$ models with more general expansion histories, considering both a constant but different than -1 and a time-varying DE equation of state. We analyze in details all the imprints of these models on the different observables. Finally, we switch gears and instead of adopting a known model of modified gravity, we study some ghost-free power law parametrizations of the EFT background functions that display a phantom-divide crossing background. The examples that we present should highlight the versatility of our EFTCAMB code: it can be used to evolve the full dynamics of linear perturbations for any given DE/MG model that can be cast into the EFT language, without the need to resort to the QS approximation; it provides a powerful and versatile tool to implement the EFT formalism as a model-independent parametrization to test gravity with large scale structure; it allows us to investigate some poorly understood models which are permitted by the symmetries and stability conditions of EFT, such as the phantom-divide crossing ones.

In combination with the check for stability of the theory embedded in EFTCAMB, EFTCosmoMC allows to explore the parameter space of models of cosmic acceleration under general viability criteria that are well motivated from the theoretical point of view. It comes with built-in likelihoods for several cosmological data sets. We illustrate the use of these patches obtaining constraints on different models within the EFT framework using data from *Planck* temperature and lensing potential spectra, WMAP low-ℓ polarization (WP) spectra as well as baryon acoustic oscillations (BAO). In particular we consider designer $f(R)$ models and an EFT linear parametrization involving only background operators, on both a ΛCDM and wCDM background.

Let us note that while our setup takes into account all contributions from operators that are at most quadratic in the perturbations, for the numerical analysis presented in Refs. [397, 398], we focus on models that involve only background operators, leaving the analysis with second order terms for future work. For a previous investigation of cosmological implications on a subset of models within the framework of effective field theory of cosmic acceleration see Ref. [422].

Finally, we publicly released the EFTCAMB and EFTCosmoMC patches at `http://www.lorentz.leidenuniv.nl/~hu/codes/` with a set of detailed notes that will guide the reader through the structure of the codes [423].

The work is organized as follows. In Section 7.4.1 we describe how EFTCAMB deals with the background cosmology. In Section 7.4.2, we present the equations for scalar linear perturbations, we discuss some general theoretical requirements for the stability of the theory in Section 7.4.3 and review the cosmological observables of interest in Section 7.4.4. In Section 7.4.5 we present numerical results, including an in depth comparison of our outputs to those of MGCAMB for $f(R)$ models, new results for designer $f(R)$ with time-varying DE equation of state and some EFT parametrizations with a phantom-divide crossing. In Section 7.4.8 we introduce EFTCosmoMC describing its main features and in Section 7.4.9 we present the data sets and the results obtained for some selected models. We finally discuss our results in Section 7.4.10.

7.4.1 Code implementation of the background cosmology

We envisage our code to serve two purposes: One being the application of the EFT framework in a model-independent way, to study the effect of the different operators in action (7.1) on the dynamics of linear perturbations; and eventually constrain the time-dependent coefficients multiplying these operators. And the second one, having a versatile full Boltzmann code to study the evolution of perturbations in virtually any single field DE/MG model for which a mapping to the EFT formalism can be worked out. The twofold nature of the code translates into the following two different procedures for the implementation of the background:

- *pure* EFT: in this case one works with a given subset of the operators in action (7.1), possibly all, treating their coefficients as free functions. The background is treated via the EFT designer approach, i.e. a given expansion history is fixed, a viable form for Ω [396] is chosen and then use the EFT designer approach discussed in Section (7.1.1) to get c, Λ and either Eqs. (7.10) or the prescription described below (see Eq. (7.69)) to get the Q quantities. The code allows for ΛCDM and wCDM expansion histories, as well as for the Chevallier-Polarski-Linder (CPL) [91, 92] parametrization of the DE equation of state. In addition it offers a selection of functional forms for $\Omega(a)$: the minimal coupling, corresponding to $\Omega = 0$; the linear model, that can be thought of as a first order approximation of a Taylor expansion; power law, inspired by $f(R)$, and exponential ones. There is also the possibility for the user to choose an arbitrary form of Ω according to any ansätz the user wants to investigate. At the level of perturbations, more operators come into play, each with a free function of time in front of it, and one needs to choose some ansätze in order to fix their functional form. To this extent, we adopted the same scheme as for the background function Ω, still providing the possibility to define and use other forms that might be of interest. Of course the possibility to set all/some second order EFT functions to zero is included. The code evolves the full perturbed equations consistently implemented to account for the inclusion of more than one second order operator per time, ensuring that even more and more complicated models can be studied.

- *mapping* EFT: in this case a particular DE/MG model is chosen, the corresponding background equations are solved and then everything is mapped into the EFT formalism [228, 229, 394, 395] to reconstruct the corresponding EFT functions and Eqs. (7.10) to obtain the Q quantities. Finally, we can evolve the full EFT perturbed equations. Built-in to the first code release there are $f(R)$ models for which a designer approach is used for the ΛCDM, wCDM and CPL backgrounds following Refs. [260, 264]. In the future other theories will be added to gradually cover the wide range of models included in the EFT framework.

Let us comment on a fundamental difference between the *pure* and *mapping* EFT cases. In the former, the designer approach serves solely the purpose of fixing the background, and therefore only the EFT functions $\{\Omega, \Lambda, c\}$; when studying the dynamics of linear perturbations one needs to independently choose a form for the EFT functions multiplying second order operators, (which of course includes the case in which all those coefficients are set to zero). In the mapping

case instead, once the model is chosen and the corresponding background is solved, one can reconstruct *all* the time-dependent coefficients in the EFT action through the matching procedure, including the higher order ones if the model under consideration involve them. Therefore in the mapping case, once the model is specified one has all the necessary ingredients to study the dynamics of cosmological perturbations. We will give explicit examples of the two cases above in Section 7.4.5, when we present numerical results of our code.

For the actual implementation of the *pure* EFT cases, we fix the expansion history to

$$\mathcal{H}^2 = \frac{8\pi G}{3} a^2(\rho_m + \rho_{\rm DE}), \tag{7.67}$$

with

$$\rho_{\rm DE} = 3H_0^2 M_P^2 \Omega_{\rm DE}^0 \exp\left[-3\int_1^a (1 + w_{\rm DE}(a'))\, d\ln a'\right], \tag{7.68}$$

where $w_{\rm DE}$ represents the equation of state of the effective DE component and can be set accordingly to the model that one wants to study. In particular we will consider the following three cases:

- $w_{\rm DE} = -1$, corresponding to a ΛCDM expansion history;

- $w_{\rm DE} = \text{const} \neq -1$, we will refer to this case as wCDM;

- $w_{\rm DE}(a) = w_0 + w_a(1-a)$, i.e. the CPL parametrization [91, 92], where w_0 and w_a are constant, respectively the value and the derivative of $w_{\rm DE}$ today.

From a comparison of (7.8), (7.9) with (7.67), (7.68), one obtains the following correspondence:

$$\begin{aligned} \rho_Q &= (1+\Omega)\,\rho_{\rm DE} + \Omega\rho_m\,, \\ P_Q &= (1+\Omega)\,P_{\rm DE} + \Omega P_m\,. \end{aligned} \tag{7.69}$$

After fixing $w_{\rm DE}$, we use Eqs. (7.69) to determine the Q quantities; we then choose an $\Omega(\tau)$ and use Eq. (7.12) and Eq. (7.13) to get c and Λ. Let us note that the quantity $\rho_{\rm DE}$ represents one possible way of modeling the contribution of the dark component, alternative to the quantity ρ_Q introduced above. The Q and DE quantities coincide in the case $\Omega = 0$, i.e. when the dark sector is minimally coupled to gravity. However, when $\Omega \neq 0$, Eq. (7.10) gives a more proper representation of the effective scalar DoF of the dark sector, taking into account the coupling to matter and the corresponding exchange of energy between the dark and the matter sectors. In fact, the continuity equation (7.11) and that one for Eq. (7.68) coincide when $\dot{\Omega} = 0$, while for $\dot{\Omega} \neq 0$ the density ρ_Q receives an extra contribution from the coupling to matter. We choose to formulate the designer approach for our code in terms of $(\rho_{\rm DE}, w_{\rm DE})$, which allows for a more direct implementation of the background cosmology in CAMB. However, we express the equations for linear perturbations in terms of the Q quantities, as it is usually done in the EFT framework, since those better represent the contributions to the evolution of perturbations from the EFT dark component.

While in the linearly perturbed equations of next Section we keep c and the Q quantities, we implicitly assume that once the background is fixed, those

will be expressed in terms of the expansion history and Ω via a combination of Eqs. (7.12)-(7.13)-(7.69) for the *pure* EFT cases, and via the matching recipe and Eq. (7.10) in the *mapping* EFT cases.

7.4.2 Scalar linear perturbations

We shall now derive the linearly perturbed Einstein equations that are needed in order to evolve scalar perturbations in CAMB. We work in synchronous gauge with the line element given by

$$ds^2 = a(\tau)^2 \left[-d\tau^2 + \left(\delta_{ij} + h_{ij} dx^i dx^j\right)\right], \tag{7.70}$$

where the scalar mode of h_{ij} in Fourier space can be decomposed into

$$h_{ij} = \int dk^3 e^{i\mathbf{k}\cdot\mathbf{x}} \left[\hat{k}_i \hat{k}_j h(k,\tau) + \left(\hat{k}_i \hat{k}_j - 2\delta_{ij}\eta(k,\tau)\right)\right], \tag{7.71}$$

with h denoting the trace of h_{ij}. Unless explicitly stated otherwise, we work with Fourier transforms of all cosmological perturbations.

While the functions $\{\Omega, \Lambda, c\}$ are the only ones affecting the background dynamics in the EFT formalism, when we move to linear perturbations, more operators come into play; indeed, all the remaining functions in action (7.1), or equivalently (7.4), that multiply second order operators, will also affect the dynamics of linear perturbations. For the sake of brevity, here we focus on the terms contributed by background operators and we list the contributions from second order operators in Appendix D.

Starting from the action in terms of the Stückelberg field (7.4), and simplifying the background terms, to linear order in scalar perturbations we have:

time-time Einstein equation:

$$\begin{aligned} k^2\eta = &- \frac{a^2}{2m_0^2(1+\Omega)} \left[\delta\rho_m + \dot{\rho}_Q \pi + 2c\left(\dot{\pi} + \mathcal{H}\pi\right)\right] + \left(\mathcal{H} + \frac{\dot{\Omega}}{2(1+\Omega)}\right) k\mathcal{Z} \\ &+ \frac{\dot{\Omega}}{2(1+\Omega)} \left[3(3\mathcal{H}^2 - \dot{\mathcal{H}})\pi + 3\mathcal{H}\dot{\pi} + k^2\pi\right], \end{aligned} \tag{7.72}$$

momentum Einstein equation:

$$\frac{2}{3}k^2\left(\sigma_* - \mathcal{Z}\right) = \frac{a^2}{m_0^2(1+\Omega)} \left[(\rho_m + P_m)v_m + (\rho_Q + P_Q)k\pi\right] + k\frac{\dot{\Omega}}{(1+\Omega)}\left(\dot{\pi} + \mathcal{H}\pi\right), \tag{7.73}$$

space-space off-diagonal Einstein equation:

$$k\dot{\sigma}_* + 2k\mathcal{H}\sigma_* - k^2\eta = -\frac{a^2 P \Pi_m}{m_0^2(1+\Omega)} - \frac{\dot{\Omega}}{(1+\Omega)}\left(k\sigma_* + k^2\pi\right), \tag{7.74}$$

space-space trace Einstein equation:

$$\ddot{h} = -\frac{3a^2}{m_0^2(1+\Omega)}\left[\delta P_m + \dot{P}_Q\pi + (\rho_Q + P_Q)\left(\dot{\pi} + \mathcal{H}\pi\right)\right] - 2\left(\frac{\dot{\Omega}}{1+\Omega} + 2\mathcal{H}\right)k\mathcal{Z} + 2k^2\eta - 3\frac{\dot{\Omega}}{(1+\Omega)}\left[\ddot{\pi} + \left(\frac{\ddot{\Omega}}{\dot{\Omega}} + 3\mathcal{H}\right)\dot{\pi} + \left(\mathcal{H}\frac{\ddot{\Omega}}{\dot{\Omega}} + 5\mathcal{H}^2 + \dot{\mathcal{H}} + \frac{2}{3}k^2\right)\pi\right], \tag{7.75}$$

π field equation:

$$c\ddot{\pi} + (\dot{c} + 4\mathcal{H}c)\dot{\pi} + \left[\frac{3}{2}\frac{m_0^2\dot{\Omega}}{a^2}(\ddot{\mathcal{H}} - 2\mathcal{H}^3) - 2\dot{\mathcal{H}}c + \mathcal{H}\dot{c} + 6\mathcal{H}^2c + k^2c\right]\pi + ck\mathcal{Z} - \frac{m_0^2\dot{\Omega}}{4a^2}\left[\ddot{h} - 4k^2\eta + 6k\mathcal{H}\mathcal{Z}\right] = 0, \tag{7.76}$$

where $2k\mathcal{Z} \equiv \dot{h}$ and $2k\sigma_* \equiv \dot{h} + 6\dot{\eta}$ are the standard CAMB variables [399]. As we will discuss shortly in Section 7.4.3, it is important to demix the degrees of freedom in order to perform the appropriate stability analysis of perturbations in the dark sector [228]. Namely, one shall substitute for η and $\ddot{h}$ using Eq. (7.72) and Eq. (7.75), respectively, in order to obtain the following equation:

$$\left(c + \frac{3m_0^2}{4a^2}\frac{\dot{\Omega}^2}{(1+\Omega)}\right)\ddot{\pi} + \left[\frac{3m_0^2}{4a^2}\frac{\dot{\Omega}}{(1+\Omega)}\left(\ddot{\Omega} + 4\mathcal{H}\dot{\Omega} + \frac{(\rho_Q + P_Q)a^2}{m_0^2}\right) + \dot{c} + 4\mathcal{H}c - \frac{\dot{\Omega}}{2(1+\Omega)}c\right]\dot{\pi} + \left[\frac{3}{4}\frac{m_0^2}{a^2}\frac{\dot{\Omega}}{(1+\Omega)}\left(\frac{(3\dot{P}_Q - \dot{\rho}_Q)a^2}{3m_0^2} + \frac{3\mathcal{H}(\rho_Q + P_Q)a^2}{3m_0^2} + \mathcal{H}\ddot{\Omega} + 8\mathcal{H}^2\dot{\Omega} + 2(1+\Omega)(\ddot{\mathcal{H}} - 2\mathcal{H}^3)\right) - 2\dot{\mathcal{H}}c + \left(\dot{c} - \frac{\dot{\Omega}}{2(1+\Omega)}c\right)\mathcal{H} + 6\mathcal{H}^2c + \left(c + \frac{3m_0^2}{4a^2}\frac{\dot{\Omega}^2}{(1+\Omega)}\right)k^2\right]\pi + \left[c + \frac{3}{4}\frac{m_0^2}{a^2}\frac{\dot{\Omega}^2}{(1+\Omega)}\right]k\mathcal{Z} + \frac{1}{4}\frac{\dot{\Omega}}{(1+\Omega)}\left(3\delta P_m - \delta\rho_m\right) = 0. \tag{7.77}$$

In our numerical code, we set the standard initial conditions for matter components and curvature perturbations in the radiation dominated epoch, at a time when the corresponding momentum mode re-enter the horizon. For the Stückelberg field instead, we set initial conditions at a later time, corresponding to $a_\pi = 0.01$. The reasons for this choice are several. First of all, we are interested in the late time accelerating universe and we typically want our theory to reproduce standard GR at early times ($a < a_\pi$). In other words, we expect the Stückelberg field not to be excited at early times.[1] This fact also makes

[1] We impose initial conditions in order to have our model to be very close to GR at early times. At that time there is an attractor for the system and we set initial conditions such that the π field does not oscillate around the attractor solution but instead it assumes this exact value. A cutoff decides if a model is close to GR or not at early times and it depends on the data one is using. Initial conditions for models that are not GR-like at early times are subject of current investigation.

initial conditions for this scalar field less motivated at deep redshift, when the other matter components initial conditions are instead well defined. Finally, from the numerical point of view, the system is more easily controlled since, not evolving the π equation at early times, we avoid some potential high frequency dynamics that would make the integration time longer, while keeping track of the underlying mode of evolution of the scalar field. Indeed, since the equation of motion for the Stückelberg field, Eq. (7.77), is coupled to metric and matter perturbations, which behaves as an external driving source, we set the π field to trace the dynamics of the source at times earlier than a_π. In this way we can get regular and proper initial conditions for the π field at a_π, while avoiding potential high frequency dynamics around the underlying growing mode which anyhow are not expected to leave imprints on physical observables.

7.4.3 Stability of perturbations in the dark sector

In this subsection we shall focus on some requirements for theoretical stability that can be enforced on the EFT functions to ensure that the underlying gravitational theory is acceptable. To this purpose we implement in our code a consistency check for the fulfillment of such stability conditions. For the following discussion it is more convenient to write the π field equation as follows:

$$A(\tau)\,\ddot{\pi} + B(\tau)\,\dot{\pi} + C(\tau)\,\pi + k^2\,D(\tau)\,\pi + E(\tau,k) = 0 \tag{7.78}$$

where the coefficients $\{A,\ldots,E\}$ can be easily read from Eq. (7.77) (and the results of Appendix D if second order operators are at play. In that case also A, B and D may display $k-$dependence). Relying on the discussion of Ref. [227], we place the following theoretical constraints:

- $1+\Omega > 0$: this condition on the non-minimal coupling function is required in order to ensure that the effective Newtonian constant does not change sign. Violating this condition, classically, would imply a Universe quickly becoming inhomogeneous and anisotropic [409, 410], while at the quantum level it will correspond to the graviton turning into a ghost [424];
- $A > 0$: this second condition follows from requiring that our effective scalar DoF should not be a ghost, i.e. the corresponding kinetic energy term should be positive. At the classical level there is no serious danger in this situation while at the quantum level the underlying physical theory can show instability of the vacuum [425];
- $c_s^2 \equiv D/A \leq 1$: the third condition ensures that the sound speed of π does not exceed the speed of light to prevent scalar perturbations from propagating super-luminary. This condition is no longer true when treating, for example, Lorentz violating theories [426];
- $m_\pi^2 \equiv C/A \geq 0$: last, we enforce the mass of the scalar DoF to be real [427], to avoid tachyonic instabilities. In $f(R)$ gravity, that we consider in Section 7.4.6, this condition is necessary to guarantee a stable high-curvature regime [264].

The above conditions could be relaxed in certain cases depending on the specific theory of gravity one is interested in and, of course, our code can be easily edited

to check different stability requirements. Let us briefly comment on this. The first two conditions are quite general and can be relaxed just in elaborated models that can associate a physical meaning to the negative branch of A and $1+\Omega$. Furthermore, their positive and negative branches are disconnected so that no theory can allow these two quantities to cross zero as this will violate the mathematical consistency of the initial value problem for Eqs. (7.8) and (7.77). The last two conditions are milder and more strictly related to the particular theory one wants to test. Therefore, they can be relaxed in many ways if the EFT formalism is used to test some peculiar model that naturally permits their violation. In this regards, we recall, among others, cosmological models which allow for viable DE models in Lorentz violating theories [428, 429] and rolling tachyon condensates [430, 106, 431, 432, 216].

As pointed out in Ref. [227], there are other types of instabilities that can be studied efficiently within the EFT framework. We leave their thorough investigation for future work.

7.4.4 Observables

In view of using our code to test gravity with upcoming and future cosmological surveys, the observables of interest are all the two-point auto- and cross-correlations between Weak Lensing (WL), Galaxy Clustering (GC) and Cosmic Microwave Background (CMB) temperature and polarization anisotropy. We refer the reader to Ref. [417] for a thorough discussion of these observables and the corresponding angular power spectra. In our work we show outputs of our code for the temperature-temperature auto-correlation, the CMB lensing potential auto-correlation, the cross-correlation between temperature and lensing potential for the CMB and the matter power spectrum.

It is expected that the dynamics of the Stückelberg field will mainly affect the time evolution of the metric potentials and matter perturbations at late times. Therefore we expect to see the more noticeable effects in observables such as the Integrated Sachs-Wolfe (ISW) effect of the CMB and WL. The former is a secondary anisotropy induced by the time evolution of the Weyl potential ($\psi \equiv (\Phi+\Psi)/2$ in Newtonian gauge [2]) at late times. The latter involves the distortion of light rays when they pass close to clustering objects, such as galaxies and clusters; it is sourced by the spatial gradients of the Weyl potential. During the accelerated epoch, no significant polarization modes of the CMB photon are generated, therefore we will not consider them here.

The CMB temperature angular spectrum can be computed via the line of sight integration method [433]

$$C_\ell^{TT} = (4\pi)^2 \int \frac{\mathrm{d}k}{k}\, \mathcal{P}(k) \left|\Delta_\ell^{\mathrm{T}}(k)\right|^2, \tag{7.79}$$

where $\mathcal{P}(k) = \Delta^2_{\mathcal{R}}(k)$ is the primordial power spectrum and the radiation transfer function

$$\Delta_\ell^T(k) = \int_0^{\tau_0} \mathrm{d}\tau\; e^{ik\mu(\tau-\tau_0)} S_{\mathrm{T}}(k,\tau) j_\ell[k(\tau_0-\tau)] \tag{7.80}$$

[2] where we assume the following convention for the Newtonian gauge: $\mathrm{d}s^2 = a^2(\tau)[-(1+2\Psi)\mathrm{d}\tau^2 + (1-2\Phi)\mathrm{d}x^2]$. The gauge transformations between Newtonian and synchronous gauges are given by: $\Psi = \dot{\sigma}_*/k + \mathcal{H}\sigma_*/k$, $\Phi = \eta - \mathcal{H}\sigma_*/k$.

is sourced by

$$S_{\rm T}(k,\tau) = e^{-\kappa}\left(\dot{\eta}+\frac{\ddot{\sigma_*}}{k}\right)+g\left(\Delta_{\rm T,0}+2\frac{\dot{\sigma_*}}{k}+\frac{\dot{v}_{\rm B}}{k}+\frac{\Pi}{4}+\frac{3\ddot{\Pi}}{4k^2}\right) + \dot{g}\left(\frac{\sigma_*}{k}+\frac{v_B}{k}+\frac{3\dot{\Pi}}{4k^2}\right)+\frac{3}{4k^2}\ddot{g}\Pi\,, \tag{7.81}$$

where τ_0, μ, κ, g, $\Delta_{\rm T,0}$, $v_{\rm B}$ and Π are, respectively, the present conformal time, angular separation, optical depth, visibility function, intrinsic CMB density perturbations at the last scattering surface, velocity of baryonic matter and total anisotropic stress of normal matter (which includes CMB photons, massless/massive neutrino). Since the recombination of electrons and protons happens very fast, the visibility function g peaks sharply at that early moment, so we do not expect the Stückelberg field to affect the terms proportional to the visibility function and its derivatives. As already discussed, the only relevant term of (7.81) for our analysis is the ISW one, which can be expressed as follows:

$$\ddot{\sigma}_*+k\dot{\eta} = -2\mathcal{H}\dot{\sigma_*}-2\dot{\mathcal{H}}\sigma_*+\frac{v_m}{1+\Omega}\frac{a^2(\rho_m+P_m)}{m_0^2}-\frac{1}{k(1+\Omega)}\frac{d}{d\tau}\left(\frac{a^2P}{m_0^2}\Pi\right) + \frac{k\pi}{1+\Omega}\frac{a^2(\rho_Q+P_Q)}{m_0^2}+\frac{\dot{\Omega}}{1+\Omega}\left[k\mathcal{H}\pi-\dot{\sigma}_*+\frac{1}{k(1+\Omega)}\frac{a^2P}{m_0^2}\Pi\right]. \tag{7.82}$$

As for WL, we calculate its angular power spectrum following the convention of [399, 434]:

$$C_\ell^{\psi\psi} = 4\pi\int\frac{{\rm d}k}{k}\mathcal{P}(k)\left[\int_0^{\chi_*}{\rm d}\chi\; S_\psi(k;\tau_0-\chi)j_\ell(k\chi)\right]^2, \tag{7.83}$$

where the source S_ψ is given in terms of the transfer function of the Weyl potential ψ, i.e.:

$$S_\psi(k;\tau_0-\chi) = 2T_\psi(k;\tau_0-\chi)\left(\frac{\chi_*-\chi}{\chi_*\chi}\right), \tag{7.84}$$

$$T_\psi(k,\tau) = \frac{\dot{\sigma_*}+k\eta}{2} = \frac{1}{2}\left[-2\mathcal{H}\sigma_*+2k\eta-\frac{1}{k(1+\Omega)}\frac{a^2P}{m_0^2}\Pi - \frac{\dot{\Omega}}{1+\Omega}(\sigma_*+k\pi)\right]. \tag{7.85}$$

Conventionally, the line of sight integral in the lensing source is expressed in terms of comoving distance χ. Here χ_* is the comoving distance of the source objects. Here we will focus on CMB lensing, for which the source object is a single distant plane (since the electron-proton recombination is approximately instantaneous), i.e. χ_* corresponds to the comoving distance to last scattering surface. At leading order, the relationship between comoving distance and conformal time reads $\chi = \tau_0 - \tau$. Since ISW and WL are sourced by the same potential, one being sensitive to time derivatives and the other to spatial gradients of the Weyl potential, it is expected that the two effects are strongly

correlated and this correlation produces a non-zero cross-spectrum $C_\ell^{\mathrm{T}\psi}$ [435]:

$$C_\ell^{\mathrm{T}\psi} = 4\pi \int \frac{\mathrm{d}k}{k}\mathcal{P}(k)\left\{\int_0^{\tau_0} \mathrm{d}\tau\; e^{ik\mu(\tau-\tau_0)}e^{-\kappa}(\dot{\Phi}+\dot{\Psi})j_\ell\Big[k(\tau_0-\tau)\Big] \times \int_{\tau_*}^{\tau_0} \mathrm{d}\tau S_\psi(k;\tau)j_\ell\Big[k(\tau_0-\tau)\Big]\right\}\,, \tag{7.86}$$

with τ_* denoting for the conformal time at recombination.

Finally, the matter power spectrum can be computed via

$$P(k) = \frac{2\pi^2}{k^3}\mathcal{P}(k)\Delta_{\mathrm{T}}(k)^2, \tag{7.87}$$

with the matter transfer function defined as [436]

$$\Delta_{\mathrm{T}}(k) = \frac{\delta_m(k,z=0)\delta_m(0,z=\infty)}{\delta_m(k,z=\infty)\delta_m(0,z=0)}\,, \tag{7.88}$$

which describes the evolution of matter density perturbations through the epochs of horizon crossing and radiation/matter transition. A proper calculation of $\Delta_{\mathrm{T}}(k)$ requires that in our code we take all types of non-relativistic matter into account, and follow the growth of each mode outside and inside the horizon.

7.4.5 Numerical Results

In this Section we showcase the reliability and scope of EFTCAMB by comparing it with an existing code, as well as producing some interesting new results. While we have all the necessary ingredients to consider models which involve also second order operators in action (7.1), for the numerical analysis we focus on the cases that involve only the background operators. The examples that we present should convey the wide range of applicability of our code.

We will first focus on $f(R)$ models and compare our code to the common implementation of these theories in MGCAMB [417, 418, 413], restricting to a ΛCDM expansion history. Then, we extend to designer $f(R)$ models with generic constant and time-varying DE equation of state in the part of this Section devoted to new results. As we will illustrate with an example in the $f(R)$ case, given the accuracy of ongoing and upcoming surveys, as well as the range of scales that they cover, in order to extract predictions about observables such as CMB lensing, it is important to employ a code that evolves the full dynamics of the system on linear scales, without employing the QS approximation. This is one of the qualities of our code which allows for an implementation of the full dynamics of a given model, without the need of reducing to the QS regime.

EFTCAMB of course can be used also to fulfill the true purpose the EFT formalism has been envisaged for, i.e. a framework for model-independent tests of gravity on cosmological scales. To this extent, presumably one fixes the expansion history as discussed in Refs. [228, 229] and briefly reviewed in Section 7.4.1, and then focuses on the dynamics of cosmological perturbations studying the effects of the different operators in action (7.1). In this case it is necessary to select some parametrization for the functions of time multiplying the operators

under consideration. Restricting to the background operators, we show the outputs for power law parametrizations of the remaining EFT free function $\Omega(a)$ on a phantom-divide crossing background.

For the present work we will always use the following cosmological parameters: $H_0 = 70\,\mathrm{Km/s/Mpc}$, $\Omega_b = 0.05$, $\Omega_{cdm} = 0.22$, $T_{\mathrm{CMB}} = 2.7255\,\mathrm{K}$.

7.4.6 $f(R)$ gravity: comparison and new results

As an illustration of how EFTCAMB can be used in its *mapping* mode, we shall perform a thorough analysis of $f(R)$ models (See Section 6.1.1). For a detailed discussion of the cosmology in $f(R)$ theories we refer the reader to Refs. [260, 261, 264, 238]. Here we will briefly review the main features that are of interest for our analysis. The higher order nature of the theory translates into having an extra scalar DoF which can be identified with the field $f_R \equiv df/dR$, commonly dubbed the *scalaron* [437]. Implementing the matching to EFT, we have that Stückelberg field for $f(R)$ theories is given by $\pi = \delta R/\dot{R}^{(0)}$ [228], which can be easily related to the perturbation of the scalaron, δf_R.

Viable $f(R)$ models need to satisfy certain conditions of stability and consistency with local tests of gravity [264], which can be inferred from the conditions in Section 7.4.3 once the matching is implemented, as shown in Section 7.2. Finally, given the higher order of the theory, it is possible to reproduce any given expansion history by an appropriate choice of the $f(R)$ function [260, 264]. In other words, $f(R)$ models can be treated with the so called *designer* approach which consists in fixing the expansion history and then using the Friedmann equation as a second order differential equation for $f[R(a)]$. As we will recap shortly, generically one finds a family of viable models that reproduce this expansion and that are commonly labeled by the boundary condition at present time, f_R^0. Equivalently, they can be parametrized by the present day value of the function:

$$B = \frac{f_{RR}}{1+f_R}\frac{\mathcal{H}\dot{R}}{\dot{\mathcal{H}}-\mathcal{H}^2}\,. \tag{7.89}$$

Let us recall that the heavier the scalaron the smaller B_0 and $|f_R^0|$.

Comparison with MGCAMB in a ΛCDM background

We shall start comparing our results for $f(R)$ theories with those of the publicly available MGCAMB code [417, 418]. Since we construct our code on the CAMB version of March 2013, in order to make a senseful comparison we use an updated version of MGCAMB based on the same version of CAMB and developed by the authors of Ref. [305].

MGCAMB relies on two functions of time and scale to parametrize deviations in the Poisson and anisotropy equations, closing the system of equations for matter in conformal Newtonian gauge with the two following equations:

$$k^2\Psi \equiv -\frac{a^2}{2M_P^2}\mu(a,k)\rho_m\Delta_m, \qquad\qquad \frac{\Phi}{\Psi} \equiv \gamma(a,k)\,. \tag{7.90}$$

In order to evolve perturbations in $f(R)$ models one has to specify the corresponding forms for $\mu(a,k)$ and $\gamma(a,k)$, and this can be achieved by taking

the QS limit of the linearly perturbed equations, which corresponds to neglecting time-derivatives of the metric potentials and of the scalar field, as well as focusing on sub-horizon scales $k \gg \mathcal{H}$. In this limit we have:

$$\begin{aligned} k^2\Psi &= -\frac{1}{1+f_R}\frac{1+4f_{RR}/(1+f_R)k^2/a^2}{1+3f_{RR}/(1+f_R)k^2/a^2}\frac{a^2\rho_m\Delta_m}{2M_P^2}, \\ \frac{\Phi}{\Psi} &= \frac{1+2f_{RR}/(1+f_R)k^2/a^2}{1+4f_{RR}/(1+f_R)k^2/a^2}. \end{aligned} \tag{7.91}$$

On sub-horizon scales the dynamics of linear perturbations in $f(R)$ is generally described sufficiently well by this QS approximation [413]. Eqs. (7.91) have inspired the following parametrization [270, 438, 413, 418]:

$$\begin{aligned} \mu^{\rm BZ}(a,k) &= \frac{1}{1-B_0\Omega_m a^{s-1}/2}\frac{1+2/3B_0\left(k/H_0\right)^2 a^s}{1+\frac{1}{2}B_0\left(k/H_0\right)^2 a^s}, \\ \gamma^{\rm BZ}(a,k) &= \frac{1+1/3B_0\left(k/H_0\right)^2 a^s}{1+2/3B_0\left(k/H_0\right)^2 a^s}, \end{aligned} \tag{7.92}$$

to which we will refer as the *BZ* parametrization that consists in assuming

$$\frac{f_{\rm RR}}{1+f_{\rm R}} \equiv \frac{B_0}{6H_0^2}a^{s+2}. \tag{7.93}$$

A standard way of extracting predictions for cosmological observables and comparing $f(R)$ models to data is the one of modeling the late time universe by inserting Eq. (7.92) into MGCAMB, leaving B_0 as a free parameter and fixing $s = 4$ [417]. Let us recall that a $f(R)$ model defined by Eq. (7.92) with a constant value for s will not in general be capable of reproducing the full ΛCDM expansion history. However, it works as a good approximation for each epoch alone [282], as can be inferred from Eq. (7.93). Indeed a reasonable value of s is given by $s \approx 5$ during radiation domination, $s \geq 4$ during matter domination and $s < 4$ during the late time phase of accelerated expansion. For small values of B_0, it is customary to fix $s = 4$ as discussed in Ref. [413], however here we will re-examine this choice in view of the precision and extent of upcoming surveys.

In order to compute observables for these theories with MGCAMB it suffices to fix the expansion history to that of ΛCDM, $s = 4$ and input (7.92) for μ and γ for several choices of B_0. EFTCAMB, on the contrary, does not rely on the quasi-static BZ parametrization, but rather solves the full equations; therefore even after fixing the expansion history to ΛCDM we need to feed the code a form for the EFT functions. We consider two cases:

- BZ case: from Eq. (7.93) we read off the implications of the BZ parametrizations for $f(R)$ and then we reconstruct the corresponding Ω and Λ to input in the full equations for linear perturbations. We again stress that our code does not rely on any QS approximation;
- Designer case: we implement in our code the $f(R)$ designer approach to reconstruct viable $f(R)$ models that mimic the ΛCDM expansion history and determine the corresponding Ω, Λ via the matching, Eq. (7.20).

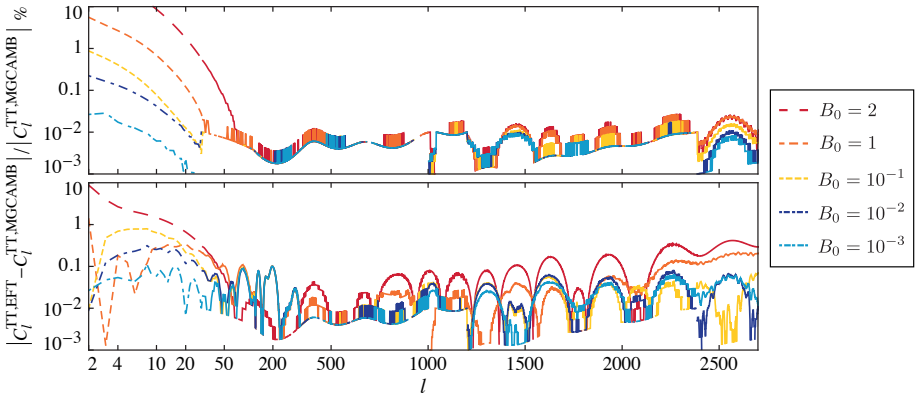

Figure 7.7: *Upper panel*: comparison between the temperature anisotropy angular power spectra of EFTCAMB and MGCAMB for $f(R)$ models with a ΛCDM expansion history but different values of B_0 and modeled via the BZ approach described in Section 7.4.6. *Lower panel*: same comparison for the case of a designer $f(R)$ model with ΛCDM background. For a detailed interpretation of the plots see Section 7.4.6.

The BZ case allows us to make a check of reliability of our code with minimal changes with respect to the way $f(R)$ theories are treated in MGCAMB. The designer case corresponds to a proper full treatment of $f(R)$ models and therefore let us fully exploit the potential of our code, avoiding spurious effects due to the BZ approximation; this will allow us to check the accuracy of the QS approximation in $f(R)$ models to a new extent. The latter case corresponds to the proper treatment of the background operators in the *mapping* EFT cases.

Let us start with the BZ case. Using the matching formulae (7.20) we see that the BZ ansätz (7.93) can be mapped into the EFT formalism as follows:

$$\begin{aligned}\Omega &= -1 + e^{-\frac{3B_0\Omega_m a^{s-1}}{2(s-1)}} = -\frac{3}{2}\frac{B_0\Omega_m a^{s-1}}{s-1} + O(B_0^2),\\ \frac{\Lambda}{m_0^2} &= -\frac{\rho_{\rm DE}}{m_0^2} + B_0H_0^2\frac{27a^4\Omega_m^2 - 9\Omega_m a^s\left(4a^3(s-4)\Omega_\Lambda + (s-1)\Omega_m\right)}{4a^4(s-4)(s-1)} + O(B_0^2).\end{aligned} \tag{7.94}$$

As in MGCAMB, we fix $s = 4$ and we use different values of B_0 ranging from very large ones ($B_0 = 2$) to small ones ($B_0 = 10^{-3}$). The comparison of the temperature spectra from the two codes is shown in the upper panel of Fig. 7.7. As we can clearly see the agreement on small scales is very good ($\lesssim 0.01\%$) and remains under control ($\lesssim 0.1\%$) even on very large scales for small values of B_0 ($\lesssim 0.01$). We get some tension between the two codes, (relative difference $> 1\%$), at low multipoles for large values of B_0 ($\gtrsim 0.1$). This is partially due to the way we treat the background in this case; first of all when $B_0 \gtrsim 1$ the correction term in Eq. (7.94) cannot be neglected anymore. For example, for $B_0 = 2$ this introduces an order of magnitude approximation error in Ω and Λ. Secondly, there is some fictitious dynamics of the scalar DoF, excited by the fact that the BZ parametrization (7.93) does not give an exact representation

of the background dynamics. We also expect this discrepancy to be partially due to the fact that the QS approximation inherent in the treatment of $f(R)$ in MGCAMB does not give a full account of the ISW effect. However, in order to make meaningful statements about the latter, we need to make a comparison between the output of MGCAMB and the output of EFTCAMB with the full treatment of the background, i.e. consider the designer case mentioned above.

Let us then abandon the BZ parametrization for our background cosmology, and rather adopt the designer approach that allows us to reconstruct all the viable $f(R)$ models that reproduce a ΛCDM expansion history. As mentioned earlier, $f(R)$ models are able to reproduce any given expansion history by means of a designer approach firstly discussed in Ref. [260] and later generalized to include radiation and a time varying DE equation of state in Ref. [264]. The Friedmann equation for $f(R)$ theories can indeed be written as a second order differential equation for $f[R(a)]$, namely:

$$f'' - \left(1 + \frac{H'}{H} + \frac{R''}{R'}\right) f' + \frac{R'}{6H^2} f = -\frac{R'}{3M_P^2 H^2}\rho_{\rm DE}, \tag{7.95}$$

where primes denote differentiation w.r.t. $\ln a$ and $\rho_{\rm DE}$ is the energy density of the effective DE component. The procedure consists then in fixing the expansion history by choosing an equation of state of DE $w_{\rm DE}(a)$, determining the corresponding energy density like in Eq. (7.68) and solving Eq. (7.95) for f. For any given expansion history the solution will consist of a family of $f(R)$ models labeled by B_0. We implement this procedure in EFTCAMB and show the output in Fig. 7.8; for the ΛCDM and wCDM cases one can notice that the reconstructed $f(R)$ are in agreement with those of Ref. [260]. We show also the results for the case of a CPL background.

We start with a ΛCDM expansion history, consider different values of B_0 and compare our results with those of MGCAMB in the lower panel of Fig. 7.7. The overall agreement for values of $B_0 < 0.1$ is within 0.1% in the high multipoles regime and within 1% in the low multipoles regime. For larger values, i.e. $B_0 \gtrsim 1$ (which are in tension with constraints from current data [439, 305, 440, 441]) we notice that at large scales there is a better agreement, while on smaller scales we get some systematic offset. In what follows we analyze this discrepancy using $B_0 = 2$ which emphasizes the offset of the codes and facilitates the investigation.

We choose to investigate the source of the above mentioned discrepancy by comparing the functions $\mu(z,k)$ and $\gamma(z,k)$ in the BZ parametrization (7.92) to those inferred from our code. The latter are obtained evolving the full dynamics for the designer $f(R)$ model in EFTCAMB and then substituting the perturbations into Eqs. (7.90), therefore we indicate them with a subscript 'des'. In Fig. 7.9 we plot all these quantities in the (z,k) space, as well as the fractional difference between the BZ and designer quantities both for μ and for γ. Overall we get good agreement between the BZ quantities and our designer ones, reproducing the known pattern of recovery of the standard GR behavior at early times on large scales, and having some significant deviations from the standard behavior on small scales at late times. After a more careful look, we see that on super-horizon scales the differences between $\mu_{\rm BZ}(\gamma_{\rm BZ})$ and $\mu_{\rm des}$ ($\gamma_{\rm des}$) are relatively small and are simply due to the fact that our full-Boltzmann code catches some well known dynamics of the scalaron at those scales, and the return to GR

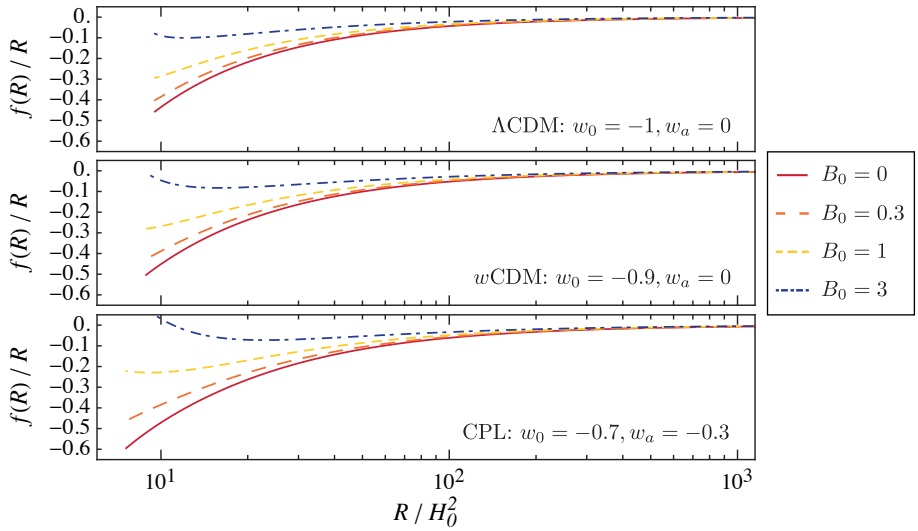

Figure 7.8: We show designer $f(R)$ models that mimic different expansion histories as reconstructed with our code: ΛCDM in the top panel, a constant $w_{\rm DE} = -0.9$ in the middle panel and a time-varying $w_{\rm DE}$ in the bottom panel. For each case we plot four curves corresponding to four different values of the boundary condition B_0. The values of $w_{\rm DE}$ in the first two panels are chosen to facilitate the comparison with Ref. [260]. See Section 7.4.6 for a detailed explanation.

is not as exact as in the quasi-static BZ where it is imposed a priori. On smaller scales, in particular on scales around the Compton wavelength of the scalaron, the fractional difference plot shows some non-trivial differences between the BZ and designer quantities. In other words, at late times and on scales around the Compton one, EFTCAMB is able to catch some dynamics of the scalaron which is not entirely negligible and perhaps is the source of the discrepancies that we noticed in the CMB lensing spectrum on small scales. The latter appears especially in models for which the Compton wavelength of the scalaron is close to the horizon scale and the sub-horizon and sub-Compton regimes are not clearly distinguished.

To investigate the non-trivial sub-horizon dynamics further, we introduce the following indicator:

$$\xi \equiv \frac{\dot{\pi}}{\mathcal{H}\pi}\,, \tag{7.96}$$

which quantifies deviations from quasi-staticity for the scalar degree of freedom. In this context with quasi-staticity we mean the fact that time derivatives of the quantities of interest can be neglected. We plot ξ in the left panel of Fig. 7.10; from that contour plot one can notice that the scalaron has some dynamics on super-horizon scales, it then slows on scales of the order of its Compton wavelength and finally resumes evolving in time below the latter scale, especially at low redshift. Let us stress that ξ is a good indicator of whether one can neglect the time derivatives of the scalar field, but does not necessarily carry information

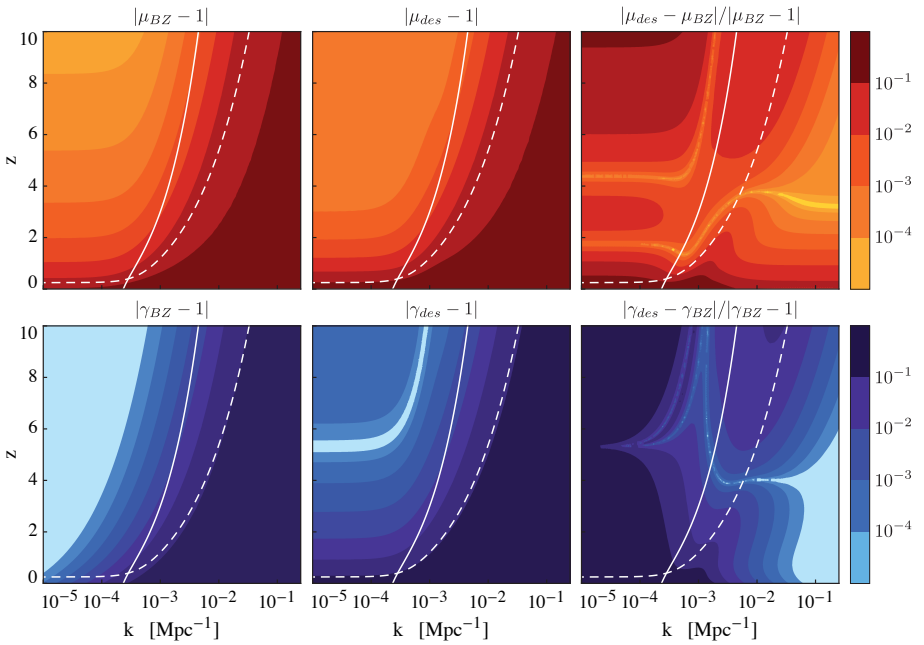

Figure 7.9: We compare the functions $\mu(z,k)$ and $\gamma(z,k)$ in Eq. (7.92), with $B_0 = 2$ and $s = 4$, to those computed in EFTCAMB evolving the full set of Einstein-Boltzmann equations for $f(R)$ models that reproduce a ΛCDM expansion history and have $B_0 = 2$. In all plots, the solid line represents the physical horizon while the dashed line represents the Compton wavelength of the scalaron (7.89). *Upper panel*: respectively $|\mu_{\rm BZ} - 1|$, $|\mu_{\rm des} - 1|$ and $|\mu_{\rm BZ} - \mu_{\rm des}|/|\mu_{\rm BZ} - 1|$. *Lower panel*: $|\gamma_{\rm BZ} - 1|$, $|\gamma_{\rm des} - 1|$ and $|\gamma_{\rm BZ} - \gamma_{\rm des}|/|\gamma_{\rm BZ} - 1|$. See Section 7.4.6 for a detailed explanation.

on the dynamics of the metric potentials and therefore on the overall validity of the QS approximation. The latter will depend on how the scalar field couples with gravity and the matter sector. In the right panel of Fig. 7.10 we plot the behavior of π as a function of redshift for four different scales, comparing it with the evolution of the source term in Eq. (7.78). The curves confirm what we inferred about the dynamics of π from the behavior of the indicator ξ; on very large scales the scalaron evolves slowly, following the source term at early times and then almost stops evolving at extremely late times. On the other hand, on smaller scales, the field evolves slowly at early times, tracking the source and continues to evolve even at later times eventually crossing zero at some point. At this point the QS approximation for the dark sector breaks down because the field becomes very small while its derivatives remains finite.

To summarize, we see that the strongest deviations from the BZ parametrization of $f(R)$ gravity are found close to the Compton wavelength of the scalaron ($k_c^2 = 6H_0^2/B_0$ is roughly the Compton scale today). Below this scale, depending on the value of B_0, the dynamics of the scalar field might be non-negligible even if we are on sub-horizon scales; and depending on the coupling of π to gravity and DM, this might generate a non-standard dynamics of matter per-

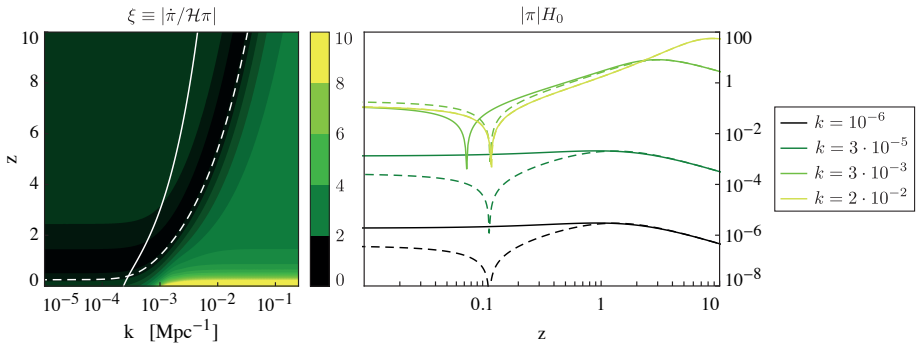

Figure 7.10: *Left:* time and scale dependence of ξ Eq. (7.96), which is the quantity we introduce as an indicator of the applicability of the QS approximation. *Right:* time evolution of the Stückelberg field $|\pi|H_0$ (solid curve) compared to that of the source $|H_0E/(C + k^2D)|$ (7.78) (dashed curve) for four different scales (dark curves are for large scales, light curves are for smaller, but linear, scales). Notice that for $k = 2 \cdot 10^{-2}$ the source and the field coincide. In both panels we use an $f(R)$ model with a ΛCDM expansion history and $B_0 = 2$. See Section 7.4.6 for a detailed explanation.

turbations. For what concerns the CMB, this effect will show up, for very large values of B_0, both on very large scales due to the differences induced on the ISW effect and on small scales due to the modified evolution of perturbations that will influence the lensing of the CMB. As the value of B_0 decreases the Compton wavelength will move to scales that just contribute to the lensing, but the magnitude of the effect will decrease as well. In the end, for small values of B_0, this will just introduce some very small, negligible, discrepancies that we can see in Fig. 7.7. We however stress that ongoing experiments, such as *Planck*, and forthcoming ones, like Euclid, are expected to be much more sensitive to these effects which will have to be properly accounted for when extracting predictions for the observables of interest.

Designer $f(R)$ models on non-ΛCDM background

In this section we shall use EFTCAMB to compute the power spectra of different cosmological observables for $f(R)$ models that mimic more general expansion histories. As above, after choosing an expansion history, we reconstruct viable models via an implementation in our code of the $f(R)$ designer approach and the matching formulae (7.20). We consider a wCDM expansion history with $w_0 = -0.7$, a CPL model with $w_0 = -0.7$, $w_a = -0.3$ and we compare the results with those of the ΛCDM models analyzed in 7.4.6. In all cases we fix $B_0 = 1$ in order to make the various effects clearly visible. In particular we choose the parameters of the CPL model in order to resemble a cosmological constant at high redshift while evolving toward the wCDM case at late times.

We show the power-spectra observables calculated with our code in Fig. 7.11 and in what follows we give a detailed overview of each result. The first, top left panel shows the ISW part of the CMB temperature power spectrum. On

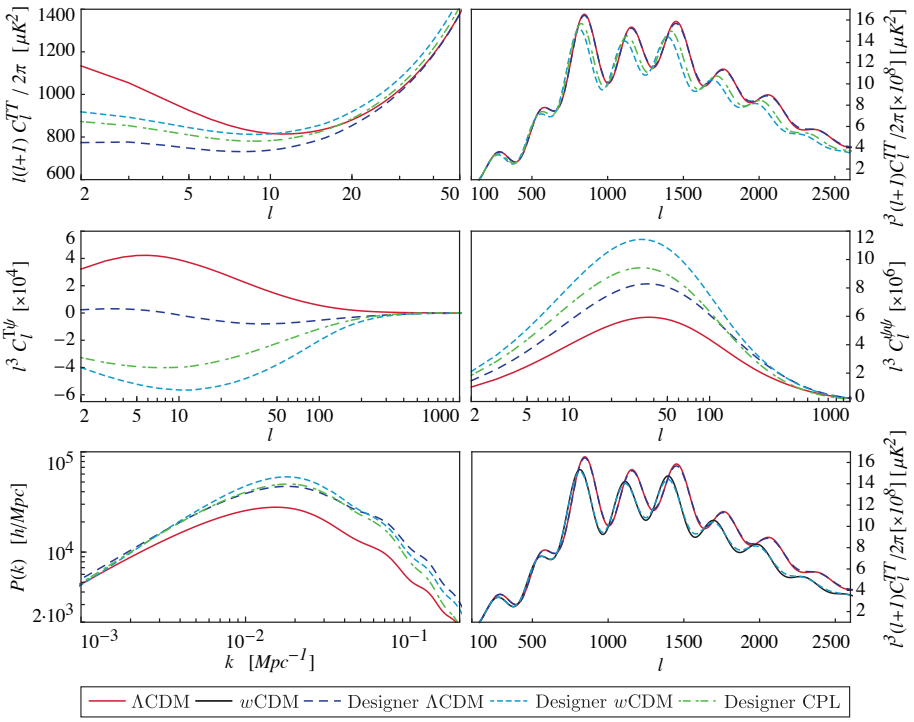

Figure 7.11: Power spectra of several cosmological observables for $f(R)$ models mimicking both ΛCDM and non-ΛCDM expansion histories. The red solid line represents predictions for the ΛCDM model while the black solid one stands for a wCDM with $w_0 = -0.7$ (shown only in the bottom right panel). Dashed lines portray designer $f(R)$ models with different expansion histories but same boundary condition $B_0 = 1$: the long-dashed dark blue line corresponds to models with a ΛCDM background, the short-dashed blue to models with a wCDM background with $w_0 = -0.7$ and the dashed-dotted light blue to models with a CPL background with $w_0 = -0.7$ and $w_a = -0.3$. *Upper panels:* CMB temperature power spectra; *central panels:* lensing-temperature cross-correlation (left) and the lensing potential power spectra (right); *lower panels:* total matter (left) and CMB temperature power spectra (right) for ΛCDM / wCDM and the corresponding designer $f(R)$ models. See Section 7.4.6 for a detailed explanation.

these angular scales we notice the effects of a modified time evolution of the gravitational potentials at late times, that results in an overall suppression of power at low multipoles. This effect will, however, be shaded by cosmic variance which lowers the statistical significance of these deviations. In fact, we expect differences from the ΛCDM behavior at small scale to acquire a primary role in testing alternative models with ongoing and upcoming surveys [442]. We zoom in on the modifications to C_ℓ^{TT} at small scales in the top right panel, where we can more clearly see the part of the temperature power spectrum which is influenced by gravitational lensing. As expected, we notice that the change in the expansion history shifts the position of the peaks and reduces their

amplitudes, while the modification of gravity could further smear the acoustic peaks in the lensing part. This can be clearly seen in the lower right figure which compares explicitly the resulting temperature spectra from CAMB and our designer EFTCAMB on ΛCDM and wCDM background. The impact of modifications of gravity on the CMB lensing potential is shown in the center right figure where we plot $C_\ell^{\psi\psi}$; one can appreciate that the different expansion histories change the angular size of the lenses slightly shifting the position of the peak, while the different dynamics of perturbations greatly impact the amplitude of the spectrum. Ongoing CMB experiments like *Planck*, ACT and SPT [419, 443, 42] have directly measured this observable, and in the upcoming future they will measure it with even greater accuracy, so to this extent codes like ours, that evolve the full dynamics and capture interesting features at those scales of the CMB spectrum, will be very useful.

Another quantity which is greatly influenced by modification of gravity is the power spectrum of the cross-correlation between temperature and lensing potential, i.e. $C_\ell^{\psi T}$. As we already commented, the evolution of the Weyl potential sources both the ISW and weak lensing effect inducing a correlation between these two. From the center left panel of Fig. 7.11 one can notice that for the ΛCDM model the cross-correlation is large and positive, while for $f(R)$ models with a ΛCDM expansion history but $B_0 = 1$, the cross-correlation oscillates around zero. Interestingly, the signal can be increased by changing the expansion history while keeping $B_0 = 1$; in this case the cross-correlation will become large and negative.

Finally, we shall comment on the effects that appear in the total matter power spectrum. In the bottom left panel of Fig. 7.11 we can appreciate that as soon as B_0 is different from zero the spectrum is shifted, both in amplitude and in scale, with respect to the ΛCDM one. In addition a non-standard expansion history changes the amplitude of the spectrum at the peak and also the slope at smaller, but still linear, scales as we can see comparing the light blue lines to the dark blue ones. Interestingly, we can clearly see that the CPL model lies between the ΛCDM and the wCDM one; the amplitude of the peak, which is influenced by the early time expansion history, lies close to the ΛCDM one while the slope at smaller scales, which is affected by the late time evolution of matter perturbations, stays close to the wCDM model as w is approaching $w_0 = -0.7$.

7.4.7 Pure EFT parametrizations with phantom-divide crossing

In this subsection we shall use our code to explore deviations from ΛCDM cosmology parametrized with the EFT language. We will focus on models that contain only background operators. On the lines of Section 7.4.1 for the *pure* EFT cases, we fix the desired expansion history and we make a choice for $\Omega(a)$, deriving the remaining quantities from the EFT designer procedure.

For the present analysis, we consider power laws for Ω, leaving the analysis of the perturbations for other viable choices [396] for future work. Specifically we set:

$$\Omega(a) = \Omega_0 a^n \,, \tag{7.97}$$

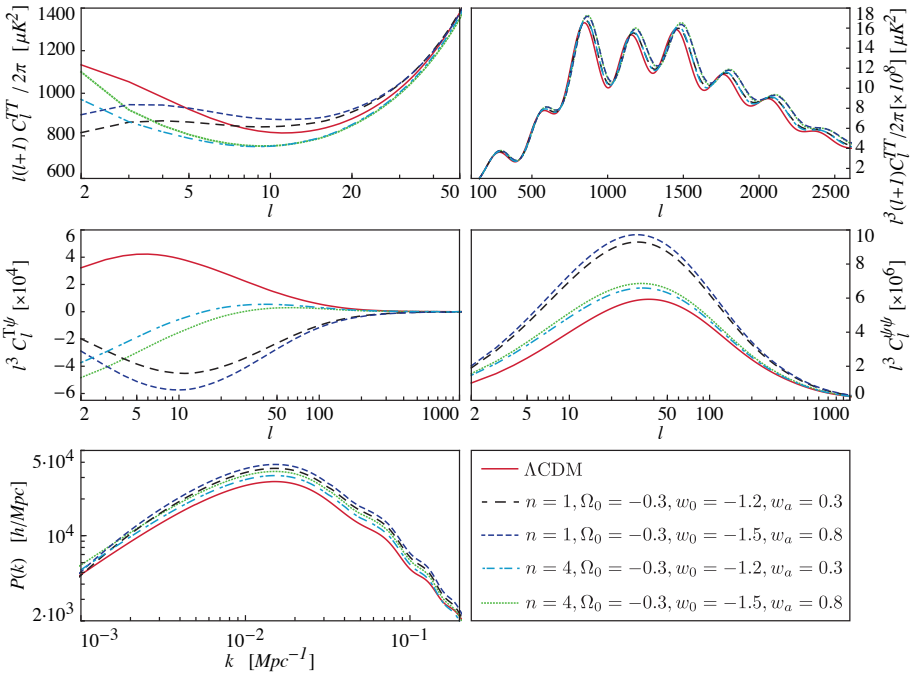

Figure 7.12: Power spectra of several cosmological observables for parametrized EFT models with a phantom-divide crossing background. The red solid line represents predictions for the ΛCDM model. Dashed lines portray models corresponding to several choices of parameters defining the function Ω. *Upper panels:* CMB temperature power spectra; *central panels:* lensing-temperature cross-correlation (left) and the lensing potential power spectra (right); *lower panels:* total matter power spectra (left). See Section 7.4.7 for a detailed explanation.

which gives an Ω analogous to the one of the BZ parametrization of $f(R)$ models when $\Omega_0 = -B_0\Omega_m/2$ and $n = 3$. We fix the expansion history to be the one of a DE model displaying an extreme phantom-divide crossing which is a phenomenological feature that is naturally and consistently accounted for by the EFT approach. Let us stress that with our code we have checked that these models satisfy the stability constraints listed in Section 7.4.3. In this case, given that we are not choosing a specific model of DE/MG, but rather a form for Ω, these stability requirements acquire the meaning of a validity check on the time dependence of the EFT functions in view of the corresponding behavior of the perturbations. In particular, the stability conditions will constrain the parameter space describing the expansion history, (w_0, w_a), and Ω, in this case n, offering a complementary constraining power.

We plot the resulting power spectra in Fig. 7.12 for two ghost-free phantom model: $n = 1, 4$ and $\Omega_0 = -0.3$ in two different background specified by $(w_0 = -1.2, w_a = 0.3)$ and $(w_0 = -1.5, w_a = 0.5)$. Aside from the wide array of phenomenological changes that we commented on in the previous Section we shall outline here some interesting features. We can notice that the CMB power

spectrum at small scales is mostly influenced by the change in the expansion history while all the other observables are more sensitive to the change in the power law exponent. Between the linear ($n = 1$) and the non-linear ($n = 4$) models we can see a pronounced qualitative difference while the different expansion histories induce just quantitative changes. This is particularly clear in the ISW part of the CMB temperature power spectrum, in the lensing potential and in the lensing-temperature cross correlation. Interestingly enough we see that the effects on the total matter power spectrum are limited even if the models that we considered are chosen to be rather extreme. At last we notice that no pathological feature arises in these spectra associated to the crossing of the phantom-divide.

7.4.8 EFTCosmoMC: sampling of the parameter space under stability conditions

To fully exploit the power of EFTCAMB we equipped it with a modified version of the standard Markov-Chain Monte-Carlo code CosmoMC [401] that we dubbed EFTCosmoMC [398]. The complete code now allows to explore the parameter space performing comparisons with several cosmological data sets, and it does so with a built-in stability check that we shall discuss in the following.

In the EFT framework, the stability of perturbations in the dark sector can be determined from the equation for the perturbation π Eq. (7.78), which is an inhomogeneous Klein-Gordon equation with coefficients that depend both on the background expansion history and the EFT functions. Following the arguments of Ref. [227], in Section 7.4.3 we listed general viability requirements in the form of conditions to impose on the coefficients of the equation for π.

When exploring the parameter space one needs to check the stability of the theory at every sampling point. While this feature at first might seem a drawback, however, it is one of the main advantages of the EFT framework and a virtue of EFTCAMB/EFTCosmoMC. Indeed, as we outlined in Ref. [397], checking the stability of the theory ensures not only that the dynamical equations are mathematically consistent and can be reliably numerically solved, but also, perhaps more importantly, that the underlying physical theory is acceptable. This of course is desired when considering specific DE/MG models and, even more, when adopting the *pure* EFT approach. In the latter case indeed, one makes a somewhat arbitrary choice for the functional form of the EFT functions and satisfying the stability conditions will ensure that there is an underlying, theoretically consistent model of gravity corresponding to that given choice.

Imposing stability conditions generally results in a partition of the parameter space into a stable region and an unstable one. In order not to alter the statistical properties of the MCMC sampler [444], like the convergence to the target distribution, when dealing with a partitioned parameter space we implement the stability conditions as priors so that the Monte Carlo step is rejected whenever it would fall in the unstable region. We call these constraints *viability priors* as they represent the degree of belief in a viable underlying single scalar field DE/MG theory encoded in the EFT framework. We would like to stress that they correspond to specific conditions that are theoretically well motivated and, hence, they represent the natural requirements to impose on a

model/parametrization. One of the virtues of the EFT framework, and consequently of EFTCAMB/EFTCosmoMC, is to allow their implementation in a straightforward way. We shall emphasize that our EFTCosmoMC code automatically enforces the *viability priors* for every model considered, both in the *pure* and *mapping* EFT approach.

7.4.9 Data sets and Results

In this Section we shall briefly review the data sets we used and discuss the resulting constraints obtained for some selected *pure* and *mapping* EFT models on both ΛCDM and wCDM backgrounds. While we will work with models that involve only background operators, EFTCAMB/EFTCosmoMC are fully equipped to handle also second order operators; the same procedure that we shall outline here can be followed when the latter are at play.

Data sets

We adopt *Planck* temperature-temperature power spectra considering the 9 frequency channels ranging from 30 $\sim$ 353 GHz for low-ℓ modes ($2 \leq \ell < 50$) and the 100, 143, and 217 GHz frequency channels for high-ℓ modes ($50 \leq \ell \leq 2500$) [3] [445, 21]. In addition we include the *Planck* collaboration 2013 data release of the full-sky lensing potential map [419], by using the 100, 143, and 217 GHz frequency bands with an overall significance greater than 25σ. The lensing potential distribution is an indicator of the underlying large-scale structure, and as such it is sensitive to the modified growth of perturbations contributing significant constraining power for DE/MG models.

In order to break the well-known degeneracy between the re-ionization optical depth and the amplitude of CMB temperature anisotropy, we include WMAP low-ℓ polarization spectra ($2 \leq \ell \leq 32$) [27]. Finally, we consider the external baryon acoustic oscillations measurements from the 6dFGS ($z = 0.1$) [446], SDSS DR7 (at effective redshift $z_{\rm eff} = 0.35$) [35, 37], and BOSS DR9 ($z_{\rm eff} = 0.2$ and $z_{\rm eff} = 0.35$) [38] surveys to get complementary constraining power on cosmological distances.

To explicitly show the effect of individual data sets on the different parameters that we consider, we adopt three different combinations of data, namely: *Planck*+WP; *Planck*+WP+BAO; *Planck*+WP+BAO+lensing, where with lensing we mean the CMB lensing potential distributions as measured by *Planck*. In all cases we assume standard flat priors from CMB on cosmological parameters while we impose the *viability priors* discussed in Section 7.4.8 on model parameters.

Linear EFT model

We start our exploration of CMB constraints on DE/MG theories in the *pure* EFT mode. We adopt the designer approach choosing two different models for the expansion history, the ΛCDM one and the wCDM one (corresponding to a constant DE equation of state). As we reviewed in Section 7.4.1, after fixing the

[3] `http://pla.esac.esa.int/pla/aio/planckProducts.html`

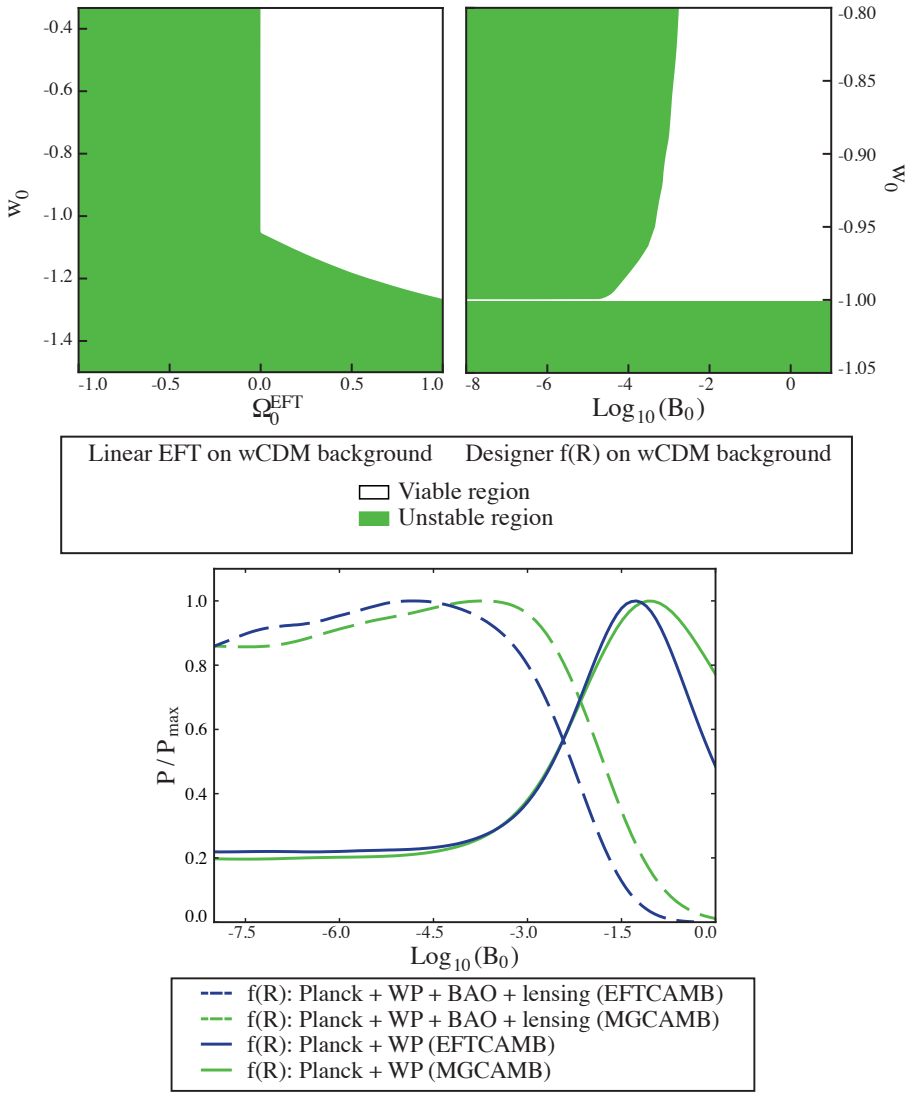

Figure 7.13: *Top panel*: stability regions of linear EFT and designer $f(R)$ models on a wCDM background. The cosmological parameters defining the expansion history are set to their CAMB default values: $H_0 = 70\,\mathrm{Km/s/Mpc}$, $\Omega_b = 0.05$, $\Omega_c = 0.22$, $T_{\mathrm{CMB}} = 2.7255\,\mathrm{K}$. *Bottom panel*: marginalized constraints on $\mathrm{Log}_{10}(B_0)$ describing designer $f(R)$ models on ΛCDM background for two data sets differing by CMB lensing and BAO. For each data set we compare the results obtained with EFTCAMB with those obtained by MGCAMB [417, 418] for the same designer $f(R)$ models.

background expansion history, one can use the Friedmann equations to solve for two of the three EFT background functions in terms of the third one; as it is common, we use this to eliminate Λ and c. We are then left with Ω as a free background function that will leave an imprint only on the behavior of

perturbations. We assume the following functional form:

$$\Omega(a) = \Omega_0^{\rm EFT}\, a\,, \tag{7.98}$$

which can be thought of as a first order approximation of a Taylor expansion in the scale factor. We set to zero the coefficients of all the second order EFT operators. In the remaining we refer to this model as the linear EFT model.

Before proceeding with parameter estimation, it is instructive to study the shape of the viable region in the parameter space of the model. As we discussed in Section 7.4.8, the check on the stability of any given model is a built-in feature of EFTCAMB/EFTCosmoMC, so that the user does not need to separately perform such an investigation prior to implementing the model in the code. Nevertheless, in some cases it might be useful to look at the outcome of such analysis as one can learn interesting things about the model/parametrization under consideration. Let us briefly discuss the stability of the linear EFT model.

In the case of a ΛCDM expansion history, it is easy to show that all the stability requirements that we listed in Ref. [397], and reviewed in Section 7.4.8, imply the following *viability prior*:

$$\Omega_0^{\rm EFT} \geq 0\,. \tag{7.99}$$

On the other hand, the case of a wCDM expansion history can not be treated analytically so we used our EFTCAMB code along with a simple sampling algorithm, included in the code release, to explore the stability of the model in the parameter space. We varied the parameters describing the dark sector physics while keeping fixed all the other cosmological parameters. The result is shown in Fig. 7.13 and includes interesting information on the behavior of this model. First of all, also in this case the stable region correspond to $\Omega_0^{\rm EFT} > 0$; furthermore it is possible to have a viable gravity model with $w_0 < -1$, although in this case $\Omega_0^{\rm EFT}$ needs to acquire a bigger and bigger value to stabilize perturbations in the dark sector. Finally, we see that if $\Omega_0^{\rm EFT} = 0$ we recover the result, found in the context of quintessence models [103], that $w_0 > -1$. This case corresponds, in fact, to minimally coupled quintessence models with a potential that is crafted so that the resulting expansion history mimics that of a wCDM model.

For the ΛCDM background case, the 1D marginalized posterior distributions, obtained with the three different data compilations discussed above, are shown in Fig. 7.14 (a). The corresponding marginalized statistics are summarized in Tab. 7.3. We find that the three different data compilations produce similar results, with *Planck*+WP+BAO+lensing giving:

$$\Omega_0^{\rm EFT} < 0.061 \quad (95\%\text{C.L.})\,. \tag{7.100}$$

Next we consider a wCDM expansion history, characterized by an equation of state for DE constant in time, w_0, but different from -1. Upon inspecting Fig. 7.14 (b) one can notice that the marginalized posterior distributions of $(\Omega_m, \Omega_\Lambda, H_0, w_0)$ obtained from *Planck*+WP data are significantly skewed, i.e. their right tail goes to zero much more sharply than the left one. The situation changes significantly when one adds BAO data. This is due to the combination of two effects. On one hand, when BAO data are not included, the constraints

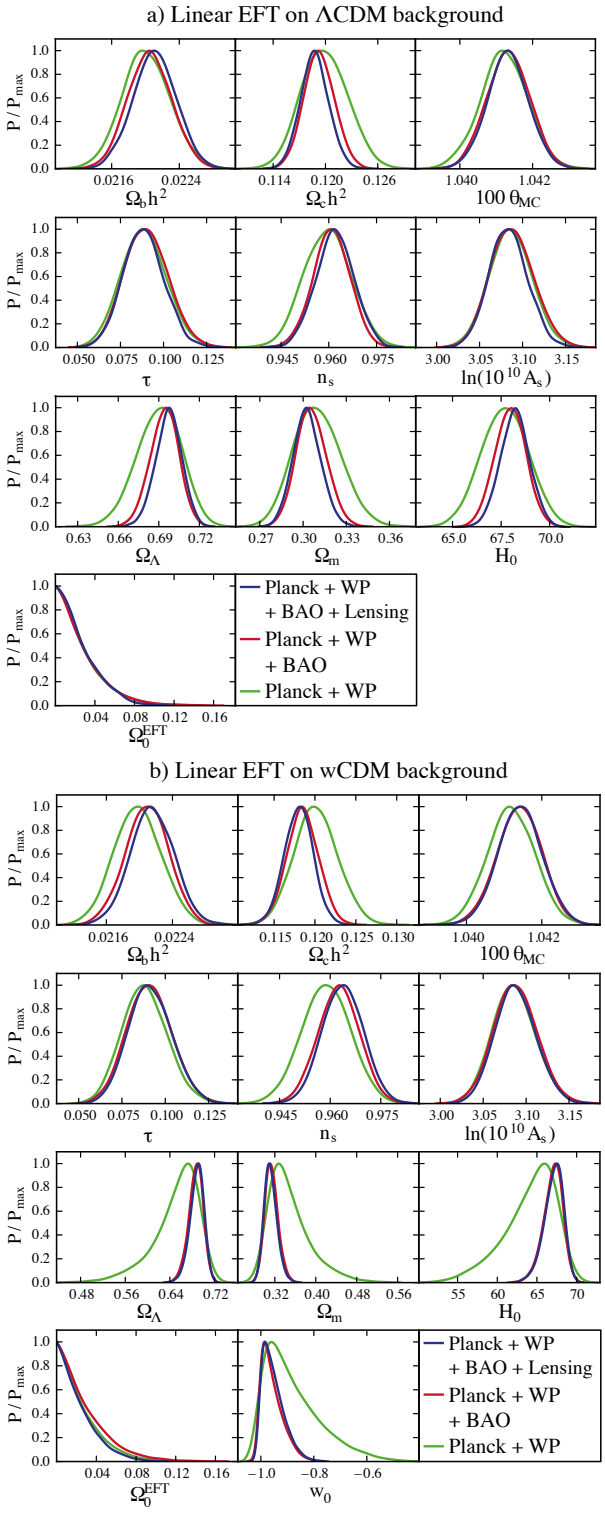

Figure 7.14: 1D Marginalized posterior distributions of cosmological and model parameters for *pure* linear EFT both on a ΛCDM (top) and wCDM (bottom) background. Different colors represent different combinations of cosmological data sets.

on $(\Omega_m, \Omega_\Lambda, H_0, w_0)$ are relatively loose since one is lacking the complementary high precision information on the expansion history. In other words, the gain/loss of likelihood value in the vicinity of best-fit points is not very significant, so the sampling points of cosmological parameters broadly spread around their central values. In this case, the stability requirements on $\Omega_0^{\rm EFT}$ and w_0 dominate over the data constraining power. On the other hand, as shown in the top panel of Fig. 7.13, the viable region in the space $(\Omega_0^{\rm EFT}, w_0)$ for the linear EFT model on a wCDM background covers mostly $w_0 > -1$, i.e. it is highly asymmetric in the range around $w_0 = -1$. This explains the asymmetry in the posterior distribution of w_0 since the marginalized posterior distribution in Monte-Carlo integration algorithms follows the number of projected sampling points in the given volume. Furthermore, from the top panel of Fig. 7.15 (green curve), one can see that $(\Omega_m, \Omega_0^{\rm EFT}, H_0)$ are degenerate, as expected, with w_0 and this explains while their posterior distributions are skewed as well. As soon as complementary measurements of cosmological distances, such as BAO, are added to the data sets, the constraining power is strong enough and the posterior distributions become more symmetric; indeed BAO data significantly helps to localize the confidence regions close to $w_0 \sim -1$, making the posterior distribution less affected by the global profile of *viability priors*.

Finally, from the top panel of Fig. 7.15 we can see that the degeneracy of $\Omega_0^{\rm EFT}$ with the other parameters is not very significant after adding BAO data (blue and red curves). As a result the bounds on $\Omega_0^{\rm EFT}$ remain at the same level of those obtained for a ΛCDM background. With *Planck*+WP+BAO+lensing data we obtain:

$$\Omega_0^{\rm EFT} < 0.058 \quad (95\%\text{C.L.}) \, . \tag{7.101}$$

One can notice that the addition of lensing data does not significantly improve the constraint on $\Omega_0^{\rm EFT}$ in neither the ΛCDM nor the wCDM case.

$f(R)$ gravity

The $f(R)$ theory of gravity has already been introduced in Section (6.1.1) and its implementation in the EFTCAMB solver has been presented and discussed in Section (7.4.6).

As described at length in Section (7.4.1), EFTCAMB treats the background of $f(R)$ gravity with a built-in designer routine that is specific to these models and can handle ΛCDM, wCDM and CPL backgrounds. Furthermore, the viability of the reconstructed model is automatically checked by the code via the procedure described in Section 7.4.8.

Like in the *pure* EFT case, it proves very instructive to investigate the shape of the parameter space as dictated by the stability conditions of Section 7.4.8. For the designer $f(R)$ model on ΛCDM background it is easy to show that the latter reproduce the known result that in order to have a positive mass of the scalaron B_0 should be greater than zero. It is much more interesting to investigate the shape of the parameter space for $f(R)$ models mimicking a wCDM background expansion history. We do it numerically, through the built-in routine of EFTCAMB, and we show the results in Fig. 7.13. The first noticeable feature is that for wCDM models the value of the equation of state of DE can not go below -1, which is consistent with what was found in Ref. [264].

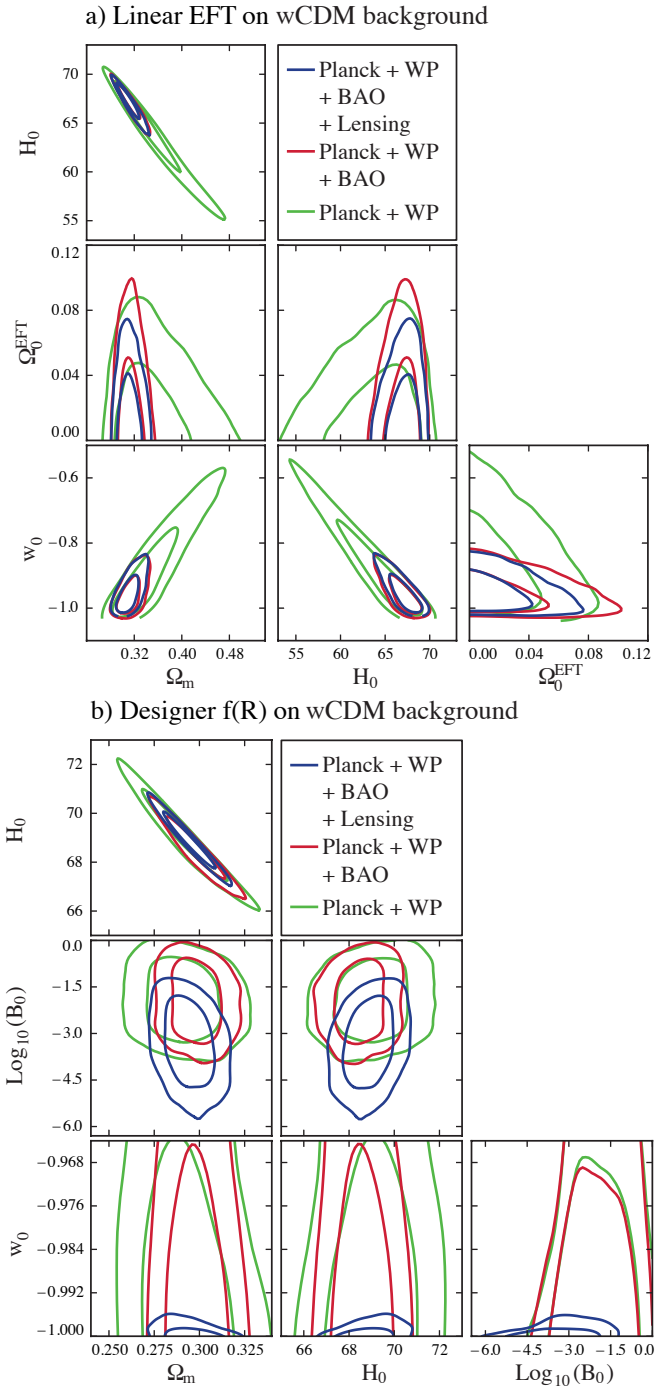

Figure 7.15: 68% and 95% confidence regions on combinations of cosmological parameters for linear *pure* EFT and designer $f(R)$ models on wCDM background. Different combinations of observables are indicated with different colors.

Linear EFT+ΛCDM			
	Planck+WP	*Planck*+WP+BAO	*Planck*+WP+BAO+lensing
Parameters	mean ± 68% C.L.	mean ± 68% C.L.	mean ± 68% C.L.
$100\Omega_b h^2$	2.201±0.028	2.205±0.025	2.211±0.025
$\Omega_c h^2$	0.1199±0.0026	0.1193±0.0017	0.1188±0.0016
$100\theta_{\rm MC}$	1.04121±0.00063	1.04133±0.00058	1.04132±0.00055
τ	0.089±0.013	0.090±0.013	0.088±0.012
n_s	0.9596±0.0073	0.9608±0.0057	0.9619±0.0059
$\log(10^{10}A_s)$	3.086±0.024	3.088±0.025	3.084±0.022
$\Omega_0^{\rm EFT}$	< 0.066 (95%CL)	< 0.072 (95%CL)	< 0.061 (95%CL)
Ω_m	0.310±0.016	0.306±0.010	0.3028±0.0096
H_0[km/s/Mpc]	67.71±1.20	67.99±0.79	68.22±0.75
$\chi^2_{\rm min}/2$	4902.799	4904.074	4908.849

Linear EFT+wCDM			
	Planck+WP	*Planck*+WP+BAO	*Planck*+WP+BAO+lensing
Parameters	mean ± 68% C.L.	mean ± 68% C.L.	mean ± 68% C.L.
$100\Omega_b h^2$	2.198±0.028	2.209±0.026	2.216±0.026
$\Omega_c h^2$	0.1201±0.0026	0.1185±0.0019	0.1180±0.0018
$100\theta_{\rm MC}$	1.04119±0.00062	1.04141±0.00058	1.04142±0.00058
τ	0.088±0.013	0.091±0.013	0.091±0.012
n_s	0.9588±0.0071	0.9625±0.0060	0.9637±0.0060
$\log(10^{10}A_s)$	3.086±0.025	3.088±0.025	3.088±0.023
$\Omega_0^{\rm EFT}$	< 0.065 (95%CL)	< 0.076 (95%CL)	< 0.058 (95%CL)
$w_0^{\rm EFT}$	$-0.88^{+0.21}_{-0.14}$ (95%CL)	$-0.96^{+0.09}_{-0.06}$ (95%CL)	$-0.95^{+0.08}_{-0.07}$ (95%CL)
Ω_m	0.349±0.041	0.314±0.013	0.312±0.013
H_0[km/s/Mpc]	64.10±3.26	66.99±1.22	67.08±1.21
$\chi^2_{\rm min}/2$	4902.921	4903.957	4908.846

Table 7.3: Constraints on cosmological parameters, using different combinations of CMB data sets, of linear *pure* EFT on both ΛCDM (up) and wCDM (down) background.

The second one is that the parameter B_0 controls the limit to GR of the theory i.e. when B_0 gets smaller the expansion history is forced to go back to that of the ΛCDM model in order to preserve a positive mass of the scalaron. The converse is not true and this same feature do not appear in *pure* EFT models where the $\Omega_0^{\rm EFT} = 0$ branch contains viable theories and corresponds to the wide class of minimally coupled quintessence models.

In what follows, we shall first investigate the constraints on B_0 in models reproducing ΛCDM background, performing also a comparison with analogous results obtained using MGCAMB [417, 418]. We will then move to study constraints on designer models on a wCDM background, which is a novel aspect of our work.

In the bottom panel of Fig. 7.13, we compare the 1D marginalized posterior distributions of $\mathrm{Log}_{10}B_0$ from our EFTCAMB to those from MGCAMB. Overall there is good agreement between the two results. Moreover, one can notice that generally the constraints obtained with EFTCAMB are a little bit tighter than those obtained with MGCAMB. This is because in the latter code $f(R)$ models are treated with the quasi-static approximation which loses out on some of

$f(R)$+ΛCDM			
	Planck+WP	*Planck*+WP+BAO	*Planck*+WP+BAO+lensing
Parameters	mean ± 68% C.L.	mean ± 68% C.L.	mean ± 68% C.L.
$100\Omega_b h^2$	2.224±0.033	2.220±0.027	2.214±0.025
$\Omega_c h^2$	0.1185±0.0027	0.1187±0.0017	0.1184±0.0016
$100\theta_{\rm MC}$	1.04149±0.00067	1.04142±0.00057	1.04136±0.00056
τ	0.088±0.013	0.087±0.013	0.087±0.012
n_s	0.9634±0.0076	0.9624±0.0058	0.9625±0.0057
$\log(10^{10}A_s)$	3.083±0.025	3.082±0.025	3.080±0.022
$\log_{10} B_0$	$< 0.0^*$	< 0.0 (95%CL)	< -2.37 (95%CL)
Ω_m	0.300±0.017	0.302±0.010	0.3005±0.0092
H_0[km/s/Mpc]	68.51±1.30	68.35±0.81	68.41±0.72
$\chi^2_{\rm min}/2$	4900.765	4901.399	4907.901

$f(R)$+wCDM			
	Planck+WP	*Planck*+WP+BAO	*Planck*+WP+BAO+lensing
Parameters	mean ± 68% C.L.	mean ± 68% C.L.	mean ± 68% C.L.
$100\Omega_b h^2$	2.255±0.033	2.246±0.029	2.226±0.026
$\Omega_c h^2$	0.1162±0.0027	0.1174±0.0019	0.1174±0.0016
$100\theta_{\rm MC}$	1.04186±0.00066	1.04166±0.00060	1.04149±0.00056
τ	0.086±0.013	0.084±0.012	0.082±0.012
n_s	0.9695±0.0078	0.9665±0.0062	0.9647±0.0057
$\log(10^{10}A_s)$	3.075±0.025	3.072±0.024	3.067±0.024
$\log_{10} B_0$	$-1.97^{+1.61}_{-1.52}$ (95%CL)	$-2.01^{+1.60}_{-1.51}$ (95%CL)	$-3.35^{+1.79}_{-1.77}$ (95%CL)
$w_0^{\rm EFT}$	$(-1, -0.94)$ (95%CL)	$(-1, -0.94)$ (95%CL)	$(-1, -0.9997)$ (95%CL)
Ω_m	0.291±0.015	0.2982±0.0099	0.2944±0.0093
H_0[km/s/Mpc]	69.04±1.18	68.50±0.80	68.89±0.75
$\chi^2_{\rm min}/2$	4900.656	4901.140	4908.286

Table 7.4: Constraints on cosmological parameters, using different combinations of CMB data sets, of the designer $f(R)$ model, on both ΛCDM (up) and wCDM (down) background. (*) No significant upper bound found in the parameter range we investigated.

the dynamics of the scalaron [413], which is instead fully captured by our full Einstein-Boltzmann solver, as discussed already in Ref. [397].

The detailed 1D posterior distributions and corresponding marginalized statistics are summarized in Fig. 7.16 (c) and Tab. 7.4 and they are consistent with previous studies employing the quasi-static approximations [447]. The bottom panel of Fig. 7.13 and Fig. 7.16 (c) show that lensing data add a significant constraining power on B_0. This is because *Planck* lensing data are helpful in breaking the degeneracy between Ω_m and B_0 which affect the lensing spectrum in different ways. Indeed, in $f(R)$ gravity the growth rate of linear structure is enhanced by the modifications, hence the amplitude of the lensing potential spectrum is amplified whenever B_0 is different than zero (see our work [397]); however, the background angular diameter distance is not affected by B_0, so the position of the lensing potential spectrum is not shifted horizontally. On the other hand, Ω_m affects both the background and linear perturbation so that both the amplitude and position of the peaks of the lensing potential are sensitive to it.

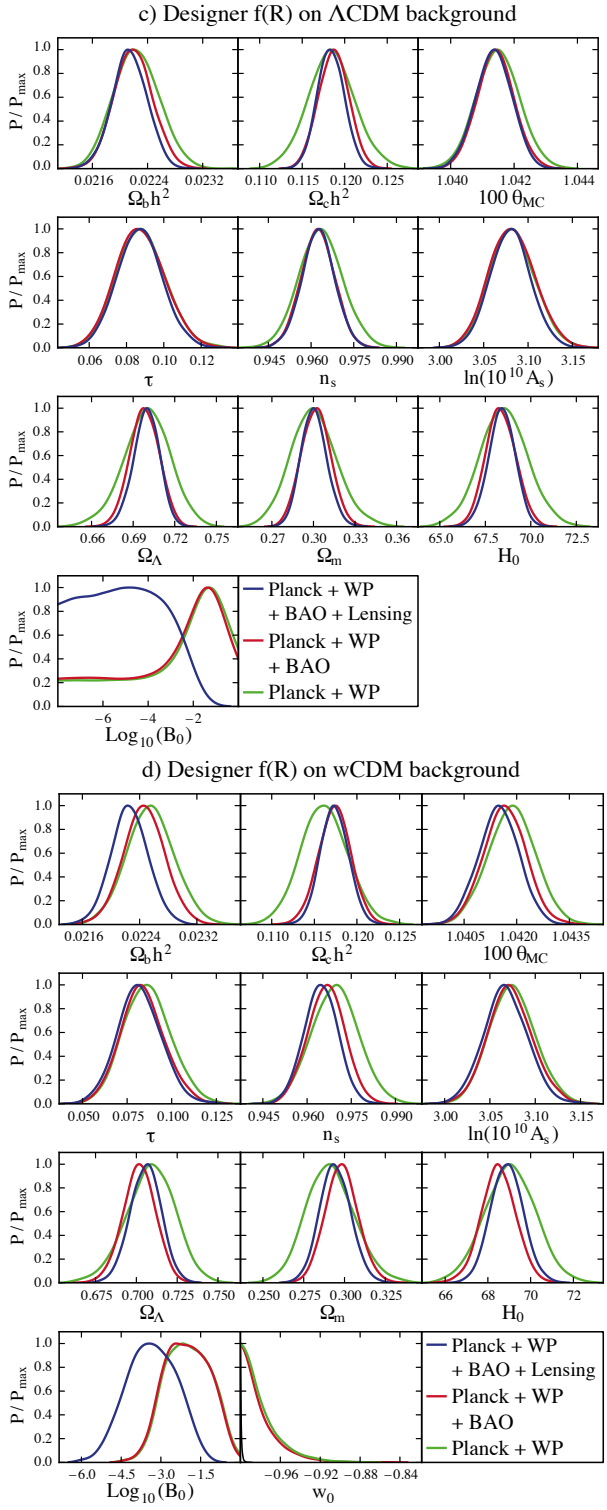

Figure 7.16: 1D Marginalized posterior distributions of cosmological and model parameters for $f(R)$ models both on a ΛCDM (top) and wCDM (bottom) background. Different colors represent different combinations of cosmological data sets.

Similarly to what happens in the linear EFT model, $f(R)$ gravity shows some novel features in the case of a wCDM background. Once again we find a non-trivial likelihood profile of $\mathrm{Log}_{10}B_0$ (see Fig. 7.16 (d)) for all the three data compilations, with the shape of the marginalized posterior distribution of $\mathrm{Log}_{10}B_0$ being dominated by the shape of the stable region. In the top right panel of Fig. 7.13 one can see indeed that when B_0 tends to smaller values, i.e. the theory tends to GR, the stable regions becomes narrower and narrower, with a tiny tip pointing to the GR limit. Since the width of this tip is so narrow compared with the current capability of parameter estimation from *Planck* data, the gains of likelihood of the sampling points inside this parameter throat are not significant, i.e. they are uniformly sampled in the throat. Hence, even though the full data set has a very good sensitivity to B_0, the marginalized distribution of $\mathrm{Log}_{10}B_0$ is dominated by the volume of the stable region in the parameter space. A complementary consequence of the shape of the stable region in the (B_0, w_0) space is the fact that when B_0 tends to zero, w_0 is driven to -1. In other words the stability conditions induce a strong correlation between B_0 and w_0 and, as a consequence, in $f(R)$ models, no matter in the ΛCDM or wCDM background case, the GR limit is effectively controlled by a single parameter, i.e. B_0.

Finally one can notice that the bound on w_0 with *Planck* lensing data is quite stringent compared to those without lensing, namely:

$$\begin{aligned} w_0 &\in (-1, -0.94)\ (95\%\text{C.L.})\ \text{without lensing}, \\ w_0 &\in (-1, -0.9997)\ (95\%\text{C.L.})\ \text{with lensing}. \end{aligned} \tag{7.102}$$

We argue that this stringent constraint actually is a consequence of the combination of the strong correlation between B_0 and w_0 induced by the viability prior, as discussed above, and the sensitivity of lensing data to B_0, that we capture well with our code. As shown in Ref. [305] *Planck* lensing data is very sensitive to MG parameters such as B_0; indeed, in our analysis with *Planck*+WP+BAO+lensing data we get

$$\mathrm{Log}_{10}B_0 = -3.35^{+1.79}_{-1.77} \quad (95\%\text{C.L.})\ . \tag{7.103}$$

Furthermore, from Fig. 7.15 (b), one can see that the ellipse in the $(\mathrm{Log}_{10}B_0, w_0)$ space corresponding to *Planck*+WP+BAO+lensing data (blue) is orthogonal to those without lensing (red and green). In other words, when lensing data is included, $\mathrm{Log}_{10}B_0$ and w_0 display a degeneracy which propagates the stringent constraint on the scalar Compton wavelength from CMB lensing data to w_0. Besides this, we do not find other remarkable degeneracies between B_0 and standard cosmological parameters.

7.4.10 Discussion

Solving the puzzle of cosmic acceleration is one of the major challenges of modern cosmology. In this respect, cosmological surveys will provide a large amount of high quality data allowing to test gravity on large scales with unprecedented accuracy. The effective field theory framework for cosmic acceleration will prove useful in performing model independent tests of gravity as well as in testing specific theories since, while being a parametrization of the quadratic action, it preserves a direct link to a wide range of DE/MG models. Indeed, any single

scalar field DE/MG models with a well defined Jordan frame can be cast into the EFT language and most of the cosmological models of interest fall into this class.

In Ref. [397], we presented the implementation of the EFT formalism into the Einstein-Boltzmann solver CAMB [399], resulting into EFTCAMB. The latter code has several virtues. It allows for the implementation of the parametrized EFT framework in what we dub the *pure* EFT approach, and for the implementation of specific DE/MG models in the *mapping* mode, we gave an example of the latter case by studying the dynamics of perturbations in viable $f(R)$ models with different expansion histories. EFTCAMB does not rely on any quasi-static approximation, but rather it implements the full perturbative equations on all linear scale for both the *pure* and the *mapping* case ensuring that no potentially interesting physics is lost. To this extent, we presented an example of signature on the small scales of the CMB lensing potential angular power spectrum from the sub-horizon dynamics of the scalaron in $f(R)$ models. Effects like the latter will be measured at increasing accuracy in the next years, and our code offers a way to exploit these data as complementary tests of gravity. It has a built-in check of the stability conditions of perturbations in the dark sector in order to guarantee that the underlying gravitational theory is viable. In particular we require: a positive Newtonian constant, absence of ghost instabilities, absence of super-luminary propagating perturbations and, finally, a positive mass of the extra scalar degree of freedom. Finally, our code can handle very different expansion histories, namely ΛCDM, wCDM and CPL backgrounds, naturally allowing phantom-divide crossing, as we have shown with some results.

Let us briefly recap the main results we obtained with EFTCAMB. We started comparing our code with the outputs of MGCAMB for $f(R)$ theories on a ΛCDM background. To this extent, we focused on the CMB temperature angular spectrum and showed an agreement of the two code within 0.1% for values of the scalaron Compton wavelength consistent with existing bounds from *Planck*. For larger values of B_0 we found some tension both at the low and high multipoles; the former is due to the fact that not relying on any QS approximation, EFTCAMB gives a more accurate account of the ISW effect. To investigate the latter discrepancy instead, we considered the functions $\mu(z,k)$ and $\gamma(z,k)$, Eqs. (7.90), commonly used to parametrize deviations from GR and implemented in MGCAMB. We compared their shape in (z,k)-space as reconstructed from the full evolution of the perturbations in our code, to their form under the BZ approximation (7.92) employed to study $f(R)$ in MGCAMB. This comparison showed that EFTCAMB catches the mild dynamics of the scalaron at early times and on large scales, as well as some non-trivial dynamics on scales around and below the Compton wavelength. We confirmed this by analyzing the time- and scale-dependence of a quantity that we propose as an indicator of quasi-staticity in the dark sector, ξ Eq. (7.96). After this thorough check of consistency with MGCAMB, we moved on to fully exploit the flexibility of the EFT framework applying our code to two different DE scenarios. First, as an example of what we called the *mapping* EFT approach, we extended the implementation of the $f(R)$ designer approach to more general expansion histories like the wCDM and CPL one, examining the effects of the combined change in the background dynamics and in the growth of structure on cosmological observables like the CMB temperature and lensing power spectra (auto- and

cross-correlation), and matter power spectrum. Second, we used the *pure* EFT approach, i.e. we chose an expansion history and a parametrized form for the EFT function Ω and again explored signatures on power-spectra observables. In this case we focused on backgrounds with a phantom-divide crossing demonstrating how, within the EFT framework, there is no special pathology arising when $w_{\rm DE} = -1$is crossed.

In Ref. [398], we equipped EFTCAMB with a modified version of CosmoMC, that we dubbed EFTCosmoMC, creating a bridge between the EFT parametrization of the dynamics of perturbations and observations. EFTCosmoMC allows to practically perform tests of gravity and get constraints analyzing the cosmological parameter space with, in its current version, data sets, such as *Planck*, WP, BAO and *Planck* lensing. Further data sets, mainly from large-scale structure surveys, will be included in the near future.

As discussed in Section 7.4.8, exploring the parameter space requires a step by step check of the stability of the theory. We implemented the resulting stability conditions as *viability priors* that makes the Monte Carlo step be rejected whenever it would fall in the unstable region of the parameter space. The latter procedure, in our view, represents a clean and natural way to impose priors on parameters describing the dark sector.

To illustrate the use of the EFTCAMB/EFTCosmoMC package, we have derived constraints on two different classes of models, namely a *pure* linear EFT model and a *mapping* designer $f(R)$. We used three different combinations of *Planck*, WP, BAO and CMB lensing data sets to show their different effects on constraining the parameter space. For both models we have adopted the designer approach built-in in EFTCAMB and have considered the case of a ΛCDM as well as of a wCDM background.

For the linear EFT model, we have derived bounds on the only model parameter, i.e the present value of the conformal coupling functions $\Omega_0^{\rm EFT}$, as described in Section 7.4.9. In the case of a ΛCDM background, we have found that the latter needs to satisfy $\Omega_0^{\rm EFT} \geq 0$ as a viability condition and with *Planck*+WP+BAO+lensing data we get a bound of $\Omega_0^{\rm EFT} < 0.061$ (95%C.L.) (the three different data compilations give similar results). For the wCDM expansion history, the outcome of the stability analysis is shown in Fig. 7.13; specifically, there is a stable region in parameter space where the DE equation of state can be smaller than -1 as long as the corresponding value of $\Omega_0^{\rm EFT}$ is high enough to stabilize perturbations in the dark sector; finally, the value $\Omega_0^{\rm EFT} = 0$ corresponds to a minimally coupled model and requires $w_0 > -1$, like in the case of quintessence. The combined bound on $\Omega_0^{\rm EFT}$ with *Planck*+WP+BAO+lensing data gives $\Omega_0^{\rm EFT} < 0.058$ (95%C.L.).

Finally, we have investigated designer $f(R)$ models on ΛCDM/wCDM backgrounds, in terms of constraints on the model parameter B_0, as described in Section (7.4.9). For the ΛCDM case we also compared our results to those that we obtained with the quasi-static treatment of these models via MGCAMB [417, 418]. The two treatments give results that are in good agreement, with bounds from EFTCAMB/EFTCosmoMC being a little tighter thanks to the full treatment of the dynamics of perturbations. On wCDM background we have found a non-trivial likelihood profile of $\mathrm{Log}_{10}B_0$ (see Fig. 7.16 (d)) for all the three data compilations and the shape of the marginalized posterior

distribution in this case strongly reflects that of the viable region in parameter space. In the wCDM background, with *Planck*+WP+BAO+lensing data we get $\mathrm{Log}_{10}B_0 = -3.35^{+1.79}_{-1.77}$ (95% C.L.). The bounds on w_0 with *Planck* lensing data ($w_0 \in (-1, -0.9997)$ (95% C.L.)) are quite stringent compared to those without this data set ($w_0 \in (-1, -0.94)$ (95% C.L.)) due to the high constraining power of lensing measurements on B_0 and the strong correlation between w_0 and B_0 via the *viability prior*.

Within the *pure* EFT approach, the code we released contains already all operators relevant for the dynamics of linear perturbations. In particular, while in Refs. [397, 398] we showed results for a model involving only background operators, we shall stress that the code is fully functional for second order operators too. As for the *mapping* mode, the code currently allows for a *full* treatment of $f(R)$ models via a specific designer approach that can handle both ΛCDM, wCDM and CPL backgrounds.

In conclusion, we will gradually implement the *mapping* procedure for many other single scalar field DE/MG models which are of relevance for cosmological tests. More data sets will be added into EFTCosmoMC allowing to test gravity with the most recent data releases with a particular emphasis toward large scale structure observations in view of surveys such as Euclid [312].

The complete EFTCAMB/EFTCosmoMC bundle is now publicly available at `http://www.lorentz.leidenuniv.nl/~hu/codes/`.

Chapter 8

Conclusions

In the first part of this thesis we have presented the state of the art of Modern Cosmology. The observational data reveal the emergence of a dark Universe, in which the Dark Energy, commonly used to parameterize the recent acceleration of the Universe, and Dark Matter, constitute about 95% of the energy content of the Universe. We presented the most widely used and accepted cosmological model to describe Universe's evolution, the ΛCDM model, and we discussed its merits and limitations in the light of the theoretical predictions and observational data. The lack of a fully satisfactory model gives rise to alternatives to the cosmological standard model. In Part II and Part III, we presented the results published in Refs. [162, 207, 379, 396, 397, 398]. These papers are the result of my collaboration with T. P. Sotiriou, R. K. Sheth, P. Salucci, A. Silvestri, J. M. Cannon, E. C. Elson, B. Hu, S. Y. Zhou, M. Raveri and D. Vernieri. In these works we investigated some outstanding problems in cosmology, such as DM, the early and late acceleration of the Universe. Let us briefly recap our main findings and highlight possible future development of them.

At small scales, dwarf galaxies are good candidates to investigate the nature of DM, because their kinematics are dominated by this component down to the center. In Chapter 4, we presented the results of detailed kinematic analysis and mass modeling of the Orion dwarf galaxy, for which we derived a high quality and high resolution RC that contains negligible non-circular motions and we corrected it for the asymmetric drift. Moreover, we exploited the proximity (D = 5.4 Mpc) and convenient inclination (47°) to produce reliable mass models for the galaxy. We found that the URCH mass model (Freeman disk + Burkert halo + gas disk) fits the observational data accurately. In contrast, the NFW halo + Freeman disk + gas disk mass model is unable to reproduce the observed RC as the Orion dwarf reveals a cored DM density distribution. Finally, we modeled the velocity profile using the MOND proposal. With the present data and with the present assumptions on distance, stellar mass, constant inclination and reliability of the gaseous mass, the MOND "amplification" of the baryonic component appears to be too small to mimic the required "dark component". On the other hand, allowing for adjustments of the distance and/or value of the gas mass, the kinematic data can be reproduced in the MOND formalism. In particular, we found that adopting a distance $\sim$ 10 Mpc, i.e. 1.9 farther than the nominal distance the RC is well fitted. A direct measurement of the distance

would be a crucial test for the MOND paradigm. More in general, at galactic scales, the study of DM through RCs is a field still opened. The extension, to a larger sample of dwarf galaxies, of the analysis we proposed for the Orion dwarf, might help in testing different mass models and in particular to investigate the validity of modifications to the newtonian law, such as MOND.

Most of the matter in the Universe is dark and it was initially rather smoothly distributed. The luminous galaxies are biased tracers of the DM distribution, meaning that galaxies mass distribution does not trace the mass in the Universe. This is an obstacle to the comparison between perturbation theories and observations. The exact relation between the spatial distribution of galaxies and DM is called bias and it depends on the complex, nonlinear process of galaxy formation. In order to do precision cosmology an important step is to understand how to model the bias. The simplest version for bias was proposed by Fry & Gaztañaga (1993) [191] and it is based on the assumptions that the bias is non-linear, local and deterministic. Then, the biased tracers can be written as a Taylor expansion in terms of the mass field. In this model one expects that the cross correlation between the biased tracers and the initial field involves the higher order terms present in the Taylor expansion while this does not happen for example in peaks, and patches which form halos, in a Gaussian random field. In Chapter 5, we showed that if this Lagrangian bias is local, and the initial conditions are Gaussian, then the two-point cross-correlation between halos and mass should be linearly proportional to the mass-mass auto-correlation function. This statement is exact and valid on all scales; there are no higher order contributions, which one might have thought would appear upon truncating the Taylor series of the halo bias function. The constant of proportionality is easily related to the first coefficient of the Taylor series expansion of the biased field, although they are not equal in general. In addition, the auto-correlation function of locally biased tracers can be written as a Taylor series in the auto-correlation function of the mass. We also explored the consequences of truncating these expansions, demonstrating that it is better to renormalize all truncated expansions than to not. Finally, it could be of interest to investigate how the bias factor changes in presence of modification of gravity, as it is expected that the scale of the screening mechanism affects the growth of structures and their formation. Our findings could in principle hold for MG models, however, for these models the bias factor shows a scale dependence even on large scale with the consequence that the assumption that Lagrangian halo bias is local is no longer so attractive.

In Part III, we have illustrated some approach to modify the theory of General Relativity. In particular, we focused on the modifications that come from the introduction of a scalar field in the action. These theories can be used to describe the recent acceleration of the Universe, as well as the Inflationary phase. A possible way to discriminate among different inflationary models is to look for non-Gaussianity. NG should be investigated using non-linear perturbation theory and standard perturbation theory can be used up to the horizon exists. A complementary method is the gradient expansion technique, which provides a fully non linear analysis and naturally tackles the superhorizon perturbations. In this approach physical quantities are expanded in terms of their inverse wavelengths, as compared to a pivotal length scale which in the inflationary epoch is the Hubble length. Hence, every spatial derivative adds one perturbative order.

In Sections 6.3 - 6.4, we develop the gradient expansion formalism for shift-symmetric Galileon-type actions up to second order. This method allowed us to have a glimpse into the phenomenology associated with the non-linear derivative interactions of the scalar field. We focused on backgrounds that undergo inflation, worked in the synchronous gauge, and finally we obtained a general solution up to second order without imposing extra conditions at first order. We also showed that the general solution simplifies during the late stages of inflation, where the background becomes de Sitter space-time. Moreover physically, perturbations coming from the late time inflation are observationally most important as it is these perturbations that seed the large scale structure of the observable Universe. It would be of interest to continue this work and get the Bispectrum. Then combining our results with the conventional non-linear perturbation analysis inside the horizon, one can use the existing data to constrain the model parameters. As already discussed, in our case some complications arises. We are able to define a curvature perturbation conserved at first order, while at second order is not something that can be done straightforwardly, as one should define a new non-linear curvature perturbation. In light of the results in Ref. [373], it seems that the complications can be traced back in one assumption, i.e. $\dot{\gamma}_{ij} = \epsilon^2$. In our work we did not impose such a condition as it is unclear how restrictive it is, hence, more investigation is needed.

Finally, in Chapter 7 we consider a recent proposal to parametrize in a model-independent way single field DE/MG models, the EFT approach to cosmic acceleration. The EFT relies on three functions of time to describe the dynamics of background cosmology. In Section 7.3, we investigated the viability of these functions by means of a thorough dynamical analysis of the background cosmology. We identified a set of variables that allowed us to transform the non-autonomous system of background equations into an infinite-dimensional one characterized by a significant recursive structure. We analyzed several autonomous sub-systems, obtained truncating the original one at increasingly higher dimension, that correspond to increasingly general DE/MG models. Furthermore, we exploit the recursive nature of the system to draw some general conclusions on the different cosmologies that can be recovered within the EFT formalism and the corresponding compatibility requirements for the EFT functions. The machinery that we set up serves different purposes. The general results, obtained with this technique, can be projected into specific models, as we showed in the Quintessence case. It also can be used to determine appropriate ansätze for the three EFT background functions when studying the dynamics of cosmological perturbations in the context of large scale structure tests of gravity. The approach that we used leaves open several fronts for new investigation. In this analysis we explored models with an increasingly more general conformal coupling, however, it would be of interest to investigate also other realizations of the system. Finally, we did not analyze the scaling configurations of some critical points, that instead could provide a dynamical solution to the coincidence problem.

In Section 7.4, we showed the implementation of the EFT framework in the public Einstein-Boltzmann solver CAMB. The resulting code, which we dubbed EFTCAMB, is a powerful and versatile tool that can be used for several objectives. It can be employed to evolve the full dynamics of linear scalar perturbations of a broad range of single field DE/MG model, once the model of

interest is mapped into the EFT formalism. It offers a numerical implementation of EFT as a model-independent framework to test gravity on cosmological scales. EFTCAMB has a built-in check for the fulfillment of general stability conditions such as the absence of ghost and superluminal propagation of perturbations. It handles phantom-divide crossing models and does not contain any quasi-static approximation, but rather evolves the full dynamics of perturbations on linear scales. As we showed, the latter is an important feature in view of the accuracy and scale range of upcoming surveys. We showed the reliability and applicability of our code by evolving the dynamics of linear perturbations and extracting predictions for power spectra in several models. In particular we performed a thorough analysis of $f(R)$ theories, comparing our outputs with those of an existing code for ΛCDM backgrounds, and finding an agreement that can reach 0.1% for models with a Compton wavelength consistent with current cosmological data. We then studied two different scenarios. First we produced new results for designer $f(R)$ models with a time-varying DE equation of state. Second, we extracted predictions for linear observables in some parametrized EFT models with a phantom-divide crossing equation of state for DE. In order to interface EFTCAMB with data we equipped it with EFTCosmoMC, the code implementation of EFT formalism in the CosmoMC code. Let us point out that the stability conditions required for a viable gravity theory, now become viability priors. To illustrate the use of these patches, we obtained constraints on parametrized *pure* EFT and designer $f(R)$ models, both on ΛCDM and wCDM background expansion histories, using data from *Planck* temperature and lensing potential spectra, WMAP low-ℓ polarization spectra, and BAO. Upon inspecting theoretical stability of the models on the given background, we find non-trivial parameter spaces that we translate into *viability priors*. We used different combinations of data sets to show their individual effects on cosmological and model parameters. Our data analysis results show that, depending on the adopted data sets, in the wCDM background case these *viability priors* could dominate the marginalized posterior distributions. Interestingly, with *Planck*+WP+BAO+lensing data, in $f(R)$ gravity models, we get very strong constraints on the constant DE equation of state, $w_0 \in (-1, -0.9997)$ (95%C.L.). Let us conclude with some remarks about future directions. We will gradually implement the *mapping* procedure for many other single scalar field DE/MG models which are of relevance for cosmological tests and perform parameter space exploration on some of these models. We will perform an analysis of viable parametrized EFT models based also on the findings of our dynamical analysis [396], as well as a thorough investigation of the validity of the QS approximation on sub-horizon scales for general models of DE/MG. Furthermore, more data sets will be added into EFTCosmoMC allowing to test gravity with the most recent data releases with a particular emphasis toward large scale structure observations in view of surveys such as Euclid [312]. Finally, an interesting development will be also to add some third order operators to study mildly non-linear scales.

Appendix A

Dependence of equations of motion in general covariant scalar-tensor theory

Consider a general covariant scalar-tensor theory of ϕ and $g_{\mu\nu}$, given by the action $S(\phi, g_{\mu\nu})$. The equations of motion for this system are

$$\mathcal{E} = \frac{1}{\sqrt{-g}}\frac{\delta S}{\delta \phi} = 0, \qquad \mathcal{E}_{\mu\nu} = \frac{1}{\sqrt{-g}}\frac{\delta S}{\delta g^{\mu\nu}} = 0, \tag{A.1}$$

with the variation of the action (modulo boundary terms) is given by

$$\delta S = \int \mathrm{d}x^D \sqrt{-g}\left(\mathcal{E}\delta\phi + \mathcal{E}_{\mu\nu}\delta g^{\mu\nu}\right). \tag{A.2}$$

Now, we assume this action is covariant, which means it is invariant under the following transformation ($\delta_\xi x^\mu = -\xi^\mu$)

$$\delta_\xi \phi = \mathcal{L}_\xi \phi = \xi^\mu \nabla_\mu \phi, \qquad \delta_\xi g^{\mu\nu} = \mathcal{L}_\xi g^{\mu\nu} = 2\nabla^{(\mu}\xi^{\nu)}. \tag{A.3}$$

That is, we have

$$\delta_\xi S = \int \mathrm{d}^D x \sqrt{-g}\left(\mathcal{E}\cdot\xi^\nu\nabla_\nu\phi + \mathcal{E}_{\mu\nu}\cdot 2\nabla^\mu\xi^\nu\right) = 0. \tag{A.4}$$

After integration by parts, we get $\int \mathrm{d}^D x\sqrt{-g}\xi^\nu\left(\mathcal{E}\nabla_\nu\phi + 2\nabla^\mu\mathcal{E}_{\mu\nu}\right) = 0$. Since ξ^ν is arbitrary, we have

$$\mathcal{E}\nabla_\nu\phi = 2\nabla^\mu\mathcal{E}_{\mu\nu}. \tag{A.5}$$

So if the Einstein equations are satisfied ($\mathcal{E}_{\mu\nu} = 0$), the scalar equation of motion is automatically satisfied ($\mathcal{E} = 0$).

Appendix B

Gradient expansion of the equations of motion in synchronous gauge

Here we list the Einstein tensor, the effective energy momentum tensor and the scalar current (the t component) up to order $\mathcal{O}(\epsilon^2)$ in the superhorizon gradient expansion. As in the main text, we suppress the background quantities' order indication $^{(0)}$. For example, $\dot{\phi}^{(0)}$ *is written as* $\dot{\phi}$

The quantities at the $\mathcal{O}(\epsilon^0)$ order:

$$G^{(0)}_{tt} = 3H^2, \tag{B.1}$$

$$G^{(0)}_{ti} = 0, \tag{B.2}$$

$$G^{(0)i}{}_{j} = -\delta^i_j \left(2\dot{H} + 3H^2\right), \tag{B.3}$$

$$T^{(0)}_{\phi}{}_{tt} = -K + 2K_X X + 6H\dot{\phi}G_X X, \tag{B.4}$$

$$T^{(0)}_{\phi}{}_{ti} = 0, \tag{B.5}$$

$$T^{(0)i}_{\phi}{}_{j} = K - 2G_X X\ddot{\phi}, \tag{B.6}$$

$$J^{t(0)} = K_X\dot{\phi} + 6HG_X X. \tag{B.7}$$

The quantities at the $\mathcal{O}(\epsilon)$ order:

$$G^{(1)}_{tt} = 6H\dot{\zeta}^{(1)}, \tag{B.8}$$

$$G^{(1)}_{ti} = \frac{2}{3}\nabla_i \mathcal{K}^{(0)} = 0, \tag{B.9}$$

$$G^{(1)i}{}_{j} = -2\left(\ddot{\zeta}^{(1)} + 3H\dot{\zeta}^{(1)}\right)\delta^i_j - \left(3HA^{(1)i}{}_{j} + \dot{A}^{(1)i}{}_{j}\right), \tag{B.10}$$

$$T^{(1)}_{\phi}{}_{tt} = \left(\dot{\phi}K_X + 2\dot{\phi}K_{XX}X + 18HG_X X + 12HG_{XX}X^2\right)\dot{\phi}^{(1)} + 6\dot{\phi}G_X X\dot{\zeta}^{(1)}, \tag{B.11}$$

$$T^{(1)}_{\phi}{}_{ti} = 0, \tag{B.12}$$

$$T^{(1)i}_{\phi}{}_{j} = \left[\left(\dot{\phi}K_X - 2\dot{X}(G_X + G_{XX}X)\right)\dot{\phi}^{(1)} - 2G_X X\ddot{\phi}^{(1)}\right]\delta^i_j, \tag{B.13}$$

$$J^{t(1)} = \left(K_X + 2K_{XX}X + 6H\dot{\phi}(G_X + G_{XX}X)\right)\dot{\phi}^{(1)} + 6G_X X\dot{\zeta}^{(1)}. \tag{B.14}$$

The quantities at the $\mathcal{O}(\epsilon^2)$ order:

$$G^{(2)}_{tt} = \frac{1}{2}\left({}^{[3]}R^{(2)} + 6\left(\dot{\zeta}^{(1)}\right)^2 + 12H\dot{\zeta}^{(2)} - A^{(1)}{}^k_l A^{(1)}{}^l_k\right), \tag{B.15}$$

$$G^{(2)}_{ti} = -2\bar{\nabla}_i\dot{\zeta}^{(1)} - \bar{\nabla}_k A^{(1)}{}^k_i, \tag{B.16}$$

$$\begin{aligned} G^{(2)}{}^i_j = {}& {}^{[3]}G^{(2)}{}^i_j - \dot{A}^{(2)}{}^i_j - 3HA^{(2)}{}^i_j - 3\dot{\zeta}^{(1)}A^{(1)}{}^i_j \\ & - \left(2\ddot{\zeta}^{(2)} + 6H\dot{\zeta}^{(2)} + 3\left(\dot{\zeta}^{(1)}\right)^2 + \frac{1}{2}A^{(1)}{}^k_l A^{(1)}{}^l_k\right)\delta^i_j, \end{aligned} \tag{B.17}$$

$$\begin{aligned} T^{(2)}_{\phi}{}_{tt} = {}& (\dot{\phi}K_X + 2\dot{\phi}K_{XX}X + 18HG_X X + 12HG_{XX}X^2)\dot{\phi}^{(2)} + 6\dot{\phi}G_X X\dot{\zeta}^{(2)} \\ & + \Big(\frac{1}{2}K_X + 4K_{XX}X + 2K_{XXX}X^2 + 9H\dot{\phi}G_X + 21H\dot{\phi}G_{XX}X \\ & + 6H\dot{\phi}G_{XXX}X^2\Big)\left(\dot{\phi}^{(1)}\right)^2 + (18G_X X + 12G_{XX}X^2)\dot{\zeta}^{(1)}\dot{\phi}^{(1)}, \end{aligned} \tag{B.18}$$

$$T^{(2)}_{\phi}{}_{ti} = (\dot{\phi}K_X + 6HG_X X)\partial_i\phi^{(1)} - 2G_X X\partial_i\dot{\phi}^{(1)}, \tag{B.19}$$

$$\begin{aligned} T^{(2)}_{\phi}{}^i_j = {}& \delta^i_j\Big[-2G_X X\ddot{\phi}^{(2)} + \left(\dot{\phi}K_X - 2\dot{X}(G_X + G_{XX}X)\right)\dot{\phi}^{(2)} \\ & - 2\dot{\phi}(G_X + G_{XX}X)\dot{\phi}^{(1)}\ddot{\phi}^{(1)} \\ & + \left(\frac{1}{2}K_X + K_{XX}X - \ddot{\phi}G_X - 5\ddot{\phi}G_{XX}X - 2\ddot{\phi}G_{XXX}X^2\right)\left(\dot{\phi}^{(1)}\right)^2\Big], \end{aligned} \tag{B.20}$$

$$\begin{aligned} J^{t(2)} = {}& 6G_X X\dot{\zeta}^{(2)} + \left(K_X + 2K_{XX}X + 6H\dot{\phi}G_X + 6H\dot{\phi}G_{XX}X\right)\dot{\phi}^{(2)} \\ & + \Big(\frac{3}{2}\dot{\phi}K_{XX} + \dot{\phi}K_{XXX}X + 3HG_X + 15HG_{XX}X \\ & + 6HG_{XXX}X^2\Big)\left(\dot{\phi}^{(1)}\right)^2 + \left(6\dot{\phi}G_X + 6\dot{\phi}G_{XX}X\right)\dot{\zeta}^{(1)}\dot{\phi}^{(1)}. \end{aligned} \tag{B.21}$$

Appendix C

EFT background Dynamical analysis

C.1 A complete second order analysis

In this Appendix we complete the analysis of the critical points of the second order system. In particular, all critical points (including those already discussed in Section 7.3.2) and their stability analysis are reported in Tabs. C.1-C.2; while in the following we present the eigenvalues and discuss the cosmology of the points that were not considered in Section 7.3.2.

- *Phantom DE points*
  From the splitting of the first order point P_4, we have two critical points characterized by a phantom effective equation of state:

$$P_{4a}: \quad \mu_1 = -6,\ \mu_2 = -5,\ \mu_3 = -3,\ \mu_4 = -2-\alpha_2,\ \mu_5 = -2-\lambda_0. \tag{C.1a}$$

$$P_{4b}: \quad \mu_1 = \frac{1}{2}(\alpha_2 - 4),\ \mu_2 = \alpha_2 - 4,\ \mu_3 = \alpha_2 - 3,\ \mu_4 = \alpha_2 + 2,\ \mu_5 = \alpha_2 - \lambda_0. \tag{C.1b}$$

  The first one has $w_{\rm eff} = -\frac{7}{3}$ and is a stable attractor for $\alpha_2 > -2 \wedge \lambda_0 > -2$, while the second one is an accelerated stable node for $\alpha_2 < \lambda_0 \wedge \alpha_2 < -2$ with $w_{\rm eff} < -\frac{7}{3}$. We do not consider these points viable as such values of $w_{\rm eff}$ have been already excluded by experiments (e.g. Refs. [21, 411]).

- *ϕ-MDE and ϕ-RDE points*
  There are two critical points characterized by, respectively, matter and radiation domination with a non-negligible DE density:

$$P_5: \qquad \mu_1 = -\frac{15}{2},\ \mu_2 = -3,\ \mu_3 = -1,\ \mu_4 = 3-\alpha_2,\ \mu_5 = 3-\lambda_0. \tag{C.2}$$

$$P_8: \qquad \mu_1 = -6,\ \mu_2 = -6,\ \mu_3 = 1,\ \mu_4 = -\frac{1}{2}-\alpha_2,\ \mu_5 = 4-\lambda_0. \tag{C.3}$$

  The first point has $\Omega_m = 5$, $\Omega_{\rm DE} = -4$ and a stiff matter equation of state, while the second one has $\Omega_r = 9$ and $\Omega_{\rm DE} = -8$ with $w_{\rm eff} = \frac{5}{3}$. Both these points are not considered cosmologically relevant.

Point	$[x_c, y_c, u_c, \alpha_{0,c}, \alpha_{1,c}]$	Stability	$\Omega_{\rm DE}$	$w_{\rm eff}$
P_{1a}	$[0,0,0,0,0]$	**Saddle point:** $\lambda_0 \neq 3 \wedge \alpha_2 \neq \frac{3}{2}$	0	0
P_{1b}	$\left[0,0,0,0,\alpha_2-\frac{3}{2}\right]$	**Saddle point:** $\lambda_0 \neq 3 \wedge \alpha_2 \neq \frac{3}{2} \wedge \alpha_2 \neq 3$	0	0
P_{2a}	$[1,0,0,0,0]$	**Unstable node:** $\alpha_2 < 3 \wedge \lambda_0 < 6$ **Saddle point:** otherwise	1	1
P_{2b}	$[1,0,0,0,-3+\alpha_2]$	**Unstable node:** $3 < \alpha_2 < 6 \wedge \lambda_0 < 6$ **Saddle point:** otherwise	1	1
P_{3a}	$\left[\frac{\lambda_0}{6}, 1-\frac{\lambda_0}{6}, 0, 0, 0\right]$	**Stable node:** $(\alpha_2 \geq 0 \wedge \lambda_0 < 0) \vee (\alpha_2 < 0 \wedge \lambda_0 < 2\alpha_2)$, **Unstable node:** $(\lambda_0 > 6 \wedge \alpha_2 < 3) \vee (\lambda_0 > 2\alpha_2 \wedge \alpha_2 \geq 3)$, **Saddle point:** otherwise	1	$\frac{1}{3}(\lambda_0 - 3)$
P_{3b}	$\left[\frac{\lambda_0}{6}, 1-\frac{\lambda_0}{6}, 0, 0, \alpha_2-\frac{\lambda_0}{2}\right]$	**Stable node:** $\alpha_2 < 0 \wedge 2\alpha_2 < \lambda_0 \wedge \lambda_0 < \alpha_2$, **Unstable node:** $(\alpha_2 \geq 6 \wedge \alpha_2 < \lambda_0 \wedge \lambda_0 < 2\alpha_2) \vee (\alpha_2 > 3 \wedge \lambda_0 > 6 \wedge \alpha_2 < 6 \wedge \lambda_0 < 2\alpha_2)$, **Saddle point:** otherwise	1	$\frac{1}{3}(\lambda_0 - 3)$
P_{4a}	$[-1,0,0,2,0]$	**Stable node:** $\alpha_2 > 2 \wedge \lambda_0 > -2$ **Saddle point:** otherwise	1	$-\frac{7}{3}$
P_{4b}	$\left[-1,0,0,2,1+\frac{\alpha_2}{2}\right]$	**Stable node:** $\alpha_2 < -2 \wedge \lambda_0 > \alpha_2$, **Unstable node:** $\alpha_2 > 4 \wedge \lambda_0 < \alpha_2$ **Saddle point:** otherwise	1	$\frac{1}{3}(-5 + \alpha_2)$

Table C.1: Hyperbolic critical points for the second order system with $\alpha_2, \lambda_0 =$ constant. Taking into account also the additional constraints $\Omega_{\rm m} \geq 0$ and $\Omega_{\rm r} \geq 0$, the domain for last two critical points is $\mathcal{D} \equiv \{\alpha_2 < 4, \lambda_0 \in \mathbb{R}\}$, while all other points have $\mathcal{D} \equiv \{\alpha_2, \lambda_0 \in \mathbb{R}\}$.

- P_9: *unstable DE point*

$$\mu_1 = \alpha_2 - 4,\ \mu_2 = \alpha_2 - 3,\ \mu_3 = \alpha_2 - \lambda_0,$$
$$\mu_4 = 6 - \frac{3}{4}\alpha_2 - \frac{1}{4}\sqrt{3}\sqrt{-\alpha_2(-32+5\alpha_2)},\ \mu_5 = 6 - \frac{3}{4}\alpha_2 + \frac{1}{4}\sqrt{3}\sqrt{-\alpha_2(-32+5\alpha_2)}. \tag{C.4}$$

Point	$[x_c, y_c, u_c, \alpha_{0,c}, \alpha_{1,c}]$	Stability	Ω_{DE}	w_{eff}
P_5	$[-1, 0, 0, -3, 0]$	**Stable node:** $\alpha_2 > 3 \wedge \lambda_0 > 3$, **Saddle point:** otherwise	-4	1
P_6	$\left[\frac{\lambda_0}{2}, 1 + \frac{\lambda_0}{2}, 0, -\lambda_0, 0\right]$	**See Fig. 7.6**	1	$-1 + \frac{2\lambda_0}{3}$
P_{7a}	$[0, 0, 1, 0, 0]$	**Saddle point:** $\lambda_0 \neq 4 \wedge \alpha_2 \neq \frac{3}{2}$	0	$\frac{1}{3}$
P_{7b}	$\left[0, 0, 1, 0, -\frac{3}{2} + \alpha_2 1\right]$	**Saddle point:** $\lambda_0 \neq 4 \wedge \alpha_2 \neq \frac{7}{2} \wedge \alpha_2 \neq \frac{3}{2}$	0	$\frac{1}{3}$
P_8	$[-4, 0, 9, -4, 0]$	**Saddle point:** $\lambda_0 \neq 4 \wedge \alpha_2 \neq -\frac{1}{2}$	-8	$\frac{5}{3}$
P_9	$[\alpha_2 - 5, 0, 0, 6 - \alpha_2, 3]$	**See Fig. 7.6**	1	$-3 + \frac{2\alpha_2}{3}$
P_{10}	$\left[-9 + 2\sqrt{8 - 2\alpha_2} + 2\alpha_2, 0, 8 - 2\alpha_2, 2 - 2\sqrt{8 - 2\alpha_2}, 3 - \sqrt{8 - 2\alpha_2}\right]$	**See Sec. 7.3.2**	$-7 + 2\alpha_2$	$\frac{1}{3}\left(-1 + 2\sqrt{8 - 2\alpha_2}\right)$
P_{11}	$\left[-9 - 2\sqrt{8 - 2\alpha_2} + 2\alpha_2, 0, 8 - 2\alpha_2, 2 + 2\sqrt{8 - 2\alpha_2}, 3 + \sqrt{8 - 2\alpha_2}\right]$	**See Appendix C.1**	$-7 + 2\alpha_2$	$\frac{1}{3}\left(-1 - 2\sqrt{8 - 2\alpha_2}\right)$

Table C.2: Hyperbolic critical points for the second order system with $\alpha_2, \lambda_0 =$ constant. Taking into account also the additional constraints $\Omega_{\text{m}} \geq 0$ and $\Omega_{\text{r}} \geq 0$, the domain for last two critical points is $\mathcal{D} \equiv \{\alpha_2 < 4, \lambda_0 \in \mathbb{R}\}$, while all other points have $\mathcal{D} \equiv \{\alpha_2, \lambda_0 \in \mathbb{R}\}$.

This point corresponds to a DE dominated configuration, albeit one that is always unstable.

- P_{11}: *radiation scaling point*
  The stability analysis of this point is too complicated to be reported, nevertheless we are able to deduce something about its cosmological behavior. From Tab. C.2 one can see that the point corresponds to a scaling solution for radiation and DE with $\Omega_{DE} = 2\alpha_2 - 7$. However, the constraint $\Omega_r \geq 0$ imposes $\alpha_2 < 4$, and for this range of values the point cannot be neither a proper DE or radiation dominated point.

C.2 N$^{\text{th}}$ order analysis

In this Appendix we continue with the analysis of the critical points for the N^{th} order system giving an overview of the points that were not presented in Section 7.3.3 since they either did not have the desired cosmological characteristics or stability. The general structure of the critical points for the N^{th} order system was explained in detail in Section 7.3.3, however here we will give a brief review. Critical points belonging to the same family can be of three types:

$(x_c, y_c, \alpha_{0,c}, \alpha_{1,c}, \alpha_{n,c} = 0)$ with $n \geq 2$, $(x_c, y_c, \alpha_{0,c}, \alpha_{1,c}, \alpha_{n,c} \neq 0)$ with $n \geq 2$ or $(x_c, y_c, \alpha_{0,c}, \alpha_{1,c}, \text{combinations})$, where 'combinations' correspond to all the different combinations of $\{\alpha_{2,c}, \ldots, \alpha_{N-1,c}\}$ for which a different A thorough description of how to build all the combinations is given in Section 7.3.3. Here we simply remind the reader that we use the index j for the $\alpha_{n,c}$ in non-zero blocks that are followed by a zero-block (rule (7.59)); while we use the index l for the $\alpha_{n,c}$ of the non-zero block that closes the combination, when it exists (rule (7.60)). Every time we substitute into Eq. (7.59) and Eq. (7.60) the specific value of $\dot{H}/H^2$ that corresponds to the point in consideration.

- *Phantom DE points:*
  There are different families of critical points which are DE dominated but give rise to cosmological behaviors which are in tension with current observations (i.e. $w_{\text{eff}} \lesssim -2$). However, their stable node configuration gives an attractor that, in principle, could be reached in the far future, provided that the duration of the matter era would remain long enough to allow for structure to form ([216] and references therein). The first family that we shall consider is P_{4a}-like, which is a set of DE dominated critical points with $w_{\text{eff}} = -\frac{7}{3}$.

$$P_{4a,1} \equiv (-1, 0, 2, 0, \alpha_{n,c} = 0), \tag{C.5a}$$

$$P_{4a,2} \equiv (-1, 0, 2, 0, \alpha_{n,c} = \alpha_N + 2(N - n)), \tag{C.5b}$$

$$P_{4a,c} \equiv (-1, 0, 2, 0, \text{combinations}),$$
$$\alpha_{j,c} = 2(s + 1 - j),\ \alpha_{l,c} = \alpha_N + 2(N - l). \tag{C.5c}$$

  From an investigation of the eigenvalues, one finds that the first point is a stable node for $\lambda_0 > -2$ while the second one exhibits this behavior for $\lambda_0 > -2 \wedge \alpha_N < -2\,(N - 2) \wedge \alpha_N > 3N - 8$. The last sub-family of critical points $P_{4a,c}$ also displays stable configurations for some combinations. In that case we have $\lambda_0 > -2 \wedge \alpha_N < -2$ and $\lambda_0 > -2 \wedge \alpha_N > -2$. The second family that we shall consider does not have a unique cosmological behavior, though in all the cases the critical points are DE dominated and resemble the P_{4b} point of the second order analysis.

$$P_{4b,1} \equiv (-1, 0, 2, 1, \alpha_{n,c} = 0), \tag{C.6a}$$

$$P_{4b,2} \equiv \left(-1, 0, 2, \frac{2N - 2 + \alpha_N}{N + 1}, \frac{-2n + 2N + n\,\alpha_N}{N}\right), \tag{C.6b}$$

$$P_{4b,c} \equiv \left(-1, 0, 2, \frac{2s_1}{1 + s_1}, \text{combinations}\right),$$
$$\alpha_{j,c} = \frac{2(s + 1 - j)}{s + 1},\ \alpha_{l,c} = \frac{\alpha_N + 2(N - l) + s\alpha_N}{s + 1}, \tag{C.6c}$$

  where s_1 is the value of s for the first non-zero block. The first critical point $P_{4b,1}$ has a well defined cosmology. It is a DE dominated point with a phantom equation of state, $w_{\text{eff}} = -\frac{5}{3}$, and it resembles the point P_{4b} of the second order with $\alpha_2 = 0$. We can infer its stability from Tab. C.1, which shows that it is a saddle, therefore it does not have the desired nature for a DE point and we do not analyze it further. The second critical point $P_{4b,2}$ can be written as

$$\left(-1, 0, 2, 1 + \frac{\alpha_{2,c}}{2}, \alpha_{n,c} = \frac{4 - 2n + n\alpha_{2,c}}{2}\right), \tag{C.7}$$

  where we have used the solution of α_2 to substitute for α_N in terms of $\alpha_{2,c}$; comparing it with Tab. C.1 we can see a clear connection with the P_{4b} critical

point. As expected the equation of state for the effective fluid equation can be written as

$$w_{\text{eff}} = \frac{-3N - 4 + 2\alpha_N}{3N} = -\frac{5 - \alpha_{2,c}}{3}, \tag{C.8}$$

which is equivalent to the one found at second order for the point P_{4b}, and shows an accelerated behavior for $\alpha_{2,c} < 4$. For this critical point is very difficult to calculate explicitly the eigenvalues but looking at Tab. C.1 we can infer that for $\alpha_2 < 4$ it will be a saddle, therefore we do not consider it cosmologically viable. In the latter case the critical points $P_{4b,c}$ has $w_{\text{eff}} = -\frac{7+3s}{3(s+1)}$, which for all the combinations is ≈ -1. The stability analysis, however, reveals that this is a set of saddle points, thus preventing them from being viable accelerated attractors.

The third family of DE dominated critical points is P_6-like with $w_{\text{eff}} = \frac{2}{3}\lambda_0 - 1$:

$$P_{6a} \equiv \left(\frac{\lambda_0}{2}, 1 + \frac{\lambda_0}{2}, -\lambda_0, 0, \alpha_{n,c} = 0\right), \tag{C.9a}$$

$$P_{6b} \equiv \left(\frac{\lambda_0}{2}, 1 + \frac{\lambda_0}{2}, -\lambda_0, 0, \alpha_{n,c} = \alpha_N - \lambda_0\ (N - n)\right), \tag{C.9b}$$

$$P_{6c} \equiv \left(\frac{\lambda_0}{2}, 1 + \frac{\lambda_0}{2}, -\lambda_0, 0, \text{combinations}\right),$$
$$\alpha_{j,c} = -(s + 1 - j)(3 + \lambda_0),\ \alpha_{l,c} = \alpha_N - (N - l)(3 + \lambda_0). \tag{C.9c}$$

The eigenvalues of the linearized system around these critical points are too complicated to be reported. However it can be shown that the first one is an accelerated attractor for $(-\frac{12}{5} < \alpha_N \leq -2 \wedge -\frac{12}{5} \leq \lambda_0 < \alpha_N) \vee (\alpha_N > -2 \wedge -\frac{12}{5} \leq \lambda_0 < -2)$ while the second one displays the same cosmological behavior for $(\alpha_N < \frac{1}{5}(24 - 12N) \wedge -\frac{12}{5} \leq \lambda_0 < -2) \vee (\alpha_N = \frac{1}{5}(24 - 12N) \wedge -\frac{12}{5} < \lambda_0 < -2) \vee (\frac{1}{5}(24 - 12N) < \alpha_N < 4 - 2N \wedge \frac{\alpha_N}{-2+N} < \lambda_0 < -2)$. Both these points, as well as P_{6c} have $w_{\text{eff}} < -2.3$, therefore we do not consider them cosmologically viable.

The last family of, P_9-like, DE dominated critical points contains configurations which all have a different effective equation of state.

$$P_{9a} \equiv (-5, 0, 6, 3, \alpha_{n,c} = 0), \tag{C.10a}$$

$$P_{9b} \equiv \left(\frac{-1 - 2N + \alpha_N}{(N-1)}, 0, \frac{3N - \alpha_N}{(N-1)}, 3, \frac{3N + n(\alpha_N - 3) - \alpha_N}{(N-1)}\right)$$
$$= (\alpha_2 - 5, 0, 6 - \alpha_2, 3, \alpha_{n,c} = 6 + n(\alpha_2 - 3) - \alpha_2), \tag{C.10b}$$

$$P_{9c} \equiv \left(-2 - \frac{3}{s_1}, 0, 3 + \frac{3}{s_1}, 3, \text{combinations}\right),$$
$$\alpha_{j,c} = \frac{3(s + 1 - j)}{s},\ \alpha_{l,c} = \frac{3(N - l) + s\alpha_N}{s}, \tag{C.10c}$$

where s_1 is the value of s for the first non-zero block. The equation of state parameter in these three configurations is, respectively:

$$w_{\text{eff}}(P_{9a}) = -3,\ w_{\text{eff}}(P_{9b}) = -\frac{3 + 3N - 2\alpha_N}{3\,(N-1)} = -3 + \frac{2}{3}\alpha_2,\ w_{\text{eff}}(P_{9c}) = -\frac{2 + s_1}{s_1}. \tag{C.11}$$

The stability analysis reveals that all the points of this family are saddles in the range for which they are accelerated and therefore we do not investigate them further.

- *Scaling solutions:*
  This family of critical points is characterized by a scaling between matter and DE:

$$P_{sc1} \equiv \Big(\frac{-3-6\,(N-1)^2+5\alpha_N-2\alpha_N^2+(N-1)\,(-9+7\alpha_N)}{3(N-2)^2}, 0, \frac{3N-2\alpha_N}{N-2}, \frac{3\,(N-1)-\alpha_N}{N-2}, \alpha_{n,c}=\frac{3N+n(-3+\alpha_N)-2\alpha_N}{N-2}\Big), \tag{C.12a}$$

$$P_{sc2} \equiv \left(-\frac{(s_1+1)(2s_1+1)}{(s_1-1)^2}, 0, \frac{3(s_1+1)}{s_1-1}, \frac{3s_1}{s_1-1}, \text{combinations} \right), \quad \alpha_{j,c}=\frac{3(s+1-j)}{s-1},\ \alpha_{l,c}=\frac{-\alpha_N+3(N-l)+s\alpha_N}{s-1}, \tag{C.12b}$$

  where s_1 is the value of s for the first non-zero block. These configurations correspond to a matter density and equation of state parameter:

$$\Omega_m(P_{sc1}) = -\frac{(4+N-2\alpha_N)(-3+\alpha_N)}{3(N-2)^2},\ w_{\text{eff}}(P_{sc1}) = \frac{3N-2\alpha_N}{6-3N}, \tag{C.13}$$

$$\Omega_m(P_{sc2}) = \frac{5+s_1}{(s_1-1)^2},\ w_{\text{eff}}(P_{sc2}) = \frac{s_1+1}{1-s_1}. \tag{C.14}$$

  The study of the stability for these critical points is very complicated due to the unknown value of N. It is, however, simple to determine that, for both points, neither of the two configurations in which they are, respectively, matter ($\Omega_m = 1$) and DE dominated ($\Omega_{\text{DE}} = 1$) is cosmologically viable.

  In this work we choose not to perform a full analysis of the scaling configurations, but rather focus on the two extrema for which either of the two components has fractional energy density equal to unity. While we leave a thorough investigation of the scaling regime for future work, we want to stress that this family of critical points is expected to display all the late-time scaling cosmologies that can offer a dynamical solution to the coincidence problem [101, 448, 449].

- *DE points:*
  The last family of critical points is made of DE dominated configurations

$$P_{d1} \equiv \Big(\frac{-2\alpha_N^2-\lambda_0(-3+(N-1)^2\,(\lambda_0+1)+(N-1)\,(\lambda_0+2))}{6(N-2)^2} + \frac{\alpha_N(-4+\lambda_0+(N-1)\,(4+3\lambda_0))}{6(N-2)^2}, \frac{(\alpha_N-3)(-2+2\alpha_N-\lambda_0)}{6(N-2)^2} + \frac{+(N-1)^2\,(6-5\lambda_0+\lambda_0^2)+(N-1)\,(-12+\alpha_N(8-3\lambda_0)+2\lambda_0+\lambda_0^2)}{6(N-2)^2}, \frac{\lambda_0+(N-1)\,\lambda_0-2\alpha_N}{N-2}, \frac{(N-1)\,\lambda_0-\alpha_N}{N-2}, \alpha_{n,c}=\frac{(n-2)\alpha_N+(N-n)\lambda_0}{N-2}\Big), \tag{C.15a}$$

$$P_{d2} \equiv \Big(-\frac{\lambda_0(-3+s_1^2(\lambda_0+1)+s_1(\lambda_0+2))}{6(s_1-1)^2}, \frac{3(2+\lambda_0)+s_1^2(6-5\lambda_0+\lambda_0^2)+s_1(-12+2\lambda_0+\lambda_0^2)}{6(s_1-1)^2}, \frac{\lambda_0(s_1+1)}{s_1-1}, \frac{s_1\lambda_0}{s_1-1}, \text{combinations}\Big),$$

$$\alpha_{j,c} = \frac{(s+1-j)\lambda_0}{s-1},\ \alpha_{l,c} = \frac{\alpha_N(s-1)+(N-l)\lambda_0}{s-1}, \tag{C.15b}$$

with different values of the equation of state, respectively

$$w_{\text{eff}}(P_{d1}) = \frac{6-3N+2\alpha_N-2\lambda_0}{3(N-2)}\,, \quad w_{\text{eff}}(P_{d2}) = \frac{3-3s_1-2\lambda_0}{3(s_1-1)}, \tag{C.16}$$

where s_1 is the value of s for the first non-zero block. The first point has a viable cosmological behavior for $\alpha_N < N-2+\lambda_0$ and would have $w_{\text{eff}} = -1$ if $\lambda_0 = \alpha_N$; however we are not able to analyze its stability. The second point gives a viable cosmological behavior for $s_1 + \lambda_0 > 1$; however requiring $w_{\text{eff}} = -1$ gives $\lambda_0 = 0$ and the stability analysis reveals that the point is non-hyperbolic for such a value.

- *ϕ-MDE:*
  This family contains the following P_5-like:

$$P_{5a} \equiv (-1, 0, -3, 0, \alpha_{n,c} = 0), \tag{C.17a}$$

$$P_{5b} \equiv (-1, 0, -3, 0, \alpha_{n,c} = \alpha_N - 3(N-n)), \tag{C.17b}$$

$$P_{5c} \equiv (-1, 0, -3, 0, \text{combinations}),\ \alpha_{j,c} = -3(s+1-j),\ \alpha_{l,c} = \alpha_N - 3(N-l), \tag{C.17c}$$

  which are characterized by $\Omega_m = 5$, $\Omega_{\text{DE}} = -4$ and $w_{\text{eff}} = 1$, therefore we do not consider them further.

Appendix D

EFT: Contributions to the perturbative equations from second order operators

In what follows we list the contributions to the linearly perturbed equations of Section 7.4.2 from the second order operators in (7.4). Let us make an itemized list where for each operator we list its contributions to the r.h.s. of Eq. (7.72) by Δ_{00}, to the r.h.s. of Eq. (7.73) by Δ_{0i}, to the r.h.s. of Eq. (7.74) by $\Delta_{ij,i\neq j}$, to the r.h.s of Eq. (7.75) by Δ_{ii} and to the l.h.s. of Eq. (7.76) by Δ_π. Notice that in order to perform a correct stability analysis on the equation for π, along the lines of Section 7.4.3, it is important to demix the degrees of freedom; specifically, *once the contributions from all operators have been taken into account*, one needs to use the Einstein equations to substitute for any $\ddot{h}, \eta, \sigma_*$ appearing in the final form of the equation for π.

$\underline{(\delta g^{00})^2}$:

$$\begin{aligned}
&\Delta_{00} = -\frac{2M_2^4 a^2}{m_0^2(1+\Omega)}\left(\dot\pi + \mathcal{H}\pi\right) ,\\
&\Delta_{0i} = 0 ,\\
&\Delta_{ij,i\neq j} = 0 ,\\
&\Delta_{ii} = 0 ,\\
&\Delta_\pi = 2M_2^4\left[\ddot\pi + 4\left(\mathcal{H} + \frac{\dot M_2}{M_2}\right)\dot\pi + \left(3\mathcal{H}^2 + \dot{\mathcal{H}} + 4\frac{\mathcal{H}\dot M_2}{M_2}\right)\pi\right] .
\end{aligned} \tag{D.1}$$

$\underline{\delta g^{00}\delta\mathcal{K}^\mu_\mu}$:

$$\begin{aligned}
&\Delta_{00} = \frac{a\bar M_1^3}{2m_0^2(1+\Omega)}\left[k\mathcal{Z} - 3\left(\dot{\mathcal{H}} - 2\mathcal{H}^2 - \frac{k^2}{3}\right)\pi + 3\mathcal{H}\dot\pi\right] ,\\
&\Delta_{0i} = \frac{a\bar M_1^3 k}{m_0^2(1+\Omega)}\left(\dot\pi + \mathcal{H}\pi\right) ,
\end{aligned}$$

$$
\begin{aligned}
&\Delta_{ij,i\neq j} = 0\,,\\
&\Delta_{ii} = -\frac{3a\bar{M}_1^3}{m_0^2(1+\Omega)}\left[\ddot{\pi} + \left(4\mathcal{H} + 3\frac{\dot{\bar{M}}_1}{\bar{M}_1}\right)\dot{\pi} + \left(3\mathcal{H}^2 + \dot{\mathcal{H}} + 3\frac{\mathcal{H}\dot{\bar{M}}_1}{\bar{M}_1}\right)\pi\right],\\
&\Delta_\pi = \frac{\bar{M}_1^3}{2a}\left[\left(3\mathcal{H} + 3\frac{\dot{\bar{M}}_1}{\bar{M}_1}\right)\left(-k\mathcal{Z} + 3(\dot{\mathcal{H}} - \mathcal{H}^2)\pi - k^2\pi\right) - \frac{\ddot{h}}{2}\right.\\
&\qquad\left. + \mathcal{H}k\mathcal{Z} + 2\mathcal{H}k^2\pi + 3(\ddot{\mathcal{H}} - 4\mathcal{H}\dot{\mathcal{H}} + 2\mathcal{H}^3)\pi\right].
\end{aligned}
\tag{D.2}
$$

$\underline{(\delta\mathcal{K})^2}$:

$$
\begin{aligned}
&\Delta_{00} = \frac{3\mathcal{H}\bar{M}_2^2}{2m_0^2(1+\Omega)}\left[k\mathcal{Z} - 3(\dot{\mathcal{H}} - \mathcal{H}^2)\pi + k^2\pi\right],\\
&\Delta_{0i} = \frac{\bar{M}_2^2 k}{m_0^2(1+\Omega)}\left[k\mathcal{Z} - 3(\dot{\mathcal{H}} - \mathcal{H}^2)\pi + k^2\pi\right],\\
&\Delta_{ij,i\neq j} = 0\,,\\
&\Delta_{ii} = -\frac{3\bar{M}_2^2}{m_0^2(1+\Omega)}\left(2\mathcal{H} + \partial_\tau + 2\frac{\dot{\bar{M}}_2}{\bar{M}_2}\right)\left[k\mathcal{Z} - 3(\dot{\mathcal{H}} - \mathcal{H}^2)\pi + k^2\pi\right],\\
&\Delta_\pi = \frac{\bar{M}_2^2}{2a^2}\left(3(\dot{\mathcal{H}} - \mathcal{H}^2) - k^2\right)\left[-k\mathcal{Z} + 3(\dot{\mathcal{H}} - \mathcal{H}^2)\pi - k^2\pi\right].
\end{aligned}
\tag{D.3}
$$

$\underline{\delta\mathcal{K}^\mu_\nu\delta\mathcal{K}^\nu_\mu}$:

$$
\begin{aligned}
&\Delta_{00} = \frac{\mathcal{H}\bar{M}_3^2}{m_0^2(1+\Omega)}\left[k\mathcal{Z} - 3\left(\dot{\mathcal{H}} - \mathcal{H}^2 - \frac{k^2}{3}\right)\pi\right],\\
&\Delta_{0i} = \frac{\bar{M}_3^2 k}{m_0^2(1+\Omega)}\left[\frac{k\mathcal{Z}}{3} + \frac{2}{3}k\sigma_* - (\dot{\mathcal{H}} - \mathcal{H}^2 - k^2)\pi\right],\\
&\Delta_{ij,i\neq j} = \frac{\bar{M}_3^2}{m_0^2(1+\Omega)}\left(2\mathcal{H} + 2\frac{\dot{\bar{M}}_3}{\bar{M}_3} + \partial_\tau\right)\left(k\sigma_* + k^2\pi\right),\\
&\Delta_{ii} = \frac{\bar{M}_3^2}{m_0^2(1+\Omega)}\left(2\mathcal{H} + 2\frac{\dot{\bar{M}}_3}{\bar{M}_3} + \partial_\tau\right)\left[-k\mathcal{Z} + 3\left(\dot{\mathcal{H}} - \mathcal{H}^2 - \frac{1}{3}k^2\right)\pi\right],\\
&\Delta_\pi = \frac{\bar{M}_3^2}{a^2}\left[\left(\frac{k^4}{2} - k^2(\dot{\mathcal{H}} - \mathcal{H}^2)\right.\right.\\
&\qquad\left.\left. + \frac{3}{2}(\dot{\mathcal{H}} - \mathcal{H}^2)^2\right)\pi + \left(\frac{k^2}{2} - \frac{\dot{\mathcal{H}} - \mathcal{H}^2}{2}\right)k\mathcal{Z} + \frac{k^3}{3}(\sigma_* - \mathcal{Z})\right].
\end{aligned}
\tag{D.4}
$$

$\underline{\delta g^{00}\delta R^{(3)}}$:

$$
\begin{aligned}
&\Delta_{00} = -\frac{2\hat{M}^2}{m_0^2(1+\Omega)}k^2\left(\eta + \mathcal{H}\pi\right),\\
&\Delta_{0i} = 0\,,\\
&\Delta_{ij,i\neq j} = 2\frac{\hat{M}^2}{m_0^2(1+\Omega)}k^2\left(\dot{\pi} + \mathcal{H}\pi\right),\\
&\Delta_{ii} = \frac{4\hat{M}^2}{m_0^2(1+\Omega)}k^2\left(\dot{\pi} + \mathcal{H}\pi\right),\\
&\Delta_\pi = \frac{2k^2}{a^2}\left[\hat{M}^2\frac{k}{3}(\sigma_* - \mathcal{Z}) + \left(\mathcal{H}\hat{M}^2 + 2\hat{M}\dot{\hat{M}}\right)\eta + \left(2\mathcal{H}\hat{M}\dot{\hat{M}} + \dot{\mathcal{H}}\hat{M}^2\right)\pi\right].
\end{aligned}
\tag{D.5}
$$

$\underline{(\mathrm{g}^{\mu\nu} + \mathrm{n}^{\mu}\mathrm{n}^{\nu})\partial_{\mu}\delta\mathrm{g}^{00}\partial_{\nu}\delta\mathrm{g}^{00}}$:

$$
\begin{aligned}
&\Delta_{00} = -\frac{4m_2^2}{m_0^2(1+\Omega)}k^2\left(\dot{\pi} + \mathcal{H}\pi\right) , \\
&\Delta_{0i} = 0 , \\
&\Delta_{ij,i\neq j} = 0 , \\
&\Delta_{ii} = 0 , \\
&\Delta_{\pi} = 4m_2^2\left(2\mathcal{H} + \frac{\dot{m}_2}{m_2} + \partial_{\tau}\right)k^2\left(\dot{\pi} + \mathcal{H}\pi\right) .
\end{aligned}
\tag{D.6}
$$

Acknowledgments

First, I would like to thank my Supervisors T. P. Sotiriou, R. K. Sheth and A. Silvestri, who provided for my scientific growth during these years. In particular, I would like to thank Thomas who helped and encouraged me in finding my way, making me stronger and more secure. I am particularly grateful to Alessandra for useful conversations and invaluable advice. It was a pleasure working with you and I am sure that in the future it will be even more fruitful and interesting.

I am grateful to my thesis examiners, Pedro G. Ferreira and Kazuya Koyama, for accepting the review of my thesis.

I am very grateful to my collaborators Paolo Salucci, Jhon M. Cannon, Ed C. Elson, Bin Hu, Shuang Y. Zhou, Marco Raveri and Daniele Vernieri, for their help, support and for interesting discussions. I enjoyed working with you.

I would like to thank C. Baccigalupi, J. Bloomfield, M. Calabrese, P. Creminelli, G. Gentile, T. Grava, L. Heltai, T. Kobayashi, S. Liberati, S. Luzzatto, M. Martinelli, A. Mohd, S. Mukohyama, M. Musso, A. Paranjape, F. Piazza, L. Pogosian, P. Saffin, R. Scoccimarro, R. Valdarnini and G.-B. Zhao for fruitful conversations.

To Daniele for his loving patience during these long four years and for all the moments we spent together.

Let me thank my office mates Xiaoting and Marco with whom I spent everyday life during this last year. In particular Marco, for scientific collaborations and mostly for his color schemes, which have made my thesis more colorful.

Thanks to Claudia M. for her Christmas gift, it is a great anti-stress and you know, we need it !

To Gianluca, Eolo, Claudia and Juan Manuel, travel friends, good scientists and loving people. In particular, thanks to Eolo because with his anecdotes, and his knowledge of the best patisseries in Trieste, makes my stay more enjoyable and tasty. His descriptions of the desserts were enough to make me fat.

I thank all the people I met in SISSA, colleagues, friends, staff, who make my life in SISSA very enjoyable.

Finally, thanks to my family for being always present with their support and love.

Bibliography

[1] F.W. Dyson, A.S. Eddington, C.R. Davidson, Phil. Trans. Roy. Soc. A 220 (571-581), 291333 (1920).

[2] T. Damour, *"On Einsteins Path"*, Springer New York, pp 171-187 (1999).

[3] K. Schwarzschild, Sitzungsber. Preuss. Akad. D. Wiss., 189196 (1916).

[4] K. Schwarzschild, Sitzungsber. Preuss. Akad. D. Wiss., 424434 (1916).

[5] H. Reissner, Annalen der Physik 355 (9), 106120 (1916).

[6] G. Nordström, Verhandl. Koninkl. Ned. Akad. Wetenschap., 26, 12381245 (1918).

[7] J. R. Oppenheimer and H. Snyder, Physical Review, vol. 56, Issue 5, pp. 455-459 (1939).

[8] M. Ostrogradski, Mem. Ac. St. Peterbourg **VI 4**, 385 (1850)

[9] E. Cartan, Jour. de Math. **1**, 141 (1922).

[10] H. Weyl, *"Space-Time-Matter"*, Dover Publications, New York (1922).

[11] H. Vermeil, Nachr. Ges. Wiss. Göttingen, 334 (1917)

[12] D. Lovelock, J. Math. Phys. **12**, 498 (1971).

[13] D. Lovelock, J. Math. Phys. **13**, 874 (1972).

[14] T. Clifton, P. G. Ferreira, A. Padilla and C. Skordis, Phys. Rept. **513**, 1 (2012) [arXiv:1106.2476 [astro-ph.CO]].

[15] A. Joyce, B. Jain, J. Khoury and M. Trodden, arXiv:1407.0059 [astro-ph.CO].

[16] H. Ruegg and M. Ruiz-Altaba, Int. J. Mod. Phys. A **19**, 3265 (2004) [hep-th/0304245].

[17] E. Hubble and M. L. Humason, Astrophys. J. **74**, 43 (1931).

[18] A. G. Riess *et al.* [Supernova Search Team Collaboration], Astron. J. **116**, 1009 (1998).

[19] S. Perlmutter *et al.* [Supernova Cosmology Project Collaboration], Astrophys. J. **517**, 565 (1999).

[20] P. A. R. Ade *et al.* [Planck Collaboration], arXiv:1303.5062 [astro-ph.CO].

[21] P. A. R. Ade *et al.* [Planck Collaboration], arXiv:1303.5076 [astro-ph.CO].

[22] http://www.sdss.org/

[23] http://www2.aao.gov.au/ TDFgg/

[24] E. A. Milne, "*Relativity, Gravitation and World Structure*", Oxford: Clarendon Press, 1935.

[25] http://map.gsfc.nasa.gov/

[26] N. Suzuki, D. Rubin, C. Lidman, G. Aldering, R. Amanullah, K. Barbary, L. F. Barrientos and J. Botyanszki *et al.*, Astrophys. J. **746**, 85 (2012) [arXiv:1105.3470 [astro-ph.CO]].

[27] G. Hinshaw *et al.* [WMAP Collaboration], Astrophys. J. Suppl. **208**, 19 (2013) [arXiv:1212.5226 [astro-ph.CO]].

[28] H. Kodama and M. Sasaki, Prog. Theor. Phys. Suppl. **78**, 1 (1984).

[29] E. Aver, K. A. Olive and E. D. Skillman, JCAP **1204**, 004 (2012) [arXiv:1112.3713 [astro-ph.CO]].

[30] M. Pettini and R. Cooke, Mon. Not. Roy. Astron. Soc. **425**, 2477 (2012) [arXiv:1205.3785 [astro-ph.CO]].

[31] F. Iocco, G. Mangano, G. Miele, O. Pisanti and P. D. Serpico, Phys. Rept. **472**, 1 (2009) [arXiv:0809.0631 [astro-ph]].

[32] V. Springel, S. D. M. White, A. Jenkins, C. S. Frenk, N. Yoshida, L. Gao, J. Navarro and R. Thacker *et al.*, Nature **435**, 629 (2005) [astro-ph/0504097].

[33] http://supernova.lbl.gov/Union/

[34] http://sci.esa.int/planck

[35] W. J. Percival *et al.* [SDSS Collaboration], Mon. Not. Roy. Astron. Soc. **401** (2010) 2148 [arXiv:0907.1660 [astro-ph.CO]].

[36] C. Blake, E. Kazin, F. Beutler, T. Davis, D. Parkinson, S. Brough, M. Colless and C. Contreras *et al.*, Mon. Not. Roy. Astron. Soc. **418**, 1707 (2011) [arXiv:1108.2635 [astro-ph.CO]].

[37] N. Padmanabhan, X. Xu, D. J. Eisenstein, R. Scalzo, A. J. Cuesta, K. T. Mehta and E. Kazin, Mon. Not. Roy. Astron. Soc. **427**, no. 3, 2132 (2012) [arXiv:1202.0090 [astro-ph.CO]].

[38] L. Anderson, E. Aubourg, S. Bailey, D. Bizyaev, M. Blanton, A. S. Bolton, J. Brinkmann and J. R. Brownstein *et al.*, Mon. Not. Roy. Astron. Soc. **427**, no. 4, 3435 (2013) [arXiv:1203.6594 [astro-ph.CO]].

[39] A. Conley *et al.* [SNLS Collaboration], Astrophys. J. Suppl. **192**, 1 (2011) [arXiv:1104.1443 [astro-ph.CO]].

[40] A. G. Riess, L. Macri, S. Casertano, H. Lampeitl, H. C. Ferguson, A. V. Filippenko, S. W. Jha and W. Li *et al.*, Astrophys. J. **730**, 119 (2011) [Erratum-ibid. **732**, 129 (2011)] [arXiv:1103.2976 [astro-ph.CO]].

[41] J. L. Sievers *et al.* [Atacama Cosmology Telescope Collaboration], JCAP **1310**, 060 (2013) [arXiv:1301.0824 [astro-ph.CO]].

[42] A. van Engelen, R. Keisler, O. Zahn, K. A. Aird, B. A. Benson, L. E. Bleem, J. E. Carlstrom and C. L. Chang *et al.*, Astrophys. J. **756**, 142 (2012) [arXiv:1202.0546 [astro-ph.CO]].

[43] http://science.nasa.gov/missions/cobe/

[44] S. Dodelson, *"Modern Cosmology"*, Academic Press, an Imprint of Elsevier, San Diego California (USA), 2003.

[45] J. Martin, C. Ringeval and V. Vennin, Phys. Dark Univ. (2014) [arXiv:1303.3787 [astro-ph.CO]].

[46] J. Martin, C. Ringeval, R. Trotta and V. Vennin, JCAP **1403**, 039 (2014) [arXiv:1312.3529 [astro-ph.CO]].

[47] P. A. R. Ade *et al.* [Planck Collaboration], arXiv:1303.5082 [astro-ph.CO].

[48] L. F. Abbott, E. Farhi and M. B. Wise, Phys. Lett. B **117**, 29 (1982).

[49] A. Albrecht, P. J. Steinhardt, M. S. Turner and F. Wilczek, Phys. Rev. Lett. **48**, 1437 (1982).

[50] Y. Shtanov, J. H. Traschen and R. H. Brandenberger, Phys. Rev. D **51**, 5438 (1995) [hep-ph/9407247].

[51] L. Kofman, A. D. Linde and A. A. Starobinsky, Phys. Rev. Lett. **73**, 3195 (1994) [hep-th/9405187].

[52] L. Kofman, A. D. Linde and A. A. Starobinsky, Phys. Rev. D **56**, 3258 (1997) [hep-ph/9704452].

[53] A. H. Guth, Phys. Rev. D **23**, 347 (1981).

[54] A. D. Linde, Phys. Lett. B **108**, 389 (1982).

[55] A. Linde, *"Particle Physics and Inflationary Cosmology"*, Harwood Academic Publishers, Switzerland, 1990.

[56] E. W. Kold and M. S. Turner, *"The Early Universe"*, Addison-Wesley, California, 1990.

[57] P. J. E. Peebles, *"Principles of Physical Cosmology"*, Princeton University Press, Princeton, 1993.

[58] D. H. Lyth, hep-th/0311040.

[59] V. Mukhanov, *"Physical Foundations of Cosmology"*, Cambridge University Press, Cambridge, 2005.

[60] J.P. Preskill, Phys. Rev. Lett, 43 (1979), p. 1365.

[61] M.B. Einhorn, D.L. Stein, D. Toussaint Phys. Rev., **D** 21 (1980), p. 3295.

[62] A.H. Guth, S.-H.H. Tye, Phys. Rev. Lett., 44 (1980), p. 631.

[63] A.H. Guth, S.-H.H. Tye, Phys. Rev. Lett., 44 (1980), p. 963.

[64] M. B. Einhorn, K. Sato, Nuclear Physics B, 180 (1981), p. 385.

[65] E. R. Harrison, Phys. Rev. D **1**, 2726 (1970).

[66] C. G. Wynn-Williams, E. E. Becklin and G. Neugebauer, Mon. Not. Roy. Astron. Soc. **160**, 1 (1972).

[67] P. J. E. Peebles and J. T. Yu, Astrophys. J. **162**, 815 (1970).

[68] F. Lucchin and S. Matarrese, Phys. Rev. D **32**, 1316 (1985).

[69] J. D. Barrow, Phys. Lett. B **235**, 40 (1990).

[70] L. McAllister, E. Silverstein and A. Westphal, Phys. Rev. D **82**, 046003 (2010) [arXiv:0808.0706 [hep-th]].

[71] N. Bartolo, S. Matarrese and A. Riotto, Phys. Rev. D **65**, 103505 (2002) [hep-ph/0112261].

[72] F. Bernardeau and J. -P. Uzan, Phys. Rev. D **66**, 103506 (2002) [hep-ph/0207295].

[73] F. Vernizzi and D. Wands, JCAP **0605**, 019 (2006) [astro-ph/0603799].

[74] G. I. Rigopoulos, E. P. S. Shellard and B. J. W. van Tent, Phys. Rev. D **73**, 083522 (2006) [astro-ph/0506704].

[75] A. D. Linde and V. F. Mukhanov, Phys. Rev. D **56**, 535 (1997) [astro-ph/9610219].

[76] D. H. Lyth and D. Wands, Phys. Lett. B **524**, 5 (2002) [hep-ph/0110002].

[77] D. H. Lyth, C. Ungarelli and D. Wands, Phys. Rev. D **67**, 023503 (2003) [astro-ph/0208055].

[78] X. Chen, R. Easther and E. A. Lim, JCAP **0706**, 023 (2007) [astro-ph/0611645].

[79] C. Armendariz-Picon, T. Damour and V. F. Mukhanov, *k - inflation, Phys. Lett. B* **458**, 209 (1999) [hep-th/9904075].

[80] C. Cheung, P. Creminelli, A. L. Fitzpatrick, J. Kaplan and L. Senatore, JHEP **0803**, 014 (2008) [arXiv:0709.0293 [hep-th]].

[81] N. Bartolo, M. Fasiello, S. Matarrese and A. Riotto, JCAP **1008**, 008 (2010) [arXiv:1004.0893 [astro-ph.CO]].

[82] L. Senatore, K. M. Smith and M. Zaldarriaga, JCAP **1001**, 028 (2010) [arXiv:0905.3746 [astro-ph.CO]].

[83] P. A. R. Ade *et al.* [Planck Collaboration], arXiv:1303.5084 [astro-ph.CO].

[84] http://www.cfa.harvard.edu/CMB/bicep2/

[85] P. A. R. Ade *et al.* [BICEP2 Collaboration], Phys. Rev. Lett. **112**, 241101 (2014) [arXiv:1403.3985 [astro-ph.CO]].

[86] S. Tsujikawa, Class. Quant. Grav. **30**, 214003 (2013) [arXiv:1304.1961 [gr-qc]].

[87] Y. B. Zeldovich, Sov. Phys. JETP Lett. 6 (1967) 3167.

[88] S. Weinberg, Rev. Mod. Phys. 61 (1989), p. 123.

[89] S. Weinberg, Phys. Rev. Lett. 59 (1987), p. 2607.

[90] D. K. Hazra, S. Majumdar, S. Pal, S. Panda and A. A. Sen, arXiv:1310.6161 [astro-ph.CO].

[91] M. Chevallier and D. Polarski, Int. J. Mod. Phys. D **10**, 213 (2001), [gr-qc/0009008].

[92] E. V. Linder, Phys. Rev. Lett. **90**, 091301 (2003), [astro-ph/0208512].

[93] http://cfht.hawaii.edu/SNLS/

[94] Y. Fujii, Phys. Rev. D **26**, 2580 (1982).

[95] L. H. Ford, Phys. Rev. D **35**, 2339 (1987).

[96] C. Wetterich, Nucl. Phys. B **302**, 668 (1988).

[97] B. Ratra and P. J. E. Peebles, Phys. Rev. D **37**, 3406 (1988).

[98] T. Chiba, N. Sugiyama and T. Nakamura, Mon. Not. Roy. Astron. Soc. **289**, L5 (1997) [astro-ph/9704199].

[99] P. G. Ferreira and M. Joyce, Phys. Rev. Lett. **79**, 4740 (1997) [astro-ph/9707286].

[100] P. G. Ferreira and M. Joyce, Phys. Rev. D **58**, 023503 (1998) [astro-ph/9711102].

[101] E. J. Copeland, A. RLiddle and D. Wands, Phys. Rev. D **57**, 4686 (1998) [gr-qc/9711068].

[102] R. R. Caldwell, R. Dave and P. J. Steinhardt, Phys. Rev. Lett. **80**, 1582 (1998) [astro-ph/9708069].

[103] I. Zlatev, L. -M. Wang and P. J. Steinhardt, Phys. Rev. Lett. **82**, 896 (1999) [astro-ph/9807002].

[104] C. Armendariz-Picon, V. F. Mukhanov and P. J. Steinhardt, Phys. Rev. Lett. **85**, 4438 (2000) [astro-ph/0004134].

[105] A. Melchiorri, L. Mersini-Houghton, C. J. Odman and M. Trodden, Phys. Rev. D **68**, 043509 (2003) [astro-ph/0211522].

[106] J. S. Bagla, H. K. Jassal and T. Padmanabhan, Phys. Rev. D **67**, 063504 (2003), [astro-ph/0212198].

[107] R. R. Caldwell and E. V. Linder, Phys. Rev. Lett. **95**, 141301 (2005) [astro-ph/0505494].

[108] S. M. Carroll, Living Rev. Rel. **4**, 1 (2001) [astro-ph/0004075].

[109] C. P. Burgess, astro-ph/0207174.

[110] P. J. Steinhardt, L. M. Wang and I. Zlatev, Phys. Rev. D **59**, 123504 (1999) [astro-ph/9812313].

[111] E. V. Linder and D. Huterer, Phys. Rev. D **72**, 043509 (2005) [astro-ph/0505330].

[112] F. Zwicky, Helv. Phys. Acta **6**, 110 (1933).

[113] E. Battaner and E. Florido, Fund. Cosmic Phys. **21**, 1 (2000) [astro-ph/0010475].

[114] K. C. Freeman,Astrophys. J. 160, 881 (1970)

[115] V. C. Rubin, W. K. Ford and N. Thonnard, Astrophys. J. 238, 471 (1980)

[116] A. Bosma, Astron. J. 86, 1791 (1981)

[117] A. Bosma, Astron. J. 86, 1825 (1981)

[118] R. Massey, T. Kitching and J. Richard, Rept. Prog. Phys. **73**, 086901 (2010) [arXiv:1001.1739 [astro-ph.CO]].

[119] G. Bertone and D. Merritt, Mod. Phys. Lett. A **20**, 1021 (2005) [astro-ph/0504422].

[120] M. Aguilar *et al.* [AMS Collaboration], Phys. Rev. Lett. **110**, 141102 (2013).

[121] P. Beltrame [XENON Collaboration], arXiv:1305.2719 [astro-ph.CO].

[122] J. F. Navarro, C. S. Frenk and S. D. M. White, Astrophys. J. **490**, 493 (1997) [astro-ph/9611107].

[123] G. Gentile, A. Burkert, P. Salucci, U. Klein and F. Walter, Astrophys. J. , **634**, 2, L145, (2005) [astro-ph/0506538].

[124] A. Burkert, IAU Symp. **171**, 175 (1996) [Astrophys. J. **447**, L25 (1995)] [astro-ph/9504041].

[125] A. Borriello and P. Salucci, Mon. Not. Roy. Astron. Soc. **323**, 285 (2001) [astro-ph/0001082].

[126] van den Bosch F. C. & Swaters R. A., 2001, MNRAS, 325, 3, 1017

[127] E. de Blok,S. McGaugh, V. C. Rubin, Astrophys. J. **122**, 2396 (2001).

[128] D. Weldrake, E. de Blok and F. Walter, Mon. Not. Roy. Astron. Soc. **340**, 12 (2003) [astro-ph/0210568].

[129] G. Gentile, P. Salucci, U. Klein, D. Vergani and P. Kalberla, Mon. Not. Roy. Astron. Soc. **351**, 903 (2004) [astro-ph/0403154].

[130] J. D. Simon, A. D. Bolatto, A. Leroy, L. Blitz and E. L. Gates, Astrophys. J. **621**, 757 (2005) [astro-ph/0412035].

[131] S. H. Oh, W. J. G. de Blok, F. Walter, E. Brinks and R. C. Kennicutt, Jr, AJ **136**, 6, 2761 (2008) [arXiv:0810.2119 [astro-ph]].

[132] F. Governato, A. Zolotov, A. Pontzen, C. Christensen, S. H. Oh, A. M. Brooks, T. Quinn and S. Shen *et al.*, Mon. Not. Roy. Astron. Soc. **422**, 1231 (2012) [arXiv:1202.0554 [astro-ph.CO]].

[133] P. Madau, S. Shen and F. Governato, Astrophys. J. **789**, L17 (2014) [arXiv:1405.2577 [astro-ph.GA]].

[134] B. Moore, S. Ghigna, F. Governato, G. Lake, T. R. Quinn, J. Stadel and P. Tozzi, Astrophys. J. **524**, L19 (1999) [astro-ph/9907411].

[135] A. A. Klypin, A. V. Kravtsov, O. Valenzuela and F. Prada, Astrophys. J. **522**, 82 (1999) [astro-ph/9901240].

[136] L. L. Watkins, N. W. Evans, V. Belokurov, M. C. Smith, P. C. Hewett, D. M. Bramich, G. F. Gilmore and M. J. Irwin *et al.*, Mon. Not. Roy. Astron. Soc. **398**, 1757 (2009) [arXiv:0906.0498 [astro-ph.GA]].

[137] V. Belokurov, M. G. Walker, N. W. Evans, G. Gilmore, M. J. Irwin, D. Just, S. Koposov and M. Mateo *et al.*, Astrophys. J. Lett. **712**, 1, L103-L106 (2010) [arXiv:1002.0504 [astro-ph.GA]].

[138] F. Governato, B. Willman, L. Mayer, A. Brooks, G. Stinson, O. Valenzuela, J. Wadsley and T. R. Quinn, Mon. Not. Roy. Astron. Soc. **374**, 1479 (2007) [astro-ph/0602351].

[139] M. A. Alvarez, M. Busha, T. Abel and R. H. Wechsler, Astrophys. J. **703**, L167 (2009) [arXiv:0812.3405 [astro-ph]].

[140] A. M. Brooks, M. Kuhlen, A. Zolotov and D. Hooper, Astrophys. J. **765**, 22 (2013) [arXiv:1209.5394 [astro-ph.CO]].

[141] M. Boylan-Kolchin, J. S. Bullock and M. Kaplinghat, Mon. Not. Roy. Astron. Soc. **415**, L40 (2011) [arXiv:1103.0007 [astro-ph.CO]].

[142] P. Bode, J. P. Ostriker and N. Turok, Astrophys. J. **556**, 93 (2001) [astro-ph/0010389].

[143] M. Milgrom, Astrophys. J. **270**, 365 (1983).

[144] M. Milgrom, Astrophys. J. **270**, 371 (1983).

[145] J. Einasto, Astronomy and Astrophysics 2010, [Eds. Oddbjorn Engvold, Rolf Stabell, Bozena Czerny, John Lattanzio], in Encyclopedia of Life Support Systems (EOLSS), Developed under the Auspices of the UNESCO, Eolss Publishers, Oxford ,UK [arXiv:0901.0632 [astro-ph.CO]].

[146] R. A. Swaters, B. F. Madore, F. C. V. D. Bosch and M. Balcells, Astrophys. J. **583**, 732 (2003) [astro-ph/0210152].

[147] P. Cote, D. E. McLaughlin, J. G. Cohen and J. P. Blakeslee, Astrophys. J. **591**, 850 (2003) [astro-ph/0303229].

[148] A. J. Romanowsky, N. D. Douglas, M. Arnaboldi, K. Kuijken, M. R. Merrifield, N. R. Napolitano, M. Capaccioli and K. C. Freeman, Science **301**, 1696 (2003) [astro-ph/0308518].

[149] F. Prada *et al.* [SDSS Collaboration], Astrophys. J. **598**, 260 (2003) [astro-ph/0301360].

[150] A. Klypin, S. Trujillo-Gomez and J. Primack, Astrophys. J. **740**, 102 (2011) [arXiv:1002.3660 [astro-ph.CO]].

[151] P. Salucci, A. Lapi, C. Tonini, G. Gentile, I. Yegorova and U. Klein, Mon. Not. Roy. Astron. Soc. **378**, 41 (2007) [astro-ph/0703115 [ASTRO-PH]].

[152] J. Einasto, Trudy Inst. Astrofiz. Alma-Ata 51, 87 (1965).

[153] K. G. Begeman, A. H. Broeils and R. H. Sanders, Mon. Not. Roy. Astron. Soc. **249**, 523 (1991).

[154] B. Famaey and J. Binney, Mon. Not. Roy. Astron. Soc. **363**, 603 (2005) [astro-ph/0506723].

[155] B. Famaey, G. Gentile, J. P. Bruneton and H. S. Zhao, Phys. Rev. D **75**, 063002 (2007) [astro-ph/0611132].

[156] H. -S. Zhao and B. Famaey, Astrophys. J. **638**, L9 (2006) [astro-ph/0512425].

[157] J. D. Bekenstein, Phys. Rev. D **70**, 083509 (2004) [Erratum-ibid. D **71**, 069901 (2005)] [astro-ph/0403694].

[158] T. Richtler, Y. Schuberth, M. Hilker, B. Dirsch, L. Bassino and A. J. Romanowsky, Astron. Astrophys. **478**, L23 (2008) [arXiv:0711.4077 [astro-ph]].

[159] R. H. Sanders and S. S. McGaugh, Ann. Rev. Astron. Astrophys. **40**, 263 (2002) [astro-ph/0204521].

[160] M. Persic, P. Salucci and F. Stel, Mon. Not. Roy. Astron. Soc. **281**, 27 (1996) [astro-ph/9506004].

[161] P. Salucci, I. A. Yegorova and N. Drory, Mon. Not. Roy. Astron. Soc. **388**, 159 (2008) [arXiv:0708.1440 [astro-ph]].

[162] N. Frusciante, P. Salucci, D. Vernieri, J. M. Cannon and E. C. Elson, Mon. Not. Roy. Astron. Soc. **426**, 751 (2012) [arXiv:1206.0314 [astro-ph.CO]].

[163] R. H. Sanders, Astrophys. J. **473**, 117 (1996) [astro-ph/9606089].

[164] R. H. Sanders and M. A. W. Verheijen, Astrophys. J. **503**, 97 (1998) [astro-ph/9802240].

[165] R. H. Sanders and E. Noordermeer, Mon. Not. Roy. Astron. Soc. **379**, 702 (2007) [astro-ph/0703352 [ASTRO-PH]].

[166] J. M. Cannon, K. Haynes, H. Most, J. J. Salzer, K. Haugland, J. Scudder, A. Sugden and J. Weindling, Astron. J. , **139**, 6, (2010) [arXiv:1003.3797 [astro-ph.CO]].

[167] O. Vaduvescu, M. L. McCall, M. G. Richer and R. L. Fingerhut, Astron. J. **130**, 1593 (2005) [astro-ph/0506706].

[168] A. N. Cox, *"Allens Astrophysical Quantities"*, 4th ed., New York, Springer (2000).

[169] M. S. Bessell, PASP, 91, 589 (1979).

[170] C. M. Springob, M. P. Haynes, R. Giovanelli and B. R. Kent, Astrophys. J. Suppl. **160**, 1, 149 (2005) [astro-ph/0505025].

[171] A. Begum and J. N. Chengalur, Astron. Astrophys. **413**, 525 (2004) [astro-ph/0310138].

[172] R. H. M. Schoenmakers, M. Franx and P. T. de Zeeuw, Mon. Not. Roy. Astron. Soc. **292**, 349 (1997) [astro-ph/9707332].

[173] E. Hayashi and J. F. Navarro, Mon. Not. Roy. Astron. Soc. **373**, 1117 (2006) [astro-ph/0608376].

[174] K. C. Freeman, Astrophys. J. **160**, 811 (1970).

[175] J. F. Navarro, C. S. Frenk and S. D. M. White, Astrophys. J. **462**, 563 (1996) [astro-ph/9508025].

[176] V. R. Eke, S. Cole and C. S. Frenk, Mon. Not. Roy. Astron. Soc. **282**, 263 (1996) [astro-ph/9601088].

[177] N. Kaiser, Astrophys. J. **284**, L9 (1984).

[178] J. M. Bardeen, J. R. Bond, N. Kaiser and A. S. Szalay, Astrophys. J. **304**, 15 (1986).

[179] H. J. Mo and S. D. M. White, Mon. Not. Roy. Astron. Soc. **282**, 347 (1996) [astro-ph/9512127].

[180] R. K. Sheth and G. Tormen, Mon. Not. Roy. Astron. Soc. **308**, 119 (1999) [astro-ph/9901122].

[181] R. Scoccimarro, R. K. Sheth, L. Hui and B. Jain, Astrophys. J. **546**, 20 (2001) [astro-ph/0006319].

[182] A. Cooray and R. K. Sheth, Phys. Rept. **372**, 1 (2002) [astro-ph/0206508].

[183] M. Davis, G. Efstathiou, C. S. Frenk and S. D. M. White, Astrophys. J. **292**, 371 (1985).

[184] V. Desjacques, Phys. Rev. D **78**, 103503 (2008) [arXiv:0806.0007 [astro-ph]].

[185] V. Desjacques and R. K. Sheth, Phys. Rev. D **81**, 023526 (2010) [arXiv:0909.4544 [astro-ph.CO]].

[186] V. Desjacques, M. Crocce, R. Scoccimarro and R. K. Sheth, Phys. Rev. D **82**, 103529 (2010) [arXiv:1009.3449 [astro-ph.CO]].

[187] M. Tegmark and B. C. Bromley, Astrophys. J. **518**, L69 (1999) [astro-ph/9809324].

[188] A. Dekel and O. Lahav, Astrophys. J. **520**, 24 (1999) [astro-ph/9806193].

[189] M. Manera, R. K. Sheth and R. Scoccimarro, Mon. Not. Roy. Astron. Soc. **402**, 589 (2010) [arXiv:0906.1314 [astro-ph.CO]].

[190] P. Coles, Mon. Not. Roy. Astron. Soc. **262**, 1065 (1993). .

[191] J. N. Fry and E. Gaztañaga, Astrophys. J. **413**, 447 (1993) [astro-ph/9302009].

[192] R. J. Scherrer and D. H. Weinberg, Astrophys. J. **504**, 607 (1998) [astro-ph/9712192].

[193] T. Matsubara, Phys. Rev. D **83**, 083518 (2011) [arXiv:1102.4619 [astro-ph.CO]].

[194] J. E. Pollack, R. E. Smith and C. Porciani, Mon. Not. Roy. Astron. Soc. **420**, 3469 (2012) [arXiv:1109.3458 [astro-ph.CO]].

[195] K. C. Chan, R. Scoccimarro and R. K. Sheth, Phys. Rev. D **85**, 083509 (2012) [arXiv:1201.3614 [astro-ph.CO]].

[196] T. Baldauf, U. Seljak, V. Desjacques and P. McDonald, Phys. Rev. D **86**, 083540 (2012) [arXiv:1201.4827 [astro-ph.CO]].

[197] L. Hui and K. P. Parfrey, Phys. Rev. D **77**, 043527 (2008) [arXiv:0712.1162 [astro-ph]].

[198] A. Shirata, T. Shiromizu, N. Yoshida and Y. Suto, Phys. Rev. D **71**, 064030 (2005) [astro-ph/0501366].

[199] S. A. Appleby and J. Weller, JCAP **1012**, 006 (2010) [arXiv:1008.2693 [astro-ph.CO]].

[200] E. V. Linder and R. N. Cahn, Astropart. Phys. **28**, 481 (2007) [astro-ph/0701317].

[201] A. Shirata, Y. Suto, C. Hikage, T. Shiromizu and N. Yoshida, Phys. Rev. D **76**, 044026 (2007) [arXiv:0705.1311 [astro-ph]].

[202] M. C. Martino, H. F. Stabenau and R. K. Sheth, Phys. Rev. D **79**, 084013 (2009) [arXiv:0812.0200 [astro-ph]].

[203] M. C. Martino and R. K. Sheth, arXiv:0911.1829 [astro-ph.CO].

[204] K. Parfrey, L. Hui and R. K. Sheth, Phys. Rev. D **83**, 063511 (2011) [arXiv:1012.1335 [astro-ph.CO]].

[205] A. S. Szalay, Astrophys. J. **333**, 21 (1988).

[206] P. McDonald, Phys. Rev. D **74**, 103512 (2006) [Erratum-ibid. D **74**, 129901 (2006)] [astro-ph/0609413].

[207] N. Frusciante and R. K. Sheth, JCAP **1211**, 016 (2012) [arXiv:1208.0229 [astro-ph.CO]].

[208] R. K. Sheth and G. Lemson, Mon. Not. Roy. Astron. Soc. **304**, 767 (1999) [astro-ph/9808138].

[209] M. Manera and E. Gaztañaga, Mon. Not. Roy. Astron. Soc. **415**, 383 (2011) [arXiv:0912.0446 [astro-ph.CO]].

[210] M. Musso, A. Paranjape and R. K. Sheth, Mon. Not. Roy. Astron. Soc. **427**, 3145 (2012) [arXiv:1205.3401 [astro-ph.CO]].

[211] P. Coles, B. Jones,Mon. Not. Roy. Astron. Soc. **248**, 1 (1991).

[212] K. C. Chan and R. Scoccimarro, Phys. Rev. D **86**, 103519 (2012) [arXiv:1204.5770 [astro-ph.CO]].

[213] H. J. Mo, Y. P. Jing and S. D. M. White, Mon. Not. Roy. Astron. Soc. **284**, 189 (1997) [astro-ph/9603039].

[214] R. K. Sheth, H. J. Mo and G. Tormen, Mon. Not. Roy. Astron. Soc. **323**, 1 (2001) [astro-ph/9907024].

[215] R. K. Sheth, K. C. Chan and R. Scoccimarro, Phys. Rev. D **87**, 083002 (2013) [arXiv:1207.7117 [astro-ph.CO]].

[216] E. J. Copeland, M. Sami and S. Tsujikawa, Int. J. Mod. Phys. D **15**, 1753 (2006) [hep-th/0603057].

[217] A. Silvestri and M. Trodden, Rept. Prog. Phys. **72**, 096901 (2009), [arXiv:0904.0024 [astro-ph.CO]].

[218] L. Amendola and S. Tsujikawa, "Dark Energy:Theory and Observations", Cambridge University Press (2010).

[219] C. Brans and R. H. Dicke, Phys. Rev. **124**, 925 (1961).

[220] A. Nicolis, R. Rattazzi and E. Trincherini, Phys. Rev. D **79**, 064036 (2009) [arXiv:0811.2197 [hep-th]].

[221] C. Deffayet, G. Esposito-Farese and A. Vikman, Phys. Rev. D **79**, 084003 (2009) [arXiv:0901.1314 [hep-th]].

[222] K. Hinterbichler, M. Trodden and D. Wesley, Phys. Rev. D **82**, 124018 (2010) [arXiv:1008.1305 [hep-th]].

[223] T. Jacobson and D. Mattingly, Phys. Rev. D **64**, 024028 (2001) [gr-qc/0007031].

[224] N. Arkani-Hamed, H. Georgi and M. D. Schwartz, Annals Phys. **305** (2003) 96 [hep-th/0210184].

[225] T. P. Sotiriou and V. Faraoni, Rev. Mod. Phys. **82**, 451 (2010) [arXiv:0805.1726 [gr-qc]].

[226] V. Faraoni, Phys. Rev. D **75**, 067302 (2007) [gr-qc/0703044 [GR-QC]].

[227] P. Creminelli, G. D'Amico, J. Norena and F. Vernizzi, JCAP **0902**, 018 (2009) [arXiv:0811.0827 [astro-ph]].

[228] G. Gubitosi, F. Piazza and F. Vernizzi, JCAP **1302**, 032 (2013) [arXiv:1210.0201 [hep-th]].

[229] J. K. Bloomfield, É. É. Flanagan, M. Park and S. Watson, JCAP **1308**, 010 (2013) [arXiv:1211.7054 [astro-ph.CO]].

[230] G. R. Dvali, G. Gabadadze and M. Porrati, Phys. Lett. B **485**, 208 (2000) [hep-th/0005016].

[231] T. Kaluza, Sitzungsber. Preuss. Akad. Wiss. Berlin (Math. Phys.) **1921**, 966 (1921).

[232] O. Klein, Zeits. Phys. 37 (1926) 895.

[233] D. Bailin and A. Love, Rept. Prog. Phys. **50**, 1087 (1987).

[234] S. 'i. Nojiri and S. D. Odintsov, Phys. Lett. B **659**, 821 (2008) [arXiv:0708.0924 [hep-th]].

[235] S. Dodelson and S. Park, arXiv:1310.4329 [astro-ph.CO].

[236] M. Maggiore and M. Mancarella, Phys. Rev. D **90**, 023005 (2014) [arXiv:1402.0448 [hep-th]].

[237] H. A. Buchdahl, Mon. Not. Roy. Astron. Soc. **150**, 1 (1970).

[238] A. De Felice and S. Tsujikawa, Living Rev. Rel. **13**, 3 (2010), [arXiv:1002.4928 [gr-qc]].

[239] M. Banados and P. G. Ferreira, Phys. Rev. Lett. **105**, 011101 (2010) [arXiv:1006.1769 [astro-ph.CO]].

[240] P. Pani, T. P. Sotiriou and D. Vernieri, Phys. Rev. D **88**, 121502 (2013) [arXiv:1306.1835 [gr-qc]].

[241] O. Pujolas, I. Sawicki, A. Vikman and , JHEP **1111**, 156 (2011) [arXiv:1103.5360 [hep-th]].

[242] C. M. Will, Living Rev. Rel. **9**, 3 (2006) [gr-qc/0510072].

[243] C. M. Will, Living Rev. Rel. **17**, 4 (2014) [arXiv:1403.7377 [gr-qc]].

[244] J. Khoury and A. Weltman, Phys. Rev. Lett. **93**, 171104 (2004) [astro-ph/0309300].

[245] J. Khoury and A. Weltman, Phys. Rev. D **69**, 044026 (2004) [astro-ph/0309411].

[246] P. Brax, C. van de Bruck, A. -C. Davis, J. Khoury and A. Weltman, Phys. Rev. D **70**, 123518 (2004) [astro-ph/0408415].

[247] P. Brax, C. van de Bruck, A. C. Davis, J. Khoury and A. Weltman, AIP Conf. Proc. **736**, 105 (2005) [astro-ph/0410103].

[248] Y. Fujii, K. Maeda, "The Scalar-Tensor Theory of Gravitation", Cambridge University Press, (2003).

[249] V. Faraoni, "Cosmology in Scalar-Tensor Gravity", Springer, (2004).

[250] S. M. Carroll, V. Duvvuri, M. Trodden and M. S. Turner, Phys. Rev. D **70**, 043528 (2004) [astro-ph/0306438].

[251] W. Hu and I. Sawicki, Phys. Rev. D **76**, 064004 (2007) [arXiv:0705.1158 [astro-ph]].

[252] A. I. Vainshtein, Phys. Lett. B **39**, 393 (1972).

[253] C. Deffayet, G. R. Dvali, G. Gabadadze and A. I. Vainshtein, Phys. Rev. D **65**, 044026 (2002) [hep-th/0106001].

[254] G. Gabadadze, Phys. Lett. B **681**, 89 (2009) [arXiv:0908.1112 [hep-th]].

[255] E. Babichev, C. Deffayet and R. Ziour, [arXiv:0905.2943 [hep-th]].

[256] K. Hinterbichler and J. Khoury, Phys. Rev. Lett. **104**, 231301 (2010) [arXiv:1001.4525 [hep-th]].

[257] K. A. Olive and M. Pospelov, Phys. Rev. D **77**, 043524 (2008) [arXiv:0709.3825 [hep-ph]].

[258] A. Lue, R. Scoccimarro and G. D. Starkman, Phys. Rev. D **69**, 124015 (2004), [astro-ph/0401515].

[259] R. Lazkoz, R. Maartens and E. Majerotto, Phys. Rev. D **74**, 083510 (2006), [astro-ph/0605701].

[260] Y. -S. Song, W. Hu and I. Sawicki, Phys. Rev. D **75**, 044004 (2007), [astro-ph/0610532].

[261] R. Bean, D. Bernat, L. Pogosian, A. Silvestri and M. Trodden, Phys. Rev. D **75**, 064020 (2007), [astro-ph/0611321].

[262] G. Dvali, S. Hofmann and J. Khoury, Phys. Rev. D **76**, 084006 (2007), [arxiv:hep-th/0703027].

[263] S. A. Appleby and R. A. Battye, Phys. Lett. B **654**, 7 (2007), [arXiv:0705.3199 [astro-ph]].

[264] L. Pogosian and A. Silvestri, Phys. Rev. D **77**, 023503 (2008), [Erratum-ibid. D **81**, 049901 (2010)], [arXiv:0709.0296[astro-ph]].

[265] P. Brax, C. van de Bruck, A. -C. Davis and D. J. Shaw, Phys. Rev. D **78**, 104021 (2008), [arXiv:0806.3415 [astro-ph]].

[266] E. Bertschinger, Astrophys. J. **648**, 797 (2006), [astro-ph/0604485].

[267] L. Amendola, M. Kunz and D. Sapone, JCAP **0804**, 013 (2008), [arXiv:0704.2421 [astro-ph]].

[268] P. Zhang, M. Liguori, R. Bean and S. Dodelson, Phys. Rev. Lett. **99**, 141302 (2007), [arXiv:0704.1932 [astro-ph]].

[269] W. Hu and I. Sawicki, Phys. Rev. D **76**, 104043 (2007), [arXiv:0708.1190 [astro-ph]].

[270] E. Bertschinger and P. Zukin, Phys. Rev. D **78**, 024015 (2008) [arXiv:0801.2431 [astro-ph]].

[271] S. F. Daniel, R. R. Caldwell, A. Cooray and A. Melchiorri, Phys. Rev. D **77**, 103513 (2008), [arXiv:0802.1068 [astro-ph]].

[272] Y. -S. Song and K. Koyama, JCAP **0901**, 048 (2009), [arXiv:0802.3897 [astro-ph]].

[273] C. Skordis, Phys. Rev. D **79**, 123527 (2009), [arXiv:0806.1238 [astro-ph]].

[274] Y. -S. Song and O. Dore, JCAP **0903**, 025 (2009), [arXiv:0812.0002 [astro-ph]].

[275] G. -B. Zhao, L. Pogosian, A. Silvestri and J. Zylberberg, Phys. Rev. Lett. **103**, 241301 (2009), [arXiv:0905.1326 [astro-ph.CO]].

[276] G. -B. Zhao, T. Giannantonio, L. Pogosian, A. Silvestri, D. J. Bacon, K. Koyama, R. C. Nichol and Y. -S. Song, Phys. Rev. D **81**, 103510 (2010), [arXiv:1003.0001 [astro-ph.CO]].

[277] J. Dossett, M. Ishak, J. Moldenhauer, Y. Gong, A. Wang, Y. Gong and A. Wang, JCAP **1004**, 022 (2010) [arXiv:1004.3086 [astro-ph.CO]].

[278] Y. -S. Song, L. Hollenstein, G. Caldera-Cabral and K. Koyama, JCAP **1004**, 018 (2010), [arXiv:1001.0969 [astro-ph.CO]].

[279] S. F. Daniel, E. V. Linder, T. L. Smith, R. R. Caldwell, A. Cooray, A. Leauthaud and L. Lombriser, Phys. Rev. D **81**, 123508 (2010), [arXiv:1002.1962 [astro-ph.CO]].

[280] L. Pogosian, A. Silvestri, K. Koyama and G. -B. Zhao, Phys. Rev. D **81**, 104023 (2010), [arXiv:1002.2382 [astro-ph.CO]].

[281] R. Bean and M. Tangmatitham, Phys. Rev. D **81**, 083534 (2010), [arXiv:1002.4197 [astro-ph.CO]].

[282] S. A. Thomas, S. A. Appleby and J. Weller, JCAP **1103**, 036 (2011), [arXiv:1101.0295 [astro-ph.CO]].

[283] T. Baker, P. G. Ferreira, C. Skordis and J. Zuntz, Phys. Rev. D **84**, 124018 (2011), [arXiv:1107.0491 [astro-ph.CO]].

[284] D. B. Thomas and C. R. Contaldi, JCAP **1112**, 013 (2011), [arXiv:1107.0727 [astro-ph.CO]].

[285] J. N. Dossett, M. Ishak and J. Moldenhauer, Phys. Rev. D **84**, 123001 (2011), [arXiv:1109.4583 [astro-ph.CO]].

[286] G. -B. Zhao *et al.*, Phys. Rev. D **85**, 123546 (2012), [arXiv:1109.1846 [astro-ph.CO]].

[287] A. Hojjati *et al.*, Phys. Rev. D **85**, 043508 (2012), [arXiv:1111.3960 [astro-ph.CO]].

[288] P. Brax, A. -C. Davis and B. Li, Phys. Lett. B **715**, 38 (2012), [arXiv:1111.6613 [astro-ph.CO]].

[289] J. Dossett and M. Ishak, Phys. Rev. D **86**, 103008 (2012) [arXiv:1205.2422 [astro-ph.CO]].

[290] P. Brax, A. -C. Davis, B. Li and H. A. Winther, Phys. Rev. D **86**, 044015 (2012), [arXiv:1203.4812 [astro-ph.CO]].

[291] I. Sawicki, I. D. Saltas, L. Amendola and M. Kunz, JCAP **1301**, 004 (2013), [arXiv:1208.4855 [astro-ph.CO]].

[292] T. Baker, P. G. Ferreira and C. Skordis, Phys. Rev. D **87**, 024015 (2013), [arXiv:1209.2117 [astro-ph.CO]].

[293] L. Amendola, M. Kunz, M. Motta, I. D. Saltas and I. Sawicki, Phys. Rev. D **87**, 023501 (2013), [arXiv:1210.0439 [astro-ph.CO]].

[294] A. Hojjati, JCAP **1301**, 009 (2013), [arXiv:1210.3903 [astro-ph.CO]].

[295] A. Silvestri, L. Pogosian and R. V. Buniy, Phys. Rev. D **87**, no. 10, 104015 (2013) [arXiv:1302.1193 [astro-ph.CO]].

[296] M. Motta, I. Sawicki, I. D. Saltas, L. Amendola and M. Kunz, Phys. Rev. D **88**, 124035 (2013), [arXiv:1305.0008 [astro-ph.CO]].

[297] S. Asaba, C. Hikage, K. Koyama, G. -B. Zhao, A. Hojjati and L. Pogosian, JCAP **1308**, 029 (2013), [arXiv:1306.2546 [astro-ph.CO]].

[298] T. Baker, P. G. Ferreira and C. Skordis, [arXiv:1310.1086 [astro-ph.CO]].

[299] J. Dossett and M. Ishak, Phys. Rev. D **88**, 103008 (2013), [arXiv:1311.0726 [astro-ph.CO]].

[300] A. Terukina, L. Lombriser, K. Yamamoto, D. Bacon, K. Koyama and R. C. Nichol, JCAP **1404**, 013 (2014) [arXiv:1312.5083 [astro-ph.CO]].

[301] F. Piazza, H. Steigerwald and C. Marinoni, JCAP **1405**, 043 (2014) [arXiv:1312.6111 [astro-ph.CO]].

[302] Lás. Á.Gergely and S. Tsujikawa, Phys. Rev. D **89**, 064059 (2014) [arXiv:1402.0553 [hep-th]].

[303] B. Hu, M. Liguori, N. Bartolo and S. Matarrese, Phys. Rev. D **88**, no. 2, 024012 (2013) [arXiv:1211.5032 [astro-ph.CO]].

[304] D. Munshi, B. Hu, A. Renzi, A. Heavens and P. Coles, Mon. Not. Roy. Astron. Soc. **442**, 821 (2014) [arXiv:1403.0852 [astro-ph.CO]].

[305] B. Hu, M. Liguori, N. Bartolo and S. Matarrese, Phys. Rev. D **88**, 123514 (2013), [arXiv:1307.5276 [astro-ph.CO]].

[306] H. Steigerwald, J. Bel and C. Marinoni, JCAP **1405**, 042 (2014) [arXiv:1403.0898 [astro-ph.CO]].

[307] L. Lombriser, Annalen der Physik (2014) [arXiv:1403.4268 [astro-ph.CO]].

[308] S. Tsujikawa, arXiv:1404.2684 [gr-qc].

[309] E. Bellini and I. Sawicki, JCAP **1407**, 050 (2014) [arXiv:1404.3713 [astro-ph.CO]].

[310] http://www.darkenergysurvey.org .

[311] http://www.lsst.org .

[312] http://sci.esa.int/euclid .

[313] M. J. Drinkwater, R. J. Jurek, C. Blake, D. Woods, K. A. Pimbblet, K. Glazebrook, R. Sharp and M. B. Pracy *et al.*, Mon. Not. Roy. Astron. Soc. **401**, 1429 (2010) [arXiv:0911.4246 [astro-ph.CO]].

[314] D. Parkinson, S. Riemer-Sorensen, C. Blake, G. B. Poole, T. M. Davis, S. Brough, M. Colless and C. Contreras *et al.*, Phys. Rev. D **86**, 103518 (2012) [arXiv:1210.2130 [astro-ph.CO]].

[315] F. Simpson, C. Heymans, D. Parkinson, C. Blake, M. Kilbinger, J. Benjamin, T. Erben and H. Hildebrandt *et al.*, arXiv:1212.3339 [astro-ph.CO].

[316] C. Heymans, E. Grocutt, A. Heavens, M. Kilbinger, T. D. Kitching, F. Simpson, J. Benjamin and T. Erben *et al.*, arXiv:1303.1808 [astro-ph.CO].

[317] L. Fu, M. Kilbinger, T. Erben, C. Heymans, H. Hildebrandt, H. Hoekstra, T. D. Kitching and Y. Mellier *et al.*, arXiv:1404.5469 [astro-ph.CO].

[318] R. A. Battye and J. A. Pearson, JCAP **1207**, 019 (2012) [arXiv:1203.0398 [hep-th]].

[319] M. Hohmann, L. Jarv, P. Kuusk and E. Randla, Phys. Rev. D **88**, no. 8, 084054 (2013) [arXiv:1309.0031 [gr-qc]].

[320] T. P. Sotiriou, arXiv:1404.2955 [gr-qc].

[321] A. Palatini, Rend. Circ. Mat. Palermo, vol. 43, (1919).

[322] A. A. Starobinsky, Phys. Lett. B **91**, 99 (1980).

[323] T. Kobayashi, M. Yamaguchi and J. 'i. Yokoyama, Phys. Rev. Lett. **105**, 231302 (2010) [arXiv:1008.0603 [hep-th]].

[324] C. Deffayet, S. Deser and G. Esposito-Farese, Phys. Rev. D **80**, 064015 (2009) [arXiv:0906.1967 [gr-qc]].

[325] C. Deffayet, X. Gao, D. A. Steer and G. Zahariade, Phys. Rev. D **84**, 064039 (2011) [arXiv:1103.3260 [hep-th]].

[326] T. Kobayashi, M. Yamaguchi and J. 'i. Yokoyama, Prog. Theor. Phys. **126**, 511 (2011) [arXiv:1105.5723 [hep-th]].

[327] G. W. Horndeski, Int. J. Theor. Phys. **10**, 363 (1974).

[328] C. de Rham and A. J. Tolley, JCAP **1005**, 015 (2010) [arXiv:1003.5917 [hep-th]].

[329] A. Padilla, P. M. Saffin and S. -Y. Zhou, JHEP **1101**, 099 (2011) [arXiv:1008.3312 [hep-th]].

[330] C. Deffayet, S. Deser and G. Esposito-Farese, Phys. Rev. D **82**, 061501 (2010) [arXiv:1007.5278 [gr-qc]].

[331] A. Padilla, P. M. Saffin and S. -Y. Zhou, Phys. Rev. D **83**, 045009 (2011) [arXiv:1008.0745 [hep-th]].

[332] S. -Y. Zhou and E. J. Copeland, Phys. Rev. D **85**, 065002 (2012) [arXiv:1112.0968 [hep-th]].

[333] G. Goon, K. Hinterbichler, A. Joyce and M. Trodden, JHEP **1206**, 004 (2012) [arXiv:1203.3191 [hep-th]].

[334] Y. -F. Cai, D. A. Easson, R. Brandenberger, JCAP **1208**, 020 (2012) [arXiv:1206.2382 [hep-th]].

[335] K. Hinterbichler, Rev. Mod. Phys. **84**, 671 (2012) [arXiv:1105.3735 [hep-th]].

[336] A. De Felice and S. Tsujikawa, JCAP **1007**, 024 (2010) [arXiv:1005.0868 [astro-ph.CO]].

[337] P. Creminelli, A. Nicolis and E. Trincherini, JCAP **1011**, 021 (2010) [arXiv:1007.0027 [hep-th]].

[338] C. Burrage, C. de Rham, D. Seery, A. J. Tolley, JCAP **1101**, 014 (2011) [arXiv:1009.2497 [hep-th]].

[339] P. Creminelli, G. D'Amico, M. Musso, J. Norena and E. Trincherini, JCAP **1102**, 006 (2011) [arXiv:1011.3004 [hep-th]].

[340] S. Renaux-Petel, S. Mizuno, K. Koyama, JCAP **1111**, 042 (2011) [arXiv:1108.0305 [astro-ph.CO]].

[341] M. Fasiello, JCAP **1312**, 033 (2013) [arXiv:1303.5015 [hep-th]].

[342] K. Kamada, T. Kobayashi, M. Yamaguchi and J. 'i. Yokoyama, Phys. Rev. D **83**, 083515 (2011) [arXiv:1012.4238 [astro-ph.CO]].

[343] T. Kobayashi, M. Yamaguchi and J. 'i. Yokoyama, Phys. Rev. D **83**, 103524 (2011) [arXiv:1103.1740 [hep-th]].

[344] A. De Felice and S. Tsujikawa, JCAP **1303**, 030 (2013) [arXiv:1301.5721 [hep-th]].

[345] X. Gao and D. A. Steer, JCAP **1112**, 019 (2011) [arXiv:1107.2642 [astro-ph.CO]].

[346] F. P. Silva and K. Koyama, Phys. Rev. D **80**, 121301 (2009) [arXiv:0909.4538 [astro-ph.CO]].

[347] N. Chow and J. Khoury, Phys. Rev. D **80**, 024037 (2009) [arXiv:0905.1325 [hep-th]].

[348] T. Kobayashi, H. Tashiro and D. Suzuki, Phys. Rev. D **81**, 063513 (2010) [arXiv:0912.4641 [astro-ph.CO]].

[349] T. Kobayashi, Phys. Rev. D **81**, 103533 (2010) [arXiv:1003.3281 [astro-ph.CO]].

[350] C. Deffayet, O. Pujolas, I. Sawicki, A. Vikman and , JCAP **1010**, 026 (2010) [arXiv:1008.0048 [hep-th]].

[351] A. De Felice and S. Tsujikawa, Phys. Rev. D **84**, 124029 (2011) [arXiv:1008.4236 [hep-th]].

[352] R. Kimura, T. Kobayashi and K. Yamamoto, Phys. Rev. D **85**, 024023 (2012) [arXiv:1111.6749 [astro-ph.CO]].

[353] A. Nicolis and R. Rattazzi, JHEP **0406**, 059 (2004) [hep-th/0404159].

[354] P. Brax, C. Burrage and A. C. Davis, JCAP **1301**, 020 (2013) [arXiv:1209.1293 [hep-th]].

[355] J. M. Maldacena, JHEP **0305**, 013 (2003) [astro-ph/0210603].

[356] V. Acquaviva, N. Bartolo, S. Matarrese and A. Riotto, Nucl. Phys. B **667**, 119 (2003) [astro-ph/0209156].

[357] K. A. Malik and D. Wands, Class. Quant. Grav. **21**, L65 (2004) [astro-ph/0307055].

[358] K. Nakamura, Prog. Theor. Phys. **117**, 17 (2007) [gr-qc/0605108].

[359] K. A. Malik, JCAP **0511**, 005 (2005) [astro-ph/0506532].

[360] D. Langlois and F. Vernizzi, JCAP **0702**, 017 (2007) [astro-ph/0610064].

[361] A. J. Christopherson, K. A. Malik, D. R. Matravers and K. Nakamura, Class. Quant. Grav. **28**, 225024 (2011) [arXiv:1101.3525 [astro-ph.CO]].

[362] E. M. Lifshitz and I. M. Khalatnikov, Adv. Phys. **12**, 185 (1963).

[363] K. Tomita, Prog. Theor. Phys. **54**, 730 (1975).

[364] D. S. Salopek and J. R. Bond, Phys. Rev. D **42**, 3936 (1990).

[365] G. L. Comer, N. Deruelle, D. Langlois and J. Parry, Phys. Rev. D **49**, 2759 (1994).

[366] N. Deruelle and D. Langlois, Phys. Rev. D **52**, 2007 (1995) [gr-qc/9411040].

[367] D. H. Lyth, K. A. Malik and M. Sasaki, JCAP **0505**, 004 (2005) [astro-ph/0411220].

[368] O. Iguchi, H. Ishihara and J. Soda, Phys. Rev. D **55**, 3337 (1997) [gr-qc/9606012].

[369] Y. Tanaka and M. Sasaki, Prog. Theor. Phys. **117**, 633 (2007) [gr-qc/0612191].

[370] Y. -i. Takamizu and S. Mukohyama, JCAP **0901**, 013 (2009) [arXiv:0810.0746 [gr-qc]].

[371] K. Izumi and S. Mukohyama, Phys. Rev. D **84**, 064025 (2011) [arXiv:1105.0246 [hep-th]].

[372] A. E. Gumrukcuoglu, S. Mukohyama and A. Wang, Phys. Rev. D **85**, 064042 (2012) [arXiv:1109.2609 [hep-th]].

[373] Y. i. Takamizu and T. Kobayashi, PTEP **2013**, no. 6, 063E03 (2013) [arXiv:1301.2370 [gr-qc]].

[374] A. Naruko, Y. i. Takamizu and M. Sasaki, PTEP **2013**, 043E01 (2013) [arXiv:1210.6525 [astro-ph.CO]].

[375] D. Wands, K. A. Malik, D. H. Lyth and A. R. Liddle, Phys. Rev. D **62**, 043527 (2000) [astro-ph/0003278].

[376] A. A. Starobinsky, JETP Lett. **42**, 152 (1985) [Pisma Zh. Eksp. Teor. Fiz. **42**, 124 (1985)].

[377] M. Sasaki and E. D. Stewart, Prog. Theor. Phys. **95**, 71 (1996) [astro-ph/9507001].

[378] S. M. Leach, M. Sasaki, D. Wands and A. R. Liddle, Phys. Rev. D **64**, 023512 (2001) [astro-ph/0101406].

[379] N. Frusciante, S. -Y. Zhou and T. P. Sotiriou, JCAP **1307**, 020 (2013) [arXiv:1303.6628 [astro-ph.CO]].

[380] R. L. Arnowitt, S. Deser and C. W. Misner, Phys. Rev. **116**, 1322 (1959).

[381] R. L. Arnowitt, S. Deser and C. W. Misner, Gen. Rel. Grav. **40**, 1997 (2008) [gr-qc/0405109].

[382] R. Arnowitt and S. Deser, Phys. Rev. **113**, 745 (1959).

[383] R. L. Arnowitt, S. Deser and C. W. Misner, Phys. Rev. **117**, 1595 (1960).

[384] R. Arnowitt, S. Deser and C. W. Misner, *"Gravitation: An introduction to current research"*, Louis Witten (editor), Wiley NY (1962).

[385] E. Gourgoulhon, gr-qc/0703035 [GR-QC].

[386] G. I. Rigopoulos and E. P. S. Shellard, Phys. Rev. D **68**, 123518 (2003) [astro-ph/0306620].

[387] Y. -i. Takamizu, S. Mukohyama, M. Sasaki and Y. Tanaka, JCAP **1006**, 019 (2010) [arXiv:1004.1870 [astro-ph.CO]].

[388] E. Bertschinger, Phil. Trans. Roy. Soc. Lond. A **369**, 4947 (2011), [arXiv:1111.4659 [astro-ph.CO]].

[389] F. Piazza and F. Vernizzi, Class. Quant. Grav. **30**, 214007 (2013) [arXiv:1307.4350 [hep-th]].

[390] S. Weinberg, Phys. Rev. D **77**, 123541 (2008)

[391] M. Park, K. M. Zurek and S. Watson, Phys. Rev. D **81**, 124008 (2010)

[392] J. J. M. Carrasco, M. P. Hertzberg and L. Senatore, JHEP **1209**, 082 (2012)

[393] M. P. Hertzberg, arXiv:1208.0839 [astro-ph.CO].

[394] J. Gleyzes, D. Langlois, F. Piazza and F. Vernizzi, JCAP **1308**, 025 (2013)

[395] J. Bloomfield, JCAP **1312**, 044 (2013) [arXiv:1304.6712 [astro-ph.CO]].

[396] N. Frusciante, M. Raveri and A. Silvestri, JCAP **1402**, 026 (2014) [arXiv:1310.6026 [astro-ph.CO]].

[397] B. Hu, M. Raveri, N. Frusciante and A. Silvestri, Phys. Rev. D **89**, 103530 (2014) [arXiv:1312.5742 [astro-ph.CO]].

[398] M. Raveri, B. Hu, N. Frusciante and A. Silvestri, Phys. Rev. D **90**, 043513 (2014) [arXiv:1405.1022 [astro-ph.CO]].

[399] http://camb.info .

[400] A. Lewis, A. Challinor and A. Lasenby, Astrophys. J. **538**, 473 (2000), [astro-ph/9911177].

[401] A. Lewis and S. Bridle, Phys. Rev. D **66**, 103511 (2002) [astro-ph/0205436].

[402] L. Amendola, R. Gannouji, D. Polarski and S. Tsujikawa, Phys. Rev. D **75**, 083504 (2007)

[403] J. Wainwright, G. F. R. Ellis, *"Dynamical Systems in Cosmology"*, Cambridge University Press (2005).

[404] S. Strogatz, *"Non linear dynamics and chaos: with applications to physics, biology, chemistry and engineering"*, Perseus Books (2001).

[405] C. Baccigalupi, S. Matarrese and F. Perrotta, Phys. Rev. D **62**, 123510 (2000) [astro-ph/0005543].

[406] S. Matarrese, C. Baccigalupi and F. Perrotta, Phys. Rev. D **70**, 061301 (2004) [astro-ph/0403480].

[407] S. -Y. Zhou, E. J. Copeland and P. M. Saffin, JCAP **0907**, 009 (2009) [arXiv:0903.4610 [gr-qc]].

[408] G. Leon and E. N. Saridakis, JCAP **1303**, 025 (2013) [arXiv:1211.3088 [astro-ph.CO]].

[409] H. Nariai, Prog. Theor. Phys. **49**, 165 (1973).

[410] V. T. Gurovich and A. A. Starobinsky, Sov. Phys. JETP **50**, 844 (1979) [Zh. Eksp. Teor. Fiz. **77**, 1683 (1979)].

[411] A. Rest *et al.* arXiv:1310.3828 [astro-ph.CO] (2013)

[412] L. Amendola *et al.* [Euclid Theory Working Group Collaboration], Living Rev. Rel. **16**, 6 (2013) [arXiv:1206.1225 [astro-ph.CO]].

[413] A. Hojjati, L. Pogosian, A. Silvestri and S. Talbot, Phys. Rev. D **86**, 123503 (2012), [arXiv:1210.6880 [astro-ph.CO]].

[414] L. Lombriser, J. Yoo and K. Koyama, Phys. Rev. D **87**, 104019 (2013), [arXiv:1301.3132 [astro-ph.CO]].

[415] J. Noller, F. von Braun-Bates and P. G. Ferreira, Phys. Rev. D **89**, 023521 (2014) [arXiv:1310.3266 [astro-ph.CO]].

[416] W. Fang, W. Hu and A. Lewis, Phys. Rev. D **78**, 087303 (2008), [arXiv:0808.3125 [astro-ph]].

[417] G. -B. Zhao, L. Pogosian, A. Silvestri and J. Zylberberg, Phys. Rev. D **79**, 083513 (2009) [arXiv:0809.3791 [astro-ph]].

[418] A. Hojjati, L. Pogosian and G. -B. Zhao, JCAP **1108**, 005 (2011) [arXiv:1106.4543 [astro-ph.CO]].

[419] P. A. R. Ade *et al.* [Planck Collaboration], arXiv:1303.5077 [astro-ph.CO].

[420] J. Bloomfield and J. Pearson, JCAP **1403**, 017 (2014) [arXiv:1310.6033 [astro-ph.CO]].

[421] R. A. Battye and J. A. Pearson, JCAP **1403**, 051 (2014) [arXiv:1311.6737 [astro-ph.CO]].

[422] E. -M. Mueller, R. Bean and S. Watson, Phys. Rev. D **87**, 083504 (2013)

[423] B. Hu, M. Raveri, N. Frusciante and A. Silvestri, arXiv:1405.3590 [astro-ph.IM].

[424] A. Nunez and S. Solganik, arXiv:hep-th/0403159.

[425] J. M. Cline, S. Jeon and G. D. Moore, Phys. Rev. D **70**, 043543 (2004), [hep-ph/0311312].

[426] S. Liberati, Class. Quant. Grav. **30**, 133001 (2013), [arXiv:1304.5795 [gr-qc]].

[427] A. E. Gumrukcuoglu *et al.*, Phys. Rev. D **88**, 024023 (2013), [arXiv:1304.0449 [hep-th]].

[428] D. Blas and S. Sibiryakov, JCAP **1107**, 026 (2011), [arXiv:1104.3579 [hep-th]].

[429] B. Audren, D. Blas, J. Lesgourgues and S. Sibiryakov, JCAP **1308**, 039 (2013), [arXiv:1305.0009 [astro-ph.CO]].

[430] T. Padmanabhan, Phys. Rev. D **66**, 021301 (2002), [hep-th/0204150].

[431] L. R. W. Abramo and F. Finelli, Phys. Lett. B **575**, 165 (2003), [astro-ph/0307208].

[432] J. M. Aguirregabiria and R. Lazkoz, Phys. Rev. D **69**, 123502 (2004), [hep-th/0402190].

[433] U. Seljak and M. Zaldarriaga, Astrophys. J. **469**, 437 (1996), [astro-ph/9603033].

[434] A. Lewis and A. Challinor, Phys. Rept. **429**, 1 (2006), [astro-ph/0601594].

[435] W. Hu, Phys. Rev. D **62**, 043007 (2000), [astro-ph/0001303].

[436] D. J. Eisenstein and W. Hu, Astrophys. J. **496**, 605 (1998), [astro-ph/9709112].

[437] A. A. Starobinsky, JETP Lett. **86**, 157 (2007), [arXiv:0706.2041 [astro-ph]].

[438] T. Giannantonio, M. Martinelli, A. Silvestri and A. Melchiorri, JCAP **1004**, 030 (2010), [arXiv:0909.2045 [astro-ph.CO]].

[439] L. Lombriser, A. Slosar, U. Seljak and W. Hu, Phys. Rev. D **85**, 124038 (2012), [arXiv:1003.3009 [astro-ph.CO]].

[440] A. Marchini and V. Salvatelli, Phys. Rev. D **88**, 027502 (2013) [arXiv:1307.2002 [astro-ph.CO]].

[441] A. Marchini, A. Melchiorri, V. Salvatelli and L. Pagano, Phys. Rev. D **87**, 083527 (2013) [arXiv:1302.2593 [astro-ph.CO]].

[442] E. Calabrese, A. Cooray, M. Martinelli, A. Melchiorri, L. Pagano, A. Slosar and G. F. Smoot, Phys. Rev. D **80**, 103516 (2009), [arXiv:0908.1585 [astro-ph.CO]].

[443] S. Das, T. Louis, M. R. Nolta, G. E. Addison, E. S. Battistelli, J. R. Bond, E. Calabrese and D. C. M. J. Devlin *et al.*, JCAP **1404**, 014 (2014) [arXiv:1301.1037 [astro-ph.CO]].

[444] W. R. Gilks, *"Markov Chain Monte Carlo In Practice"*, Chapman and Hall/CRC, 0412055511, (1999).

[445] P. A. R. Ade *et al.* [Planck Collaboration], arXiv:1303.5075 [astro-ph.CO].

[446] F. Beutler, C. Blake, M. Colless, D. H. Jones, L. Staveley-Smith, L. Campbell, Q. Parker and W. Saunders *et al.*, Mon. Not. Roy. Astron. Soc. **416**, 3017 (2011), [arXiv:1106.3366 [astro-ph.CO]].

[447] J. Dossett, B. Hu and D. Parkinson, JCAP **1403**, 046 (2014), [arXiv:1401.3980 [astro-ph.CO]].

[448] S. Tsujikawa and M. Sami, Phys. Lett. B **603**, 113 (2004) [hep-th/0409212].

[449] A. R. Gomes and L. Amendola, arXiv:1306.3593 [astro-ph.CO].